

**EFFECT OF CHARGE NEUTRALIZATION, PARTICLE
SIZE AND BIDISPERSE AEROSOL FRACTIONS ON
THE EFFICIENCY OF FIBROUS AUTOMOTIVE
AIR FILTERS USING LASER DOPPLER
VELOCIMETRY**

By

RAM SRINIVASAN

Bachelor of Technology

Banaras Hindu University

Varanasi, India

1996

Submitted to the Faculty of the
Graduate College of the
Oklahoma State University
in partial fulfillment of
the requirements for
the Degree of
MASTER OF SCIENCE
May, 2000

EFFECT OF CHARGE NEUTRALIZATION, PARTICLE


SIZE AND BIDISPERSE AEROSOL FRACTIONS ON

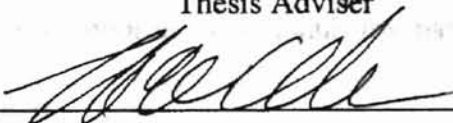
THE EFFICIENCY OF FIBROUS AUTOMOTIVE

AIR FILTERS USING LASER DOPPLER

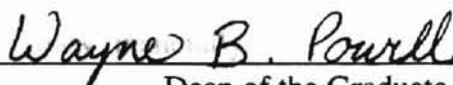
VELOCIMETRY

Thesis Approved:


Thesis Adviser







Dean of the Graduate College

ACKNOWLEDGMENTS

I would like to express my admiration and appreciation to my major advisor Dr. R. L. Dougherty for his intellectual and constructive guidance, inspiration and supervision. I also extend my sincere appreciation to my other committee members Dr. F. W. Chambers and Dr. A. J. Ghajar for their valuable suggestions and support.

Thanks are due to my colleagues, P. Saxena, S. H. Yao, A. Al-Sarkhi, and T. Gebreegziabher for their cooperation.

I would like to give my special appreciation to my fiancé, Ashley, for her special support, understanding, encouragement and love and in bearing with me in this process. I want to use this opportunity to thank my parents and my brother for their support and encouragement.

Finally, I would like to acknowledge the help of Purolator Products, Inc. and the Oklahoma Center for the Advancement of Science and Technology (OCAST) for supporting this study financially.

	Page
4.2.5	57
	59
4.4	63
4.4.1	63
4.4.2	66
4.4.3	67
CHAPTER 1 INTRODUCTION	01
1.1	2
1.2	3
CHAPTER 2 LITERATURE REVIEW	4
2.1	4
2.2	4
2.3	7
2.4	11
2.5	14
2.6	18
2.7	23
CHAPTER 3 THE LASER DOPPLER VELOCIMETRY SYSTEM: DATA MEASUREMENT CALIBRATION AND CALCULATION TECHNIQUE	26
3.1	26
3.2	26
3.3	28
3.4	31
3.5	40
CHAPTER 4 EXPERIMENTAL SETUP	48
4.1	48
4.2	48
4.2.1	50
4.2.2	51
4.2.3	52
4.2.4	55

	Page
4.2.5 The Filter and Local Efficiency Measurements	57
4.3 Laser Consistency	59
4.4 Operating Procedures and Practices.....	63
4.4.1 Experimental Procedure	63
4.4.2 Low Number Density	66
4.4.3 Procedural Precautions.....	67
4.4.4 Regular System Maintenance.....	68
4.4.5 Procedure for Maintaining Steady-State Temperature in Housing.....	68
CHAPTER 5 RESULTS AND DISCUSSION.....	71
5.1 Overview	71
5.2 Flow Measurement and Pressure Drop	72
5.3 Results for Monodisperse Aerosols	75
5.4 Local Profiles	82
5.5 Overall Results.....	89
5.6 Fractional Efficiency Results for Bidisperse Aerosols	97
5.7 Empirical Modeling of Experimental Results by Modifying Slip Factor.....	102
5.8 Empirical Model for Inertial Interception Regime	104
CHAPTER 6 SUMMARY AND RECOMMENDATIONS	109
6.1 Summary	109
6.2 Recommendations.....	111
REFERENCES	113
APPENDICES	118
APPENDIX A RESULTS FOR MONODISPERSE AEROSOLS CONTAINING 2.02 MICRON DIAMETER PSL PARTICLES IN THE SMALL ANGLE DIFFUSER HOUSING	119
APPENDIX B RESULTS FOR MONODISPERSE AEROSOLS CONTAINING 0.505 MICRON DIAMETER PSL PARTICLES IN THE SMALL ANGLE DIFFUSER HOUSING	155
APPENDIX C HIGH VOLTAGE AND PARTICLE SIZING EXPERIMENTS	190

	Page
APPENDIX D CALCULATION OF ERROR IN USING THE TSI FLOW METER FOR MEASURING DUCT VELOCITY	206
APPENDIX E DSA RAW DATA LISTING	208
APPENDIX F EFFECT OF PARTICLE SIZE ON PROBE VOLUME	223
APPENDIX G REFERENCES FROM THE INTERNET	225
APPENDIX H LIST OF EQUIPMENT	228
APPENDIX I ERROR ANALYSIS	230
APPENDIX J RESULTS FOR MONODISPERSE AEROSOLS CONTAINING 0.505 MICRON DIAMETER AND 2.02 MICRON DIAMETER PSL PARTICLES IN THE SIMULATED AUTOMOTIVE FILTER HOUSING	233
	237
	238
	238
	156
	157

LIST OF TABLES

Table		Page
2-1	Characteristics of Fibrous Filter Used by Gougeon (1994).....	17
3-1	LDV Parameters for Study of High Voltage and Particle Sizing	34
3-2	Effect of High Voltage on the Measurement of Filtration Efficiency	39
3-3	Experiments Performed to Show Consistency of High Voltage in Predicting Number Density for a Two Particle Mixture of Sizes A and B (Also Refer to Appendix C)	46
5-1	Overall Efficiency Results for Monodisperse Aerosols using the Purolator Products, Inc. A13192 Filter	77
5-2	Fractional Efficiency for Two Particle Mixtures with Varying Flow Rate	98
5-3	Mixtures Analyzed to Predict the Expected Validity Based on the Calibrations	98
A-1	Test Conditions and Average Values over the Filter Surface of Efficiency, Upstream and Downstream Velocities, and Upstream and Downstream Number Densities for 2.02 Micron Particles in the Small Angle Diffuser Housing	120
B-1	Test Conditions and Average Values over the Filter Surface of Efficiency, Upstream and Downstream Velocities, and Upstream and Downstream Number Densities for 0.505 Micron Particles in the Small Angle Diffuser Housing	156
D-1	Tabulation of Calculated Error using the TSI Flow Meter	207
J-1	Test Conditions and Average Values over the Filter Surface of Efficiency, Upstream and Downstream Velocities, and Upstream and Downstream Number Densities in the Simulated Automotive Filter Housing	234

Figure		Page
2-13	Fractional Efficiencies of Diffusion Filter Media (Mads and Uthman, 1986)	20
2-14	Fractional Efficiencies of Diffusion Filter Media (Mads and Uthman, 1986)	21
LIST OF FIGURES		
Figure		Page
2-1	Different Mechanisms of Filtrations and their Significance in Various Regimes (Spurny, 1998)	5
2-2	Stopping Distance for a Plate Impactor (Pastuszka, 1998)	6
2-3	Limiting Trajectories for Single Fiber Efficiency (Lastow and Podgorski, 1998)	8
2-4	Microscopic View of Filter Structure (Brown, 1998a)	9
2-5	Effect of Fiber Length Distribution for Filter with a Packing Density of 0.03, a Fiber Diameter Equal to 1 Micron, and a Face Velocity of 0.01 m/s.	10
2-6	Effect of Fiber Length Distribution for Filter with a Packing Density of 0.01, Fiber Diameter Equal to 20 Microns and a Face Velocity of 1 m/s.	10
2-7	Single Fiber Efficiencies Calculated from Computer Simulation for $D_p = 1$ to 12 Microns and $D_f = 10$ to 80 Microns at a Constant Velocity of 0.1 m/s in the Inertial Impaction Regime of Filtration (Lastow and Podgorski, 1998)	13
2-8	Comparison of Results in the Inertial Interception Regime for 2.04 Micron Particles (Saxena, 1998)	14
2-9	Comparison of Results in the Inertial Interception Regime for 0.497 Micron Particles (Saxena, 1998)	15
2-10	Comparison of Experimental Results with Theoretical Model of Duran (1995) (from Gebreegziabher, 1999)	16
2-11	Comparison of Gougeon's Results with Correlations of Different Authors (Boulaud and Renoux, 1998)	17
2-12	Relation of Particle Size to Signal Amplitude (Liang, 1997)	20

Figure		Page
2-13	Fractional Efficiency of Different Filter Media (Maus and Umhauer, 1996)	20
2-14	Fractional Efficiency of Two Filter Media for Limestone Dust (Maus and Umhauer, 1996)	21
2-15	Fractional Efficiencies for Microbial Aerosols for Medium Efficiency Filters (Schmidt et al., 1998)	22
2-16	Fractional Efficiencies of High Efficiency Charged Filter for Bacterial Aerosols (Schmidt et al., 1998)	23
3-1	Optical Probe Volume (Aerometrics, 1999)	27
3-2	Swept Volume Technique (Liang, 1997)	29
3-3	Effect of PMT High Voltage on the Percent of Valid Samples using Constant LDV Parameters (see Table 3-1) at Flow Rates of 85 m^3/hr , 170 m^3/hr and 255 m^3/hr in the Small Angle Diffuser Housing ...	32
3-4	Generalized Trend for Validity vs. High Voltage for a Constant Particle Size	33
3-5	Effect of High Voltage on Efficiency of 0.966 Micron Diameter Particles Showing a Standard Deviation of 2 % (see Test34.xls of Table 3-2 for Details)	38
3-6	Effect of Threshold on Signal Validity for 0.505 Micron Particle Diameter and High Voltage of 500 V at a Flow Rate of 170 m^3/hr	40
3-7	Best Fit Polynomial Equations for Calibration Based on Average Value of Validity for 2.02, 0.966 and 0.505 Micron Particles	41
3-8	Difference in Validity for the Three Different Pairs of Particle Sizes as a Function of High Voltage	45
3-9	Fractional Efficiency as a Function of High Voltage for a Bidisperse Mixture of 0.966 Micron and 2.02 Micron Particles (see Test29.xls of Table 3-3) for PMT High Voltage Parameters Defined in Table 3-1	46
4-1	Overall Layout of Test Laboratory (Not to Scale)	49
4-2	Schematic Drawing of the Air Flow Path	50

Figure		Page
4-3	Schematic of LDV Data Acquisition (Anand, 1997).....	52
4-4	Isometric View of the Small Angle Diffuser Housing.....	53
4-5	Isometric View of Mixing Box and Downstream Assembly of the Flow Housing Components.....	54
4-6	Front Views of Upstream and Downstream Small Angle Diffuser Housing Components.....	55
4-7	Side Views of Upstream and Downstream Small Angle Diffuser Housing Components.....	56
4-8	Charge Neutralization Setup (Gebreegziabher, 1999)	57
4-9	Filter Construction (Purolator Products) and the Location of the Measuring Grid over the Filter Surface	58
4-10	Sample Number Density Profile Downstream of Filter for 17 m ³ /hr (10 scfm), Grounded Housing (2.02 Micron Particles)	59
4-11	Variation of Laser Power at the Transceiver for a Constant Temperature inside the Plexiglass Box, Blower in Operation (Saxena, 1998)	61
4-12	Effect of Various Parameters on Laser Power (Gebreegziabher, 1999) ..	61
4-13	Fiber Drive Setup on an Insulated Metal Table (Gebreegziabher, 1999).....	62
4-14	Variation in Laser Power When the Temperature inside the Plexiglass Box Was Kept Constant (Saxena, 1998)	63
4-15	Procedural Flow Chart for Conducting Efficiency Measurements	65
4-16	Procedural Flow Chart for Achieving and Maintaining Constant Temperature in the Fiber Drive.....	70
5-1	Variation of LDV Velocity with TSI Flow using the Small Angle Diffuser Housing.....	73
5-2	Calibration Curve for TSI Flow Meter (Al-Sarkhi, 1999).....	74
5-3	Initial Pressure Drop as a Function of LDV Recorded Velocity	74

Figure		Page
5-21	Comparison of Theoretical and Experimental Values for	
5-4	Initial Pressure Drop as a Function of TSI Flow Meter Measured Flow Rate	96 75
5-5	Upstream Number Density Profile for a Flow Rate of 340.1 m ³ /hr	83 90
5-6	Upstream Number Density Profile for a Flow Rate of 27.2 m ³ /hr	83 83
5-7	Upstream Velocity Profile for a Flow Rate of 340.1 m ³ /hr	84 100
5-8	Upstream Velocity Profile for a Flow Rate of 27.2 m ³ /hr	84 84
5-9	Downstream Number Density Profile for a Flow Rate of 340.1 m ³ /hr....	85 101
5-10	Downstream Number Density Profile for a Flow Rate of 27.2 m ³ /hr.....	85 85
5-11	Downstream Velocity Profile for a Flow Rate of 340.1 m ³ /hr	87 91
5-12	Downstream Velocity Profile for a Flow Rate of 27.2 m ³ /hr	87 87
5-13	Efficiency Profile for a Flow Rate of 340.1 m ³ /hr.....	88 91
5-14	Efficiency Profile for a Flow Rate of 27.2 m ³ /hr.....	88 91
5-15	Overall Efficiency for 2.02 Micron Particles as a Function of LDV Recorded Velocity with and without the Effects of Charge Neutralization Compared with the Results of Saxena (1998)	90 90 90
5-16	Overall Efficiency for 2.02 Micron Particles as a Function of TSI Recorded Flow Rate with and without the Effects of Charge Neutralization Compared with the Results of Saxena (1998)	90 90 90
5-17	Overall Efficiency for 0.505 Micron Particles as a Function of LDV Recorded Velocity with and without the Effects of Charge Neutralization Compared with the Results of Saxena (1998)	91 91 91
5-18	Overall Efficiency for 0.505 Micron Particles as a Function of TSI Recorded Flow Rate with and without the Effects of Charge Neutralization Compared with the Results of Saxena (1998)	92 92 92
5-19	Comparison of Theoretical and Experimental Values for 2.02 Micron Particles	94 94
5-20	Comparison of Theoretical and Experimental Values for 0.966 Micron Particles	95 95

Figure		Page
5-21	Comparison of Theoretical and Experimental Values for 0.505 Micron Particles	96
5-22	Accuracy of Predicting Fractional Ratio in a Bidisperse Mixture of 2.02 Micron and 0.505 Micron Diameter Particles by Comparing Known Mixture Ratios with Predicted Ratios	99
5-23	Fractional Efficiency as a Function of LDV Velocity for a Bidisperse Aerosol Mixture of 2.02 Micron and 0.505 Micron Particles	100
5-24	Fractional Efficiency as a Function of LDV Velocity for a Bidisperse Aerosol Mixture of 2.02 Micron and 0.966 Micron Particles	101
5-25	Fractional Efficiency as a Function of LDV Velocity for a Bidisperse Aerosol Mixture of 0.966 Micron and 0.505 Micron Particles	102
5-26	Efficiency as a Function of Stokes Number for 2.02, 0.966 and 0.505 Micron Particle Diameters in the Charge Neutralized Setup	103
5-27	Efficiency as a Function of Stokes Number for 2.02, 0.966 and 0.505 Micron Particle Diameters in the Charged Setup	104
5-28	Efficiency as a Function of Stokes Number with Modified Slip Factor ($Q' = 2000$) for 2.02, 0.966 and 0.505 Micron Particle Diameters in the Charge Neutralized Setup	105
5-29	Efficiency as a Function of Stokes Number with Modified Slip Factor ($Q' = 2000$) for 2.02, 0.966 and 0.505 Micron Particle Diameters in the Charged Setup	105
5-30	Efficiency ($\eta\alpha/(1-\alpha)$) vs. an Inertial Interception Parameter ($St^{0.73}(D_p/D_f)^{-1}$) for 2.02, 0.966 and 0.505 Micron Diameter PSL Particles in the Grounded Setup of the Small Angle Diffuser Housing	107
5-31	Efficiency ($\eta\alpha/(1-\alpha)$) vs. Stokes Number (St) for 2.02, 0.966 and 0.505 Micron Diameter PSL Particles in the Grounded Setup of the Small Angle Diffuser Housing	107

Figure		Page
A-1	Results for 2.02 Micron Diameter Monodisperse Aerosols using a Charge Neutralized Setup for a Flow Rate of 340.06 m ³ /hr in the Small Angle Diffuser Housing (125-2ag).....	122
A-2	Results for 2.02 Micron Diameter Aerosols using a Charge Neutralized Setup for a Flow Rate of 340.06 m ³ /hr in the Small Angle Diffuser Housing (125-2bg).....	123
A-3	Results for 2.02 Micron Diameter Aerosols using a Charge Neutralized Setup for a Flow Rate of 340.06 m ³ /hr in the Small Angle Diffuser Housing (125-2cg).....	124
A-4	Results for 2.02 Micron Diameter Aerosols using a Charge Neutralized Setup for a Flow Rate of 204.04 m ³ /hr in the Small Angle Diffuser Housing (75-2ag).....	125
A-5	Results for 2.02 Micron Diameter Aerosols using a Charge Neutralized Setup for a Flow Rate of 204.04 m ³ /hr in the Small Angle Diffuser Housing (75-2bg).....	126
A-6	Results for 2.02 Micron Diameter Aerosols using a Charge Neutralized Setup for a Flow Rate of 136.02 m ³ /hr in the Small Angle Diffuser Housing (75-2cg).....	127
A-7	Results for 2.02 Micron Diameter Aerosols using a Charge Neutralized Setup for a Flow Rate of 136.02 m ³ /hr in the Small Angle Diffuser Housing (50-2ag).....	128
A-8	Results for 2.02 Micron Diameter Aerosols using a Charge Neutralized Setup for a Flow Rate of 136.02 m ³ /hr in the Small Angle Diffuser Housing (50-2bg).....	129
A-9	Results for 2.02 Micron Diameter Aerosols using a Charge Neutralized Setup for a Flow Rate of 136.02 m ³ /hr in the Small Angle Diffuser Housing (50-2cg).....	130
A-10	Results for 2.02 Micron Diameter Aerosols using a Charge Neutralized Setup for a Flow Rate of 136.02 m ³ /hr in the Small Angle Diffuser Housing (50-2dg).....	131
A-11	Results for 2.02 Micron Diameter Aerosols using a Charge Neutralized Setup for a Flow Rate of 95.21 m ³ /hr in the Small Angle Diffuser Housing (35-2ag).....	132

Figure	Page
A-12	Results for 2.02 Micron Diameter Aerosols using a Charge Neutralized Setup for a Flow Rate of 95.21 m ³ /hr in the Small Angle Diffuser Housing (35-2bg) 133
A-13	Results for 2.02 Micron Diameter Aerosols using a Charge Neutralized Setup for a Flow Rate of 95.21 m ³ /hr in the Small Angle Diffuser Housing (35-2cg) 134
A-14	Results for 2.02 Micron Diameter Aerosols using a Charge Neutralized Setup for a Flow Rate of 95.21 m ³ /hr in the Small Angle Diffuser Housing (35-2dg) 135
A-15	Results for 2.02 Micron Diameter Aerosols using a Charge Neutralized Setup for a Flow Rate of 95.21 m ³ /hr in the Small Angle Diffuser Housing (35-2eg) 136
A-16	Results for 2.02 Micron Diameter Aerosols using a Charge Neutralized Setup for a Flow Rate of 68.01 m ³ /hr in the Small Angle Diffuser Housing (25-2ag) 137
A-17	Results for 2.02 Micron Diameter Aerosols using a Charge Neutralized Setup for a Flow Rate of 68.01 m ³ /hr in the Small Angle Diffuser Housing (25-2bg) 138
A-18	Results for 2.02 Micron Diameter Aerosols using a Charge Neutralized Setup for a Flow Rate of 68.01 m ³ /hr in the Small Angle Diffuser Housing (25-2cg) 139
A-19	Results for 2.02 Micron Diameter Aerosols using a Charge Neutralized Setup for a Flow Rate of 68.01 m ³ /hr in the Small Angle Diffuser Housing (25-2dg) 140
A-20	Results for 2.02 Micron Diameter Aerosols using a Charge Neutralized Setup for a Flow Rate of 68.01 m ³ /hr in the Small Angle Diffuser Housing (25-2eg) 141
A-21	Results for 2.02 Micron Diameter Aerosols using a Charge Neutralized Setup for a Flow Rate of 40.81 m ³ /hr in the Small Angle Diffuser Housing (15-2ag) 142
A-22	Results for 2.02 Micron Diameter Aerosols using a Charge Neutralized Setup for a Flow Rate of 40.81 m ³ /hr in the Small Angle Diffuser Housing (15-2bg) 143

Figure	Page
A-23	Results for 2.02 Micron Diameter Aerosols using a Charge Neutralized Setup for a Flow Rate of 40.81 m ³ /hr in the Small Angle Diffuser Housing (15-2cg) 144
A-24	Results for 2.02 Micron Diameter Aerosols using a Charge Neutralized Setup for a Flow Rate of 40.81 m ³ /hr in the Small Angle Diffuser Housing (15-2dg) 145
A-25	Results for 2.02 Micron Diameter Aerosols using a Charge Neutralized Setup for a Flow Rate of 40.81 m ³ /hr in the Small Angle Diffuser Housing (15-2eg) 146
A-26	Results for 2.02 Micron Diameter Aerosols using a Charge Neutralized Setup for a Flow Rate of 27.2 m ³ /hr in the Small Angle Diffuser Housing (10-2ag) 147
A-27	Results for 2.02 Micron Diameter Aerosols using a Charge Neutralized Setup for a Flow Rate of 27.2 m ³ /hr in the Small Angle Diffuser Housing (10-2bg) 148
A-28	Results for 2.02 Micron Diameter Aerosols using a Charged Setup for a Flow Rate of 340.06 m ³ /hr in the Small Angle Diffuser Housing (125-2au) 149
A-29	Results for 2.02 Micron Diameter Aerosols using a Charged Setup for a Flow Rate of 204.04 m ³ /hr in the Small Angle Diffuser Housing (75-2au) 150
A-30	Results for 2.02 Micron Diameter Aerosols using a Charged Setup for a Flow Rate of 204.04 m ³ /hr in the Small Angle Diffuser Housing (75-2bu) 151
A-31	Results for 2.02 Micron Diameter Aerosols using a Charged Setup for a Flow Rate of 136.02 m ³ /hr in the Small Angle Diffuser Housing (50-2au) 152
A-32	Results for 2.02 Micron Diameter Aerosols using a Charged Setup for a Flow Rate of 136.02 m ³ /hr in the Small Angle Diffuser Housing (50-2bu) 153
A-33	Results for 2.02 Micron Diameter Aerosols using a Charged Setup for a Flow Rate of 136.02 m ³ /hr in the Small Angle Diffuser Housing (50-2cu) 154

Figure	Page
B-1	Results for 0.505 Micron Diameter Aerosols using a Charge Neutralized Setup for a Flow Rate of 340.06 m ³ /hr in the Small Angle Diffuser Housing (200-05ag) 158
B-2	Results for 0.505 Micron Diameter Aerosols using a Charge Neutralized Setup for a Flow Rate of 340.06 m ³ /hr in the Small Angle Diffuser Housing (200-05bg) 159
B-3	Results for 0.505 Micron Diameter Aerosols using a Charge Neutralized Setup for a Flow Rate of 255.04 m ³ /hr in the Small Angle Diffuser Housing (150-05ag) 160
B-4	Results for 0.505 Micron Diameter Aerosols using a Charge Neutralized Setup for a Flow Rate of 255.04 m ³ /hr in the Small Angle Diffuser Housing (150-05bg) 161
B-5	Results for 0.505 Micron Diameter Aerosols using a Charge Neutralized Setup for a Flow Rate of 212.54 m ³ /hr in the Small Angle Diffuser Housing (125-05ag) 162
B-6	Results for 0.505 Micron Diameter Aerosols using a Charge Neutralized Setup for a Flow Rate of 212.54 m ³ /hr in the Small Angle Diffuser Housing (125-05bg) 163
B-7	Results for 0.505 Micron Diameter Aerosols using a Charge Neutralized Setup for a Flow Rate of 170.03 m ³ /hr in the Small Angle Diffuser Housing (100-05ag) 164
B-8	Results for 0.505 Micron Diameter Aerosols using a Charge Neutralized Setup for a Flow Rate of 170.03 m ³ /hr in the Small Angle Diffuser Housing (100-05bg) 165
B-9	Results for 0.505 Micron Diameter Aerosols using a Charge Neutralized Setup for a Flow Rate of 170.03 m ³ /hr in the Small Angle Diffuser Housing (100-05cg) 166
B-10	Results for 0.505 Micron Diameter Aerosols using a Charge Neutralized Setup for a Flow Rate of 127.52 m ³ /hr in the Small Angle Diffuser Housing (75-05ag) 167
B-11	Results for 0.505 Micron Diameter Aerosols using a Charge Neutralized Setup for a Flow Rate of 127.52 m ³ /hr in the Small Angle Diffuser Housing (75-05bg) 168

Figure		Page
B-12	Results for 0.505 Micron Diameter Aerosols using a Charge Neutralized Setup for a Flow Rate of 85.02 m ³ /hr in the Small Angle Diffuser Housing (50-05ag)	169
B-13	Results for 0.505 Micron Diameter Aerosols using a Charge Neutralized Setup for a Flow Rate of 85.02 m ³ /hr in the Small Angle Diffuser Housing (50-05bg)	170
B-14	Results for 0.505 Micron Diameter Aerosols using a Charge Neutralized Setup for a Flow Rate of 42.51 m ³ /hr in the Small Angle Diffuser Housing (25-05ag)	171
B-15	Results for 0.505 Micron Diameter Aerosols using a Charge Neutralized Setup for a Flow Rate of 42.51 m ³ /hr in the Small Angle Diffuser Housing (25-05bg)	172
B-16	Results for 0.505 Micron Diameter Aerosols using a Charged Setup for a Flow Rate of 544.10 m ³ /hr in the Small Angle Diffuser Housing (200-05au)	173
B-17	Results for 0.505 Micron Diameter Aerosols using a Charged Setup for a Flow Rate of 476.09 m ³ /hr in the Small Angle Diffuser Housing (175-05au)	174
B-18	Results for 0.505 Micron Diameter Aerosols using a Charged Setup for a Flow Rate of 476.09 m ³ /hr in the Small Angle Diffuser Housing (175-05bu)	175
B-19	Results for 0.505 Micron Diameter Aerosols using a Charged Setup for a Flow Rate of 408.08 m ³ /hr in the Small Angle Diffuser Housing (150-05au)	176
B-20	Results for 0.505 Micron Diameter Aerosols using a Charged Setup for a Flow Rate of 408.08 m ³ /hr in the Small Angle Diffuser Housing (150-05bu)	177
B-21	Results for 0.505 Micron Diameter Aerosols using a Charged Setup for a Flow Rate of 340.05 m ³ /hr in the Small Angle Diffuser Housing (125-05au)	178
B-22	Results for 0.505 Micron Diameter Aerosols using a Charged Setup for a Flow Rate of 340.05 m ³ /hr in the Small Angle Diffuser Housing (125-05bu)	179

Figure	Page
B-23	Results for 0.505 Micron Diameter Aerosols using a Charged Setup for a Flow Rate of 272.05 m ³ /hr in the Small Angle Diffuser Housing (100-05au) 180
B-24	Results for 0.505 Micron Diameter Aerosols using a Charged Setup for a Flow Rate of 272.05 m ³ /hr in the Small Angle Diffuser Housing (100-05bu) 181
B-25	Results for 0.505 Micron Diameter Aerosols using a Charged Setup for a Flow Rate of 204.04 m ³ /hr in the Small Angle Diffuser Housing (75-05au) 182
B-26	Results for 0.505 Micron Diameter Aerosols using a Charged Setup for a Flow Rate of 204.04 m ³ /hr in the Small Angle Diffuser Housing (75-05bu) 183
B-27	Results for 0.505 Micron Diameter Aerosols using a Charged Setup for a Flow Rate of 204.04 m ³ /hr in the Small Angle Diffuser Housing (75-05cu) 184
B-28	Results for 0.505 Micron Diameter Aerosols using a Charged Setup for a Flow Rate of 136.02 m ³ /hr in the Small Angle Diffuser Housing (50-05au) 185
B-29	Results for 0.505 Micron Diameter Aerosols using a Charged Setup for a Flow Rate of 136.02 m ³ /hr in the Small Angle Diffuser Housing (50-05bu) 186
B-30	Results for 0.505 Micron Diameter Aerosols using a Charged Setup for a Flow Rate of 68.01 m ³ /hr in the Small Angle Diffuser Housing (25-05au) 187
B-31	Results for 0.505 Micron Diameter Aerosols using a Charged Setup for a Flow Rate of 68.01 m ³ /hr in the Small Angle Diffuser Housing (25-05bu) 188
B-32	Results for 0.505 Micron Diameter Aerosols using a Charged Setup for a Flow Rate of 68.01 m ³ /hr in the Small Angle Diffuser Housing (25-05cu) 189
C-1	Fractional Ratio of the Number of Particles of Each Individual Particle Size in a Bidisperse Mixture of 2.02 Micron and 0.505 Micron Diameter Particles (Test13)..... 191

Figure		Page
C-2	Fractional Ratio of the Number of Particles of Each Individual Particle Size in a Bidisperse Mixture of 2.02 Micron and 0.505 Micron Diameter Particles (Test14).....	192
C-3	Fractional Ratio of the Number of Particles of Each Individual Particle Size in a Bidisperse Mixture of 2.02 Micron and 0.505 Micron Diameter Particles (Test16).....	192
C-4	Fractional Ratio of the Number of Particles of Each Individual Particle Size in a Bidisperse Mixture of 2.02 Micron and 0.505 Micron Diameter Particles (Test17).....	193
C-5	Fractional Ratio of the Number of Particles of Each Individual Particle Size in a Bidisperse Mixture of 2.02 Micron and 0.505 Micron Diameter Particles (Test18).....	193
C-6	Fractional Ratio of the Number of Particles of Each Individual Particle Size in a Bidisperse Mixture of 2.02 Micron and 0.505 Micron Diameter Particles (Test19).....	194
C-7	Fractional Ratio of the Number of Particles of Each Individual Particle Size in a Bidisperse Mixture of 2.02 Micron and 0.505 Micron Diameter Particles (Test19).....	194
C-8	Efficiency as a Function of High Voltage for 0.505 Micron Diameter Particles (Test23)	195
C-9	Efficiency as a Function of High Voltage for 0.505 Micron Diameter Particles (Test24)	195
C-10	Efficiency as a Function of High Voltage for 2.02 Micron Diameter Particles (Test25)	196
C-11	Efficiency as a Function of High Voltage for 2.02 Micron Diameter Particles (Test26)	196
C-12	Efficiency as a Function of High Voltage for 0.966 Micron Diameter Particles (Test27)	197
C-13	Efficiency as a Function of High Voltage for 0.966 Micron Diameter Particles (Test28)	197
C-14	Efficiency as a Function of High Voltage for 0.966 Micron Diameter Particles (Test33)	198

Figure		Page
C-15	Efficiency as a Function of High Voltage for 0.966 Micron Diameter Particles (Test34) of Diameter 0.505 Micron and 0.966 Micron (Test36)	198 204
C-16	Efficiency as a Function of High Voltage for 0.966 Micron Diameter Particles (Test38)	199 204
C-17	Fractional Efficiency as a Function of High Voltage for a Mixture Containing Particles of Diameter 2.02 Microns and 0.966 Micron (Test29)	204 199
C-18	Fractional Efficiency as a Function of High Voltage for a Mixture Containing Particles of Diameter 2.02 Microns and 0.966 Micron (Test30)	205 200
C-19	Fractional Efficiency as a Function of High Voltage for a Mixture Containing Particles of Diameter 2.02 Microns and 0.966 Micron (Test40)	200 200
C-20	Fractional Efficiency as a Function of High Voltage for a Mixture Containing Particles of Diameter 2.02 Microns and 0.505 Micron (Test21)	201 201
C-21	Fractional Efficiency as a Function of High Voltage for a Mixture Containing Particles of Diameter 2.02 Microns and 0.505 Micron (Test22)	201 201
C-22	Fractional Efficiency as a Function of High Voltage for a Mixture Containing Particles of Diameter 2.02 Microns and 0.505 Micron (Test35)	202 202
C-23	Fractional Efficiency as a Function of High Voltage for a Mixture Containing Particles of Diameter 2.02 Microns and 0.505 Micron (Test39)	202 202
C-24	Fractional Efficiency as a Function of High Voltage for a Mixture Containing Particles of Diameter 0.505 Micron and 0.966 Micron (Test31)	203 203
C-25	Fractional Efficiency as a Function of High Voltage for a Mixture Containing Particles of Diameter 0.505 Micron and 0.966 Micron (Test32)	203 203

Figure		Page
C-26	Fractional Efficiency as a Function of High Voltage for a Mixture Containing Particles of Diameter 0.505 Micron and 0.966 Micron (Test36)	204
C-27	Fractional Efficiency as a Function of High Voltage for a Mixture Containing Particles of Diameter 0.505 Micron and 0.966 Micron (Test37)	204
C-28	Fractional Efficiency as a Function of High Voltage for a Mixture Containing Particles of Diameter 2.02 Microns and 0.966 Micron (Test41)	205
F-1	Effect of Particle Size on the Transit Time of the LDV Signal	224
J-1	Results for 2.02 Micron Diameter Aerosols using a Charged Setup for a Flow Rate of 136.03 m ³ /hr in the Simulated Automotive Filter Housing (80-2ausaf).....	235
J-2	Results for 2.02 Micron Diameter Aerosols using a Charged Setup for a Flow Rate of 102.01 m ³ /hr in the Simulated Automotive Filter Housing (60-2ausaf).....	236
J-3	Results for 2.02 Micron Diameter Aerosols using a Charged Setup for a Flow Rate of 76.51 m ³ /hr in the Simulated Automotive Filter Housing (45-2ausaf).....	237
J-4	Results for 2.02 Micron Diameter Aerosols using a Charged Setup for a Flow Rate of 59.51 m ³ /hr in the Simulated Automotive Filter Housing (35-2ausaf).....	238
J-5	Results for 2.02 Micron Diameter Aerosols using a Charged Setup for a Flow Rate of 42.51 m ³ /hr in the Simulated Automotive Filter Housing (25-2ausaf).....	239
J-6	Results for 2.02 Micron Diameter Aerosols using a Charged Setup for a Flow Rate of 34.00 m ³ /hr in the Simulated Automotive Filter Housing (20-2ausaf).....	240
J-7	Results for 0.505 Micron Diameter Aerosols using a Charged Setup for a Flow Rate of 136.03 m ³ /hr in the Simulated Automotive Filter Housing (80-05ausaf).....	241
J-8	Results for 0.505 Micron Diameter Aerosols using a Charged Setup for a Flow Rate of 76.51 m ³ /hr in the Simulated Automotive Filter Housing (45-05ausaf)	242

$D(2)$	diameter of particle designated as "2" in a monodisperse mixture containing particles "1" and "2" [μm]
$D(p)$	diameter of any general particle designated as "p" in a polydisperse mixture containing "p" number of particles [μm]
NOMENCLATURE	
A_p	cross-sectional area of probe volume [m^2]
$A^{\text{peak voltage}}$	Cunningham constant (1.246) <small>peak voltage (V)</small>
$B^{\text{(t)}}$	Cunningham constant (0.87) <small>voltage oscillating at frequency</small>
c_e	cumulative fractional error in number density
C_n	Cunningham slip correction factor
C_{pv}	minor diameter of the cross-section of probe volume [μm]
$C^{\text{(peak voltage)}}$	number concentration downstream of the filter [m^{-3}]
$C_o^{\text{(t)}}$	number concentration upstream of the filter [m^{-3}]
$C(D_p)^{\text{peak power}}$	number concentration downstream of the filter for particle of diameter D_p [m^{-3}]
$C_o(D_p)^{\text{peak power}}$	number concentration upstream of the filter for particle of diameter D_p [m^{-3}]
D_e	diameter of unfocussed laser beam [μm]
D_f	fiber diameter [μm]
D_p	particle diameter [μm]
D_l	diameter of light collecting aperture [μm]
$D(1)$	diameter of particle designated as 1 in a monodisperse mixture containing particles "1" and "2" [μm]

$D(2)$	diameter of particle designated as "2" in a monodisperse mixture containing particles "1" and "2" [μm]
$D(p)$	diameter of any general particle designated as "p" in a polydisperse mixture containing "p" number of particles [μm]
$e(t)$	total signal voltage [V] for particle of diameter $D(p)$ at high voltage HV
$e_D(\text{peak voltage})$	peak Doppler component of signal voltage [V]
$e_D(t)$	Doppler component of signal voltage oscillating at Doppler frequency [V]
$e_N(t)$	shot noise generated in photodetector by the light scattered from the signal produced particle noise [V]
$e_p(\text{peak voltage})$	peak pedestal component of signal voltage [V]
$e_p(t)$	pedestal component of signal voltage [V]
$\langle e_D^2 \rangle (\text{peak power})$	peak Doppler signal power [W]
$\langle e_N^2 \rangle (\text{peak power})$	peak shot noise power [W]
EU1	coarse grade filter classified as per EUROVENT 4/5
EU3	low efficiency filter classified as per EUROVENT 4/5
EU4	low efficiency filter classified as per EUROVENT 4/5
EU7	fine grade filter classified as per EUROVENT 4/5
EV	expected signal validity [%]
$EV[D(1),HV]$	expected signal validity for particle of diameter $D(1)$ at high voltage HV [%]
$EV[D(2),HV]$	expected signal validity for particle of diameter $D(2)$ at high voltage HV [%]

$EV[D(p),HV(1)]$	expected signal validity for particle of diameter $D(p)$ at high voltage $HV(1)$ [%]
I_0	intensity of the laser light at the center of the probe volume [W/m^2]
$EV[D(p),HV(2)]$	expected signal validity for particle of diameter $D(p)$ at high voltage $HV(2)$ [%]
$EV[D(p),HV(3)]$	expected signal validity for particle of diameter $D(p)$ at high voltage $HV(3)$ [%]
$EV[D(p),HV(n-1)]$	expected signal validity for particle of diameter $D(p)$ at high voltage $HV(n-1)$ [%]
Δf	bandwidth of the filtered noise [V]
ΔF	fringe spacing [μm]
f_c	focal length of the focussing lens [m]
$f[D(1)]$	fractional mixture ratio for particles having a diameter $D(1)$
$f[D(2)]$	fractional mixture ratio for particles having a diameter $D(2)$
$f[D(p)]$	fractional mixture ratio for particles having a diameter $D(p)$
\overline{G}	light scattering gain function
h	distance between the two limiting trajectories of flow around a cylindrical fiber at a point in the undisturbed flow field [m]
h_p	Planck's constant [6.6×10^{-34} J-s]
h_f	height of the filter paper [μm]
HV	high voltage amplification supplied to the PMT [V]

I_{upstream}	laser intensity at any location in the probe volume [W/m^2]
$I_{\text{O-downstream}}[D(1),HV]$	laser intensity at the center of the probe volume [W/m^2] for $D(1)$
I_p	interception parameter [$= D_p/D_f$] of the filter [eq. 2]
$k_{\text{upstream}}[D(1),HV]$	slope of a straight line concentration for particles of diameter $D(1)$
Ku	the Kuwabara hydrodynamic constant [eq. 10]
$l_{F-downstream}[D(2),HV]$	fiber length of the filter [μm] for particles of diameter $D(2)$
\bar{l}_F	mean fiber length of the filter [μm] [eq. 11]
L	filter thickness [m]
L_f	total length of fiber per unit volume of filter [m^2]
L_s	swept volume length [m]
n_{attempts}	total number of signals detected in a run
n_{valid}	number of signals detected in a run from which particle velocity can be calculated
N	number density [m^{-3}]
N_{idown}	number density downstream of filter at grid location "i" [m^{-3}]
N_{iup}	number density upstream of filter at grid location "i" [m^{-3}]
$N[D(1),HV]$	fractional number concentration for particles of diameter $D(1)$ at high voltage HV [m^{-3}]
$N[D(2),HV]$	fractional number concentration for particles of diameter $D(2)$ at high voltage HV [m^{-3}]
$N(\text{mixture},HV)$	number concentration for a mixture containing particles of diameter $D(1)$ and $D(2)$ [m^{-3}]
$N_{\text{downstream}}$	number concentration downstream of the filter [m^{-3}]

N_{upstream}	number concentration upstream of the filter [m^{-3}]
$N_{\text{downstream}}[D(1),\text{HV}]$	fractional number concentration for particles of diameter $D(1)$ at high voltage HV downstream of the filter [m^{-3}]
$N_{\text{upstream}}[D(1),\text{HV}]$	fractional number concentration for particles of diameter $D(1)$ at high voltage HV upstream of the filter [m^{-3}]
$N_{\text{downstream}}[D(2),\text{HV}]$	fractional number concentration for particles of diameter $D(2)$ at high voltage HV downstream of the filter [m^{-3}]
$N_{\text{upstream}}[D(2),\text{HV}]$	fractional number concentration for particles of diameter $D(2)$ at high voltage HV upstream of the filter [m^{-3}]
m	vertical offset between a set of straight lines
P	ambient air pressure [Pa]
P_o	power of either laser beam in a balanced dual beam [W]
Q'	Cunningham constant (0.42)
r_a	distance from the measuring volume to the light collecting aperture [m]
R_d	number density ratio [$N_{\text{idown}}/N_{\text{iup}}$]
Re_f	Reynolds number based on fiber diameter [= $\rho_a D_f V / \mu_a$]
S	stopping distance [m]
S_f	fringe spacing [μm]
SF	solidity factor
SN	sensitivity of the photodetector [V/W]
SNR_{peak}	peak signal power to peak shot noise power ratio

Stokes Symbols	Stokes number [$St = C_n \rho_p (D_p)^2 V / (18 \mu_a D_f)$] a parameter for
α	intensity of deposition by inertia
St(T,P)	Stokes number at temperature T and pressure P
St _{TSI}	Stokes number using the value of velocity calculated using the
	TSI flow meter
SV	percentage of valid signals [%]
SV[mixture, HV(1)]	signal validity for the mixture at high voltage HV(1) [%]
SV[mixture, HV(2)]	signal validity for the mixture at high voltage HV(2) [%]
SV[mixture, HV(3)]	signal validity for the mixture at high voltage HV(3) [%]
SV[mixture, HV(n-1)]	signal validity for the mixture at high voltage HV(n-1) [%]
t	run time [s]
T	ambient air temperature [T]
v	velocity of a particle measured by the LDV system [m/s]
v/v	volume of a 10 % solid solution of PSL particles ratioed to volume of distilled water [m ³ /m ³]
V	velocity of air [m/s]
\bar{V}	Doppler signal visibility at the peak of the Doppler burst
V(T,P)	velocity of air at temperature T and pressure P [m/s]
V _{TSI}	velocity of air as calculated using the TSI flow meter [m/s]
V _n	nominal face velocity for the filter [m/s]
X	axis along shorter dimension of the filter
Y	axis along the longer dimension of the filter

Greek Symbols	density of air at 15.55 °C and 1.013x10 ⁵ Pa [kg/m ³]
α	filter solidity, packing density
η	single fiber efficiency [fiber length [μm]]
η_a	kinematic viscosity of air [m ² /s]
η_b	overall efficiency of the filter bed
η_i	local filtration efficiency at grid point i
η_{IR}	combined efficiency due to the effects of interception and inertial impaction
η_{overall}	overall filtration efficiency
η_q	quantum efficiency of the photodetector
$\eta [D(1)]$	fractional efficiency for particles of diameter D(1)
$\eta [D(2)]$	fractional efficiency for particles of diameter D(2)
λ	mean free path of air molecules [μm]
λ_w	wavelength of the laser light [μm]
μ_a	dynamic viscosity of air [Pa-s]
$\mu_{\text{air}}(T, P)$	dynamic viscosity of air at temperature T and pressure P [Pa-s]
$\mu_{\text{air-standard}}$	dynamic viscosity of air at 15.55 °C and 1.013x10 ⁵ Pa [Pa-s]
ν_D	Doppler frequency [s ⁻¹]
ν_0	frequency of laser light [s ⁻¹]
π	a mathematical constant [$\pi = 3.14159265\dots$]
ρ_a	density of air [kg/m ³]
$\rho_{\text{air}}(T, P)$	density of air at temperature T and pressure P [kg/m ³]

$\rho_{\text{air-standard}}$ density of air at 15.55 °C and 1.013x10⁵ Pa [kg/m³]

CHAPTER 1

ρ_p particle density [kg/m³]

INTRODUCTION

σ_{IF} standard deviation of fiber length [μm]

τ transit time of particle [μs]

ψ half angle between interfering beams [rad]

The need to continuously improve the performance of the automotive air filter

has led to a number of studies in the past few years

for better cabin air environment. These studies have been thorough studies of automotive

and existing air filter technologies

and the need for a more efficient and effective air filter

in order to improve the overall air quality in the vehicle

models and the overall air quality

of the experimental work has been the overall air quality

in the cabin environment

and the need for a more efficient and effective air filter

and

and

the product literature has been the overall air quality

in the cabin environment

CHAPTER 1

INTRODUCTION

A good automotive air filter serves to provide a virtually undisturbed supply of dust free air to the automobile engine with no disturbance of the inlet air flow pattern. The need to continuously improve this performance and also the demand in recent years for better cabin air environmental control necessitates the thorough study of automotive air filters (Liang et al., 1994).

Much research has been and is being done on filtration performance. Several theories have been proposed to predict flow fields around fibrous filters and to predict filtration efficiency. These studies have been aimed at developing filter efficiency models and defining and predicting the overall filtration performance. In addition, most of the experimental work have been aimed at validating these theories, and have met with partial success. Studies have also been performed on fractional efficiency, which is an important parameter used to evaluate cabin air filtration performance. The fractional efficiency refers to the efficiency of a particulate filter at specific particle "size fractions" (Burroughs, 1995).

It is not possible to fully predict filter behaviour without studying the effect of all parameters affecting the filtration efficiency and flow performance. The theoretically established parameters of interception, diffusion, inertial impaction, electrostatic forces, etc. must be studied with their experimentally influential macroscopic counterparts. Some of these include the nature of the flow, the thermodynamic conditions of the flow, local velocity profiles at the inlet and outlet of the filters, overall electric charge in the flow and size of the aerosol contaminants in the flow. This study has attempted to

investigate and correlate some of these parameters. This research has also made preliminary steps in developing a technique to determine fractional efficiency. Investigation of fractional efficiency as a function of flow rate also has been initiated.

1.1 Objectives and Area of Research

The aim of this study was to investigate the filtration efficiency of type fibrous air filters and establish some experimental measurement techniques for that type of filter. Experiments were performed using polystyrene latex (PSL) particles as the flow contaminant. These particles have excellent optical and flow properties and are commonly used to characterize fibrous filters.

All of the tests were carried out on the small angle diffuser housing. This housing is similar to the housing specified in the SAE code for cabin air filtration. However, the measurement techniques, parameters and conclusions in this work can be partially applied to both the engine inlet air and cabin air filtration. The Purolator Products, Inc. A13192 pleated air filter was used to conduct all of the tests. This filter is employed in Chrysler minivans.

The effect of electrostatic charge neutralization on the overall filtration efficiency was studied for two different sized monodisperse aerosol contaminants. These overall efficiencies were compared with previous research and also with the popular filtration models. Also for each of the above tests, the local upstream and downstream profiles for velocity and number density were measured. These were used in the computation of the local filtration efficiency.

Individual PSL particles having diameters of 2.02 microns, 0.966 micron and 0.505 micron were studied for the effect of signal quality with varying high voltage from

the Laser Doppler Velocimetry (LDV) system. Using this study, a statistical technique was developed for estimating the fractional size number count in a single test run. This is used in calculating fractional efficiency for bidisperse mixtures of known particle diameters. Fractional efficiency was studied at different flow rate and Stokes numbers. These results were then compared with their monodisperse counterparts and theoretical models.

1.2 Thesis Outline

The literature review portion (Chapter 2) in this work discusses some of the theoretical studies and model prediction related to the experimental tests carried out in this research. The next chapter (Chapter 3) pertains to the optical measurement parameters and techniques used. This discussion is based on the LDV system used. The chapter on experimental setup (Chapter 4) discusses the flow system used, the test housing, the filter and the overall organizational scheme of the test setup. Important characteristic observations and results are presented and discussed in the next chapter (Chapter 5). Previous experimental work and relevant theoretical models are used to compare with the computed results. The final chapter (Chapter 5) summarizes the significant results and conclusions and also provides recommendations for future work.

CHAPTER 2

LITERATURE REVIEW

2.1 Overview

This literature review will attempt to review past work in the related fields of filtration. Section 2.2 will provide a brief description of the mechanisms of filtration. The next section (Section 2.3) will review the definition of single fiber efficiency and will also discuss characteristics with reference to the structure of fibrous filters. Next, a review of some of the attempts to model filter behaviour in the inertial impaction regime will be discussed. Section 2.5 will target some of the experimental work in the inertial impaction regime. The next section (Section 2.6) will review some of the experimental work performed for sizing particles and carrying out fractional efficiency measurements. The last section will then briefly describe the theoretical work of Adrian (1978) involved in the estimation of LDV signal quality.

2.2 Classical Mechanisms of Filtration

All classical theories of filtration are based on the superposed effect of different mechanisms of particle collection on a single cylindrical fiber (Spurny, 1998). These different mechanisms and their effects are shown in Fig. 2-1.

The main mechanisms shown in Fig. 2-1 are diffusion, interception, inertial impaction, electrostatic deposition, attraction-repulsion, gravitational effects and settling. In order to correctly model the filter performance, it is imperative to understand the correct importance of each mechanism to the appropriate flow regime.

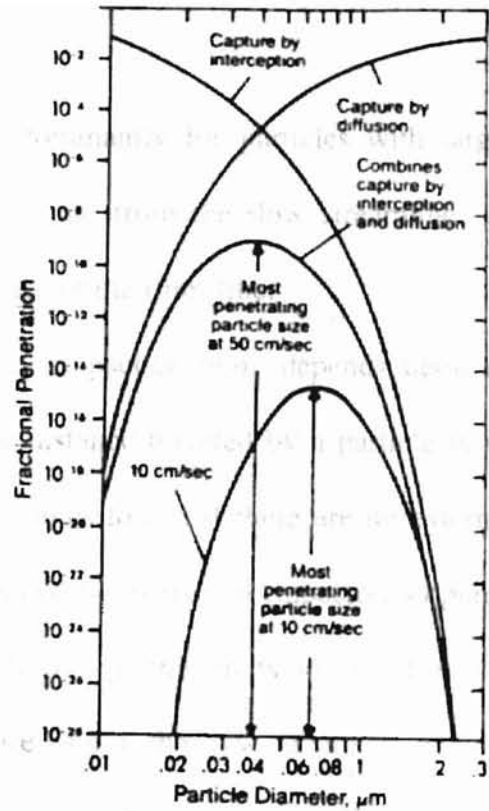
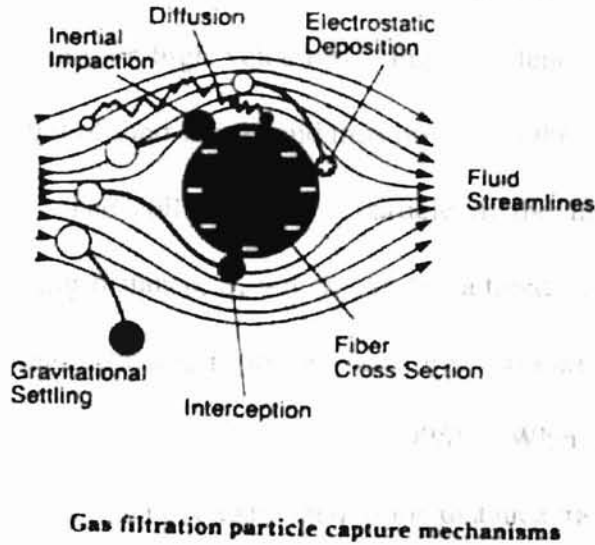


Figure 2-1 Different Mechanisms of Filtrations and their Significance in Various Regimes (Spurny, 1998)

For small particles, diffusion due to Brownian motion has a major influence on trajectory. Low velocity increases the particle residence time in the medium. Both low velocity and small particle size can increase the chances of a particle randomly settling on a filter fiber and thus increases the collection efficiency. In this study, the effect of diffusion was not considered because, for particles greater than 0.5 microns, diffusion is negligible (Flagan and Seinfeld, 1988).

Interception capture is directly related to the streamlines of the flow field and particle size. The larger the particle diameter, the greater the chance of interception. Interception by itself depends upon the interception parameter D_p/D_f (Fuchs, 1964),

where D_p is the diameter of the contaminant particle and D_f is the diameter of the filter's fibers.

The inertial deposition mechanism is predominantly for particles with larger diameters or high velocities. Particles tend to deviate from the flow streamlines on account of their inertia and thus impact on the surface of the filter fiber.

The collection of a particle in the inertial impaction zone depends upon its stopping distance, S , which can be defined as the distance traveled by a particle in its original direction in its original direction until it comes to rest if there are no external forces acting on it (Patuszka, 1998). When applied to an inertial impactor, stopping distance, S , can be explained as the distance traveled by a particle in its original direction before it recovers from an abrupt change in the direction of the flow stream if there are no external forces acting. An example of this explanation of stopping distance applied to a plate impactor is shown in Fig. 2-2. In this figure, it can be seen that a sudden turn in the flow streamlines cannot be followed by the particle owing to its inertia. It takes a distance of S to recover from this trajectory and to continue in the flow field. For this case the particle escapes collision and continues to follow the flow path.

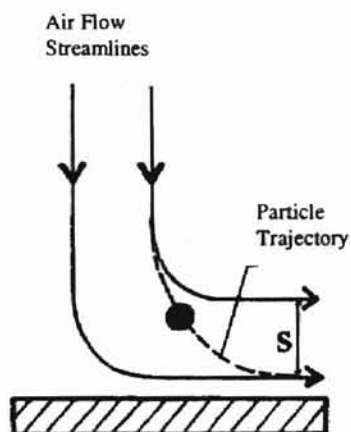


Figure 2-2 Stopping Distance for a Plate Impactor (Pastuszka, 1998)

Using Stokes Law, an expression for stopping distance can be deduced for a spherical particle moving in a fluid as (Pastuszka, 1998)

$$S = \frac{V\rho_p D_p^2 C_n}{18\mu_a} \quad (2-1)$$

As can be seen from the expression for stopping distance, a greater velocity, diameter or density causes a greater inertial force and hence a greater stopping distance.

Electrostatic deposition can cause enhanced particle capture in two separate ways. When the particles are in motion, they carry strong electrostatic charge which causes them to stick to the fiber surfaces within charged filters (Hinds, 1982). Also particle- particle attraction may cause agglomeration of particles and increase the chance of interception.

2.3 Single Fiber Model

As stated earlier, in order to study the performance of fibrous filters, the classical approach is to study the effect of flow around a single cylinder. This is because, in essence, fibrous filters are just a collection of small cylinders. This is then extrapolated to see the effect of two fibers and multiple fibers and the effect of fiber arrangement.

The single fiber efficiency is the ratio of particles captured on the fiber, when a fiber is placed in an undisturbed flow field (Davies, 1973).

The single fiber efficiency is expressed as (Lastow and Podgorski, 1998)

$$\eta = \frac{h}{D_f} \quad (2-2)$$

This definition is based on the limiting trajectory, which is the streamline closest to the particle, which can be followed by the particle without impact. Here h is defined

as the distance between the two limiting trajectories. The distance h is given for a point in the undisturbed flow field.

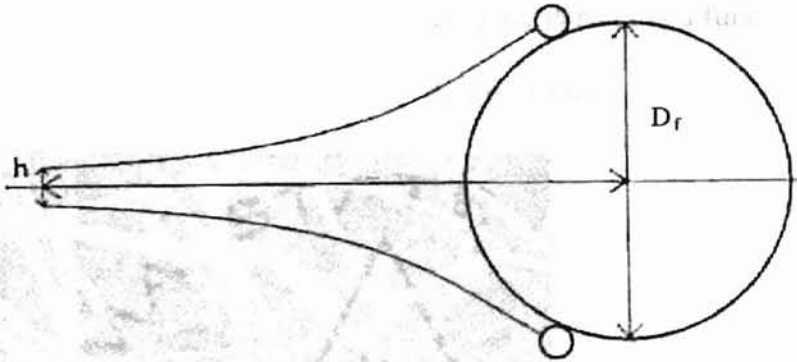


Figure 2-3 Limiting Trajectories for Single Fiber Efficiency (Lastow and Podgorski, 1998)

The overall filtration efficiency of a filter bed η_b can be related to the single fiber efficiency as (Flagan and Seinfeld, 1988)

$$\eta_b = 1 - \exp\left(\frac{-4\alpha\eta L}{\pi(1-\alpha)D_f}\right) \quad (2-3)$$

where L is taken to be the filter thickness, α is the packing density, η is the single fiber efficiency, and D_f is the diameter of the filter fiber. The packing density α is given as (Flagan and Seinfeld, 1988)

$$\alpha = \frac{\pi D_f^2 L_f}{4} \quad (2-4)$$

where L_f is the total length of the filter per unit volume of the filter bed. The packing density is most difficult to estimate due to the uncertainty in the estimation of the term L_f . A sense of the extent of uncertainty in this term is shown in Fig. 2-4.

This is a microscopic photograph of a small portion (element) of a filter. The arrangement of the filter fiber within this cell is very uneven. It is extremely difficult to determine the average length of the fiber for all of the elements of the filter. Current solutions for this problem assume that the packing density is a function of position. One of these models is described in the following discussion.

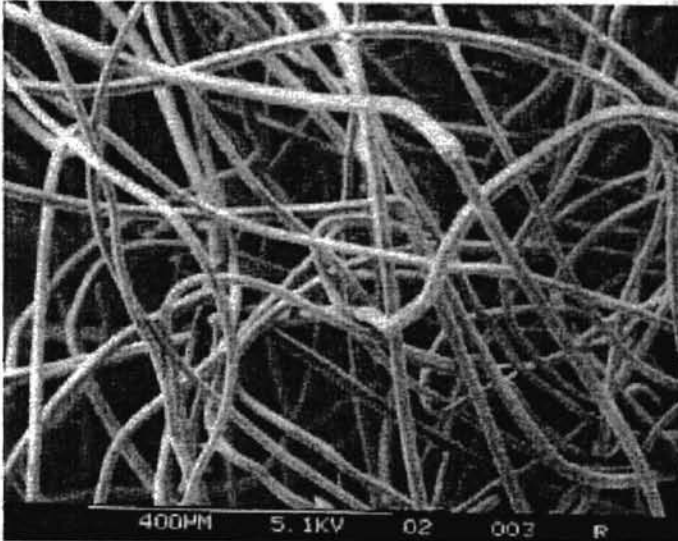


Figure 2-4 Microscopic View of Filter Structure (Brown, 1998a)

In order to account for some of these irregularities, Schweers and Loffler (1994) presented a new model explaining the filter structure. In their model, the filter is subdivided into individual elements with various structural characteristics. In accordance with structural data, the permeability of the element is calculated and hence the local flow field is determined. This is used to calculate an element specific local separation, which, together with the local volume flow weighted local effectivity, is used to calculate the total separation efficiency of the fibrous filter. Using normal distributions to describe packing density, they show that the variation in the elemental fiber length (l_f) has the most prominent effect on the total separation efficiency of the non-homogenous filter.

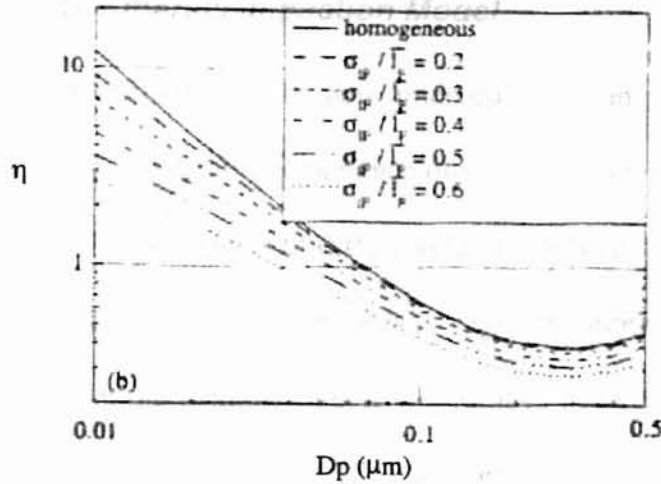


Figure 2-5 Effect of Fiber Length Distribution for Filter with a Packing Density of 0.03, a Fiber Diameter Equal to 1 Micron, and a Face Velocity of 0.01 m/s.

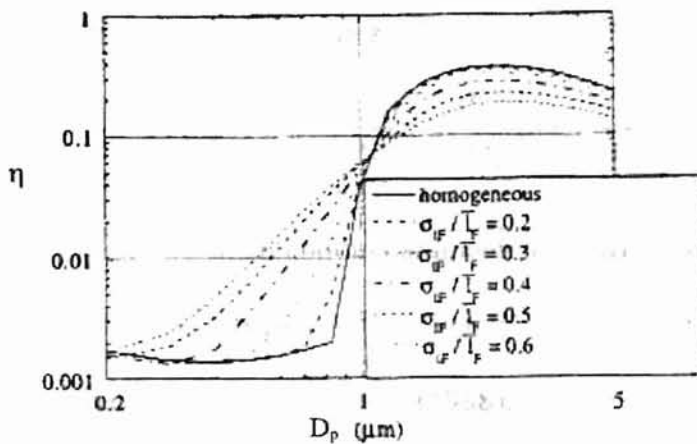


Figure 2-6 Effect of Fiber Length Distribution for Filter with a Packing Density of 0.01, Fiber Diameter Equal to 20 Microns and a Face Velocity of 1 m/s.

Figures 2-5 and 2-6 show how the effective single fiber efficiency is affected by the standard deviation of the fiber length per unit of the mean filter fiber length (σ_{lf}/\bar{l}_f) for different particle diameters (D_p). In the diffusion and interception regime (Fig. 2-5), the variation in efficiency ranges from 20% to 60%; and in the inertial interception regime (Fig. 2-6), a deviation of 50% is observed for the case having the highest fiber length distribution width.

2.4 The Inertial Impaction Model

Collection due to pure interception is an unrealistic assumption. All particles have mass and tend to experience other forces like inertia and diffusion. As explained in Section 3.1, the effects of diffusion have not been considered in this study.

The particle's mass tends to cause the purely inertial flow streamline to be further away from the cylinder than it would have been had there been no inertial force acting on the particle. Duran (1995) uses the Lee and Liu (1982) interception model and the Landahl and Herman (1949) inertial impaction model to derive a combined model for both effects. The combined efficiency due to the effects of interception and inertial impaction is given by Duran as

$$\eta_{IR} = 1 - \left[1 - \left(\frac{1-\alpha}{Ku} \right) \left(\frac{I_p^2}{1+I_p} \right) \right] \left[1 - \left(\frac{St^3}{St^3 + 0.77St^2 + 0.22} \right) \right] \quad (2-5)$$

where I_p is the interception parameter (D_p/D_f). This parameter is a function of the particle size and fiber diameter. Duran showed that this equation agrees with the exact solution of Flagan and Seinfeld (1988).

Suneja and Lee (1974) calculate the collision efficiencies of spherical particles impacting on a cylindrical fiber in an intermediate domain of Re_f (1 to 60). Per their results, they analytically derive an expression for collection efficiency as a function of Stokes number (St), Reynolds number based on fiber diameter (Re_f), and interception parameter (D_p/D_f) as

$$\eta_{IR} = + \frac{2 D_p/D_f}{3St} + \left[\frac{1.53 - 0.23 \ln(Re_f) + 0.0167 \ln(Re_f)^2}{St} \right]^{-1} \quad (2-6)$$

Here D_p is the diameter of the contaminant particle and D_f is the diameter of the filter fiber. In this expression, as St tends to zero, the collection efficiency becomes due only

to pure interception, and, as St tends to infinity, the collection efficiency becomes due only to inertial impaction.

In an attempt to calculate the combined inertial impaction and interception efficiency as a function of particle diameter, fiber diameter and air parameters (air velocity, air viscosity, air density, air temperature and air pressure), Lastow and Podgorski (1998) used a computer program which performed a real-time two-dimensional simulation of the dynamic deposition of particles on filter fibers.

Lastow and Podgorski explained that normally inertial impaction is a function of Stokes number and interception a function of D_p/D_f . However, in most studies of filtration efficiency is calculated as a unique function of Stokes number. Results expressed as a function of Stokes number cannot be compared unless two of the three parameters – air velocity, particle diameter or fiber diameter are the same. Hence, they attempted to express efficiency as a family of curves as will be shown later in this discussion.

Lastow and Podgorski calculated single fiber efficiencies at 20 °C air temperature and 1.0325×10^5 Pa air pressure. In their simulation, the air flow rate was kept constant at 0.1 m/s, the fiber diameter was varied from 10 μm to 80 μm and particle diameter was varied from 1 μm to 12 μm .

A family of lines, one line for each value of D_p , is seen in Fig. 2-7. Each of these lines can be fitted to straight lines with a slope, k , and vertical offset, m . A relation for single fiber efficiency is expressed as a family of curves whose equation is given by

$$\eta = 10^m (D_p/D_f)^k \quad (2-7)$$

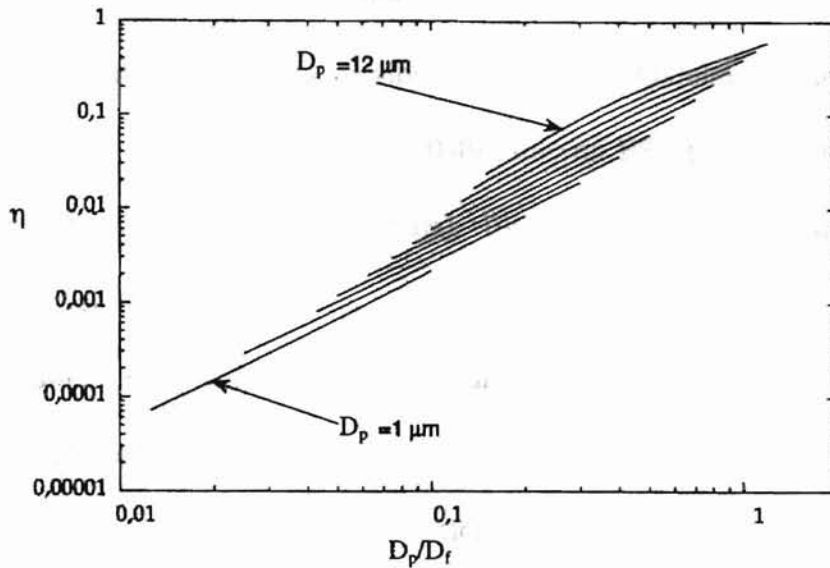


Figure 2-7 Single Fiber Efficiencies Calculated from Computer Simulation for $D_p = 1$ to 12 Microns and $D_f = 10$ to 80 Microns at a Constant Velocity of 0.1 m/s in the Inertial Impaction Regime of Filtration (Lastow and Podgorski, 1998)

where the slope, k , and the vertical offset, m , are functions of particle diameter, particle density, air velocity, air viscosity, air density, mean free path in air, air pressure, air temperature and relative humidity.

As explained earlier, a velocity of 0.1 m/s was used in this simulation. Upon comparing efficiencies calculated using Eq. (2-7) with the results from the calculation of the computer simulation, for 10%, 50% and 100% variation air temperature, air pressure and relative humidity, relative differences in efficiency of only 1% to 3% were found. However, when the air velocity was increased from 0.1 m/s to 0.11 m/s, 0.15 m/s and 0.2 m/s, relative differences in efficiency ranged from 3% to 17%.

This method is thus useful if the air velocity parameter is kept constant and only the particle diameter and fiber diameter are varied. If the air velocity is varied, then the value of k and m will have to be calculated for each of the velocities in order to accurately calculate efficiency which would be seem to be a tedious process. Their method was not experimentally verified.

2.5 Experimental Studies

Saxena (1998), a previous researcher at Oklahoma State University, carried out tests using the 2.04 micron and 0.497 micron PSL particles in the small angle diffuser housing (see Chapter 4 for details). Electrostatic charge could have been present in the flow for the Saxena's setup because he did not ground the housing or regulate the humidity inside the flow. He compared the results of his efficiency measurements with the theoretical model of Duran (1995). Saxena uses an interception parameter (D_p/D_f) of 0.01 to compare his results for particle diameters of 2.04 microns and 0.497 micron.

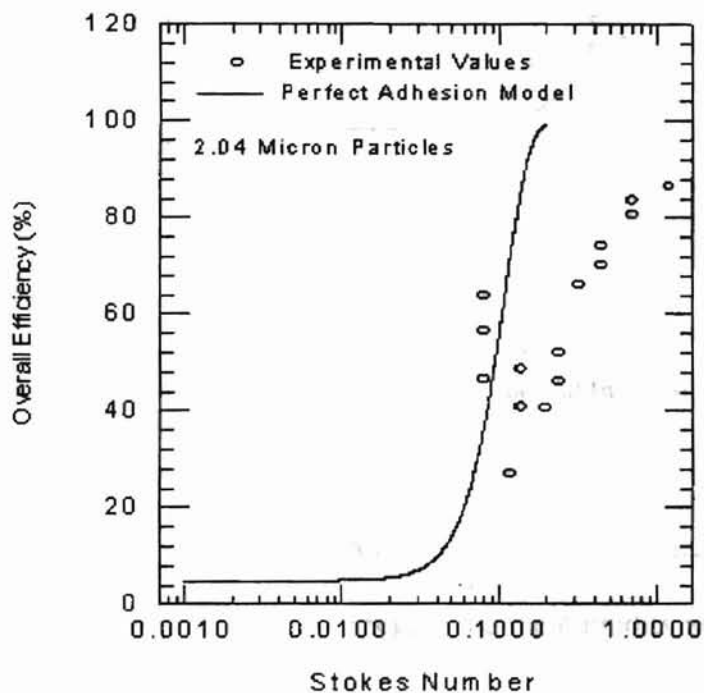


Figure 2-8 Comparison of Results in the Inertial Interception Regime for 2.04 Micron Particles (Saxena, 1998)

It would however be incorrect to use the same interception parameter (D_p/D_f) of 0.01 for both of these particle diameters, because, as particle diameter changes for the same filter fiber diameter, the interception parameter would also change. Saxena accounts for filter clogging as a possible reason for deviation of overall efficiency from

the theoretical value for the 0.497 micron particles (Fig. 2-9). However, for the 2.04 micron particles (Fig. 2-8), Saxena also concludes that higher values of measured efficiency at lower flow rates could be due to the mechanism of diffusion.

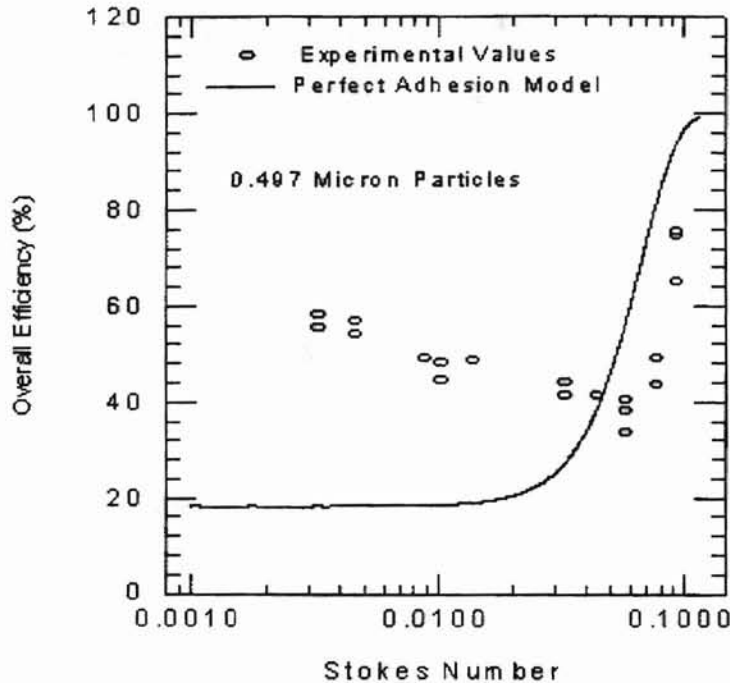


Figure 2-9 Comparison of Results in the Inertial Interception Regime for 0.497 Micron Particles (Saxena, 1998)

Gebreegiabher (1999) conducted experiments in the small angle diffuser housing using 0.966 micron PSL particles. Gebreegiabher's experiments were conducted with and without regulating the humidity and electrostatic charge in the flow. Gebreegiabher shows that Duran's model (1995) underpredicts at lower Stokes number and overpredicts at higher Stokes number (see Fig. 2-9). Gebreegiabher also shows in his work that high humidity increases the efficiency of filtration for the same Stokes number. Gebreegiabher concludes that, since theoretical models are based on the two-dimensional flow assumption and also Duran's model does not account for electrostatic

charge. Thus the model may generally underpredict or overpredict due to these simplifications.

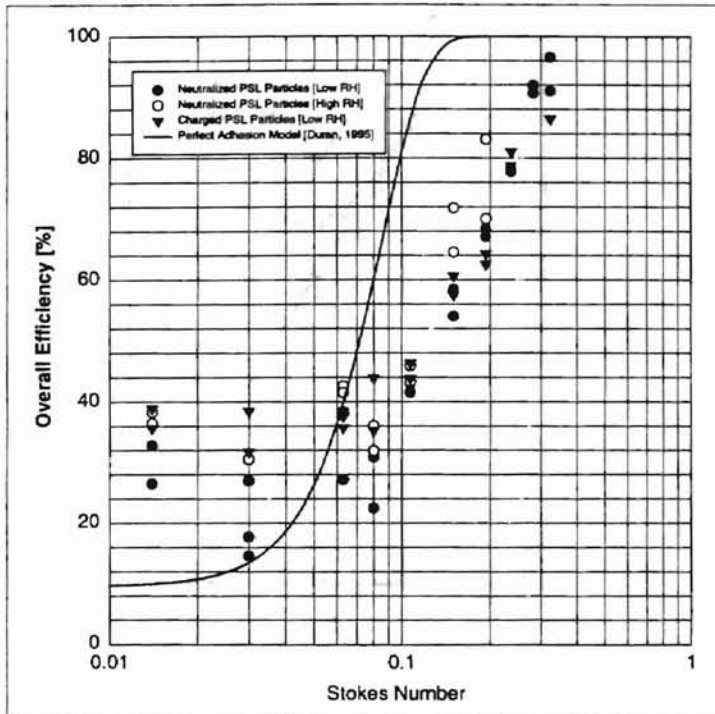


Figure 2-10 Comparison of Experimental Results with Theoretical Model of Duran (1995) (from Gebreegziabher, 1999)

Boulaud and Renoux (1998) compared the experimental work of Gougeon (1994) with the model of Suneja and Lee (1974) from Eq. (2-6), and with Friedlander (1965), but did not find satisfactory results (see Fig. 2-11). These experiments were carried out for low Reynolds numbers ($Re_f < 0.25$). Because of the unsatisfactory comparisons, an empirical correlation for efficiency of filters with characteristics shown in Table 2-1 is presented in Eqs. (2-8) and (2-9).

Using the filter with the characteristics detailed in Table 2-1, Gougeon developed an empirical correlation based on the single fiber efficiency from experiments.

$$\eta = 0.0334 St^{3/2} \quad (2-8)$$

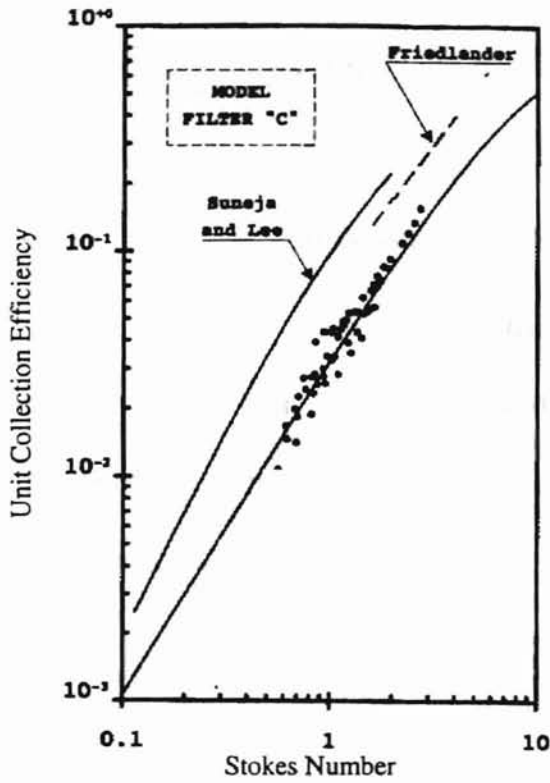


Figure 2-11 Comparison of Gougeon's Results with Correlations of Different Authors (Boulaud and Renoux, 1998)

Table 2-1 Characteristics of Fibrous Filter Used by Gougeon (1994)

	Property for filter model "C"
Diameter of fiber (mm)	2.7
Thickness of the filter (mm)	0.3
Weight by unit surface area of filter (g/m^2)	78
Density of fiber (g/cm^3)	2.657

Equation (2-8) is valid for $0.5 \leq St \leq 4.1$ and $0.0263 \leq Re_f \leq 0.25$. This correlation is extrapolated to higher Stokes numbers as

$$\eta = \frac{0.0334 St^{3/2}}{1 + 0.0334 St^{3/2}} \quad (2-9)$$

2.6 Fractional Efficiencies and Particle Sizing

In order to study filter behaviour, it is necessary to determine fractional efficiency behaviour in addition to the total efficiency behaviour. The fractional efficiency yields more information and is not dependent upon particle size distribution.

Maus and Umhauer (1996) define fractional efficiency $\eta(D_p)$ as

$$\eta(D_p) = 1 - \frac{C(D_p)}{C_0(D_p)} \quad (2-10)$$

where D_p is the particle diameter, $C_0(D_p)$ and $C(D_p)$ are the particle concentrations upstream and downstream of the filter, respectively. If the upstream and downstream particle concentrations are to be determined by counting the number of particles, it is thus imperative that the diameter of each of the counted particles must be determined in order to study fractional efficiency behaviour.

One technique established by Liang (1997) was the Particle Trajectory Method suitable for an LDV system based experimental setup. The signal amplitude of every particle passing through the probe volume (the region of the two intersecting laser beams) is a function of the particle size and the location of the particle in the probe volume (Liang, 1997). If the location of the particle in the probe volume is determined, the signal amplitude becomes a function of particle size alone. In Liang's method, the signal amplitude of every particle detected by the LDV system is measured, along with

the duration of the signal (τ). This signal duration along with the velocity (v) measured by the LDV system is used to determine a transit length ($v\tau$). Knowing the geometry of the probe volume and the transit length, it is possible to determine the location of the particle in the probe volume and hence its diameter. The two main assumptions for this method are:

1. The particle velocity is taken to be predominantly along the measuring axis of the LDV system.
2. The intensity distribution function at any location in the probe volume is known is inversely proportional to the distance of the location from the measuring axis.

Using the Particle Trajectory Method technique, Liang was able to correlate particle size with its respective signal amplitude. These results are shown in Fig. 2-12. All three data series were taken on different dates and seem to follow a similar trend with reasonable accuracy. However, in order to measure the signal amplitude, each signal detected by the oscilloscope had to be analyzed manually, which was a very tedious procedure even to analyze a few (100) samples. Maus and Umhauer (1996) used optical particle counters to measure the flux and diameters of airborne particles upstream and downstream of the filter. They used a high pressure Xenon lamp as a white light source to measure scattered light for a mean angle of 90° . Maus and Umhauer compared three different filters EU3, EU6 and EU7, which are classified as per the EUROVENT 4/5. This standard classifies filters in categories EU1 (coarse dust filters) to EU9 (fine dust filters). Thus EU7 is a high efficiency filter and EU3 is a low efficiency filter. In Fig. 2-13, the three filters are compared for their fractional efficiency performance for limestone dust with size ranging from 0.6 micron to 10

micron for nominal face velocities (V_n) shown in the figure. They conclude that EU3 and EU6 filters perform poorly in the respirable size range (5 microns to 10 microns) and are hence poor air conditioning filters. Only the EU7 filter works well within the respirable size range, eliminating most particles within this size range.

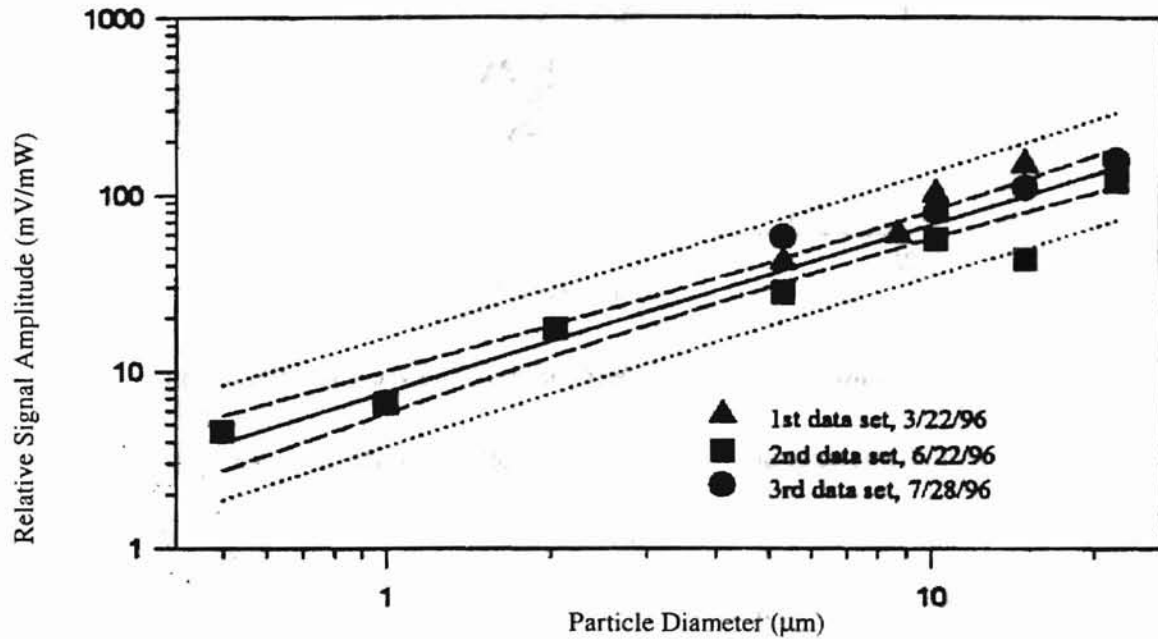


Figure 2-12 Relation of Particle Size to Signal Amplitude (Liang, 1997)

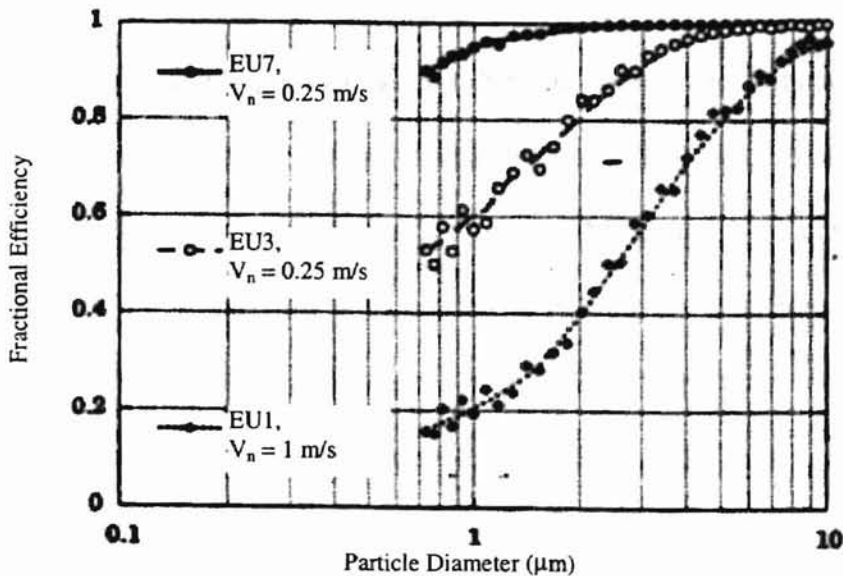


Figure 2-13 Fractional Efficiency of Different Filter Media (Maus and Umhauer, 1996)

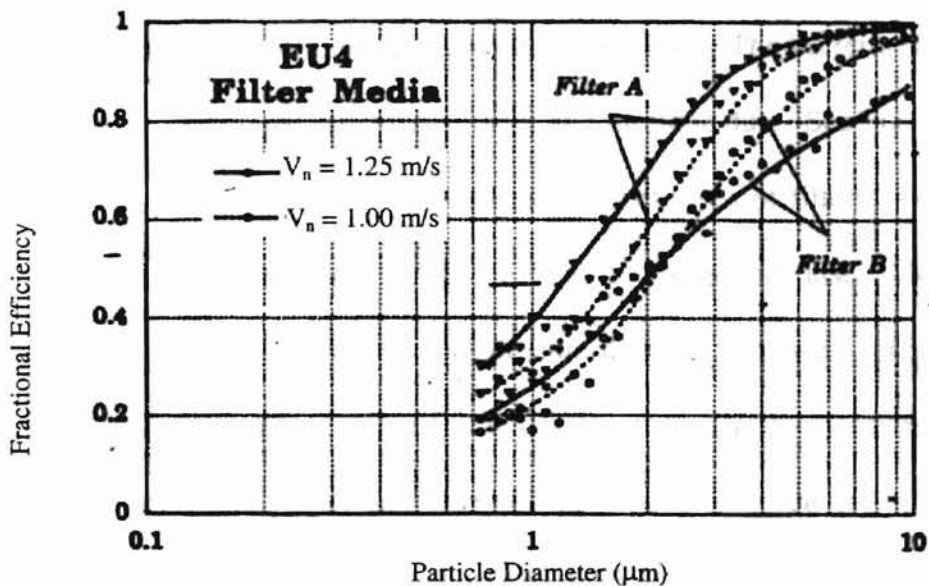


Figure 2-14 Fractional Efficiency of Two Filter Media for Limestone Dust (Maus and Umhauer, 1996)

In Fig. 2-14, two different filter media of the same type of filter (a low efficiency filter EU4 as per the EUROVENT 4/5 standard) are compared at two different velocities (1 m/s and 1.25 m/s) to see the effect of fractional efficiency. Filter A's media is made of polypropylene with a mean fiber diameter of 49 microns and a lower porosity (98.0%), and Filter B's media is made of polyester with a mean fiber diameter of 24 microns and a higher porosity (98.8%). Maus and Umhauer observed that filtration efficiency increased with particle diameter. Also, Filter A shows greater efficiency due to the difference in filter characteristics. Maus and Umhauer concluded that, for Filter B, the larger sized particles tended to exhibit lower efficiency than that for the lower flow rate, due to the increased probability of particle bounce. This mechanism of filtration was not observed for Filter B because it has a larger fiber diameter and hence a smaller probability of bounce in the data range.

In another paper, Schmidt et al. (1998) compared the fractional efficiencies of bacteria for two different filters with limestone dust. The bacteria (*E. coli*, *M. luteus* and *B. cereus*) are comparable by size range to limestone dust. See Fig. 2-15.

Schmidt et al. (1998) used two different types of filters. For the low efficiency filters, microbial aerosols behave similar to limestone dust. However, in the high efficiency filter, there was a considerable difference between efficiencies experienced with limestone and bacterial aerosols. The high efficiency electret fiber medium was charged and since water (an essential constituent of bacteria) has a higher dielectric constant of 80 as compared to limestone with a dielectric constant of 8, bacteria showed a better collection efficiency for this high efficiency electret filter medium.

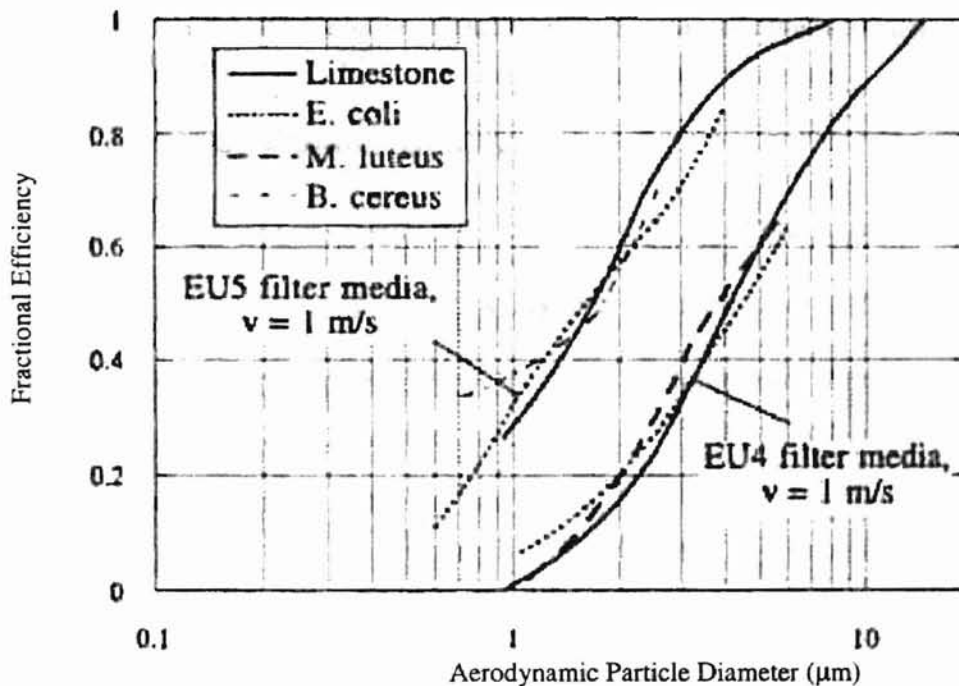


Figure 2-15 Fractional Efficiencies for Microbial Aerosols for Medium Efficiency Filters (Schmidt et al., 1998)

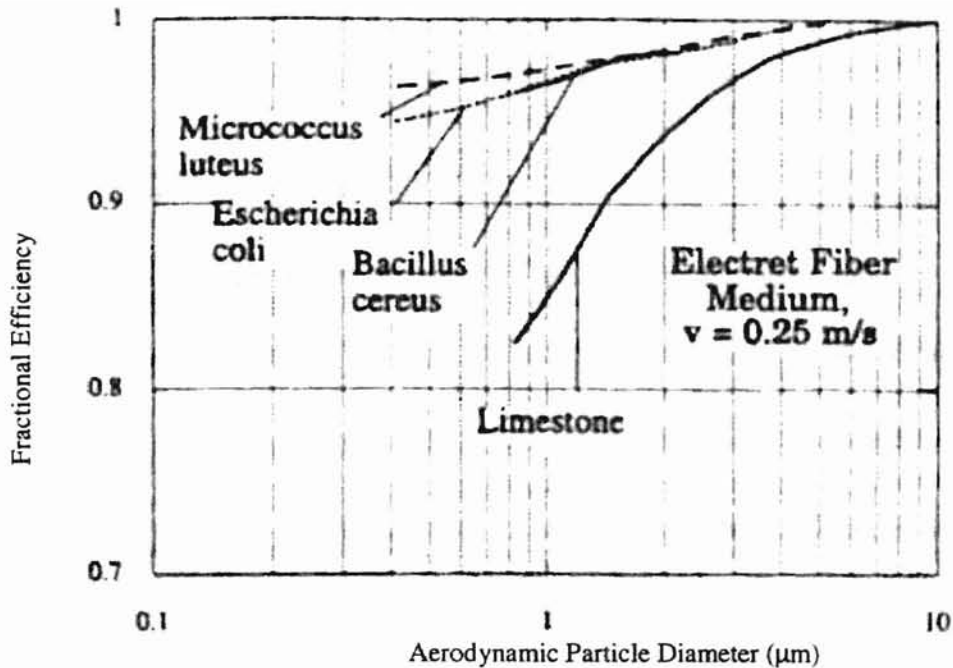


Figure 2-16 Fractional Efficiencies of High Efficiency Charged Filter for Bacterial Aerosols (Schmidt et al., 1998)

2.7 Effect of LDV Signal Quality

Adrian (1978) presented a procedure to estimate the signal-to-noise ratio of an LDV system for the purpose of analyzing its suitability for a given application. According to Adrian, signals from the LDV system have three distinct sources, as follows:

$$e(t) = e_p(t) + e_D(t) + e_N(t) \quad (2-11)$$

where $e_p(t)$ is the pedestal component of the signal voltage, $e_D(t)$ is the Doppler component of the signal voltage, and $e_N(t)$ which is the shot noise generated in photodetector by the light scattered from the signal produced particle noise. Adrian defines a peak signal-to-noise ratio as a ratio of the peak Doppler signal power to the peak shot noise power. Adrian considers the peak values of the signal components so that the time dependence of the photodetection signals can be eliminated. The peak

value of the pedestal signal component is given to be

$$e_p(\text{peak}) = (\text{SN}) \frac{\pi^2}{64} P_0 \left(\frac{D_p}{\lambda_w} \frac{D_l}{r_a} \frac{D_e^{-2}}{f c} \right)^2 \overline{G} \quad (2-12)$$

Where SN is the sensitivity (V/W) of the photodetector, D_l is the diameter of the light collecting aperture, D_e is the diameter of the unfocused laser beam, r_a is the distance from measuring volume to the light collecting aperture, $f c$ is the focal length of the focussing lens, λ_w is the wavelength of the laser light, \overline{G} is a complex light scattering gain function, and D_p is the diameter of the scattering particle. The peak amplitude of the Doppler signal is related to the peak pedestal component as

$$e_D(\text{peak voltage}) = \overline{V} e_p(\text{peak voltage}) \quad (2-13)$$

where \overline{V} is the Doppler signal visibility at the peak of the Doppler burst, which is the ratio of the Doppler signal amplitude to the pedestal signal amplitude. The peak signal power relation is given as:

$$\langle e^2_D \rangle (\text{peak power}) = \frac{1}{2} \overline{V}^2 e_p^2(\text{peak voltage}) \quad (2-14)$$

where \overline{V} is the Doppler signal visibility. The peak shot noise power is given as:

$$\langle e^2_N \rangle (\text{peak power}) = 2 \frac{h_p v_0}{\eta_q} \Delta f S e_p(\text{peak voltage}) \quad (2-15)$$

Herein, Δf is the bandwidth of the filtered noise, h_p is Planck's constant, v_0 is the frequency of the laser light, and η_q is the quantum efficiency of the photodetector. Thus, the peak signal to shot noise ratio is deduced as:

$$\text{SNR}_{\text{peak}} = 4 \times 10^{11} \frac{\eta_q P_0}{h_p v_0} \frac{1}{\Delta f} \frac{D_p D_e^{-2}}{r_a f c} D_p^2 \overline{G} \overline{V} \quad (2-16)$$

This relation can be used to determine the diameter of unknown particles if the LDV

system parameters are controlled. The author uses this method as a means of calculating the size of particles with the LDV system.

CHAPTER 3

THE LASER DOPPLER VELOCIMETRY SYSTEM: DATA MEASUREMENT CALIBRATION AND CALCULATION TECHNIQUE

3.1 Overview

Measurement techniques and the basis for particle flow and concentration using the laser Doppler system are discussed in this chapter. Being a very important and influential parameter, high voltage is discussed regarding its effect on data collection and measurement. The probe volume size is also discussed. Good and bad regions of signal quality for data measurement are classified and discussed. Calibration and analytical expressions for calculating the fractional number density are given.

3.2 LDV Measurement Principles

A simple review of the basic principles and setup of the optical system has been described in this sub-section. A backscattering LDV system based on the light scattering interferometry technique was used for making all measurements. A small ellipsoidal probe volume is generated by the crossing of two laser beams in the path of the flow (see Fig. 3-1). A 5-watt Argon-Ion laser is used to generate all of the laser beams. This crossing of the beams also produces alternate bright and dark fringes, defining the probe volume. The spacing between the fringes (ΔF), is a function of the optical wavelength and the angle between the interfering beams and can be calculated as (Aerometrics, 1999)

$$\Delta F = \frac{\lambda_w}{2 \sin \psi} \quad (3-1)$$

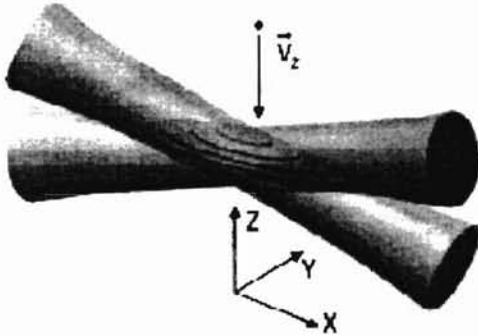


Figure 3-1 Optical Probe Volume (Aerometrics, 1999)

where ΔF , λ_w and ψ are the fringe spacing, wavelength of the laser beams and the half angle between the two interfering beams respectively. As a particle enters the probe volume, it alternatively passes through the bright and dark fringes, scattering light as per the intensity in the fringes. Thus a Doppler frequency is produced, which is directly proportional to the velocity of the particle. The relation is given as (Aerometrics, 1999)

$$v_D = \frac{2(v) \sin \psi}{\lambda_w} \quad (3-2)$$

where v_D is the measured Doppler frequency, and v is the particle velocity.

A Bragg cell is used to shift the frequency of one of the interfering light beams by 40 MHz. This shift causes the fringes to move in the probe volume along the direction of the velocity component to be measured. Fringe movement provides the directional sense of the particle whose velocity component is being measured. Otherwise, without moving fringes, the velocity magnitude can be determined, but not its direction.

The two-component LDV system was used in our case so that velocities could be measured along the flow direction and in one direction orthogonal to the flow direction

along the longer filter axis. It has been shown that the transverse component of velocity along the longer axis of the filter is just a fraction of the axial velocity as long as the flow rates do not become as low as $8.5 \text{ m}^3/\text{hr}$ (5 scfm) (Anand, 1997). As an example, for a flow rate of $17 \text{ m}^3/\text{hr}$, the upstream velocity at the center of the filter was recorded as 0.22 m/s in the axial direction and -0.01 m/s in the transverse direction (which is less than 5% of the axial component of velocity) for the test designated as 10-2ag (see Section 5.3 for an explanation of test designations). Also, the velocity along the shorter filter axis would be even smaller as compared to that along the axial direction. This velocity component along the shorter filter axis is not measured, and it is assumed in this thesis that this component does not have much influence on the total velocity, above a flow rate of $8.5 \text{ m}^3/\text{hr}$ (5 scfm). All of the experiments in this study were carried out for air flow rates above $17 \text{ m}^3/\text{hr}$ (10 scfm). Also since these experiments were carried out in the small angle housing, the axial component of the velocity was considered to be dominant.

A transceiver was used to transmit the beams and receive signals from the particles. The signals were transferred to the photomultiplier tubes (PMTs), which analyzed and interpreted the signals. This transceiver, which was mounted on a traverse, could be moved to the desired location of measurement with a maximum error of 1 mm as measured by the author. A more detailed description of the setup along with a schematic diagram is shown in Section 4.2.2.

3.3 Particle Number Density Calculation

The laser Doppler system is a reliable and proven tool for its non-invasive velocity measurement in fluid flow (Saffman, 1987). Using the particle velocity and the

particle arrival rate, the local number concentration of the contaminant in the flow can also be measured. After each run, the LDV system used for this research displays the following information.

- the mean velocity in the two directions of flow measured,
- the total number of signals which the system attempted to process,
- the total number of signals from which the velocity was calculated,
- the percentage of valid signals, and
- the time taken to detect all of these signals.

In order to determine the concentration of particles in the measuring zone, the swept volume technique developed by Liang (1997) was used. As the particles travel with a mean velocity of v for a duration of time t , they sweep a distance of $L_s = vt$ as shown in Fig. 3-2 with an area equal to the projected cross-sectional area of the probe volume.

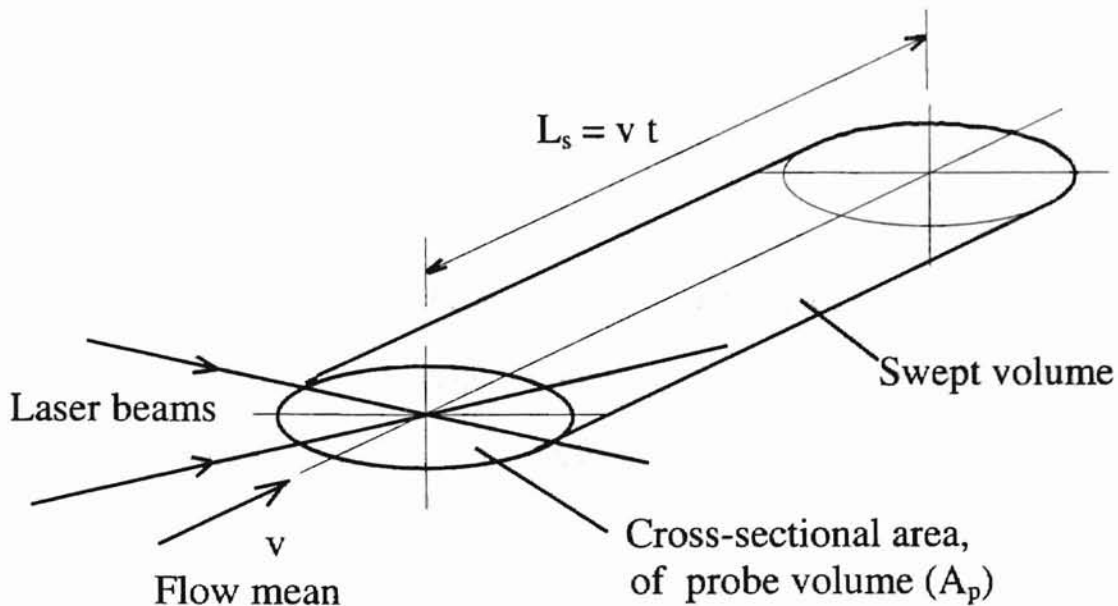


Figure 3-2 Swept Volume Technique (Liang, 1997)

Number density is given by this swept volume technique as

$$N = (n_{\text{attempts}}) / (vtA_p) \quad (3-3)$$

where N , n_{attempts} , A_p , v and t are the number density, the total number of signals detected, the projected cross-sectional area of the probe volume, the velocity of the particles, and the time taken to detect the particles. Using the local upstream and downstream values of number density, the local efficiency can be calculated using the following relation

$$\eta_i = 1 - \frac{N_{\text{idown}}}{N_{\text{iup}}} \quad (3-4)$$

Here η_i is the local efficiency measured using the swept volume technique. It is indeed important to study the parameters affecting the measurement of number density, due to its vital role in the measurement of efficiency as defined in Eq. (3-4).

The errors in velocity measurement are very small, around 2% (Anand, 1997). The LDV system however has its limitations in the accurate measurement of the particle arrival rate. The particle arrival rate can be defined as the number of signals measured in unit time. The most important factor affecting the arrival rate is the concentration of seedant in the flow. The correct amount of concentration used in the flow is discussed in the Chapter 5 (Experimental Setup). However, for the LDV system, not only should the flow be adequately seeded, but also the appropriate measuring parameters for the system ensure the ideal measurement of the particle arrival rate. This is discussed in subsequent sections of this chapter. The intensity of light in the probe volume is Gaussian in nature with the peak intensity at the center and decreasing to zero at infinity. The following equation defines the edges of the probe volume (Liang, 1997):

$$I / I_0 = 1 / e^2 \quad (3-5)$$

where I and I_0 are the intensity of the probe volume at a particular location and the intensity at the center of the probe volume. A change in the light intensity in the probe volume causes the $1/e^2$ envelope to change in size and thereby change the size of the effective probe volume, hence affecting probe volume cross-sectional area (A_p). This change in the probe volume size affects the calculation of number density as seen in Eq. (3-3). Factors affecting laser intensity in the probe volume and procedures to minimize its variation are discussed in the chapter on the experimental setup (Chapter 4).

3.4 High Voltage and Signal Quality

In an experimental run, the LDV system gives us quantitative information on the signal quality. The percentage of valid signals in a run is calculated as

$$SV = [n_{\text{valid}} / n_{\text{attempts}}] (100) \quad (3-6)$$

where n_{attempts} is the total number of signals detected, and n_{valid} is the total number of signals from which the LDV system is able to accurately measure the Doppler frequency. In order to obtain the correct value of local efficiency in Eq. (3-4), the total number of attempted signals n_{attempts} is employed. This n_{attempts} depends upon the signal validity as seen in Eq. (3-6). This dependence is further discussed later in this section. It is therefore important to understand, investigate and correctly interpret the signal validity as well as the factors affecting it.

With reference to the LDV system used by the author, high voltage is a parameter used to control the amplification of the detected signals. The signal quality

was studied by varying this parameter for this research. For the current system, high voltage has a range of 200 to 800 V.

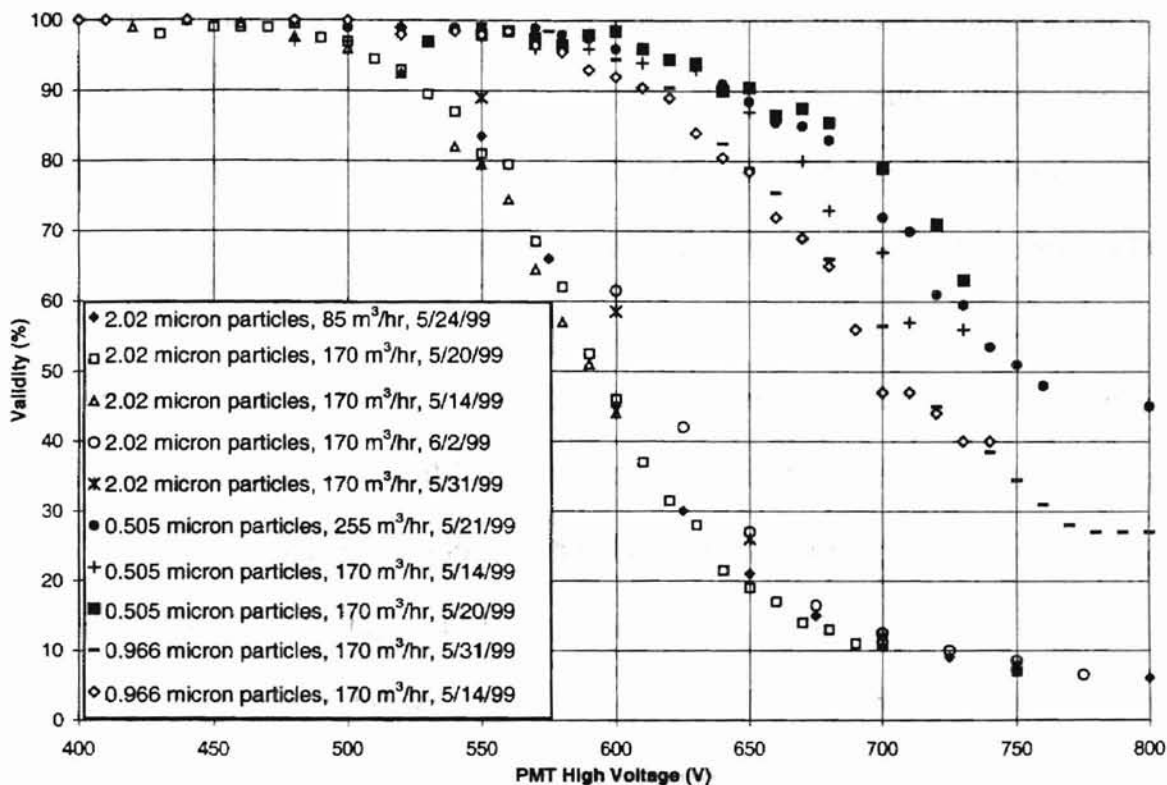


Figure 3-3 Effect of PMT High Voltage on the Percent of Valid Samples using Constant LDV Parameters (see Table 3-1) at Flow Rates of 85 m³/hr, 170 m³/hr and 255 m³/hr in the Small Angle Diffuser Housing

In order to study the effect of PMT high voltage on the on the percentage of valid signals for the three different particle diameters (2.02 microns, 0.966 micron and 0.505 micron), various tests were carried out by the author. These are shown in Fig. 3-3. All tests were carried out in order to determine the effect of PMT high voltage, with every other parameter in the LDV system held constant and are defined in Table 3-1. By a process of trial and error, the remaining LDV parameters were selected so that each of the particle sizes exhibited its full range of behaviour (explained further on in this section) between a high voltage of 500 V and 800 V for all of the tests done for the above experiments.

For all three particle diameters, the signal validity remains at 100% until a specific high voltage value is reached. Above this high voltage, the validity decreases in a nearly linear manner with increasing high voltage. This decrease continues until the saturation validity is reached. Once the validity reaches this value, validity remains constant as high voltage increases. It must be noted that 800 V is the highest possible amplification (high voltage) which can be provided to the PMTs using the current LDV system.

For example, from Fig. 3-3, for the 2.02 micron particles, the hundred percent signal validity remains until 500 V. In the region from 500 V to 700 V, high voltage decreases in a nearly linear manner. The saturation validity of between 5%-10% is reached when the high voltage is increased to a value above 700 V.

Similar trends exhibited by all three particle sizes were classified as a characteristic behaviour of the signals and is divided into three regions, each of which will be discussed (see Fig. 3-4).

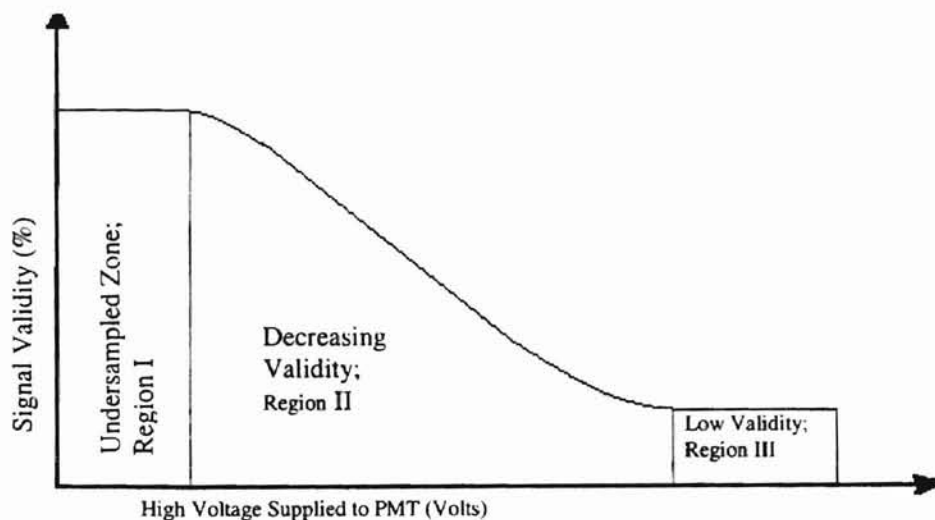


Figure 3-4 Generalized Trend for Validity vs. High Voltage for a Constant Particle Size

Table 3-1 LDV Parameters for Study of High Voltage and Particle Sizing

Frequency Shift	40 MHz
DC Offset	17.4 mV
Mixer Frequency	40 MHz
Burst Filter	40 MHz Band pass
Threshold	70 mV
Envelope Filter	3.3 μ s
Peak Detection	On
Number of Samples	64
Sampling Rate	10 MHz
Minimum Signal-to-Noise Ratio	0.3

Region I

The initial region is characterized by low amplification of signals. Background shot noise is kept at a minimum and hence the signal to noise ratio is at a maximum. Also some particles passing through the probe volume may not be detected. This is because the amplitude of the signals after amplification is not sufficient to cross the threshold value of signal acceptance. Thus, this region may also be called the undersampled region. The 2.02 micron diameter particles have the shortest undersampled region. This zone ends at 500 V for the 2.02 micron diameter particles. The 0.966 micron diameter particles show this region to extend to 550 V. The 0.505 micron diameter particles show this zone to extend unto almost 600 V. This trend is explained as follows. The lowest particle diameter (0.505 micron) scatters signals which have a small signal amplitude as compared to the particle diameters of 2.02 micron and

0.966 micron. Thus it requires a higher amplification to cross the threshold value of signal acceptance. Since all of these experiments were conducted for the constant set of parameters described in Table 3-1, the threshold voltage was accordingly constant at a value of 70 V.

The 2.02 micron particles had the least required amplification, and the 0.966 micron particles required amplification intermediate to both the 2.02 micron and 0.505 micron particles. This size dependence on signal amplitude is also consistent with Mie scattering theory (Liang, 1997). According to this theory, the smallest particle size will have the lowest signal amplitude and vice versa.

Readings should not be taken in the undersampled region. As mentioned earlier, in this region, because of low signal amplification, the scattered signal amplitude may not be high enough to cross the threshold acceptance value, and hence no signal would be detected. This is because of the random nature of the detection and acceptance of signal amplitudes. Also, in this region, longer sampling time would be required in order to statistically validate the data. This would be due to the low sampling rate. These factors go to show that the samples collected would not be true indicators of the particle concentration in the flow.

Region II

Just beyond the undersampled region, the system is able to record all particles with a signal-to-noise ratio (SNR) of 0.3 or greater. The value of 0.3 is a user-selected option recommended for proper measurement of signal velocity (Aerometrics, 1992). Once this SNR value of 0.3 is selected, the system is not capable of measuring the velocities of particles with noise ratio below 0.3. All signals lower than this value are

detected but classified as noise according to the system. As the high voltage is increased, the system records an increasing number of samples with an SNR of less than 0.3. This is because, as the high voltage increases, not only does the scattered signal amplitude increase but so also does the background noise. The increase in this background shot noise contributes to the decrease in SNR. Thus, in this region, the sample validity decreases with increasing high voltage. This trend is approximately linear for all the three particle sizes tested in this research.

Region III

All three curves tend to reduce the validity to a constant value. In this region, the PMTs receive a very high number of signals per unit time. However this constant value of validity and the region of occurrence are seen to be different for each particle diameter. The 2.02 micron particle curve starts this zone at approximately 700 V. The saturation validity for this size is seen to be about 10%. The 0.966 micron particle curve reaches this value at 725 V, and has this for signal validity of around 27%. The 0.505 micron particle curve has the highest constant value for signal validity of around 43%. This value is reached at a relatively higher value of high voltage equal to 750 V. It is interesting to note that the signal amplification-saturation value and zone depends on particle size.

As is observed for Region II, since the number of valid signals becomes constant, the signal validity is inversely proportional to the number of attempted signals. Ideally Region III would be the best region to carry out the measurements. However the low SNR can result in erroneous values for velocity. This phenomenon causes the LDV

system to record absurdly high or low values of velocities for some samples. Also, low signal validity would require huge amounts of data to be stored.

Thus this author has chosen Region II to be the best conditions under which all measurements have been recorded for this LDV system. In this region, velocity can be measured accurately, with a high sampling number density, which is directly proportional to the aerosol concentration in the flow.

If, we assume the above to be true, the following holds true for aerosol concentration, in terms of number density

$$\eta = 1 - \frac{C}{C_0} = 1 - \frac{N_{\text{downstream}}}{N_{\text{upstream}}} \quad (3-7)$$

where

$$C = \text{constant} \times N_{\text{downstream}}$$

$$C_0 = \text{constant} \times N_{\text{upstream}}$$

The efficiency measurement process will not be affected if it is shown that the number density based on the attempted counts is directly proportional to the actual concentration of the aerosol in the airflow. In order to verify this assumption, filtration efficiency was determined at various values of high voltage using the same setup and air flow rate. All the tests on shown in this chapter are performed at the center location of the filter. Increasing the value of high voltage will correspondingly increase the value of sample number density. Within the regime of Region II, if the sample number density indicates the proportional aerosol concentration, then the efficiency will remain the same for any value of the high voltage used within this region. Tests were carried out to see the dependence of high voltage on the filtration efficiency.

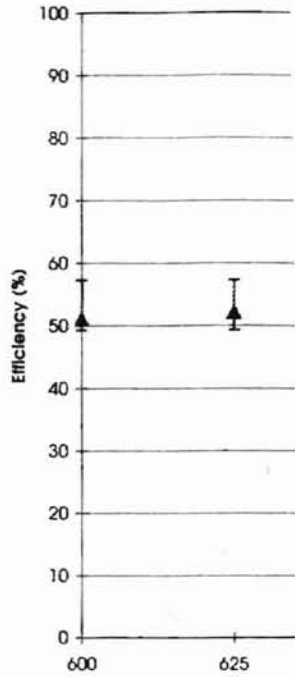


Figure 3-5 Effect of High Standard Dev

As shown in Fig
 within a narrow band of
 more sets of data were
 particles. All of these
 between 5%-10%. The
 calculated to be around
 consistency measuremer

The entire tests p
 3-2. The last column of
 indicates volume of the
 test solution.

It is concluded from these experiments that the calculation of efficiency is suitable using signals measured in the Region II regime. All of the experiments carried out by the author for the monodisperse solutions were carried out in Region II where the signal validity was between 70% to 90%.

Among the other LDV parameters, the threshold is the only other major parameter which also affects the signal arrival rate (number of signals detected in unit time) and signal quality. This parameter determines the minimum signal amplitude for burst detection (Aerometrics, 1992). Since the signal amplitude is dependent on the high voltage, increasing the high voltage will produce an effect similar to decreasing the threshold. This can also be seen from Fig. 3-6. The plot of signal validity with decreasing threshold shows a similar shape for the curves, which was explained using Fig. 3-4 in an earlier part of this section. The tests were performed for parameters described in Table 3-1. The only difference was that threshold was varied as per Fig. 3-6 and PMT high voltage was kept constant at 500 V.

Table 3-2 Effect of High Voltage on the Measurement of Filtration Efficiency

File Name	Test Date	Alignment Temperature	Flow	Size	Concentration
		Degrees C	m³/hr	microns	m³/m³
Test23.xls	6/2/99	24.2	170	0.505	1/100
Test24.xls	6/2/99	24.2	170	0.505	1/100
Test25.xls	6/2/99	24.2	170	2.02	1/100
Test26.xls	6/2/99	24.2	170	2.02	1/100
Test27.xls	6/2/99	24.2	170	0.966	1/100
Test28.xls	6/2/99	24.2	170	0.966	1/100
Test33.xls	6/2/99	24.5	170	0.505	1/100
Test34.xls	6/2/99	24.5	170	0.966	1/100
Test38.xls	6/5/99	24.5	170	0.505	1/100

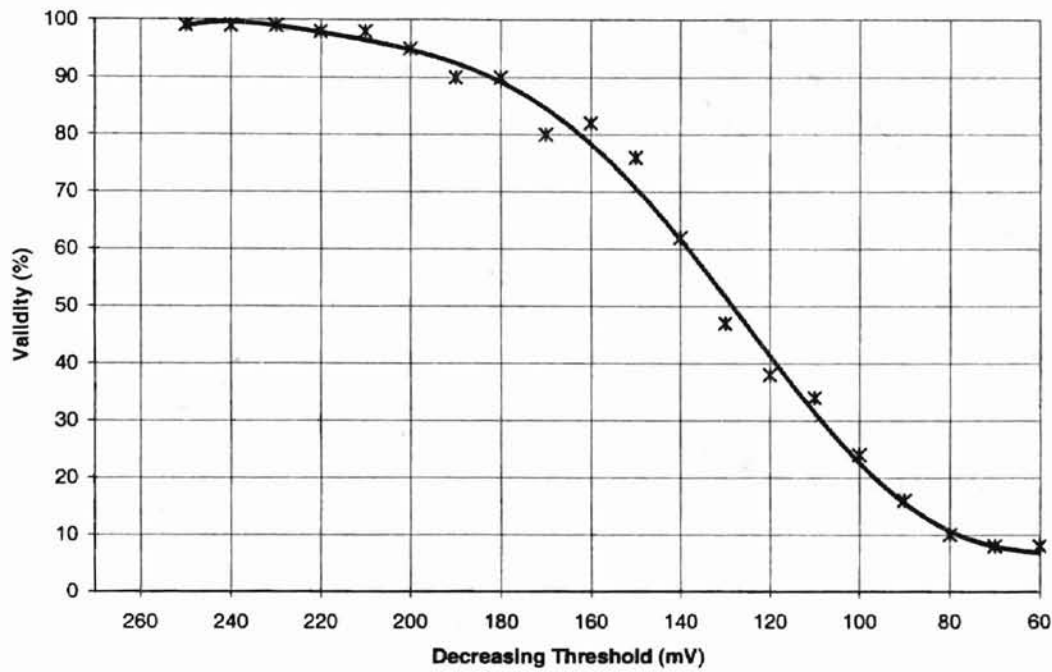


Figure 3-6 Effect of Threshold on Signal Validity for 0.505 Micron Particle Diameter and High Voltage of 500 V at a Flow Rate of 170 m³/hr

3.5 Fractional Efficiency Calculation for Bidisperse Solutions

From the discussion in Section 3.2, the signal validity gives us information on the signal-to-noise ratio in a statistical sense. This signal-to-noise ratio is a characteristic function of the particle diameter when the particle is detected by the LDV system (Agarwal and Keady, 1980). In order to be able to distinguish between two known particle sizes, the average values of signal validity measured at the centerline of the filter are plotted against high voltage, yielding the calibration curves in Fig. 3-7.

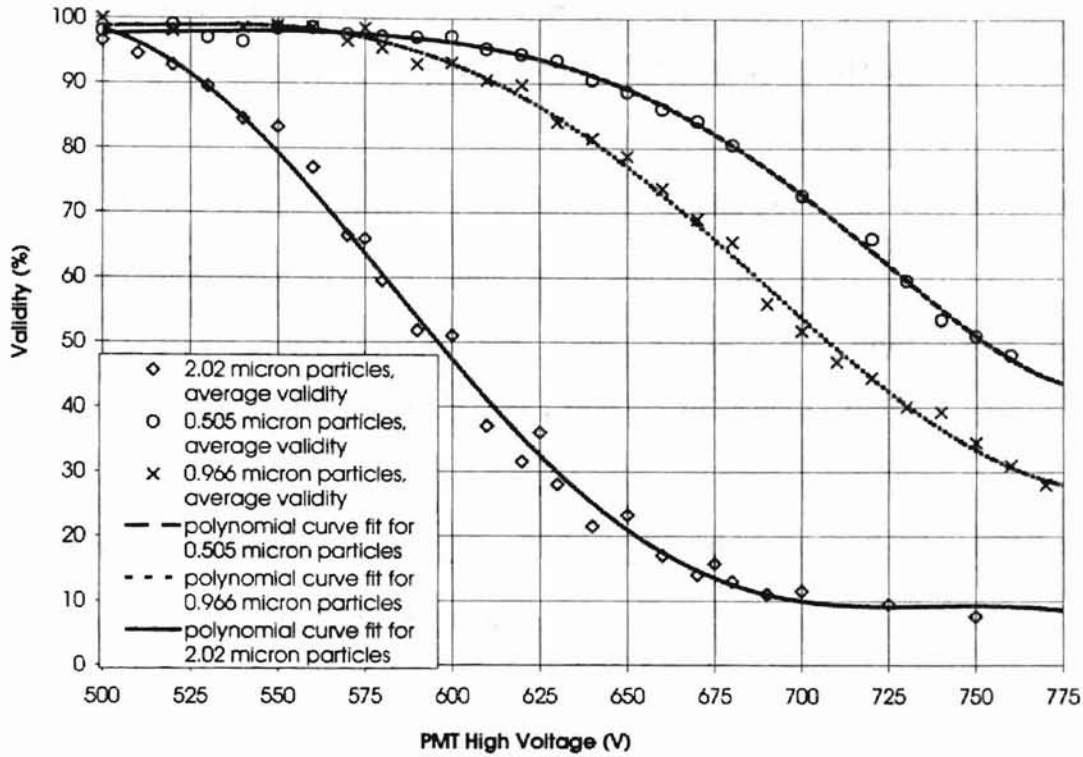


Figure 3-7 Best Fit Polynomial Equations for Calibration Based on Average Value of Validity for 2.02, 0.966 and 0.505 Micron Particles

It was found that 6th degree polynomial equations provided a very good fit to the data points for all the three particle sizes (see Fig. 3-7). The equations providing the fit are listed as follows:

- a) for the 0.966 micron diameter PSL particles, 41 data points were used to obtain a calibration curve with a correlation coefficient of 0.99

$$EV (\%) = -5.6874 \times 10^{-13} \times (HV)^6 + 2.1215 \times 10^{-09} \times (HV)^5 - 3.2339 \times 10^{-06} \times (HV)^4 + 2.5786 \times 10^{-03} \times (HV)^3 - 1.1353 \times 10^{+00} \times (HV)^2 + 2.6197 \times 10^{+02} \times (HV) - 2.4680 \times 10^{+04} \tag{3-8}$$

- b) for the 0.505 micron diameter PSL particle, 45 data points are used to obtain a calibration curve with a correlation coefficient of 0.99

$$EV (\%) = 3.1767 \times 10^{-13} \times (HV)^6 - 1.009 \times 10^{-09} \times (HV)^5 + 1.3097 \times 10^{-06} \times (HV)^4 - 8.8946593659 \times 10^{-04} \times (HV)^3 + 3.329 \times 10^{-01} \times (HV)^2 - 6.4917 \times 10^{+01} \times (HV) + 5.2180 \times 10^{+03}$$

(3-9)

c) for the 2.02 micron diameter PSL particle, 63 data points are used to obtain a calibration curve with a correlation coefficient of 0.99

$$EV (\%) = 1.1957 \times 10^{-12} \times (HV)^6 - 4.6600 \times 10^{-09} \times (HV)^5 + 7.4516 \times 10^{-06} \times (HV)^4 - 6.2505 \times 10^{-03} \times (HV)^3 + 2.8976 \times 10^{+00} \times (HV)^2 - 7.0366 \times 10^{+02} \times (HV) + 7.0054 \times 10^{+04}$$

(3-10)

where HV represents the PMT high voltage which is used to obtain the data for the test run. The three calibration equations represented in Eqs. (3-8) to (3-10) are valid from a PMT high voltage of 500 V to 775 V. Using these equations, the statistical determination of the size based number fraction in a bidisperse mixture would be determined from the following equations

$$SV(\text{mixture}, HV) = EV [D(1), HV] \times f [D(1)] + EV [D(2), HV] \times f [D(2)] \quad (3-11)$$

where

- D(1) and D(2) are the two known particle sizes in the mixture.
- SV(mixture, HV) is the signal validity recorded from the run for the bidisperse mixture.
- EV [D(1), HV] and EV [D(2), HV] are the expected validities obtained from Eqs. (3-8) to (3-10).
- $f [D(1)]$ and $f [D(2)]$ are the fractional mixture ratio for the two particle sizes.

Equation (3-11) basically assumes that the total validity of a mixture containing two different particle sizes in a test run is the weighted average of the validity of each individual particle size in the mixture. Also by definition,

$$f[D(1)] + f[D(2)] = 1 \quad (3-12)$$

The fractional number concentration can be calculated as

$$N[D(1),HV] = f[D(1)] N(\text{mixture}, HV)$$

$$N[D(2),HV] = f[D(2)] N(\text{mixture}, HV) \quad (3-13)$$

Using these concentrations, the fractional efficiencies are calculated as follows

$$\eta[D(1)] = 1 - \{N_{\text{downstream}}[D(1),HV]\}/\{N_{\text{upstream}}[D(1),HV]\}$$

$$\eta[D(2)] = 1 - \{N_{\text{downstream}}[D(2),HV]\}/\{N_{\text{upstream}}[D(2),HV]\} \quad (3-14)$$

In theory, if the validity curves for n particle sizes are known, then it is possible to determine the fractional ratio of each of the n sizes in the polydisperse mixture using $n-1$ runs, each taken at a different high voltage. Here there would be n unknown fractions to determine. The fractional ratios would give $n-1$ equations as Eq. (3-15).

$$\begin{aligned}
 & \sum_{p=1}^n \{EV[D(p), HV(1)] f [D(p)]\} = SV[\text{mixture}, HV(1)] \\
 & \sum_{p=1}^n \{EV[D(p), HV(2)] f [D(p)]\} = SV[\text{mixture}, HV(2)] \\
 & \sum_{p=1}^n \{EV[D(p), HV(3)] f [D(p)]\} = SV[\text{mixture}, HV(3)] \\
 & \cdot \\
 & \cdot \downarrow \qquad \qquad \qquad \downarrow \qquad \qquad \qquad \downarrow \\
 & \cdot \\
 & \sum_{p=1}^n \{EV[D(p), HV(n-1)] f [D(p)]\} = SV[\text{mixture}, HV(n-1)]
 \end{aligned} \quad (3-15)$$

and the n th equation would be given as

$$\sum_{p=1}^n f (D(p)) = 1 \quad (3-16)$$

This research was however limited to the study of bidisperse mixtures only.

In order to obtain a greater statistical accuracy, validity difference curves are plotted using the calibration curves of Fig. 3-7 (see Fig. 3-8). These curves show us the best region from which to pick the high voltage for testing the mixture. The higher the validity difference, the easier it is to distinguish between the two particle sizes.

This curve is useful for the especially when the validity difference is low and a good measurement region is to be determined. This is true for the bidisperse mixture of 0.966 micron and 0.505 micron particle diameters. The best region for calculating the fractional ratio appears to be between 700 V and 750 V.

Because the value of validity difference was low for the bidisperse mixture of 0.966 micron and 0.505 micron particle diameters, the values of signal validity for the 0.505 micron particles were taken from the series dated 5/20/99 as shown in Fig. 3-3. This series had higher values of signal validity for all high voltages as compared to the other series of 0.505 micron particles as seen in Fig. 3-3, and was hence able to increase the validity difference between the 0.505 micron and 0.966 micron particles.

The new validity equation based on the data of the series dated 5/20/99 as shown in Fig. 3-3 for the 0.505 micron particles is obtained as.

$$\begin{aligned} \text{EV (\%)} = & - 1.4325 \times 10^{-06} \times (\text{HV})^3 + 1.4331 \times 10^{-03} \times (\text{HV})^2 - 2.4084 \times 10^{-01} \times (\text{HV}) \\ & + 3.500 \times 10^{+01} \end{aligned} \tag{3-17}$$

18 data points were used to obtain this equation with a correlation coefficient of 0.98. For the bidisperse mixture of 0.966 micron and 0.505 micron particles, Eq. (3-17) was used to determine the EV of the 0.505 micron particles.

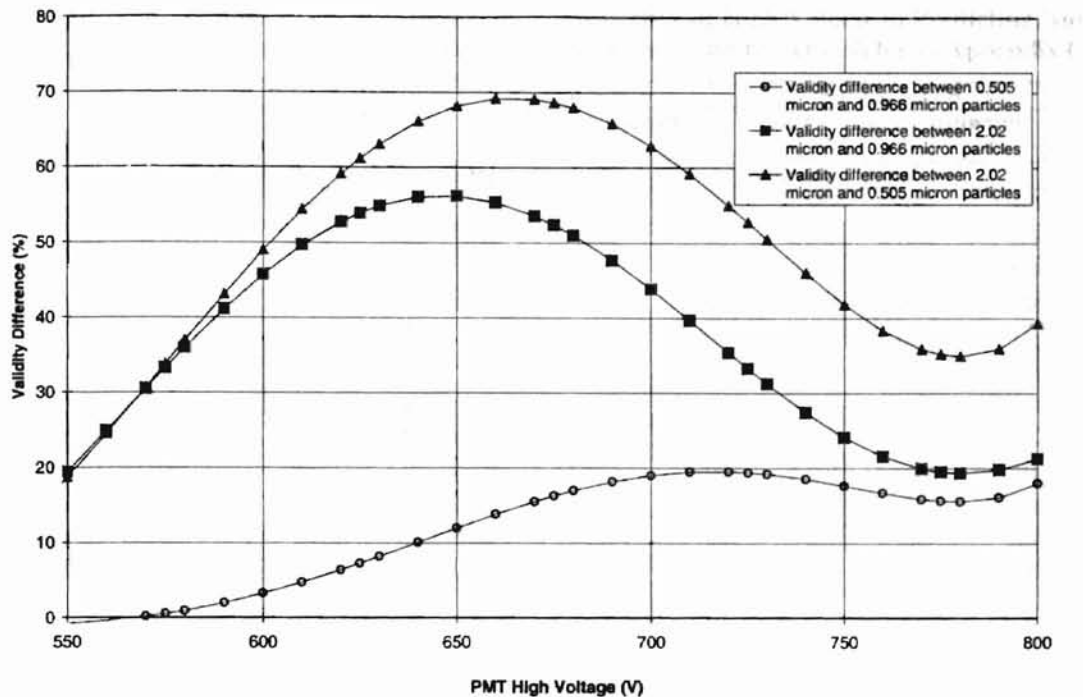


Figure 3-8 Difference in Validity for the Three Different Pairs of Particle Sizes as a Function of High Voltage

As was done for the monodisperse aerosols, the fractional efficiencies for the bidisperse mixtures were calculated at different high voltage points. This author assumed that the best high voltage regions to measure efficiencies are the regions where this fractional efficiency becomes independent of high voltage, as should be the case.

Fractional efficiency values measured at the centerline of the filter for different PMT high voltage values are plotted for a bidisperse mixture of 2.02 micron and 0.966 micron diameter particles in Fig. 3-9. Almost all of the data for the bidisperse mixture of 0.966 micron and 2.02 micron particles that is shown in Fig. 3-9 falls in a narrow band. The entire set of tests performed for this class of measurements is summarized in Table 3-3.

As an example, in Test21 of Table 3-3, a solution (Mixture A) of 10 ml of 2.02 micron PSL solution in 1000 ml of distilled water (a concentration of $1/100 \text{ m}^3/\text{m}^3$) was

Table 3-3 Experiments Performed to Show Consistency of High Voltage in Predicting Number Density for a Two Particle Mixture of Sizes A and B (Also Refer to Appendix C)

File Name	Test Date	Laser Temperature Degrees C	Flow m ³ /hr	Particle Size A			Particle Size B		
				Size Microns	Conc. m ³ /m ³	Strength	Size microns	Conc. m ³ /m ³	Strength
Test29.xls	6/2/99	24.5	170	2.02	1/100	4/5	0.966	1/100	1/5
Test30.xls	6/2/99	24.5	170	2.02	1/100	4/5	0.966	1/100	1/5
Test40.xls	6/6/99	24.2	85	2.02	1/100	4/5	0.966	1/100	1/5
Test21.xls	6/2/99	24.3	170	2.02	1/100	1/2	0.505	1/100	1/2
Test22.xls	6/2/99	24.2	170	2.02	1/100	1/2	0.505	1/100	1/2
Test35.xls	6/4/99	24.2	170	2.02	1/100	1/2	0.505	1/100	1/2
Test39.xls	6/6/99	24.2	85	2.02	1/50	1/3	0.505	1/100	2/3
Test31.xls	6/2/99	24.5	170	0.966	1/100	1/4	0.505	1/100	3/4
Test32.xls	6/2/99	24.5	170	0.966	1/100	1/4	0.505	1/100	3/4
Test36.xls	6/5/99	24.5	170	0.966	1/100	1/4	0.505	1/100	3/4
Test37.xls	6/5/99	24.5	85	0.966	1/100	1/4	0.505	1/100	3/4
Test41.xls	6/6/99	24.2	85	0.966	1/200	2/5	0.505	1/100	3/5

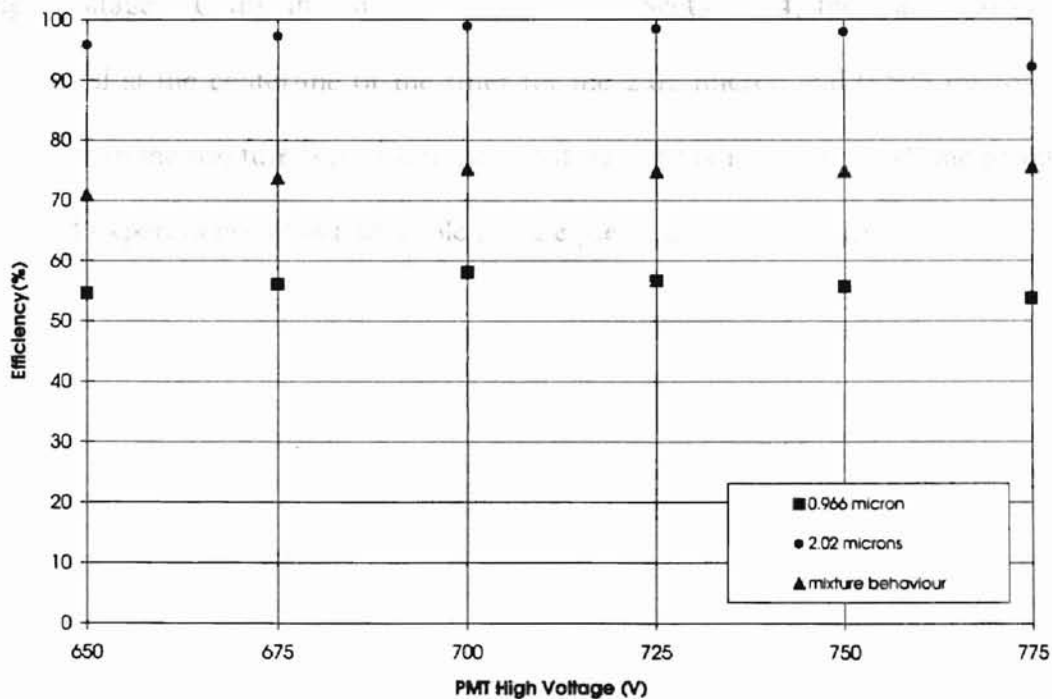


Figure 3-9 Fractional Efficiency as a Function of High Voltage for a Bidisperse Mixture of 0.966 Micron and 2.02 Micron Particles (see Test29.xls of Table 3-3) for PMT High Voltage Parameters Defined in Table 3-1

prepared. This concentration of the solution is indicated in the column with the heading labeled as "Mixture A Concentration" in Table 3-3. Number density measurements upstream of the filter for this solution were recorded for a flow rate of 170 m³/hr using the procedure described in Chapter 4. Another solution (Mixture B) of 10 ml of 0.505 micron PSL solution in 1000 ml of distilled water (a concentration of 1/100 m³/m³) was prepared. This concentration of the solution is indicated as the column heading labeled "Mixture B Concentration" in Table 3-3. The two solutions for Size A and Size B were mixed in equal volumes. Thus the strength column for Size A and Size B was the same and calculated as: volume of the solution of Size A or B in the mixture divided by the total volume of the solution mixture. The mixture was then fed through the atomizer into the small angle housing, and the signal validity was measured at different values of high voltage. Using the method described in Section 3.4, the fractional efficiencies measured at the centerline of the filter for the 2.02 micron and 0.505 micron diameter particles in the mixture were calculated at different high voltages. All the results for the class of experiments shown in Table 3-3 are presented in Appendix C.

CHAPTER 4

EXPERIMENTAL SETUP

4.1 Overview

Section 4.2 describes the general arrangement of the test equipment along with the experimental setup. Also, some measurement techniques are discussed. Section 4.3 discusses data measurement consistency with reference to constant laser power. General operating procedures and precautions observed to obtain reliable and consistent data are discussed in Section 4.4.

4.2 The Setup

All of the efficiency measurements were conducted in a prepared laboratory test setup. The overall layout and location of the system setup in the laboratory is shown in Fig. 4-1. The equipment in this layout will also be discussed in the section on the operating procedures.

As can be seen in Fig. 4-1, the laboratory was broadly divided into two areas. The first area was where the blower and flow system were located, and the second area was where the LDV system and the operator station were located. A curtain separates these two regions. The reason for this is described elsewhere in this chapter. In order to carefully regulate the laser temperature, a duct from the air conditioner was connected directly to the laser housing. An external source of pneumatic air, designated as number 15 in Fig. 4-1 is used for the atomizer and blower controls. Two computers are located in the operator's area. The first computer was used to run the LDV software and

automatically stores the raw LDV data. The second computer was used to operate the traverse and also to manually store the processed data in an MS-Excel file. The refrigerator (designated as number 10 in Fig. 4-1) is used to store the PSL solution at constant temperature.

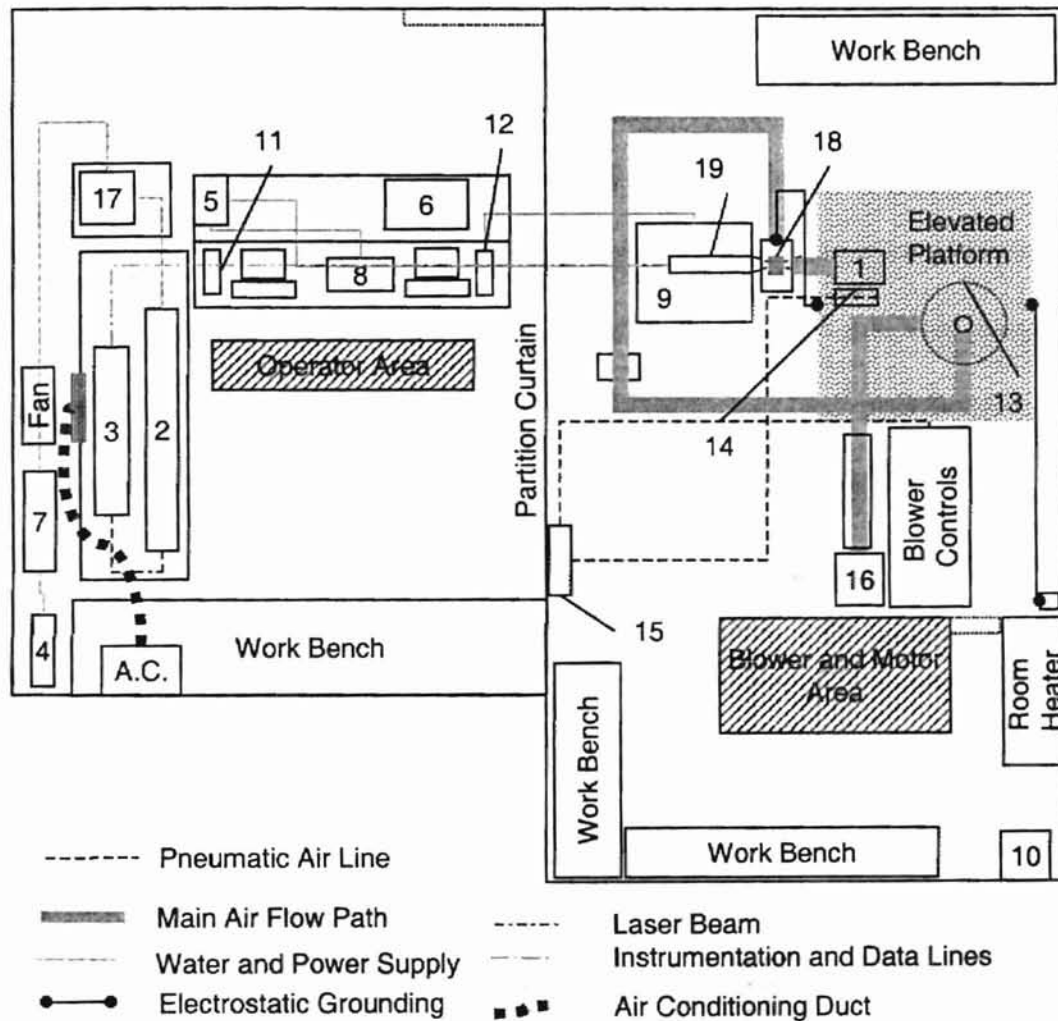


Figure 4-1 Overall Layout of Test Laboratory (Not to Scale)

The numerically designated items in Fig. 4-1 stand for the equipment listed below:

1. Heater and Fan
2. Laser
3. Fiber Drive
4. Cooling Water Supply
5. PMT

6. Printer
7. Cooling Water Filter
8. DSA
9. Transceiver Traverse Mechanism
10. Refrigerator
11. DSA Software Computer
12. Data Storage Computer
13. Final Air Filter
14. Atomizer
15. Pneumatic Air Supply
16. Blower Exhaust
17. Laser Power Supply
18. Test Filter
19. Transceiver

4.2.1 Flow System

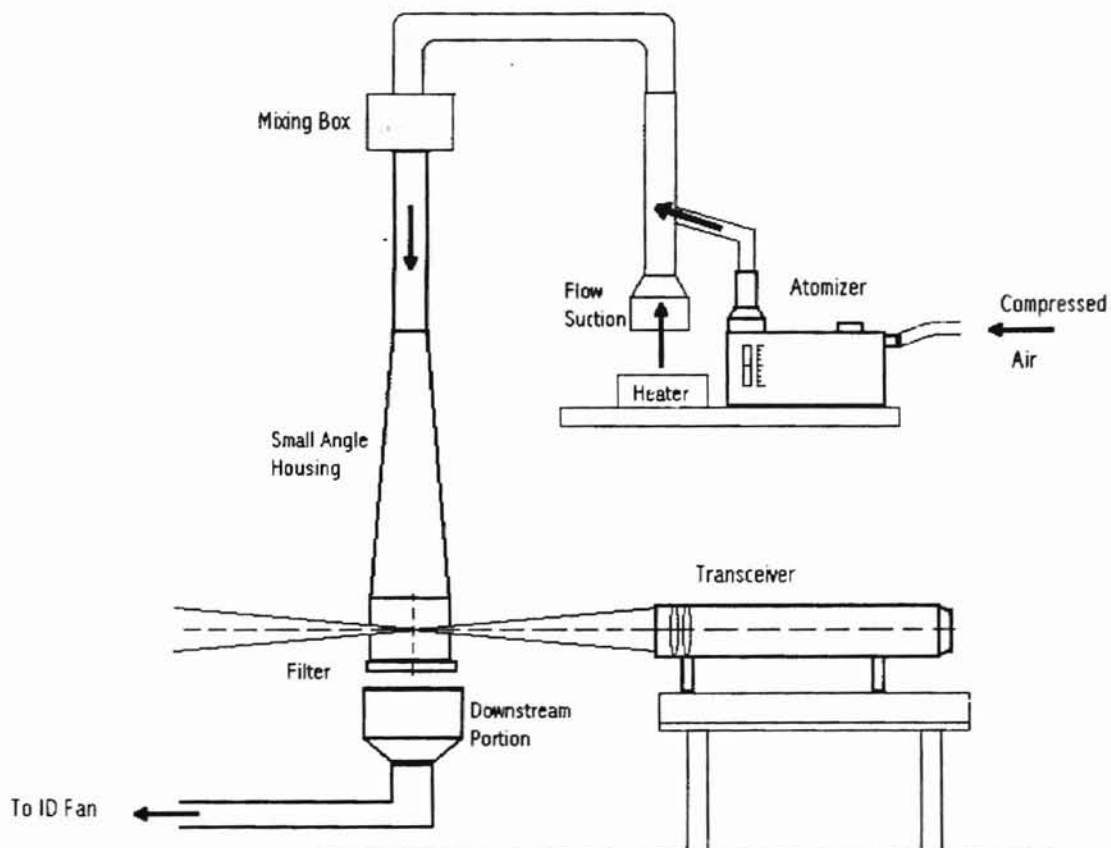


Figure 4-2 Schematic Drawing of the Air Flow Path

An induced draft system was created, with the flow path being on the suction side of the blower. This system simulated the test airflow conditions for the filter. The atomizer, located near the inlet, fed the PSL solution into the flow. The main air intake

was partly heated with a heating coil placed in the suction path. This caused the water in the PSL solution to evaporate, thus enabling only PSL particles to remain in the flow. A mixing box was located further along the flow path, but well upstream of the filter. This box was used to evenly mix the particles and distribute them uniformly in the flow. The temperature and humidity measurements were performed with the sensors placed in the mixing box. The small angle diffuser housing, located just upstream of the filter was used to create a fairly uniform velocity profile upstream of the filter. Just downstream of the filter, another housing collected the filtered air. The dimensional details of the three main flow components (upstream housing, mixing box and the downstream housing) are described later in this chapter. The filtered flow then passed through a flow meter, which recorded the equivalent mass flow rate. Finally, the flow passed through a final filter (designated as number 13 in Fig. 4-1) which collected any remaining particles without these particles being released to the atmosphere.

4.2.2 Data Analysis and Storage

As can be seen in Fig. 4-3, the light beam produced by the laser is directed into the fiber drive through carefully aligned steering mirrors. Inside the fiber drive, a prism splits the beam to blue and green colors. A Bragg cell is then used to shift the frequency of each of the two beams by 40 MHz. The 4 beams pass through fiber optic cables into the measurement zone. The shifted and unshifted green beams are directed in the vertical plane of flow in order to measure corresponding vertical velocity. The blue beams measure corresponding horizontal velocity. The signals produced by the particles crossing the interference fringes are then received by the transceiver. The signals are then transferred to a PMT where each raw signal is first processed and a basic

amplification is applied to it. The signals are then analyzed with the Doppler Signal Analyzer (DSA) which converts the raw signal data to meaningful values of velocity.

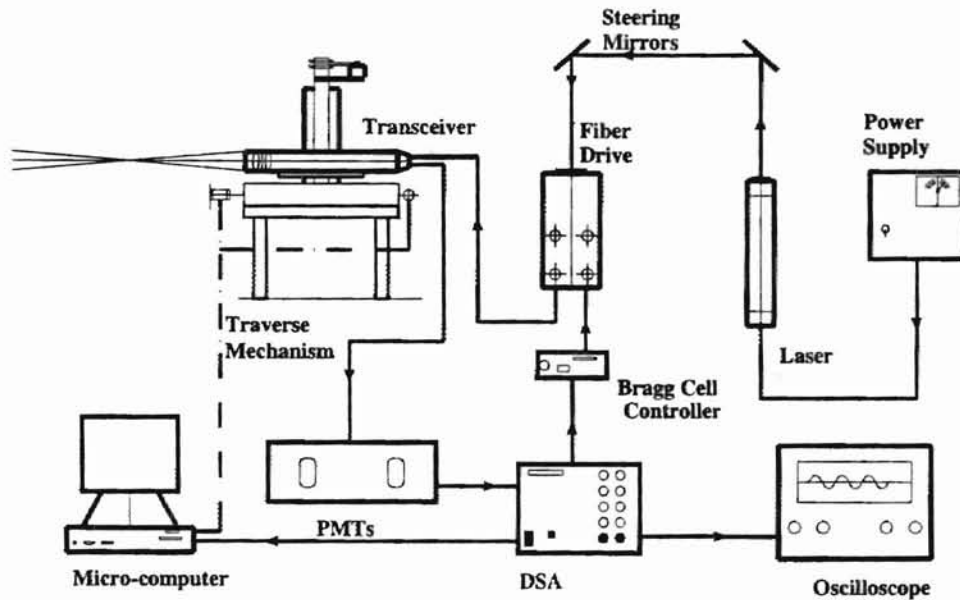


Figure 4-3 Schematic of LDV Data Acquisition (Anand, 1997)

4.2.3 The Flow Housing Components

The small angle diffuser housing was used for conducting all of the tests. Previous researchers (Anand, 1997; Jadbabaei, 1997; Saxena, 1998; and Gebreegziabher, 1999), had worked on constructing and modifying this flow housing. However there is no detailed dimensioning available in any of the previous thesis literature. The detailed dimensions of this housing construction are specified in the figures accompanying this subsection (see Figs. 4-4 to 4-7). The SAE J1669 cabin air filtration code (Society of Automotive Engineers, 1993) recommends a similar type of housing. The small diffuser angles of 1° (see Fig. 4-7) and 3° (see Fig. 4-6) helped to maintain a fairly uniform velocity entering the filter. The cube shaped mixing box, as

seen in Fig. 4-5, provides uniform mixing of particles with the air before entering the filter. The lower section of the housing receives the clean filtered air. At a distance of around 0.4 m downstream of the filter (see Fig. 4-5 and 4-6), the lower housing walls taper off at 8° to accommodate entry into the 100 mm nominal diameter PVC piping. The front faces of the upstream and downstream components of the housing are made from scratch resistant glass. This glass face minimizes distortion and has better optical properties than plexiglass (Anand, 1997). The upstream and downstream portions of the housing are clamped together in combination with an aluminium plate on which the filter is mounted. A foam seal in-between each of the housings and the aluminum plate helps to ensure an airtight connection.

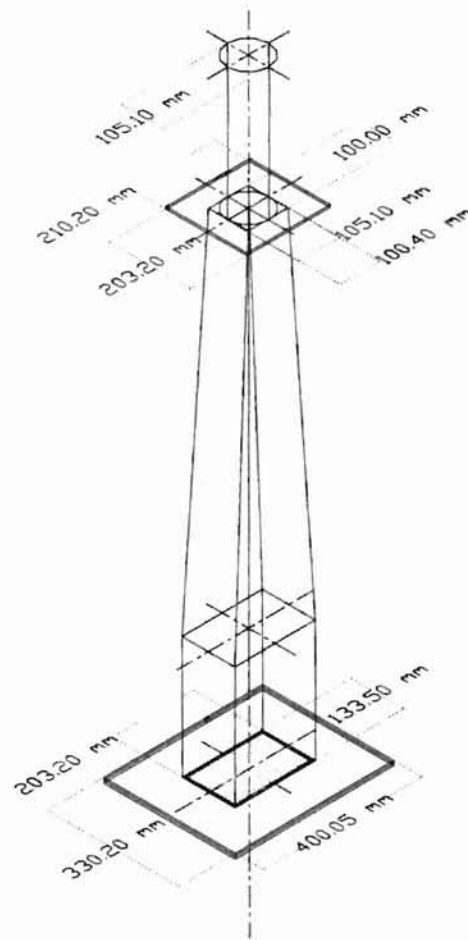
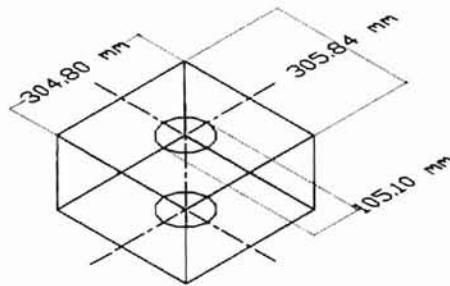


Figure 4-4 Isometric View of the Small Angle Diffuser Housing

Before proceeding with any experiment, the alignment was checked for each of the housing components with a level gauge. Care was taken to ensure that the green beams and the blue beams were in exact horizontal and perpendicular planes. Any error could result in an incorrect component of airflow being measured.

Mixing
Box



Downstream
Assembly

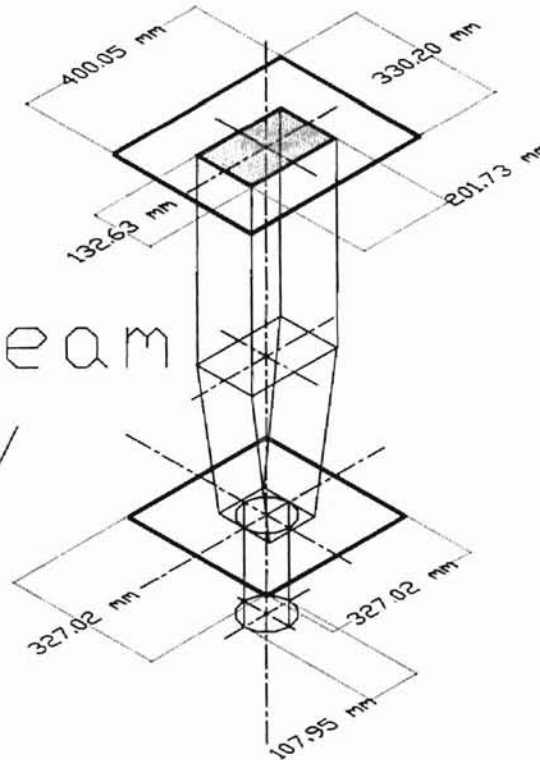


Figure 4-5 Isometric View of Mixing Box and Downstream Assembly of the Flow Housing Components

A vertical U-tube manometer was used to monitor the pressure difference across the filter. In order to measure the pressure drop across the filter, two pressure taps were installed, one in the upstream section and one in the downstream section of the housing. The remaining components were pipes and fittings including straight pipes and elbows, all made of PVC material; and the immediate entry and exit piping for the housing was made with 100 mm nominal diameter tubing.

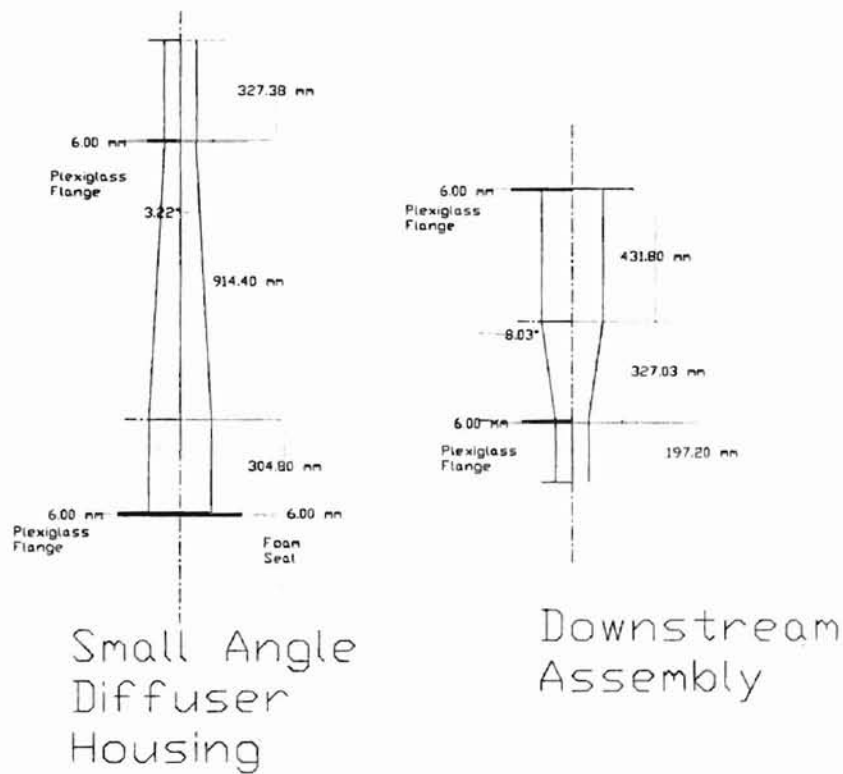


Figure 4-6 Front Views of Upstream and Downstream Small Angle Diffuser Housing Components

4.2.4 Electrostatic Charge Neutralization

Contact between PSL particles in the flow can cause the build up of electrostatic charge in the flow (Gebreegziabher, 1999). By carrying out experiments, Gebreegziabher concluded that charge neutralization might be accomplished by covering the outside of the plexiglass housing with a conducting aluminum foil.

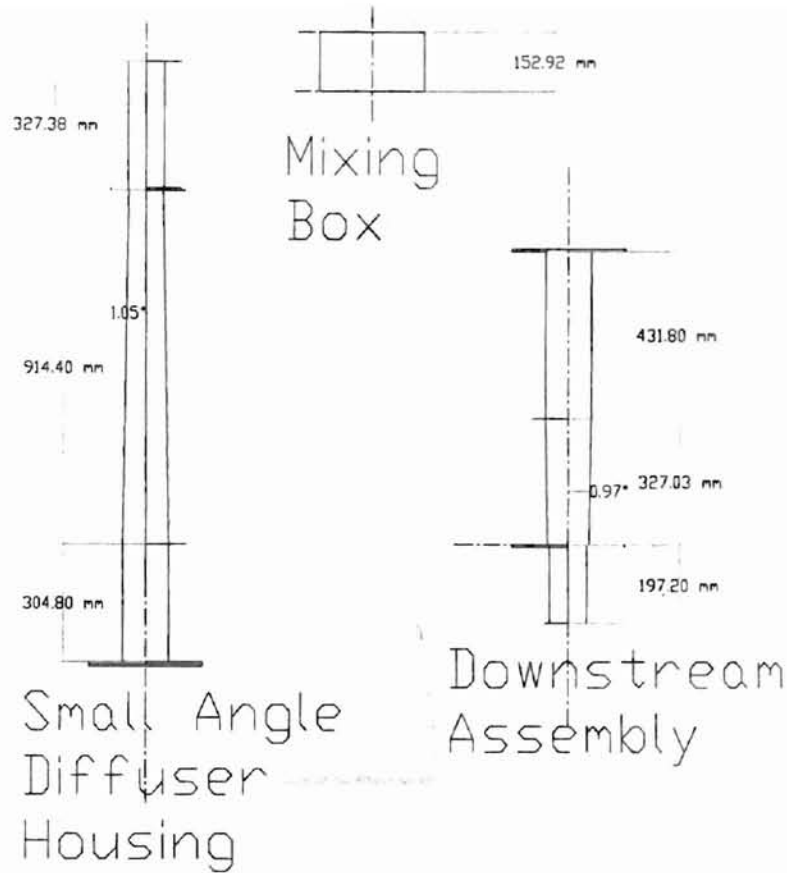


Figure 4-7 Side Views of Upstream and Downstream Small Angle Diffuser Housing Components

Some of the tests done to verify the absence of charge were also witnessed and aided by the author. All tests performed to neutralize the charge in the flow were performed using the setup shown in Fig. 4-8. Charge neutralization was accomplished by preventing charge from accumulating by continuously transferring charge to a grounded wire. However, care had to be taken to provide firm ground contact and also firm contact with the plexiglass housing. A copper wire connected to the housing was grounded by connecting the wire to a metal platform, which was in turn connected to groundwater supply piping (see Fig. 4-1). The verification of charge neutralization was done using an electrostatic field meter (see item number 22 in Appendix G). Readings of 100 V or less were assumed to be good values for zero charge. Readings were taken

just upstream of the filter to measure the amount of charge in the flow. In this study, electrostatic charge voltage refers to the voltage due to electrostatic charge resident upon the surface of the plexiglass housing or the charged particles in the flowing air.

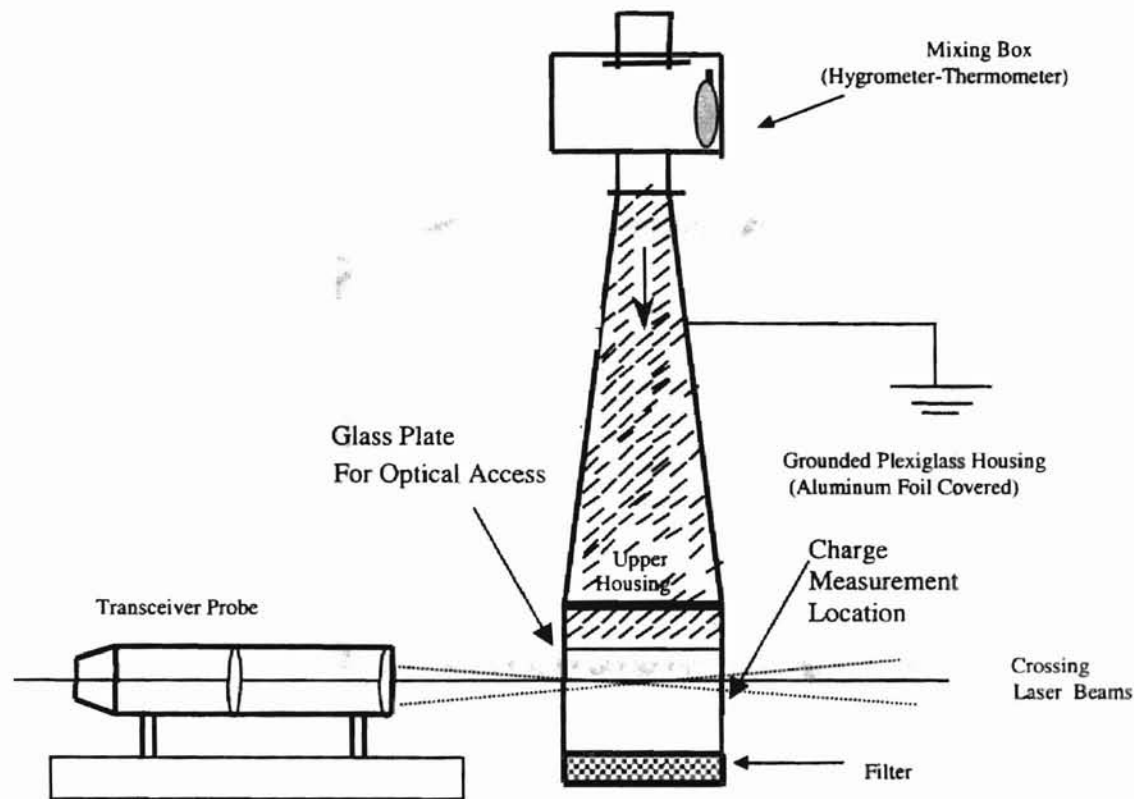


Figure 4-8 Charge Neutralization Setup (Gebreegziabher, 1999)

4.2.5 The Filter and Local Efficiency Measurements

The A13192 pleated filters (by Purolator Products, Inc.) were used as the test filters for this research. They have a pleat pitch of 3.125 mm and pleat height of 30 mm. Beams of the same color, emitted by the transceiver, intersect to form the probe volume (refer to Section 3.2 describing the probe volume in detail). This measuring volume is first located relative to the filter. With the help of the traverse mechanism (see Figs. 4-1 to 4-3), the transceiver was moved such that the probe volume was on the central grid point as shown in Fig. 4-9. The measurements of run time and particle velocity were

performed at the 35 points upstream and downstream of the filter. These grid points are shown relative to the filter in Fig. 4-9. As an example, Fig. 4-11 shows the number density profile downstream of the filter, obtained by moving the measuring volume to the locations specified in Fig. 4-9.

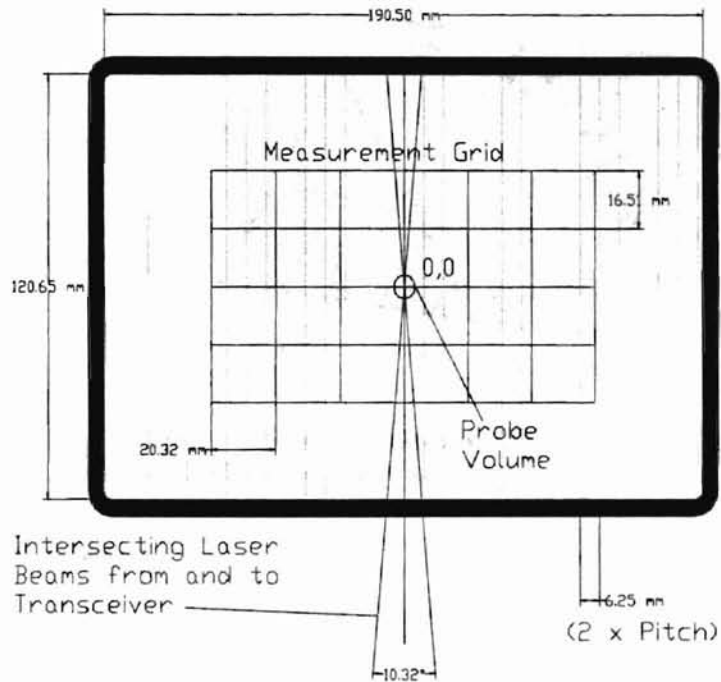


Figure 4-9 Filter Construction (Purolator Products) and the Location of the Measuring Grid over the Filter Surface

This is used to calculate the local efficiency from Eq. (4-1).

$$\eta_i = 1 - N_{i\text{down}}/N_{i\text{up}} \quad (4-1)$$

This local efficiency was used to calculate the average efficiency as follows

$$\eta_{\text{overall}} = \frac{\sum \eta_i}{35} \quad (4-2)$$

where i is the particular grid location of interest.

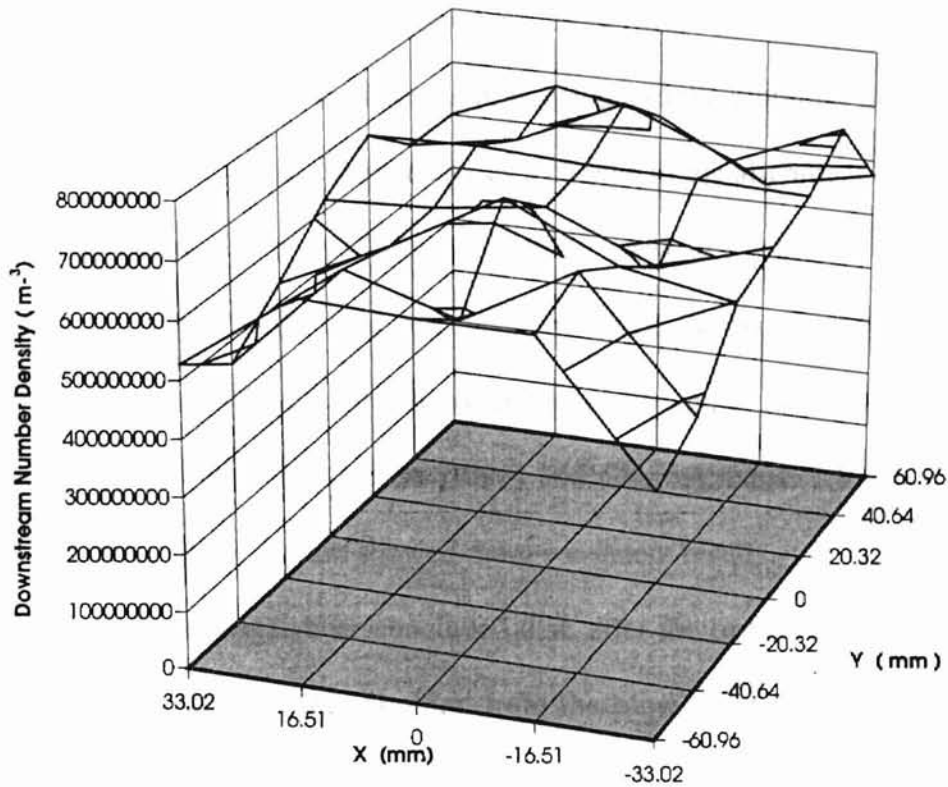


Figure 4-10 Sample Number Density Profile Downstream of Filter for 17 m³/hr (10 scfm), Grounded Housing (2.02 Micron Particles)

4.3 Laser Consistency

In order to validate data from the experiments, prior researchers working on this project performed consistency experiments. Initially there was a wide variation in earlier results for the measured efficiency ranging from 28% to 79% (Saxena, 1998).

In order to account for these efficiencies, later researchers concluded that the inconsistencies were due to deterioration in laser power. As discussed earlier, the reduction in laser power causes a reduction in the probe volume size, thus apparently reducing the number density. A bigger probe volume size detects a larger number of particles passing through it. However, for all our experiments, number density is calculated based on a constant probe volume size. Thus, if, for the same size of the probe volume, more particles are detected, the number density will increase.

The main source of power variation for the laser was initially presumed to be due to the change in temperature in the fiber drive housing and the vibration from the blower (Jadbabaei, 1997). Temperature change causes a change in the alignment of the couplers and reduces the beam efficiency (Jadbabaei, 1997). Also the vibration caused by the blower might be transferred to the optical bread-board, to which the fiber drive is attached. This in turn can lead to a reduction in beam efficiency (Jadbabaei, 1997).

The later work done by Saxena (1998) and Gebreegziabher (1999) in order to improve the stability of the system showed more consistent results.

Saxena and Gebreegziabher concluded that, after the installation of a cork sheet underneath the laser housing, the vibration from the blower had no effect on the laser power (see Fig. 4-11).

Gebreegziabher ruled out other factors such as the cooling water temperature and the breadboard temperature from being very influential. The author witnessed and aided in setting up insulation around the breadboard in order to determine its effect on laser stability.

As can be seen in Fig. 4-12, the breadboard temperature, the outlet and inlet cooling water temperature and the relative humidity inside the housing were maintained constant (within reason), but the laser power showed a considerable decline. So these factors were ruled out as having a major effect on the power deterioration. But since the effects due to variation in the bread-board temperature are not known, this author decided to keep the insulation around the breadboard while continuing all of the measurements (see Fig. 4-13).

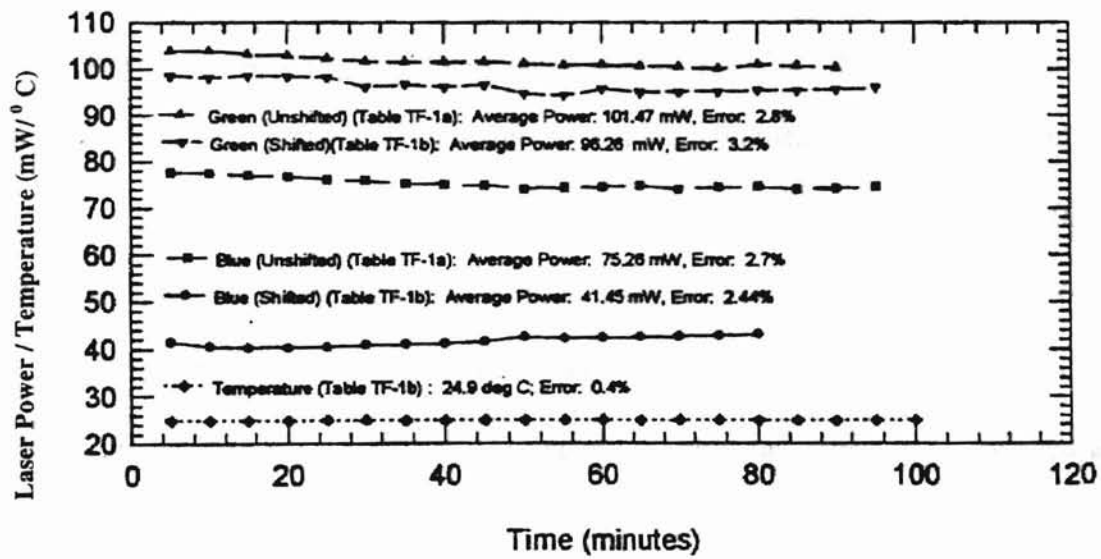


Figure 4-11 Variation of Laser Power at the Transceiver for a Constant Temperature inside the Plexiglass Box, Blower in Operation (Saxena, 1998)

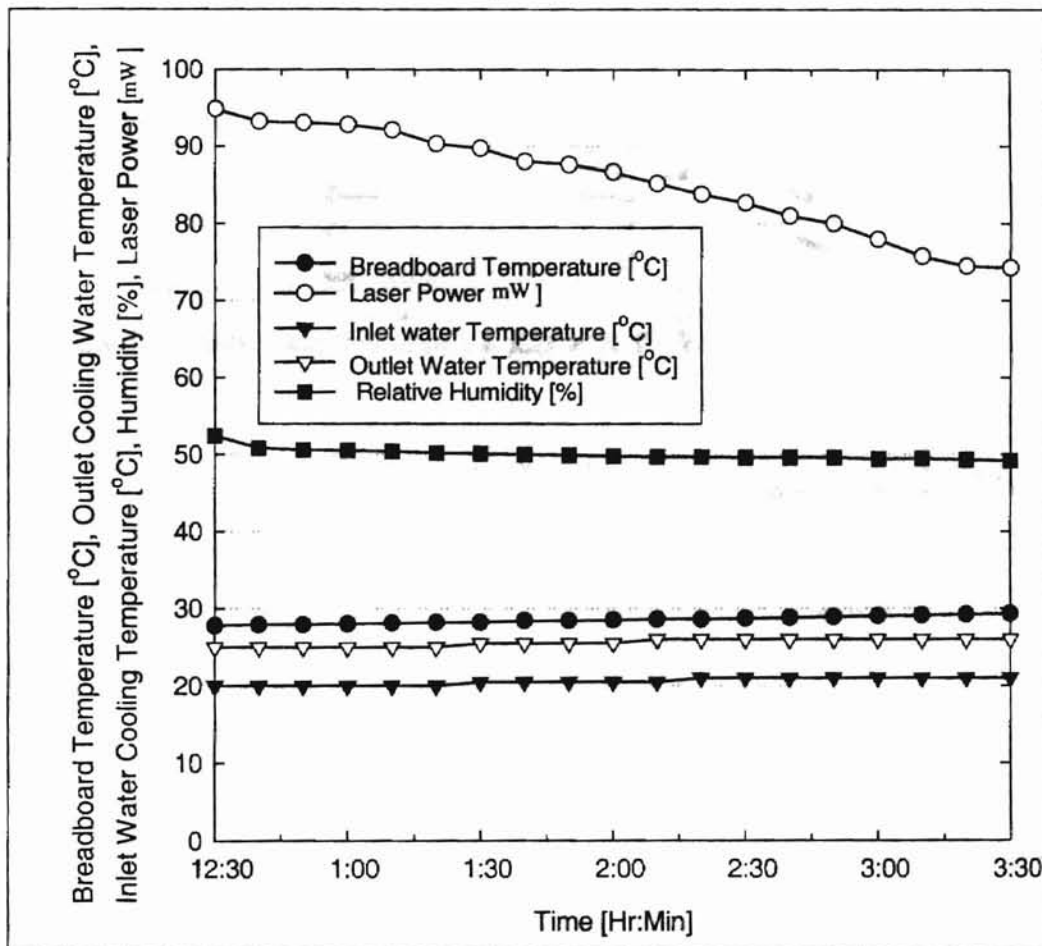


Figure 4-12 Effect of Various Parameters on Laser Power (Gebreegziabher, 1999)

Saxena and Gebreegziabher then went on to show that the temperature inside the fiber drive was the most important parameter in keeping the laser power constant. Saxena and Gebreegziabher were able to maintain constant laser power output, by maintaining the temperature around the couplers inside the housing to within $\pm 0.2^{\circ}\text{C}$ as recorded within the limits of accuracy of the temperature measuring instrument (see Fig. 4-14). It was thus concluded that the laser temperature inside the plexiglass housing must be maintained within a $\pm 0.2^{\circ}\text{C}$ temperature range as recorded by the accuracy of the temperature measuring instrument. The procedure used to monitor this temperature is discussed later in this chapter.

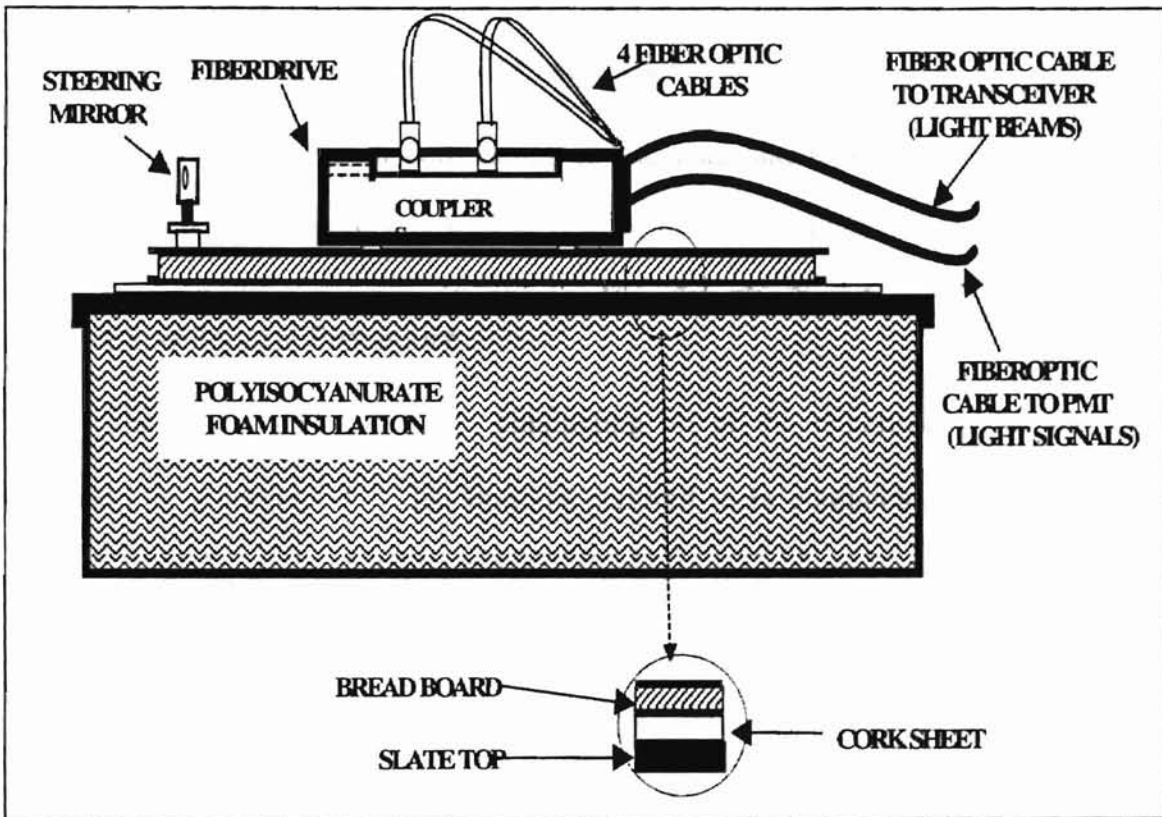


Figure 4-13 Fiber Drive Setup on an Insulated Metal Table (Gebreegziabher, 1999)

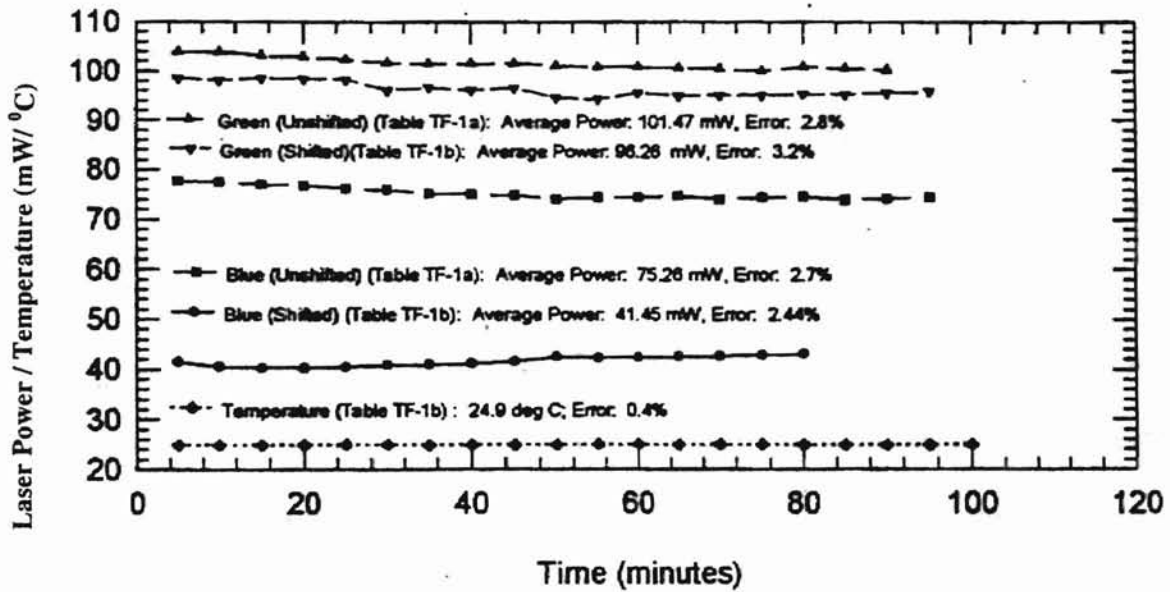


Figure 4-14 Variation in Laser Power When the Temperature inside the Plexiglass Box Was Kept Constant (Saxena, 1998)

4.4 Operating Procedures and Practices

In order to maintain consistency in the data and in order to achieve system stability, the same operational procedure was followed for all tests.

4.4.1 Experimental Procedure

The sequential method for conducting all of the experiments for measuring efficiency is given below. This must be referred to in conjunction with the general equipment layout shown in Fig. 4-1. The procedural flow chart is as shown in Fig. 4-15.

- The LDV hardware and software including the DSA, the PC software, the Bragg cell, and the oscilloscope are initiated. The laser is powered up to 0.1 W.
- The doors of the laser housing are opened and the fan is turned on to insure faster equilibrium of temperature in the room.
- The blower is started, making sure the air supply to the control panel is turned on.

- The plexiglass housing is cleaned, and a new filter is mounted along with the upper half of the housing.
- The mixing box is assembled and the connecting pieces are used to join the mixing box to the small angle diffuser housing. All jointed sections are sealed with duct tape to insure airtight flow.
- The flow is increased to 130.7 m³/hr (75 scfm), and the initial pressure drop is read from the manometer. This pressure drop should be at least equal to its expected minimum value (within a range of 10.16 mm to 12.7 mm) for the small angle diffuser housing. If the pressure drop is less than this value, the housing and filter are checked and reassembled until the minimum value is achieved. If this does not happen in repeated attempts, the filter is assumed to be defective and replaced.
- The flow rate in the blower is then increased by opening the main flow valve until the reading on the TSI flow meter, which is connected downstream of the flow setup, reads the value which is desired to perform the experiment.
- The traverse is then initialized, and the transceiver is moved upstream of the filter.
- The PSL solution is prepared, and, depending upon the duration of the experiment, a minimum of 200 ml is poured into the atomizer.
- The atomizer is positioned at the inlet of the flow housing and adjusted to a pressure of 262 kPag.
- The flow of PSL particles helps us see the laser beams cross inside the small angle housing. This view of the crossing laser beams helps in adjusting the probe volume to the center of the filter with the help of the traverse. Another technique for ensuring that the probe volume is set to the center of the filter

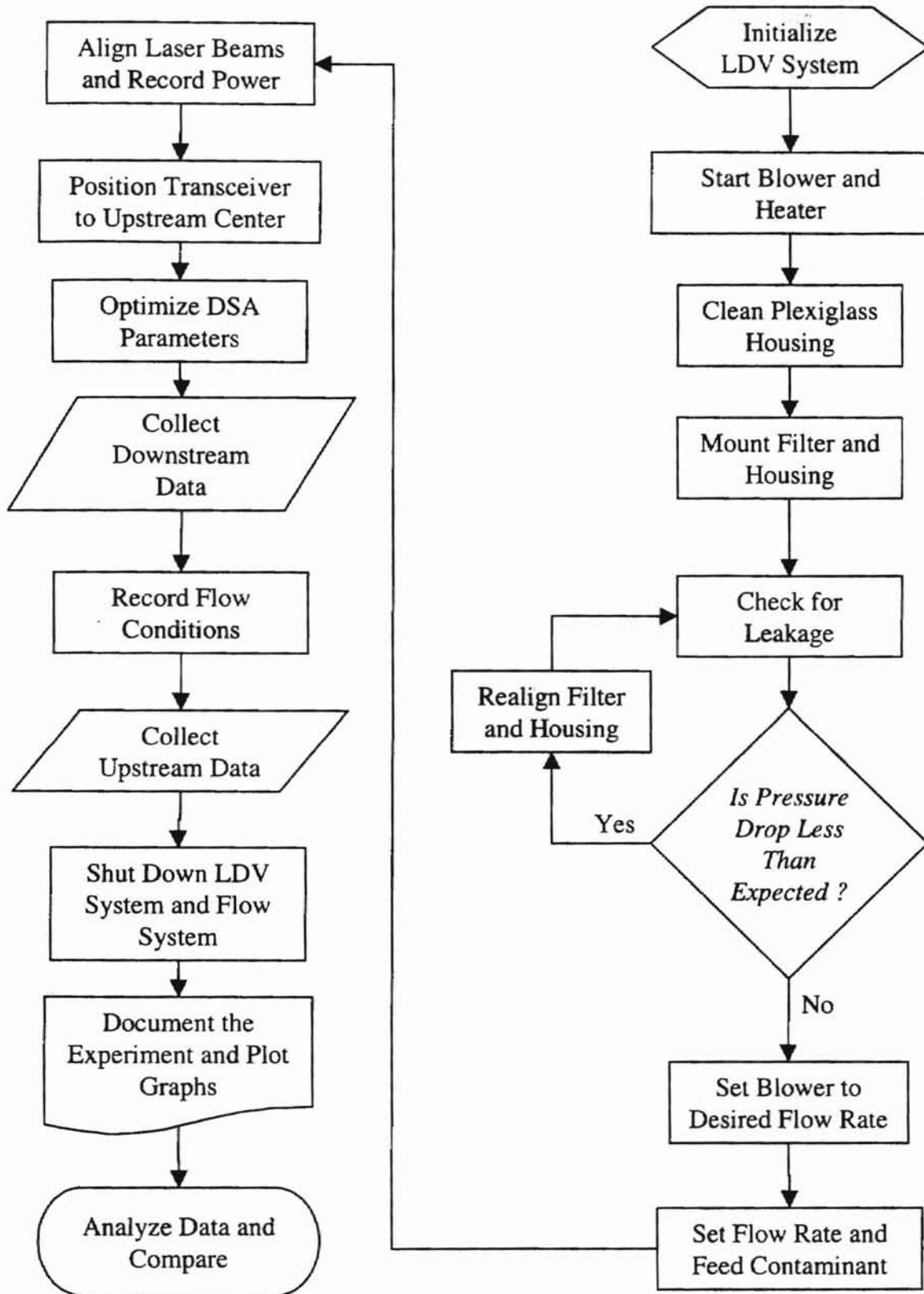


Figure 4-15 Procedural Flow Chart for Conducting Efficiency Measurements

is to bring the intersecting laser beams to the side wall of the housing and observe the path of the laser beams and thus adjust the intersection to the center of the housing.

- The DSA signal detection is turned on, and the parameters are adjusted to get good readings (see Aerometrics, 1993, for a description on setting the signal parameters).
- The transceiver is moved downstream, and the velocity, attempted samples, and the run time are recorded for each of the 35 grid points in order to calculate the number density locally.
- This data is also manually entered by the operator on a Microsoft Excel file.
- The electrostatic charge in the flow just upstream of the filter, the pressure drop, and the temperature and relative humidity at the mixing box are recorded.
- The transceiver is then moved upstream, and the velocity, attempted samples, and the run time are recorded for each of the 35 grid points in order to calculate the number density locally.
- The atomizer is switched off.
- The laser is shut down along with the blower and the heater.
- The Microsoft Excel files are saved, and the local flow and efficiency profiles are graphed.

4.4.2 Low Number Density

Many times it was observed that the same concentration of the PSL solution gave much lower number densities than expected. The PSL particles are very expensive. Thus, the particles should be used sparingly. This author followed a checklist in order to troubleshoot the problem.

- Recheck beam alignment because, the beam may have accidentally become misaligned. This could lead to lower than normal laser beam power, which could result in low number count. The beam power at the outlet of the transceiver should be maximized.
- Check and clean the plexiglass. A hazy plexiglass surface could also lead to reduction in the intensity of emitted or received signals.
- Check for leakage at the atomizer inlet. The atomized PSL solution could be escaping outside the flow path.
- Check the atomizer position. At low flow rates of the experiments, the heater, which also blows air into the flow, may resist the entry of the atomized PSL solution into the flow. In order to avoid this problem, either the atomizer pressure was reduced slightly or alternatively the distance of the blower from the suction area was reduced.
- Also the high voltage and threshold should be checked to insure that the signals are not being under sampled. (Section 3.4 describes how to select the proper sampling zone.)

4.4.3 Procedural Precautions

The following precautions were maintained for each experiment.

- The laser must be kept at minimum power before being started.
- The shutter at the outlet of the laser should be at the open position when starting.
- The shutter at the fiber drive inlet should be closed to prevent the fiber drive from receiving extra high power at startup. Such high power could damage the fiber drive.
- The blower should be always be set for minimum flow rate position before starting.

- Whenever the housing is to be disassembled, minimum flow rate should be set on the blower.

4.4.4 Regular System Maintenance

To insure good operation of the system, following the procedures described below were performed periodically.

- A compressor was used to pressurize the whole system, so that all joints could be checked for leakage with a soap solution. Whenever leakage was detected, the area was sealed with duct tape.
- General cleaning of the computer monitors, keyboards, the plexiglass box covering the laser, and the temperature measuring instruments was performed to prevent dust from damaging and destroying the instruments.
- Cleaning of the mirrors and alignment beams inside the fiber drive was done every couple of months to ensure maximum beam power. (See Coherent, 1991, for a detailed description of the procedure to align the laser beams.)

4.4.5 Procedure for Maintaining Steady-State Temperature in Housing

As discussed in Section 4.3, it is important to ensure the least amount of temperature variation inside the laser housing. In order to do so, the following procedure developed jointly by Gebreegziabher (1999) and the author was followed.

- The basic procedure to maintain the constant temperature inside the fiber drive is as charted in Fig. 4-16.
- Just after the laser is powered up and the blower is turned on, the main curtain separating the data collection area from the blower area is opened (see Fig. 4-1).

- This will insure a faster attainment of equilibrium temperature throughout the laboratory after the system has started.
- The laser housing door is opened and the fan located next to the housing (see Fig. 4-1) is switched on.
- The temperature in the room gradually rises due to the heat generated by the blower system. This rise continues until equilibrium is reached in the room.
- Rapid recirculation caused by the fan causes faster attainment of the equilibrium temperature in the laser housing.
- At this stage, the curtain (see Fig. 4-1) is closed. This temperature is noted as the equilibrium coupler temperature T_c . The fan is switched off and the laser-housing door is closed.
- After this stage in the experimental procedure, the rate of heat rise caused due to the operation of the blower is reduced and any increase in temperature due to the laser can be compensated for by the air conditioner.
- Once the experiment is started, the coupler temperature (T_{coupler}) is observed. A rise in temperature is offset by opening the housing door and turning on the air-conditioner and fan (see Fig. 4-1).
- A drop in temperature is offset by a) switching off the air-conditioner, and opening the partition curtain, and opening the laser housing door. Thus the laser housing can take additional heat generated by the blower in operation and use it to increase its temperature until the desired value is obtained.
- Using this method, it was possible to control the air temperature in the laser housing to within $\pm 0.1^\circ \text{C}$ which was the stated least count of the temperature measuring

instrument (see item number 22 in Appendix G).

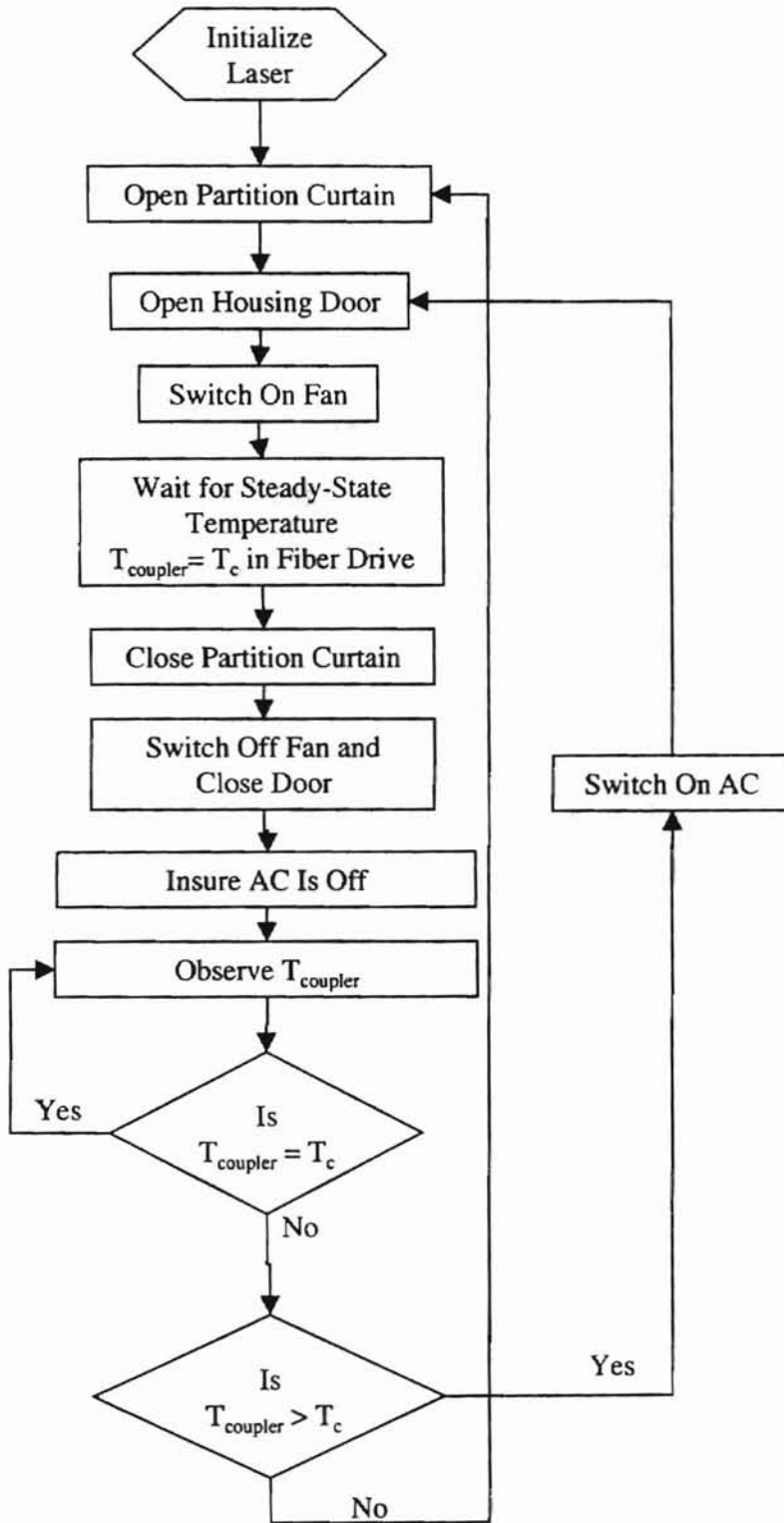


Figure 4-16 Procedural Flow Chart for Achieving and Maintaining Constant Temperature in the Fiber Drive

CHAPTER 5

RESULTS AND DISCUSSION

5.1 Overview

In order to establish the validity of experimental data, it is necessary to correlate with known experimental values and models. This chapter attempts to validate results with theoretical and experimental models. Localized efficiencies were calculated for monodisperse aerosols using PSL particle diameters of 2.02 microns and 0.505 micron. These tests were performed with and without the charge-neutralizing setup. The fractional efficiencies were calculated using binary mixtures containing 2.02 micron, 0.966 micron, and 0.505 micron diameter particles.

In order to validate the experimental results, this author mainly compared the current data with the results of two prior researchers (Saxena, 1998; and Gebreegziabher 1999). These two researchers had helped considerably in stabilizing the test setup and obtaining consistent readings from the LDV system. This was discussed in Chapters 3 and 4. Saxena performed the tests for 2.02 micron and 0.497 micron diameter particles in the small angle diffuser housing. However, he did not carry out his experiments with the charge neutralization arrangement, which is described in Section 4.2.4. On the other hand, Gebreegziabher performed efficiency measurements mainly with the 0.966 micron diameter particles. His research involved efficiency measurements with and without charge neutralization.

Also, the current results are compared with the model proposed by Duran (1995) and that of Suneja and Lee (1974). An empirical relation for determining single fiber

efficiency is explored in the last section of this chapter.

5.2 Flow Measurement and Pressure Drop

A TSI flow meter was used to measure varying flow rate, which was varied with a variable capacity blower. Also another indicator of the flow was the average upstream velocity measured by the LDV system. Ideally, a flow rate recorded by the flow meter should correspond to only one value of LDV velocity. A plot of the LDV recorded velocity as a function of the corrected flow recorded by the TSI flow meter is shown in Fig. 5-1. Here, it can be seen that for a single flow rate recorded by the flow meter, each experiment had a different velocity. This is because of two reasons.

1. The TSI flow meter measures the volume flow rate of air in the duct corresponding to standard conditions of temperature and pressure in the calibration nozzle. Thus, the flow meter measures the mass flow rate of air, which is independent of the temperature and pressure in the flow. Thus, for different temperature and pressure conditions in the calibration nozzle, there would be different volume flow rates measured. In order to obtain the correct velocity information, the exact temperature and pressure must be known inside the measuring nozzle. Since this data changes depending on the conditions occurring at the time of the experiment, there may be different values of velocity recorded for the same flow rate recorded by the TSI flow meter. See Appendix D for more details.
2. The hot film sensor, which is used by the TSI flow meter to measure the flow rate, accumulates dust and needs to be re-calibrated from time to time. In order to obtain correct information about the flow rate, the flow meter is calibrated against a

standard ASME nozzle. Al-Sarkhi (1999), a fellow research student working on the same test system, performed the calibration with the nozzle (Fig. 5-2).

This author used LDV velocity to define Stokes number in the later sections of this chapter.

A plot of the initial pressure drop for all experiments as a function of the average LDV velocity is shown in Fig. 5-3. Also, Fig. 5-4 is a plot of pressure drop with the TSI flow rate. If we compare the two plots, we can see that a better quadratic correlation is obtained for flow versus pressure drop using the LDV average velocity. Hence the LDV recorded average velocity appears to be a better indicator of the flow rate inside the housing.

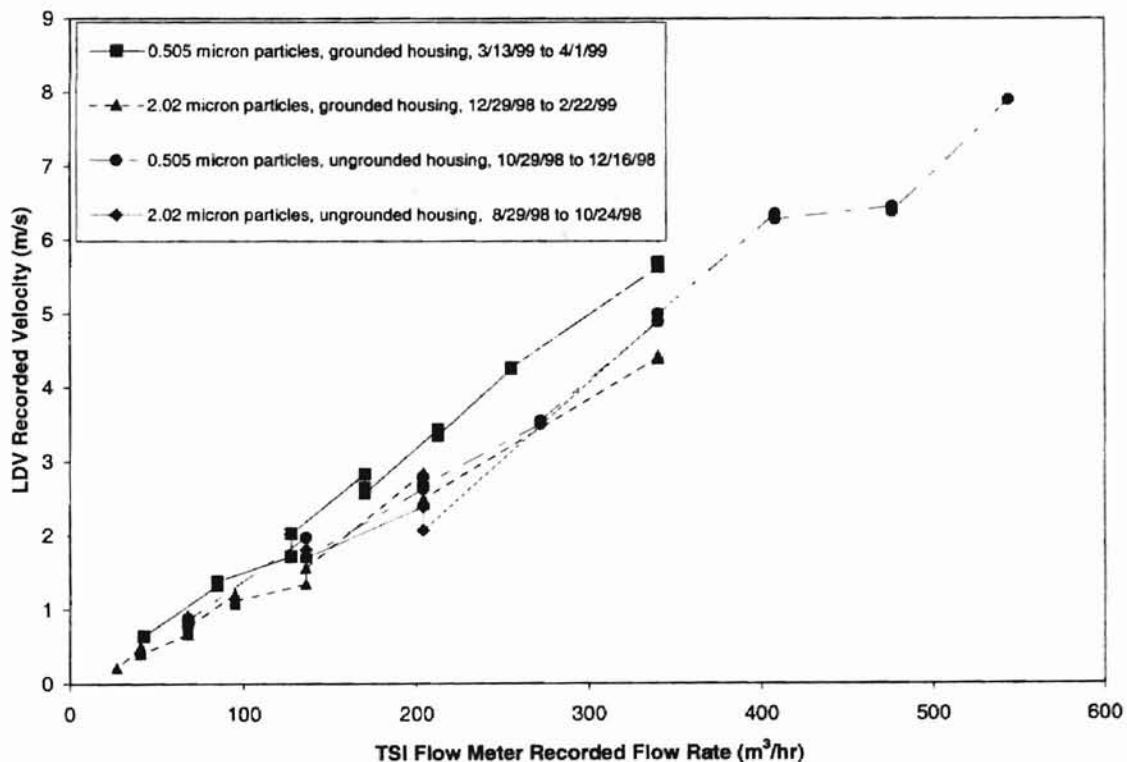


Figure 5-1 Variation of LDV Velocity with TSI Flow using the Small Angle Diffuser Housing

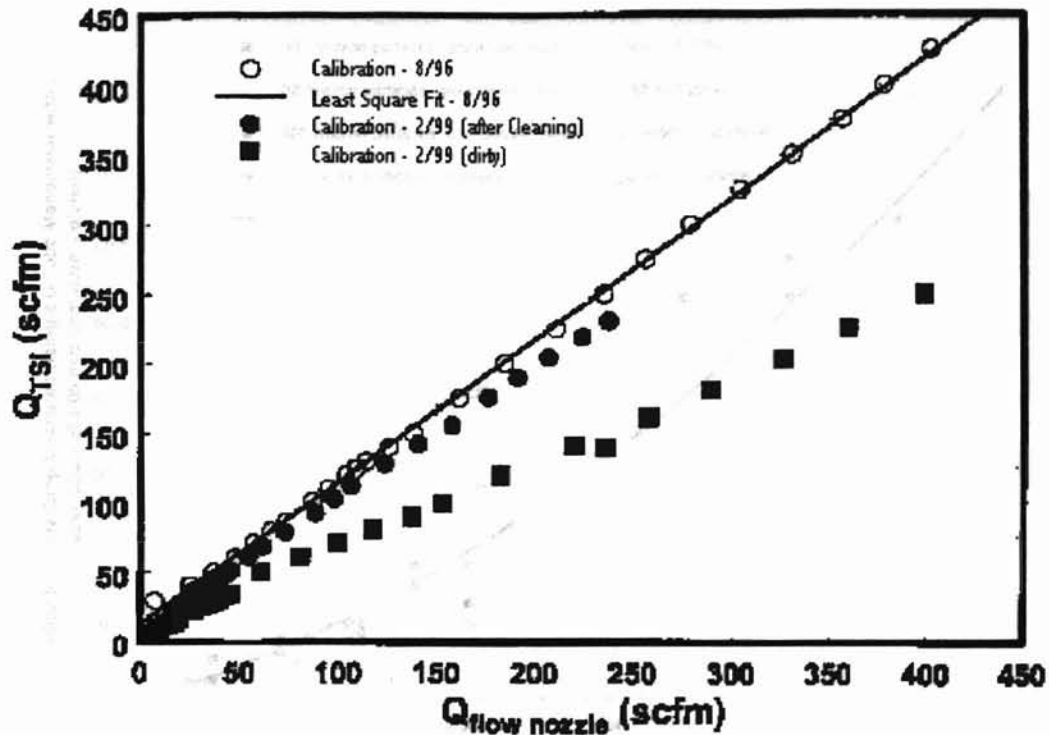


Figure 5-2 Calibration Curve for TSI Flow Meter (Al-Sarkhi, 1999)

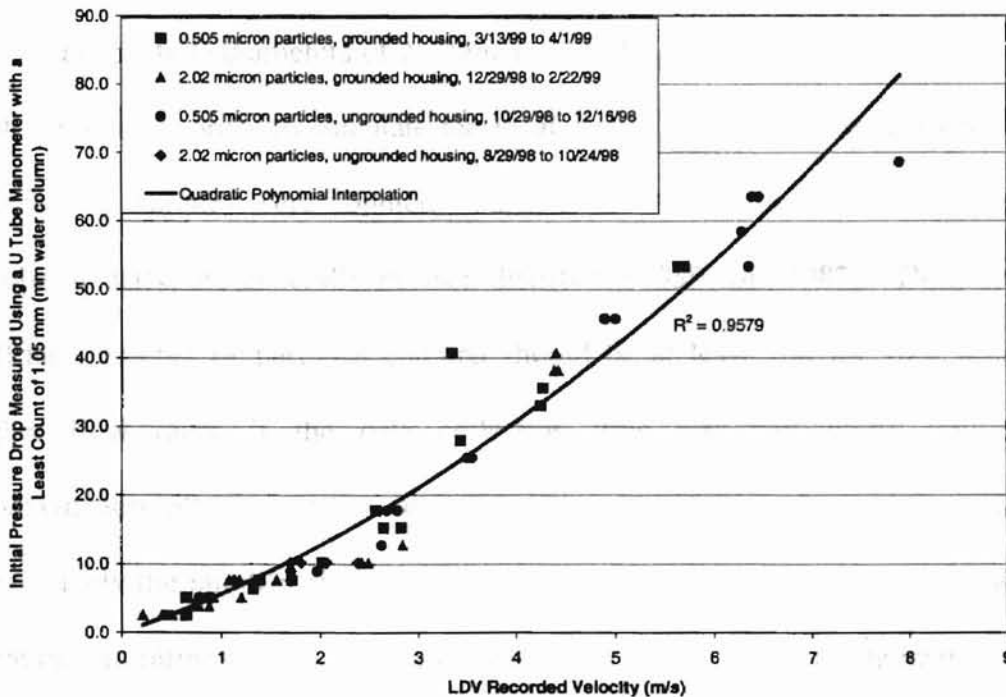


Figure 5-3 Initial Pressure Drop as a Function of LDV Recorded Velocity

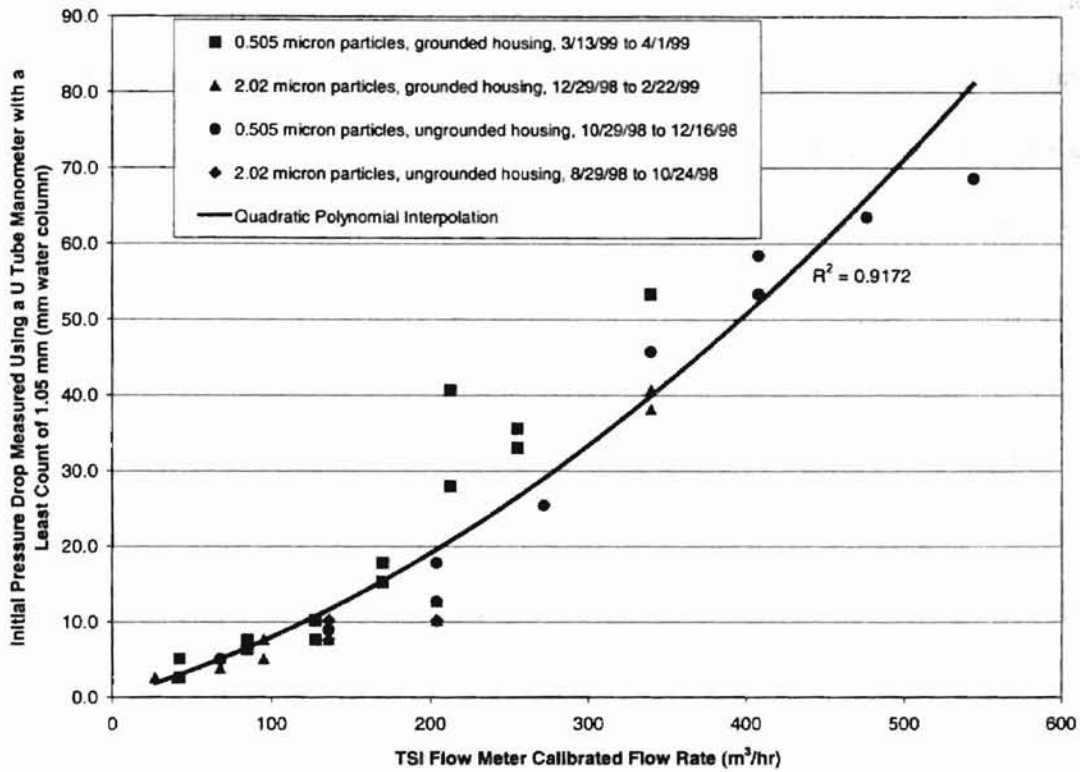


Figure 5-4 Initial Pressure Drop as a Function of TSI Flow Meter Measured Flow Rate

5.3 Results for Monodisperse Aerosols

For particle diameters of 2.02 microns and 0.505 micron, two runs were made for each location in order to calculate the local number density. During each of the runs, 200 to 500 samples were counted. Particle arrival statistics, an indirect indicator of number density, are generally Poisson distributed (Saffman, 1987). Thus, according to Saffman, number of particles counted should be at least 100 for 10% accuracy. At higher flow rates, if the data collection time was particularly low (exceeding approximately 50 seconds to count 100 samples), single measurements were made or alternatively the number of samples was reduced to 200, thus preventing prolonged test duration. Limiting the test time minimizes fluctuation in ambient temperature and also reduces the amount of clogging undergone by the filter.

The overall results are shown in Table 5-1. All of the tests are sorted in order of increasing TSI indicated flow rate. Each test is assigned a unique identification number. This identification number indicates the test flow rate, the particle diameter, the setup used and the file name under which it is stored. For example, for test code 125-2ag, "125" corresponds to the test flow rate of 212.5 m³/hr (125 scfm); "2" is the particle diameter of 2.02 microns ("05" would indicate 0.505 micron); "a" is the 1st test performed ("b" would correspond to 1st test repetition; "c" would correspond to 2nd test repetition, and so on); "g" means that the charge elimination setup is used ("u" indicates an ungrounded setup). It must be noted that the TSI flow meter indicates the flow rate in scfm at standard conditions (15.55 °C and 1.013 x 10⁵ Pa). This was used as the basis for flow variation in the experiment.

After the column showing the test code, the next four main columns of Table 5-1 indicate the date the test was conducted and the calibrated flow rate in m³/hr, the overall integrated efficiency, and the pressure drop across the filter, respectively. Some rows indicating zero rise in pressure drop should be interpreted as the pressure drop change not being above the least count of the manometer of 1.06 mm (1/20 of an inch).

The column on solution strength indicates how much of the PSL particle concentration was introduced in the flow. All PSL particles are from the supplier's solution having 10% by volume of solids. Thus, a solution strength of 5/2000 would indicate that 5 ml of the supplier's solution is mixed with 2000 ml of distilled water. This mixture is fed into the atomizer and introduced to the test flow.

The test parameters indicating the solution concentration, the temperature and relative humidity at the mixing box, and the electrostatic charge are indicated in the next

Table 5-1 Overall Efficiency Results for Monodisperse Aerosols using the Purolator Products, Inc. A13192 Filter

Test No.	Test Code	Test Date	Corrected Flow Rate	Overall Average Efficiency of the Filter (%)				Pressure Drop (mm Water Column)			PSL Solution Strength	Temp. Deg. C	RH %	Charge Above Filter Volts	Remarks
				2.02 micron		0.505 micron		Initial	Final	Rise					
			m ³ /hr (scfm)	Grounded	Not Grounded	Grounded	Not Grounded				m ³ /m ³	At Mixing Box			
1	10-2ag	2/20/99	27.21 (16)	38.13				2.5	2.5	0.0	2/1000	30	50	0	
2	10-2bg	2/22/99	27.21 (16)	37.81				2.5	2.5	0.0	2/1000	32	45	0	
3	15-2ag	1/3/99	40.81 (24)	25				2.5	2.5	0.0	2/1000	30	60	0	Low Efficiency
4	15-2bg	1/4/99	40.81 (24)	26				2.5	2.5	0.0	2/1000	20	60	0	Low Efficiency
5	15-2cg	2/7/99	40.81 (24)	38.32				2.5	3.8	1.3	15/3000	36	46	0	
6	15-2dg	2/9/99	40.81 (24)	37.98				2.5	3.8	1.3	7.5/3000	32	52	0	
7	15-2eg	2/14/99	40.81 (24)	40.59				2.5	3.8	1.3	11/1100	32	45	0	
8	25-05au	11/4/98	68.01 (40)				35.64	5.1	5.1	0.0	5/2000	39	40	Na	
9	25-05bu	11/6/98	68.01 (40)				8.58	5.1	5.1	0.0	5/2000	39	40	Na	Negative Efficiencies
10	25-05cu	12/16/98	68.01 (40)				29.55	5.1	5.1	0.0	5/2000	37	40	-50	
11	25-2ag	1/2/99	68.01 (40)	30				3.8	5.1	1.3	2/1000	25	45	0	Low Efficiency
12	25-2bg	1/9/99	68.01 (40)	32				3.8	3.8	0.0	7.5/1500	27	45	0	Low Efficiency
13	25-2cg	2/6/99	68.01 (40)	40.66				3.8	5.1	1.3	2/1000	32	58	0	
14	25-2dg	2/8/99	68.01 (40)	39.98				5.1	5.1	0.0	5/1000	32	60	0	
15	25-2eg	2/19/99	68.01 (40)	37.43				5.1	6.4	1.3	11/1100	32	45	0	
16	25-05ag	3/18/99	42.51 (25)				48.53	5.1	5.1	0.0	5/2000	35	42	0	
17	25-05bg	3/30/99	42.51 (25)				31.84	2.5	3.8	1.3	5/2000	33	50	0	
18	35-2ag	1/27/99	95.22 (56)	52.89				7.6	10.2	2.5	15/1400	35	47	0	High Efficiency
19	35-2bg	1/28/99	95.22 (56)	55.75				7.6	7.6	0.0	15/1400	30	47	0	High Efficiency

Table 5-1 (continued)

Test No.	Test Code	Test Date	Corrected Flow Rate	Overall Average Efficiency of the Filter (%)				Pressure Drop (mm Water Column)			PSL Solution Strength	Temp. Deg. C	RH %	Charge Above Filter Volts	Remarks
				2.02 micron		0.505 micron		Initial	Final	Rise					
			m ³ /hr (scfm)	Grounded	Not Grounded	Grounded	Not Grounded							m ³ /m ³	At Mixing Box
20	35-2cg	2/1/99	95.22 (56)	47.56				7.6	7.6	0.0	15/1400	31	47	0	
21	35-2dg	2/2/99	95.22 (56)	43.35				7.6	7.6	0.0	15/1400	31	43	0	
22	35-2eg	2/15/99	95.22 (56)	51.71				5.1	5.1	0.0	11/1100	32	48	0	
23	50-2au	10/16/98	136.03 (80)		63.69			10.2	10.2	0.0	15/750	35	55	Na	
24	50-2bu	10/24/98	136.03 (80)		65.94			7.6	10.2	2.5	15/750	39	39	Na	
25	50-2cu	10/16/98	136.03 (80)		54.13			10.2	10.2	0.0	16/800	NA	54.9	Na	
26	50-05au	10/30/98	136.03 (80)				28.86	8.9	10.2	1.3	5/1000	32	55	Na	
27	50-05bu	11/5/98	136.03 (80)				36.24	8.9	10.2	1.3	5/2000	32	55	Na	
28	50-2ag	1/1/99	136.03 (80)	49.15				7.6	7.6	0.0	7.5/3000	27	24	0	
29	50-2bg	2/3/99	136.03 (80)	53.35				7.6	7.6	0.0	15/3000	32	37	0	
30	50-2cg	2/3/99	136.03 (80)	54.98				7.6	7.6	0.0	15/1400	31	45	0	
31	50-2dg	2/22/99	136.03 (80)	60.28				7.6	7.6	0.0	11/1100	33	43	0	High Efficiency
32	50-05ag	3/18/99	85.02 (50)			45.62		7.6	7.6	0.0	5/2000	35	40	0	
33	50-05bg	3/31/99	85.02 (50)			30.96		6.4	6.4	0.0	5/2000	33	51	0	
34	75-2au	8/30/98	204.04 (120)		86.40			10.2	NA	NA	15/750	45	38	-500	
35	75-2bu	#####	204.04 (120)		55.85			10.2	NA	NA	15/750	36	49	-500	Negative Efficiencies

Table 5-1 (continued)

Test No.	Test Code	Test Date	Corrected Flow Rate	Overall Average Efficiency of the Filter (%)				Pressure Drop (mm Water Column)			PSL Solution Strength	Temp. Deg. C	RH %	Charge Above Filter	Remarks
				2.02 micron		0.505 micron		Initial	Final	Rise					
			m ³ /hr (scfm)	Grounded	Not Grounded	Grounded	Not Grounded				m ³ /m ³	At Mixing Box			
36	75-05au	28/10/98	204.04 (120)				23.55	17.8	17.8	0.0	5/1000	NA	51	Negative Efficiencies	
37	75-05bu	#####	204.04 (120)				34.81	17.8	22.9	5.1	5/1000	NA	51	Negative Efficiencies	
38	75-05cu	12/16/98	204.04 (120)				29.84	12.7	22.9	10.2	1.25/1000	40	37	Na	
39	75-2ag	12/29/98	204.04 (120)	65.92				10.2	12.7	2.5	15/1500	40	36	-100	
40	75-2bg	1/7/99	204.04 (120)	72.35				10.2	12.7	2.5	7.5/1500	24	47	0	
41	75-2cg	2/16/99	204.04 (120)	72.15				12.7	12.7	0.0	11/1100	24	47	0	
42	75-05ag	3/13/99	127.52 (75)			31.09		10.2	12.7	2.5	5/1000	35	42	0	
43	75-05bg	4/1/99	127.52 (75)			39.84		7.6	10.2	2.5	5/1000	33	55	0	
44	100-05au	12/15/98	272.05 (160)				45.82	25.4	27.9	2.5	1.25/1000	40	37	-100	
45	100-05bu	12/15/98	272.05 (160)				49.51	25.4	27.9	2.5	1.25/1000	41	37	-500	
46	100-05ag	3/17/99	170.03 (100)			63.41		17.8	20.3	2.5	5/1000	33	50	0	
47	100-05bg	3/27/99	170.03 (100)			38.69		15.2	17.8	2.5	5/1000	35	40	0	
48	100-05cg	3/27/99	170.03 (100)			42.25		15.2	17.8	2.5	5/1000	33	55	0	
49	125-2au	10/15/98	340.06 (200)		90.32			45.7	50.8	5.1	15/750	35	55	Na	
50	125-05au	11/4/98	340.06 (200)				63.40	45.7	50.8	5.1	5/1000	NA	47	Na	

Table 5-1 (continued)

Test No.	Test Code	Test Date	Corrected Flow Rate	Overall Average Efficiency of the Filter (%)				Pressure Drop (mm Water Column)			PSL Solution Strength	Temp. Deg. C	RH %	Charge Above Filter Volts	Remarks
				2.02 micron		0.505 micron		Initial	Final	Rise					
			m ³ /hr (scfm)	Grounded	Not Grounded	Grounded	Not Grounded				m ³ /m ³	At Mixing Box			
51	125-05bu	11/6/98	340.06 (200)				61.29	45.7	50.8	5.1	2.5/1000	31	47	Na	
52	125-2ag	1/6/99	340.06 (200)	83.71				38.1	40.6	2.5	7.5/1500	30	45	0	
53	125-2bg	12/30/98	340.06 (200)	80.31				38.1	43.0	4.9	7.5/1500	36	36	-100	
54	125-2cg	2/17/99	340.06 (200)	84.19				40.6	43.2	2.5	11/1100	33	43	-100	
55	125-05ag	3/17/99	212.54 (125)			50.67		40.6	43.2	2.5	5/1000	33	50	0	
56	125-05bg	3/17/99	212.54 (125)			54.24		27.9	27.9	0.0	5/1000	36	40	0	
57	150-05au	10/29/98	408.08 (240)				82.75	58.4	63.5	5.1	5/1000	NA	51.3	Na	
58	150-05bu	11/5/98	408.08 (240)				75.51	53.3	61.0	7.6	5/1000	NA	51.3	Na	
59	150-05ag	3/19/99	255.05 (150)			64.72		35.6	38.1	2.5	8/1000	36	42	0	
60	150-05bg	3/26/99	255.05 (150)			56.89		33.0	35.6	2.5	8/1000	35	36	0	
61	175-05au	12/10/98	476.09 (280)				79.84	63.5	71.1	7.6	5/2000	36	37	-100	
62	175-05bu	12/11/98	476.09 (280)				77.50	63.5	71.1	7.6	36647	40	35	-100	
63	200-05au	12/11/98	544.1 (320)				85.60	68.6	76.2	7.6	3.5/1400	35	40	-150	
64	200-05ag	3/19/99	340.06 (200)			75.04		53.3	58.4	5.1	8/1000	37	42	0	
65	200-05bg	3/24/99	340.06 (200)			73.06		53.3	58.4	5.1	8/1000	36	45	0	

three columns. The remarks column was used by the operator to provide comments, such as bad test data, or test data with considerable variation in the local efficiency.

Occasionally there would be inconsistencies occurring in some of the tests conducted, due to negative local efficiencies. This was thought to result, because, at some low flow rates, recirculation zones existed downstream of the filter. There could be an equal number of positive and negative velocities resulting in velocity averages close to zero. A closer look at Eq. (3-3) for calculation of number density reveals that since the velocity term is in the denominator, a low value of velocity will result in misleadingly high values of number density, which may exceed the particle count upstream for that same location. The location of these zones depended upon the precise mounting of the filter in the test stand. Since the filter is not mounted in the exact same place each time, the precise location of the zones varied from test to test by a maximum of 1 grid point location (see Fig. 4-9). Typically, these recirculating zones were observed closer to the smaller walls of the small angle diffuser housing. In order to overcome this problem, some of these tests were repeated, or the filter was remounted initially, or the measuring location was shifted to a region close to the measuring grid but just outside the re-circulating region. A detailed explanation for calculating number density in recirculation zones has been described in the thesis of Jadbabaei (1997).

Some tests gave results having considerably higher or low efficiency values. These tests were repeated until consistent results were obtained (Overall efficiency values for an experiment at a single flow rate did not vary more than around 10%). The author attempts to justify these experiments as follows.

Signal detection is dependent on the optical clarity of the measuring area (glass constructed) of the small angle diffuser housing. This author made sure that the outside glass surface was cleaned after every experiment. The inside of the glass surface was cleaned after every 5 experiments. Occasionally, a slightly misaligned filter could cause accumulation of the PSL particles on a portion of the measuring surface. If this was not observed and cleaned immediately, the quality and strength of the LDV signals passing through this dirty region could be reduced, and hence not allow detection of all particles. This in turn could cause the system to detect fewer signals and hence record a lower number density. High efficiency might have been due to poor quality glass downstream of the filter, and low efficiency might have been due to poor quality glass upstream of the filter.

5.4 Local Profiles

In order to study the local behaviour of the filters, two cases of higher and lower flow rates were used. Local measurements of upstream concentrations revealed fairly regular profiles across the filter for both high and low flow rates (see Figs. 5-5 and 5-6).

The relatively small diffuser divergence angle (see Figs. 4-4 to 4-7) and uniform mixing of particles at the mixing box (Figs. 4-5 and 4-7) helped to ensure uniform dispersion of the particles. Also, relatively regular upstream velocity profile helps to ensure this uniformity (see Figs. 5-7 and 5-8).

However, downstream of the filter, there was a greater spread in the values of number density (see Figs. 5-9 and 5-10). This is because the downstream number density profile can vary due to any of the following:

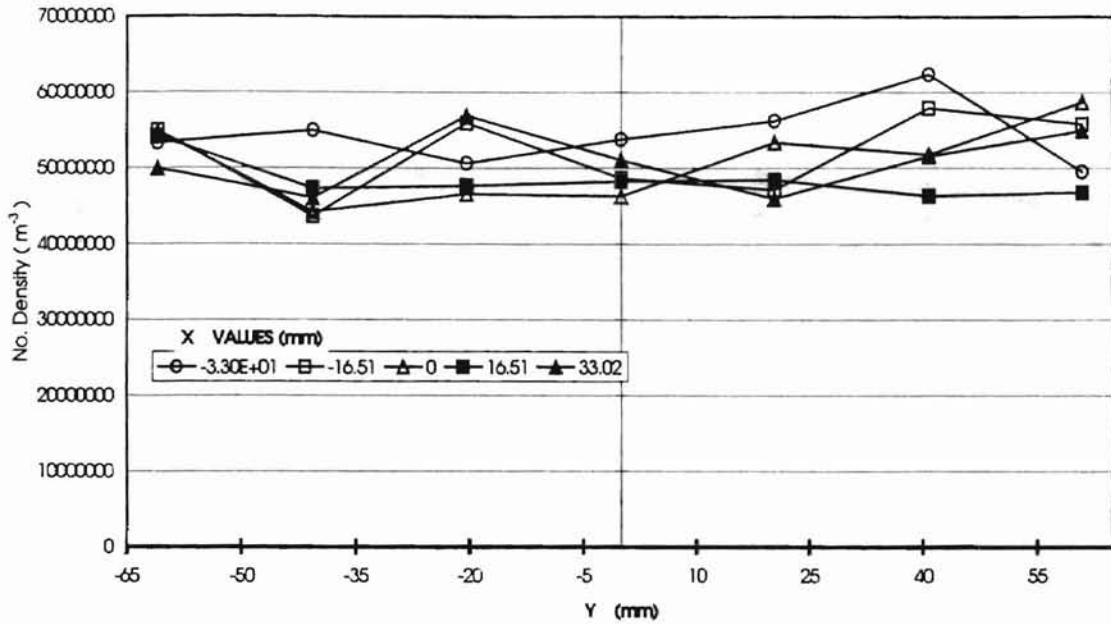


Figure 5-5 Upstream Number Density Profile for a Flow Rate of 340.1 m³/hr

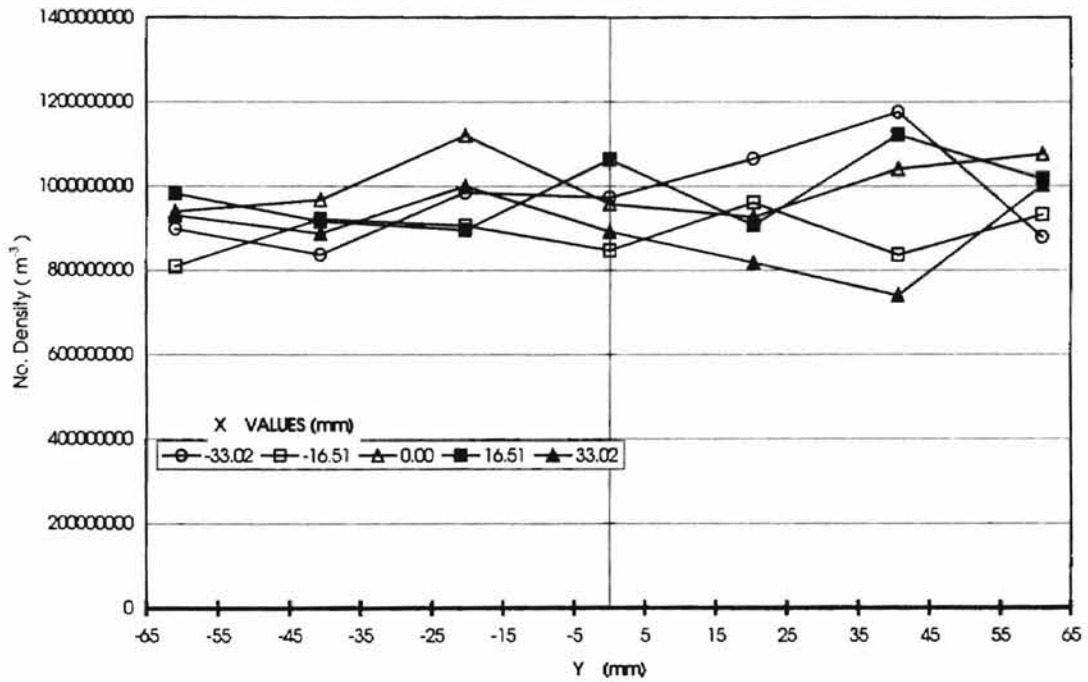


Figure 5-6 Upstream Number Density Profile for a Flow Rate of 27.2 m³/hr

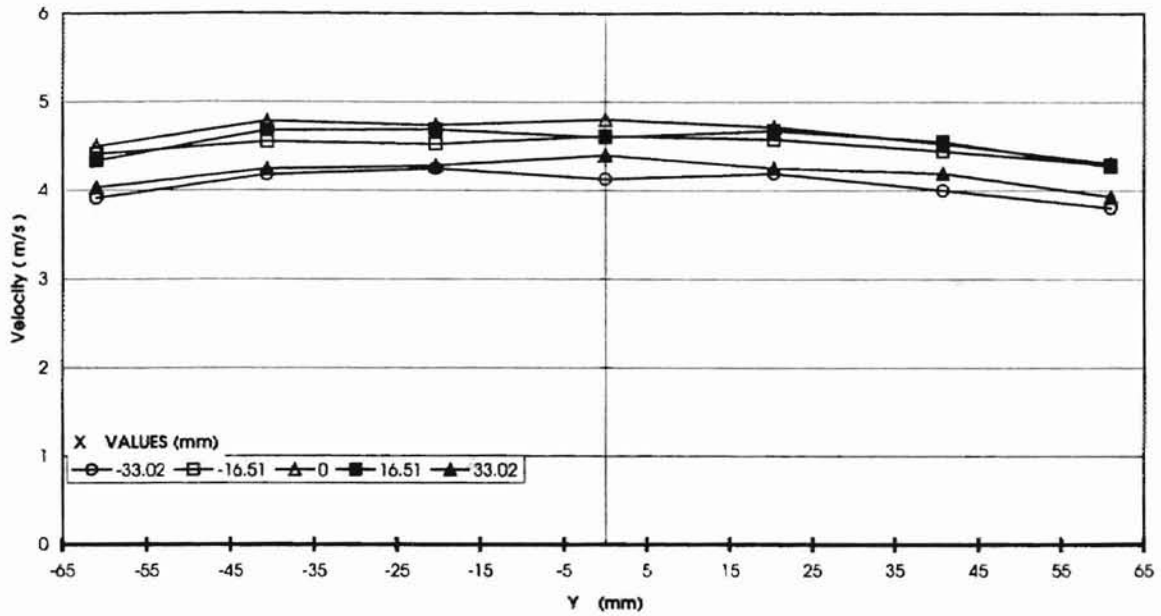


Figure 5-7 Upstream Velocity Profile for a Flow Rate of 340.1 m³/hr

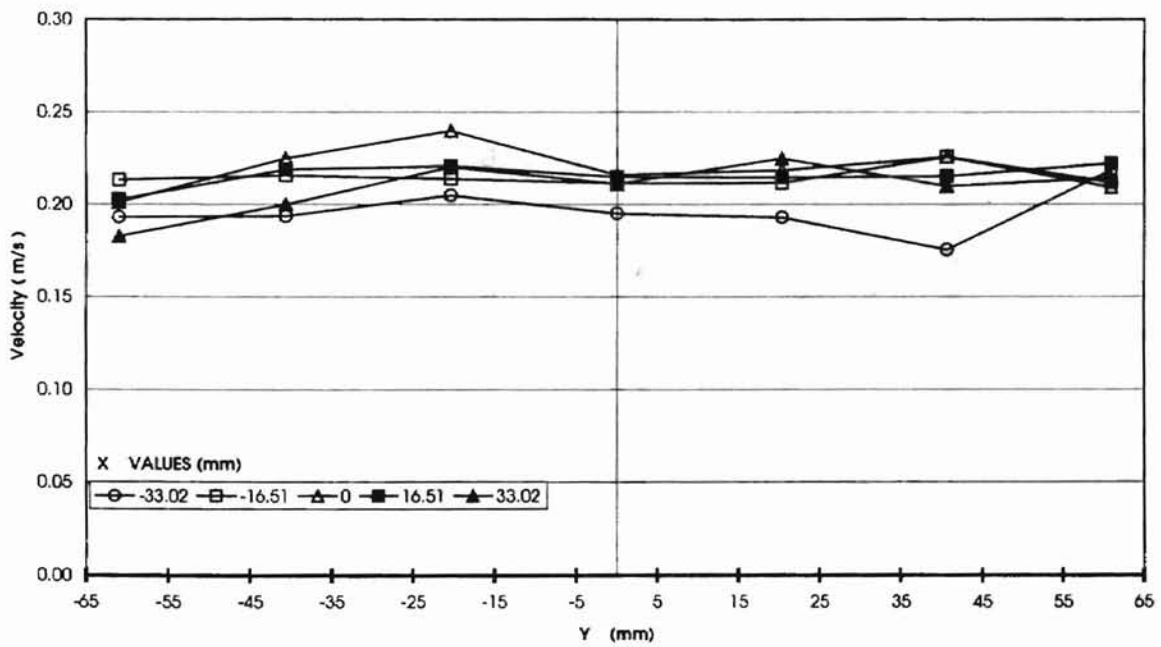


Figure 5-8 Upstream Velocity Profile for a Flow Rate of 27.2 m³/hr

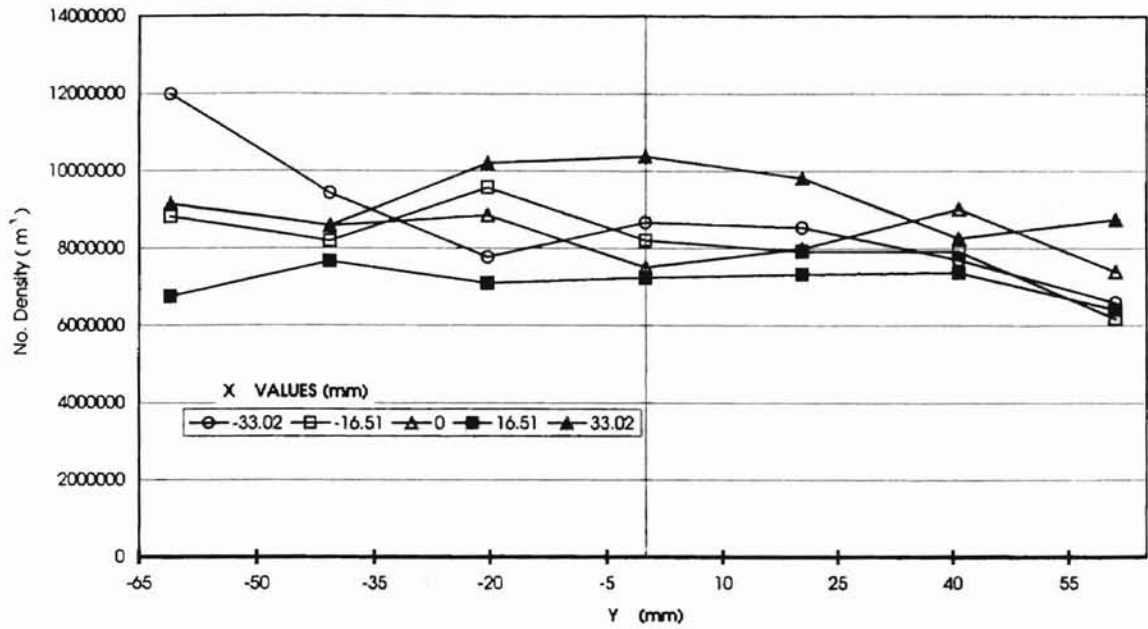


Figure 5-9 Downstream Number Density Profile for a Flow Rate of 340.1 m³/hr

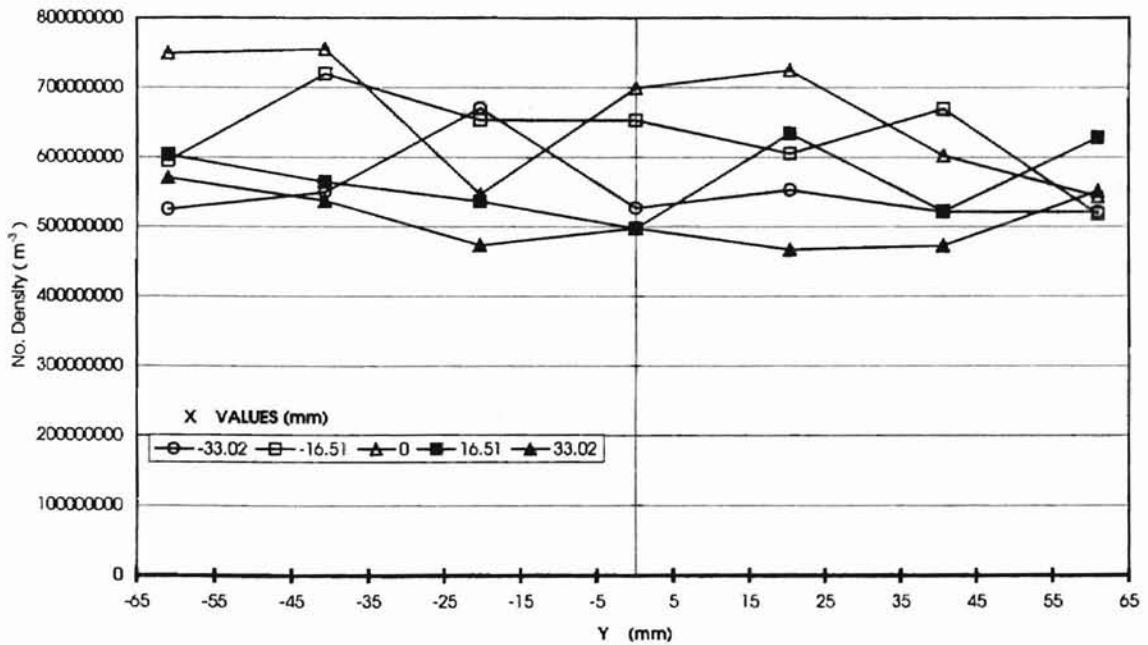


Figure 5-10 Downstream Number Density Profile for a Flow Rate of 27.2 m³/hr

- variation in the corresponding upstream number density profile,
- variation in the downstream velocity profile, which is discussed later in this section, and
- variation in the filtration efficiency profile, which is also discussed later in this section.

Another trend, as seen from Figs. 5-9 and 5-10, was that the number density profile for the lower flow rates showed a larger spread.

Velocity profiles downstream of the filter are more irregular (see Figs. 5-11 and 5-12), which was partly caused by the higher variation in number density downstream of the filter. A probable reason for this could be the rubber gasket around the filter, which can serve as an obstruction in the flow path and also cause recirculation downstream of the filter.

All of these effects influence the final efficiency profiles across the filter. Variation in the filtration efficiency profile is affected by any fluctuation in the upstream velocity across the filter surface. Also, due to the relative non-uniformities across the filter fibers, the filtration efficiency can vary across the filter surface. Packing density variation in fibrous filters can cause a variation in local efficiency of almost 60% (Schweers and Loffler, 1994).

In general, it is seen that the higher flow rate tests had a fairly regular type profile (see Fig. 5-13). Greater variation was seen for the lower flow rate case (see Fig. 5-14). This was because, at lower flow rates, the particle concentration is much more sensitive to a change in velocity.

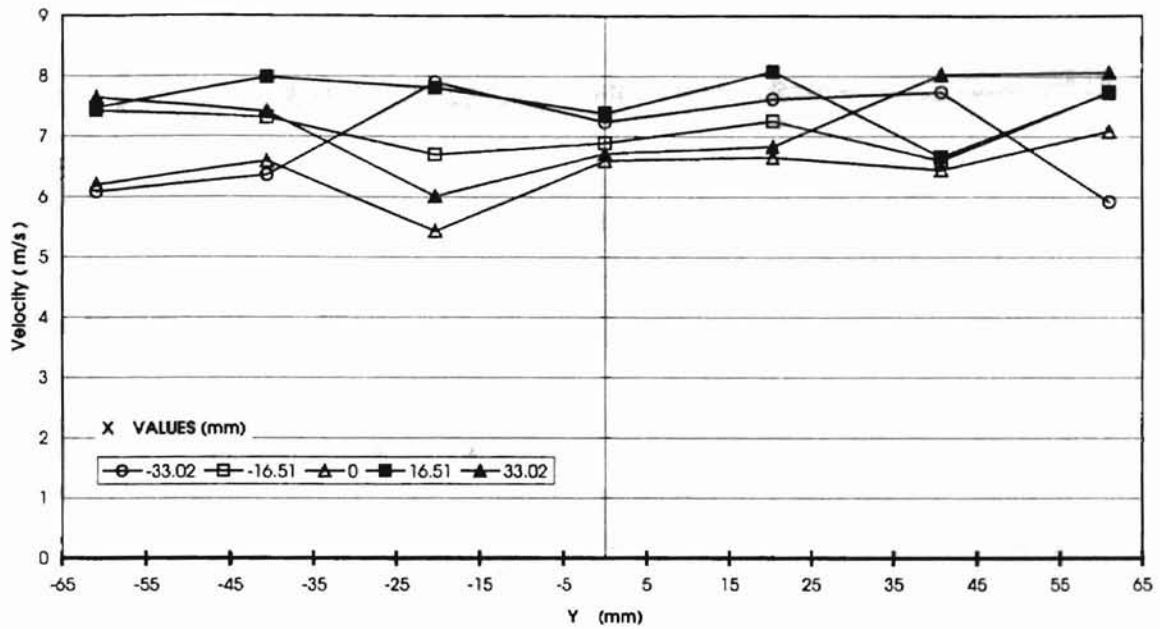


Figure 5-11 Downstream Velocity Profile for a Flow Rate of 340.1 m³/hr

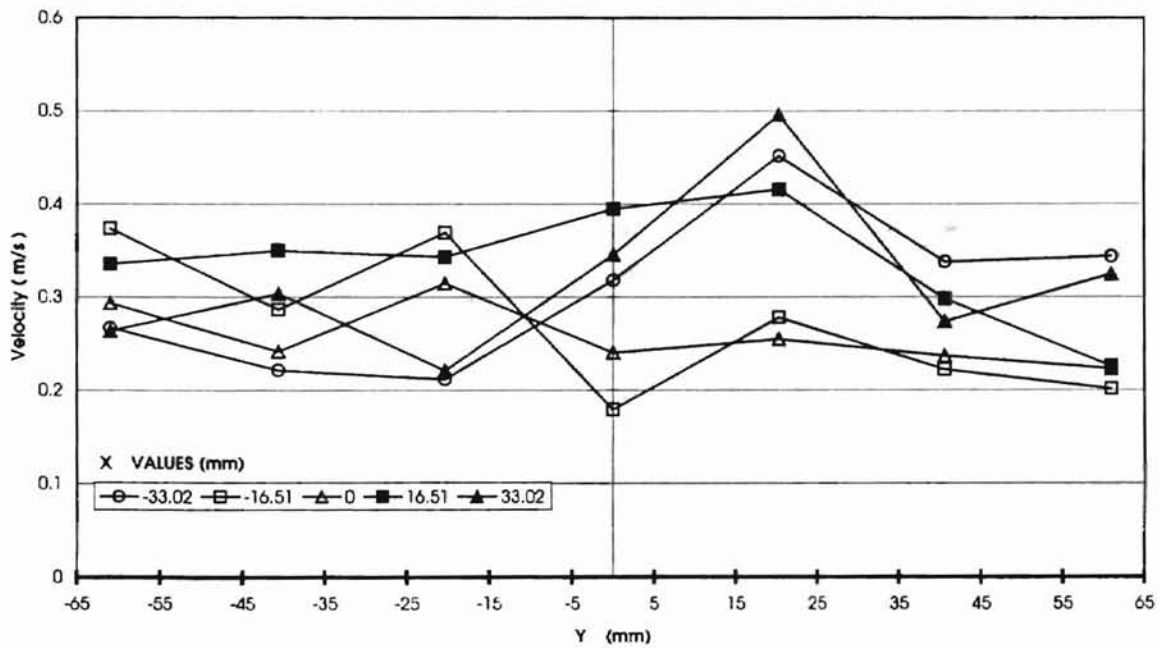


Figure 5-12 Downstream Velocity Profile for a Flow Rate of 27.2 m³/hr

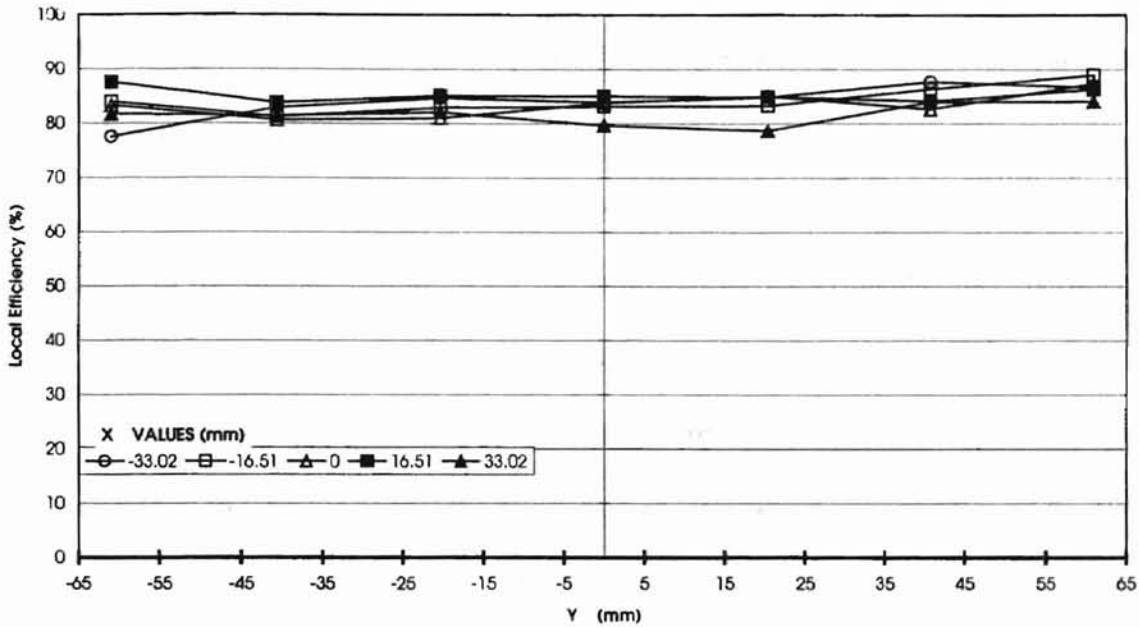


Figure 5-13 Efficiency Profile for a Flow Rate of 340.1 m³/hr

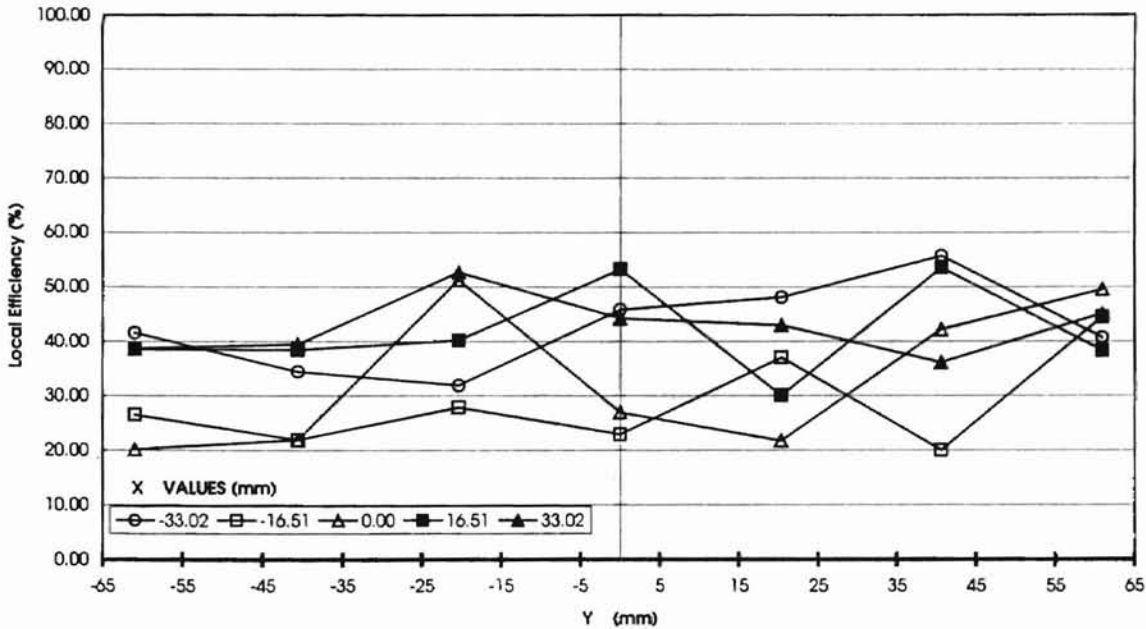


Figure 5-14 Efficiency Profile for a Flow Rate of 27.2 m³/hr

5.5 Overall Results

The integrated overall efficiency results are plotted against the flow rate and velocity shown on the abscissa.

These results are compared with those of Saxena (1998). It was explained earlier that, because of the similar conditions for the setup and the experiments, his experiments were treated as a setup without charge elimination.

The integrated overall results for the 2.02 micron diameter particles are shown in Figs. 5-15 and 5-16. As can be seen in these figures, efficiency was sensitive to the flow rate in the filter. There was a continuously rising efficiency with increasing flow rate for both of the particle diameters. This increasing variation followed a narrower band for Fig. 5-15. This is in comparison with Fig. 5-16, which showed a much broader band. The efficiency values ranged from a low of approximately 40% at 0.2 m/s to around 90% at around 5 m/s, for both the ungrounded and grounded experimental setups. The grounded (charge-neutralized) setup showed lower values of efficiency for the entire range of flow. At lower flow rates, the difference in efficiencies obtained from the grounded and ungrounded setup is even higher.

Higher efficiency occurring for the ungrounded setup (charged particles) could be attributed due to two possible reasons (Spurny, 1998).

- a) If the filter surface is charged, the charged particles may experience a Coulombic force of attraction with the filter surface, thereby increasing the collision efficiency.
- b) If the filter surface is neutral, the charged particles may induce a dipolar effect on the filter surface and thus increase the adhesion efficiency.

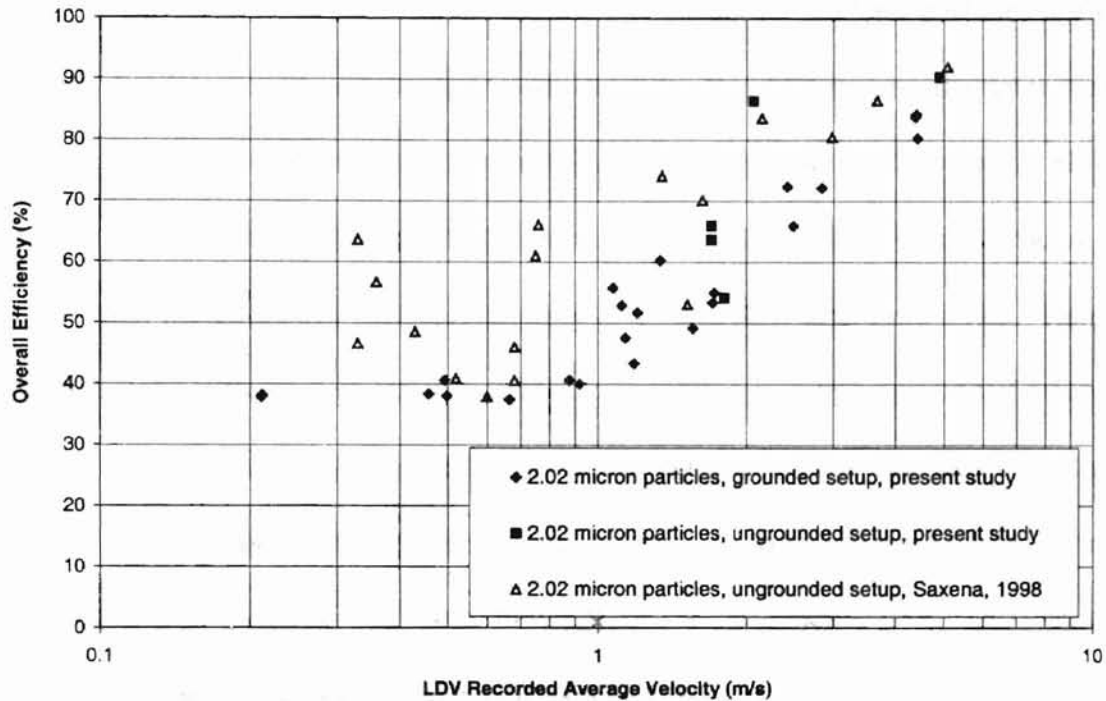


Figure 5-15 Overall Efficiency for 2.02 Micron Particles as a Function of LDV Recorded Velocity with and without the Effects of Charge Neutralization Compared with the Results of Saxena (1998)

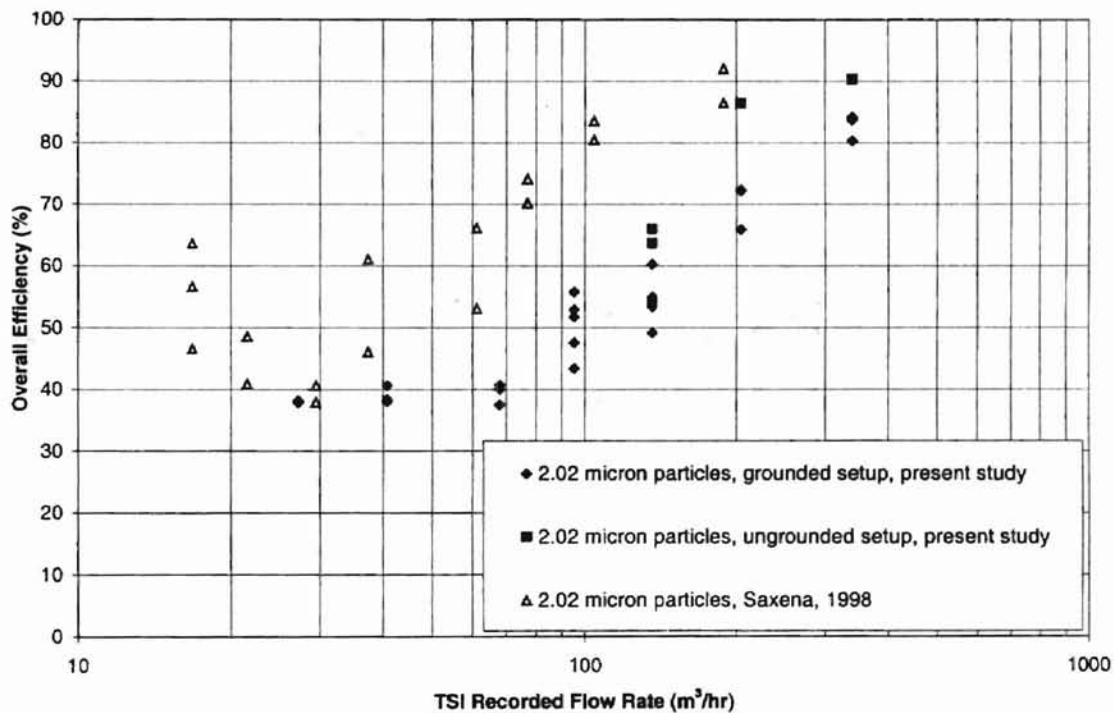


Figure 5-16 Overall Efficiency for 2.02 Micron Particles as a Function of TSI Recorded Flow Rate with and without the Effects of Charge Neutralization Compared with the Results of Saxena (1998)

The integrated overall results for the 0.505 micron diameter particles are shown in Figs. 5-17 and 5-18. These plots, like those for the 2.02 micron diameter particles, also show a trend of increasing efficiency with increasing higher flow rates. However, the range varied from 20% to 40% from a velocity of around 0.2 m/s to around 2 m/s, after which the efficiency increased sharply to around 85% at around 8 m/s. Here there was not much difference in the values for the grounded and the ungrounded setup. This is possibly because the 0.505 micron particles, being smaller in diameter than the 2.02 micron particles, produce less electrostatic charge. Also as seen for the 0.505 micron particles, the efficiency plot as a function of LDV velocity (Fig. 5-17) showed a narrower band as compared to the plot as a function of TSI flow meter recorded flow rate (Fig. 5-18).

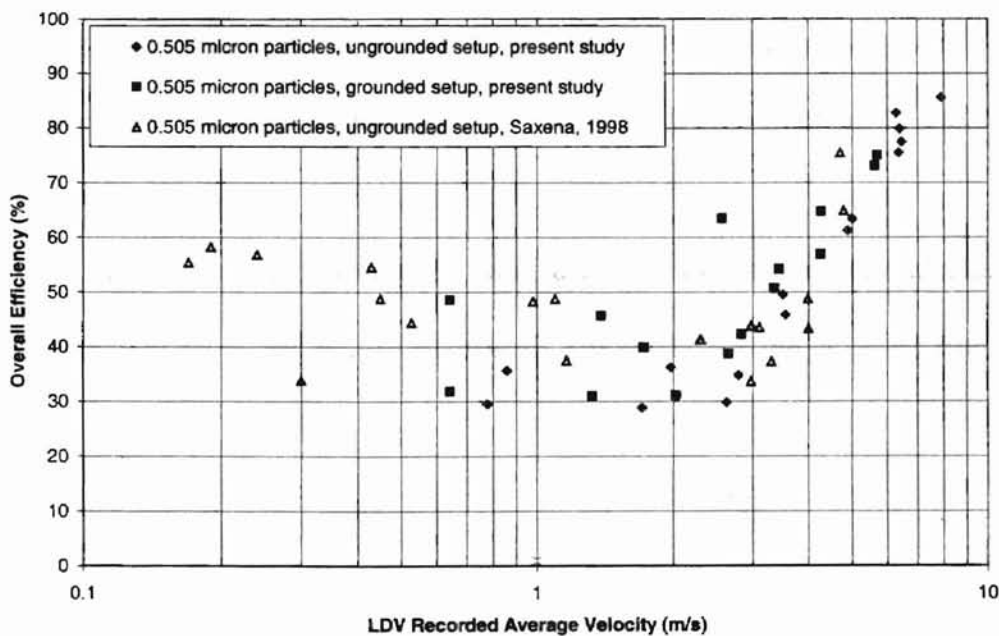


Figure 5-17 Overall Efficiency for 0.505 Micron Particles as a Function of LDV Recorded Velocity with and without the Effects of Charge Neutralization Compared with the Results of Saxena (1998)

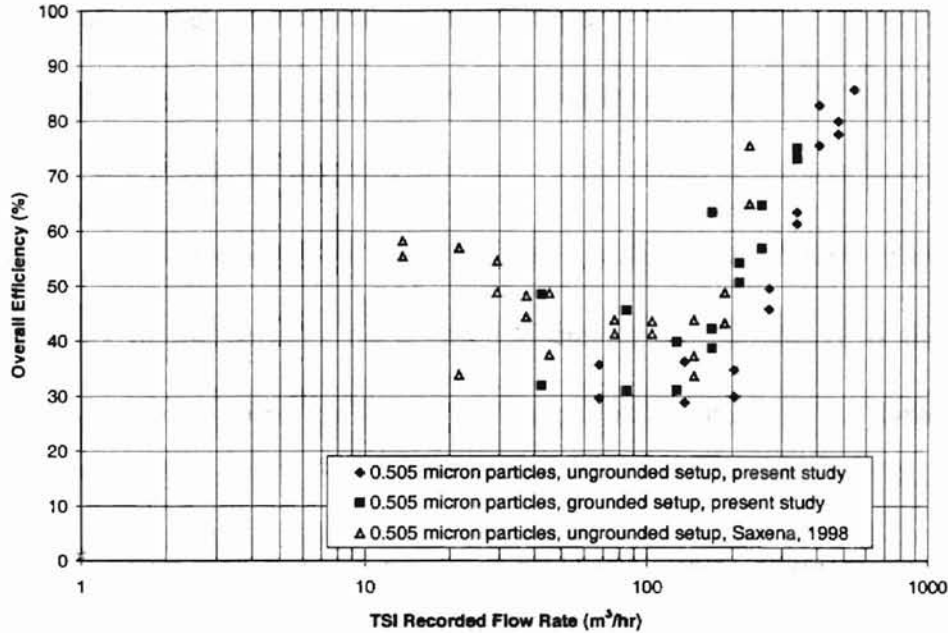


Figure 5-18 Overall Efficiency for 0.505 Micron Particles as a Function of TSI Recorded Flow Rate with and without the Effects of Charge Neutralization Compared with the Results of Saxena (1998)

In order to compare the results of the experimental work in this thesis with theory, the author employed two models. Most theoretical work in the inertial interception regime models single fiber efficiency of a filter using Stokes number as a convenient datum.

The following correlation was used by this author to calculate single fiber efficiency η from the values of overall efficiency for the A13192 filter given by the relation as

$$\eta_{\text{overall}} = 1 - e^{-\left(\frac{4\alpha\eta}{\pi(1-\alpha)D_f}\right)h_f} \quad (5-1)$$

where η_{overall} is the measured value of the overall filtration efficiency, α is the packing density whose value is not known for the filter under consideration, D_f is the diameter of the filter fiber of 38 μm , and h_f is the height of the filter paper (a value of 700 μm

(Jadbabaei, 1997)). Because the value of α is not known for the filter under consideration, the ordinate was modeled as $\eta \alpha/(1-\alpha)$.

Stokes number is defined in the following relation as

$$St = C_n \rho_p (D_p)^2 V / (18 \mu_a D_f) \quad (5-2)$$

where C_n is the Cunningham correlation factor defined elsewhere in this chapter, ρ_p is the density of the particle, D_p is the diameter of the particle, V is the velocity of air (which is assumed to be the velocity of the particle), and μ_a is the dynamic viscosity of air.

The first model, which proposed by Duran (1995), basically employs the inertial impaction model of Landahl and Hermann (1949) and the interception effects proposed by Lee and Liu (1982) (see Eq. (2-5)). Adhesion effects proposed by Ptak and Jaroszczyk (1990) are utilized.

The author also developed a model using the formula for collision efficiency in the inertial interception region as proposed by Suneja and Lee (1974) (see Eq. (2-6)) and combined it with the adhesion effects of Ptak and Jaroszczyk (1990). The model of Suneja and Lee (1974) was suitable for the transition regime where Re_f is less than 100. For the present study, all values of Re_f lie in the transition regime between 0.2 (this corresponds to a velocity of 0.1 m/s) and 20 (this corresponds to a velocity of 9 m/s).

The theoretical and experimental values of $\eta \alpha/(1-\alpha)$ are plotted against Stokes number for the particles with diameters 2.02 microns, 0.966 micron and 0.505 micron (see Figs. 5-19 to 5-21).

The model of Suneja and Lee (1974) shows good agreement with the efficiency curve for the 2.02 micron diameter particles when no charge is present in the flow (see

Fig. 5-19). However, the tests performed with the ungrounded setup, have higher efficiency values than those predicted by the model of Suneja and Lee. It was explained earlier in this section that the presence of electrostatic charge on the particles can increase filtration efficiency. The theoretical model of Suneja and Lee underpredicts efficiencies for the charged setup possibly because this model does not account for electrostatic charge effects in the calculation of filtration efficiency. Also, in Fig. 5-19, for a Stokes number less than 0.3, Duran's model underpredicts filtration efficiencies. This might be because of diffusion effects setting in at low flow rates, which serve to increase the efficiency of the filter.

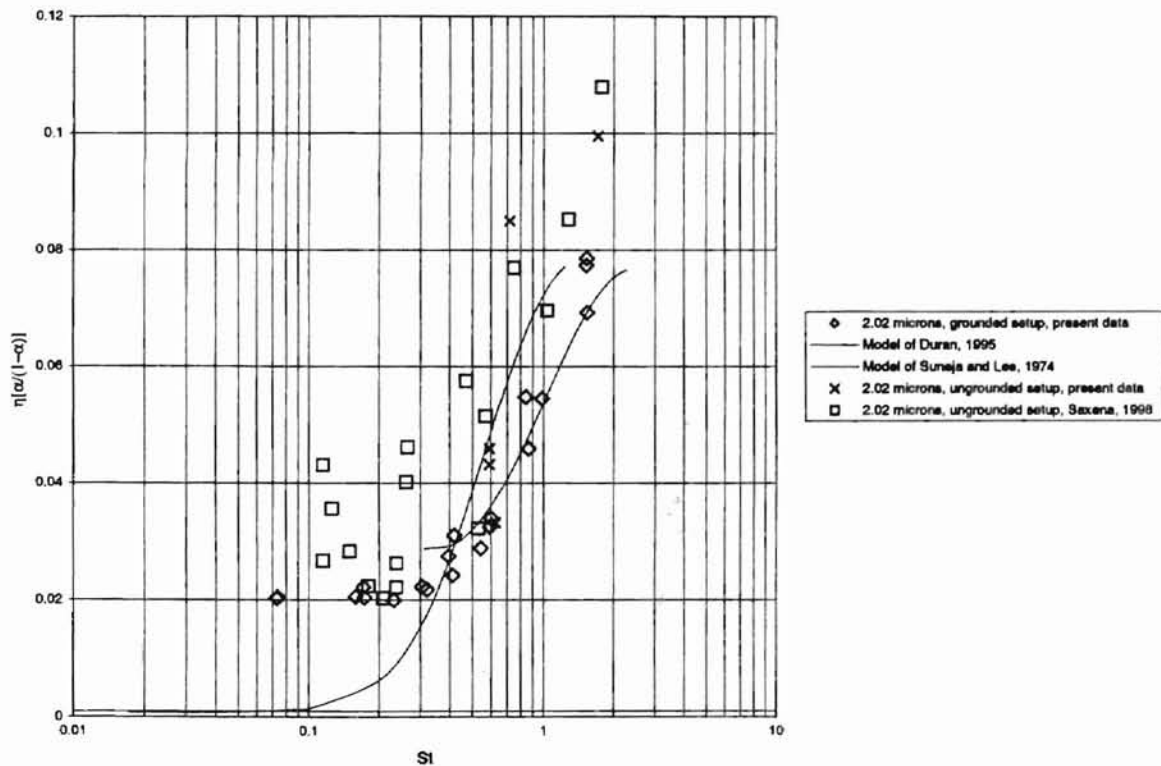


Figure 5-19 Comparison of Theoretical and Experimental Values for 2.02 Micron Particles

For the 0.966 micron particles (Fig. 5-20), the set of experiments performed by Gebreegziabher were plotted for comparison purposes. The model of Duran again vastly underpredicts $\eta\alpha/(1-\alpha)$ at lower Stokes number for the 0.966 micron particles. This again might be due to diffusion effects at those lower flow rates. For this particle size, however, there is a better prediction by the models for Stokes number between 0.3 and 0.6.

The model of Duran underpredicts $\eta\alpha/(1-\alpha)$ at all Stokes number for the 0.505 micron particles. The Suneja and Lee model is not valid for the range of Stokes number plotted in Fig. 5-21.

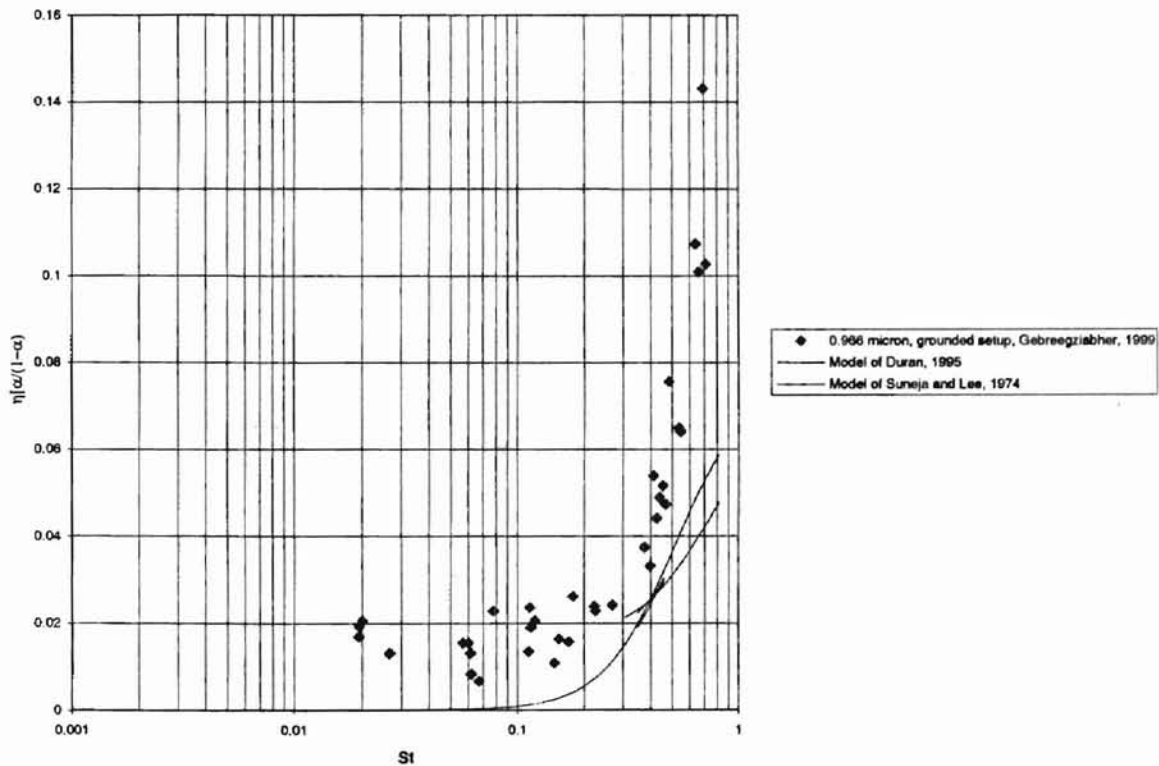


Figure 5-20 Comparison of Theoretical and Experimental Values for 0.966 Micron Particles

In general, the lower particle sizes of 0.966 micron and 0.505 micron do not

validate the theoretical models in the correlation of efficiency with Stokes number as well as the 2.02 micron particles do. A possible reason for this may be because, for the set of flow rates in this study, the Stokes number values corresponding to the 0.505 micron and 0.966 micron particle sizes were lower as compared to those for the 2.02 micron particle sizes (see Figs. 5-19 to 5-21). Thus, the inertial impaction mechanism may not be adequate as an abscissa in these models. A new abscissa to model filtration efficiency is discussed in Section 5.8.

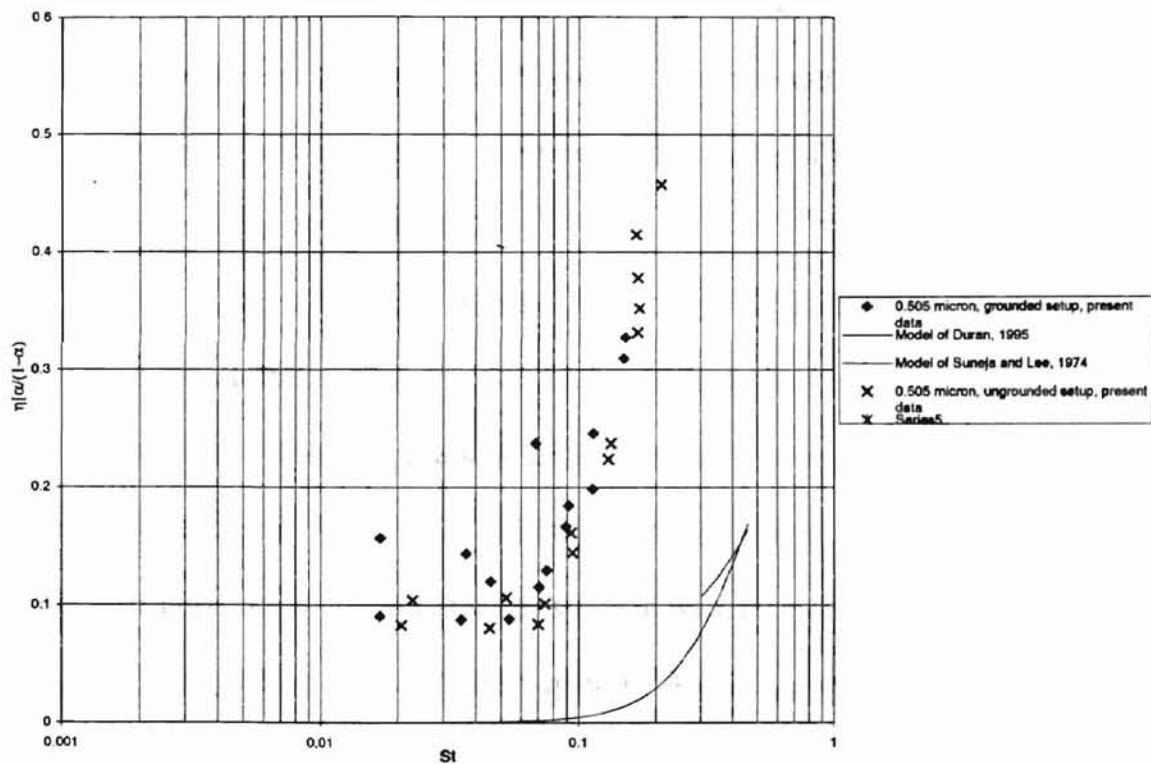


Figure 5-21 Comparison of Theoretical and Experimental Values for 0.505 Micron Particles

Gebregziabher (1999) suggested that inaccuracy in modeling of filtration efficiency may be due to the approximation of two-dimensional effects in the models.

Also, at lower flow rates, diffusion may become a more prominent mechanism of filtration (Saxena, 1998).

5.6 Fractional Efficiency Results for Bidisperse Aerosols

In Chapter 3, this author discussed how signal validity could be used to detect the fractional ratio of the number particles of a particular size in a mixture. In this section, the author attempts to establish a technique to measure the fractional efficiency of filters for a mixture with two different particle sizes.

Table 5-2 is a list of all the tests that were performed to analyze how well the measurement technique, discussed in Chapter 3, can measure the fractional number ratios of particle sizes in two particle mixtures. The results of all of the tests listed in Table 5-2 are presented in Appendix C.

As an example, in Test13 of Table 5-2 (see Fig. 5-22), a solution (Mixture A) of 10 ml of 2.02 micron PSL particles in 500 ml. of distilled water (a concentration of $1/50 \text{ m}^3/\text{m}^3$) was prepared. This concentration of the solution is indicated in the column with the heading labeled as "Mixture A Concentration" in Table 5-2. Number density measurements upstream of the filter for this solution were recorded for a flow rate of $170 \text{ m}^3/\text{hr}$ using the procedure described in Chapter 4. Another solution (Mixture B) of 10 ml of 0.505 micron PSL particles in 1000 ml of distilled water (a concentration of $1/100 \text{ m}^3/\text{m}^3$) was prepared. The concentration of this solution is indicated as the column heading labeled "Mixture B Concentration" in Table 5-2. The two solutions for Size A and Size B were mixed in equal volumes. Thus the strength column for size A and Size B was the same and calculated as volume of the solution of Size A or B in the mixture divided by the total volume of the solution mixture. The mixture was then fed

Table 5-2 Fractional Efficiency for Two Particle Mixtures with Varying Flow Rate

File Name	Test Date	Alignment Temperature	High Voltage	Mixture A			Mixture B		
				Size	Concentration	Strength	Size	Concentration	Strength
				Degrees C	V	Micron(s)	m ³ /m ³	Ratio	Micron(s)
ST2_1A.xls	6/6/99	24.20	775	2.02	10/1000	4/5	0.966	10/1000	1/5
ST2_05a.xls	6/6/99	24.20	700	2.02	15/750	1/3	0.505	10/1000	2/3
ST2_05b.xls	6/6/99	24.20	700	2.02	15/750	1/3	0.505	10/1000	2/3
ST2_05c.xls	6/7/99	24.20	700	2.02	15/750	1/3	0.505	10/1000	2/3
ST05_1a.xls	6/6/99	24.20	725	0.966	5/1000	2/5	0.505	10/1000	3/5
ST05_1b.xls	6/6/99	24.50	700	0.966	5/1000	2/5	0.505	10/1000	2/5

Table 5-3 Mixtures Analyzed to Predict the Expected Validity Based on the Calibrations

File Name	Test Date	Alignment Temperature	Flow	Mixture A			Mixture B		
				Size	Concentration	Strength	Size	Concentration	Strength
				Degrees C	m ³ /hr	Micron(s)	m ³ /m ³	Ratio	Micron(s)
Test 19.xls	5/31/99	22.60	170	2.02	1/100	1/2	0.966	1/200	1/2
Test13.xls	5/23/99	25.00	170	2.02	1/50	1/6	0.505	1/100	5/6
Test14.xls	5/23/99	25.00	170	2.02	1/50	1/2	0.505	1/100	1/2
Test16.xls	5/23/99	25.00	170	2.02	1/50	1/6	0.505	1/100	5/6
Test17.xls	5/23/99	25.00	170	2.02	1/50	1/2	0.505	1/100	1/2
Test18.xls	5/23/99	25.00	170	2.02	1/50	1/11	0.505	1/100	10/11
Test 19.xls	6/1/99	22.60	170	0.966	1/200	1/4	0.505	1/200	3/4
Test 19.xls	6/2/99	22.60	170	2.02	1/100	1/6	0.966	1/200	1/6

through the atomizer into the small angle housing, and the signal validity was measured at different values of high voltage. Using the method described in Section 3.4, the fractional amounts of the 2.02 micron and 0.505 micron particles were predicted. The fractional amounts predicted using the technique described in Section 3.4 were then compared with known values of the mixture ratio, which were calculated by measuring number density for each particle size individually and then calculating an expected number ratio. The accuracy of predicting the relative amounts for all diameters in the mixture is seen in Fig. 5-22. All of the results for the class of experiments shown in Table 5-2 are presented in Appendix C.

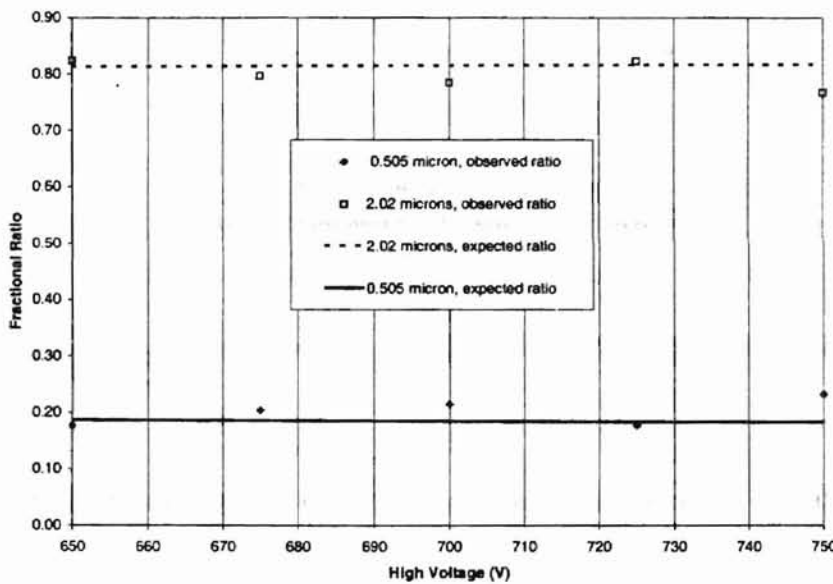


Figure 5-22 Accuracy of Predicting Fractional Ratio in a Bidisperse Mixture of 2.02 Micron and 0.505 Micron Diameter Particles by Comparing Known Mixture Ratios with Predicted Ratios

The next part of the study was aimed at studying the effect of fractional efficiency with varying flow rate. The flow rate was varied from 85.01 m³/hr (50 scfm) to 255.04 m³/hr (150 scfm). As can be seen in the Figs. 5-23 to 5-25, the overall efficiency points follow an increasing trend with increasing velocity.

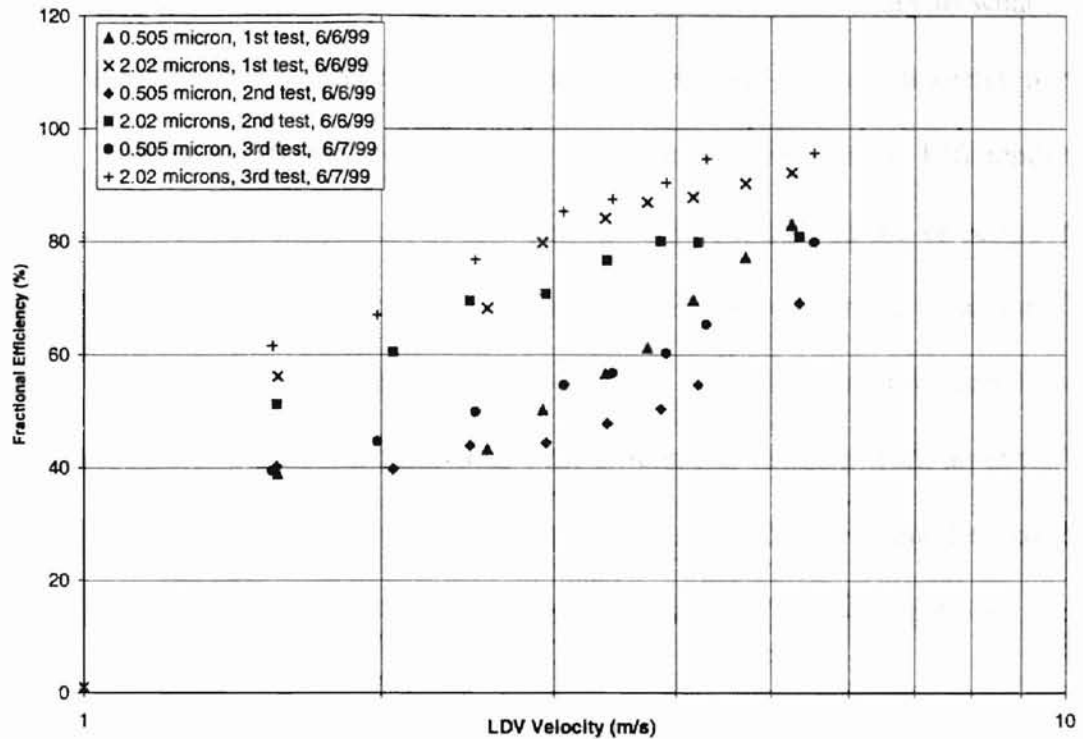


Figure 5-23 Fractional Efficiency as a Function of LDV Velocity for a Bidisperse Aerosol Mixture of 2.02 Micron and 0.505 Micron Particles

The bidisperse mixture of 2.02 micron and 0.505 micron diameter particles showed a smooth increase in efficiency from a low of 40% to a high of 80% for the lower size (see Fig. 5-23). The higher size showed a variation from 50% to 90%. This higher efficiency was expected because it corresponds to a larger particle diameter in the inertial interception regime.

For the mixture containing 2.02 micron and 0.966 micron diameter particles (Fig. 5-24) the 0.966 micron diameter particle curve shows continuously increasing efficiency from a low of 40% to high of 70%. For the 2.02 micron diameter particle, efficiencies increased from 72% to 95%.

For the mixture containing 0.966 micron and 0.505 micron diameter particles (Fig. 5-25), the 0.966 micron diameter particles show a lower efficiency than the 0.505

micron particle diameters for the entire range of flow, which is contrary to what might be expected in the inertial interception regime. The 0.505 micron diameter particle curve starts around an efficiency of 48% for a flow rate close to 1.5 m/s. Efficiency then increases to 60% at a velocity of 2 m/s and then again falls to 35% as the velocity further increases. This oscillating behaviour continues until it reaches a value of around 70% corresponding to a velocity of approximately 5.5 m/s. The 0.966 micron particle curve also shows a similar oscillating behaviour with efficiencies ranging from an initial low of 25% to a high of approximately 62%. The author was unable to explain the reason for this behaviour of the mixture containing 0.966 micron and 0.505 micron particles.

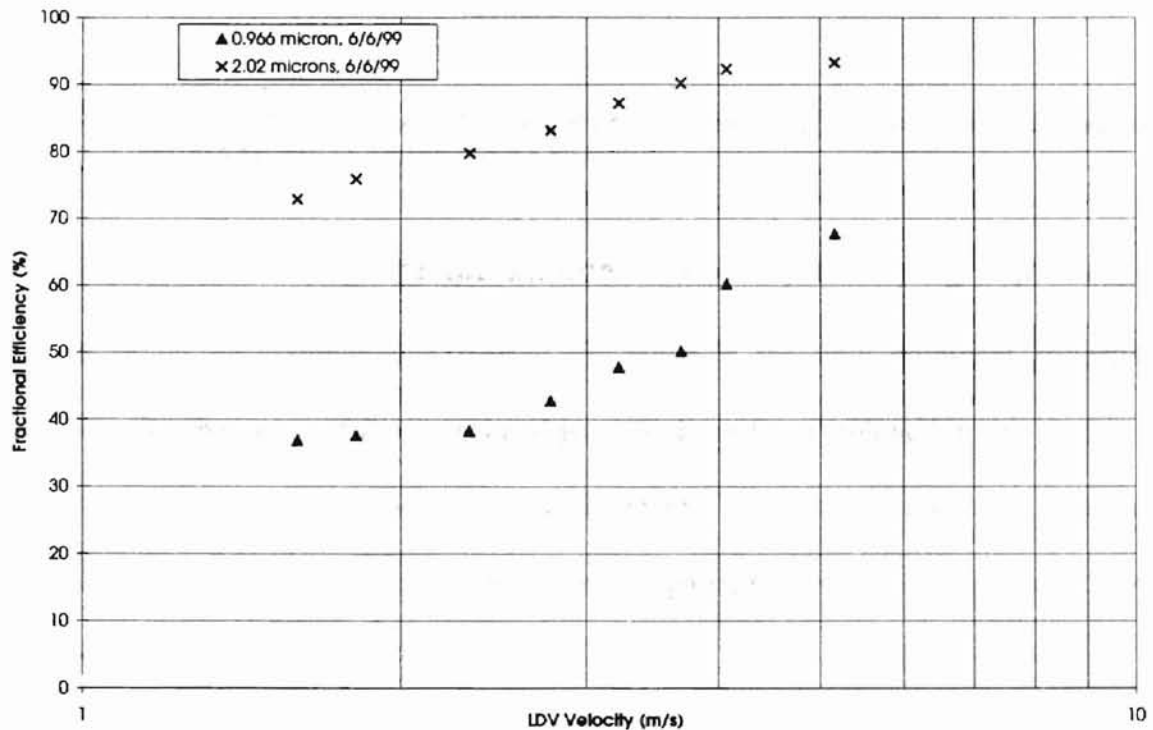


Figure 5-24 Fractional Efficiency as a Function of LDV Velocity for a Bidisperse Aerosol Mixture of 2.02 Micron and 0.966 Micron Particles

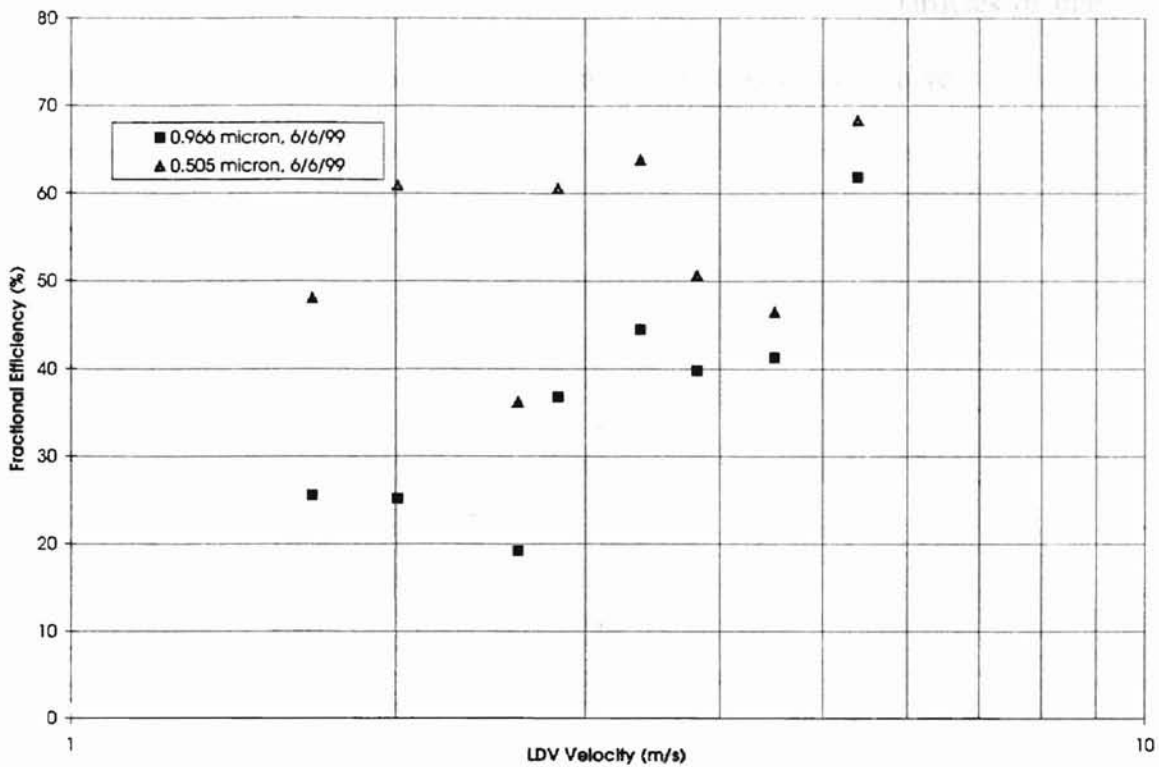


Figure 5-25 Fractional Efficiency as a Function of LDV Velocity for a Bidisperse Aerosol Mixture of 0.966 Micron and 0.505 Micron Particles

5.7 Empirical Modeling of Experimental Results by Modifying Slip Factor

It might be assumed that inertial impaction is the only dominant collection mechanism for the range of flow rates and particle diameters employed in this study. If so, the efficiency must then be explicitly dependent upon Stokes number. Thus, an efficiency versus Stokes number plot including all particle sizes should yield one curve, regardless of particle diameter.

Figures 5-26 and 5-27 are plots of overall efficiency against Stokes number for monodisperse particles with diameters of 2.02 microns, 0.966 micron and 0.505 micron. Both of these figures show a widely scattered spread of overall efficiency with Stokes number. These graphs together do not display any apparent trend in the behaviour of

efficiency with varying Stokes number. The plots for all of the particles of diameter 2.02 microns, 0.966 micron and 0.505 micron do not yield a single curve.

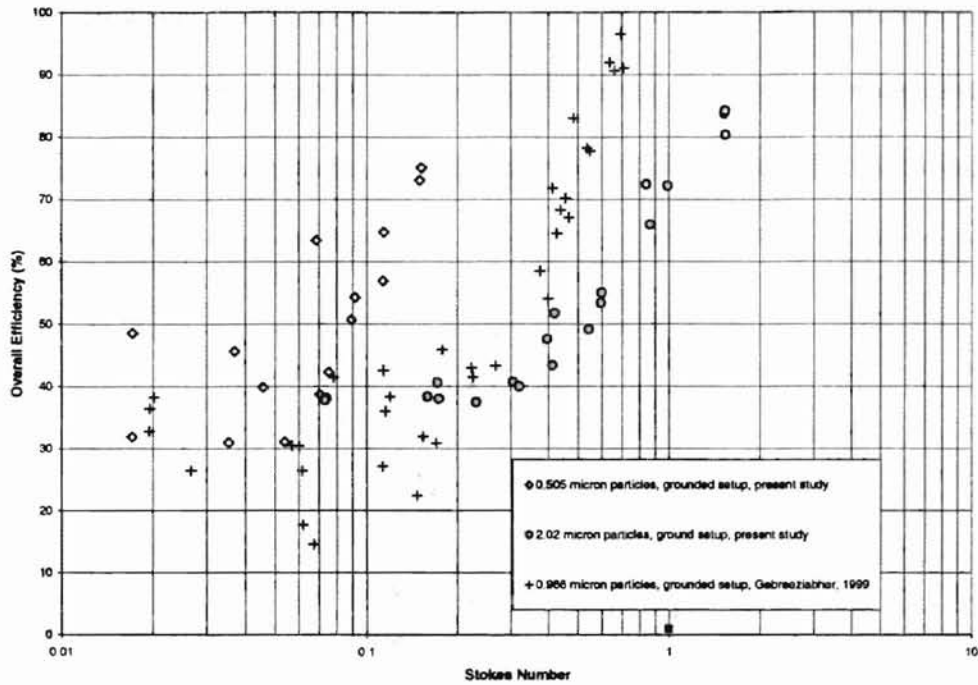


Figure 5-26 Efficiency as a Function of Stokes Number for 2.02, 0.966 and 0.505 Micron Particle Diameters in the Charge Neutralized Setup

Stokes number defined in Eq. (5-2) is directly proportional to the Cunningham Slip factor. This slip factor is defined in Eq. (5-3) below.

$$C_n = 1 + \frac{2A'\lambda}{D_p} + \frac{2Q'\lambda}{D_p} \exp\left(-\frac{B'D_p}{2\lambda}\right) \quad (5-3)$$

where $A' = 1.246$, $Q' = 0.42$, $B' = 0.87$ are essentially curve fitted constant values and λ (mean free path of air molecules) is $0.065 \mu\text{m}$ at 20°C and $1.013 \times 10^5 \text{ Pa}$. In order to collapse the curves, the constants in the defining equation of the slip factor of Eq. (5-3) were modified so that all three particle diameter curves (0.505 micron, 0.966 micron, and 2.02 microns) may collapse into a single curve on the Stokes number plot. Of the three curve fitted constants in Eq. 5-3, changing the value of Q' was seen to have

the most prominent effect in collapsing the overall efficiency curves. Changing the value of Q' in Eq. (5-3) to 1000 reduced the scatter band as seen in Fig. 5-26 and Fig. 5-27. However, the author's attempts to collapse the overall efficiency curves for the three particle sizes of 0.505 micron, 0.966 micron and 2.02 microns into a single curve against Stokes number did not meet with much success (see Figs. 5-28 and Fig. 5-29).

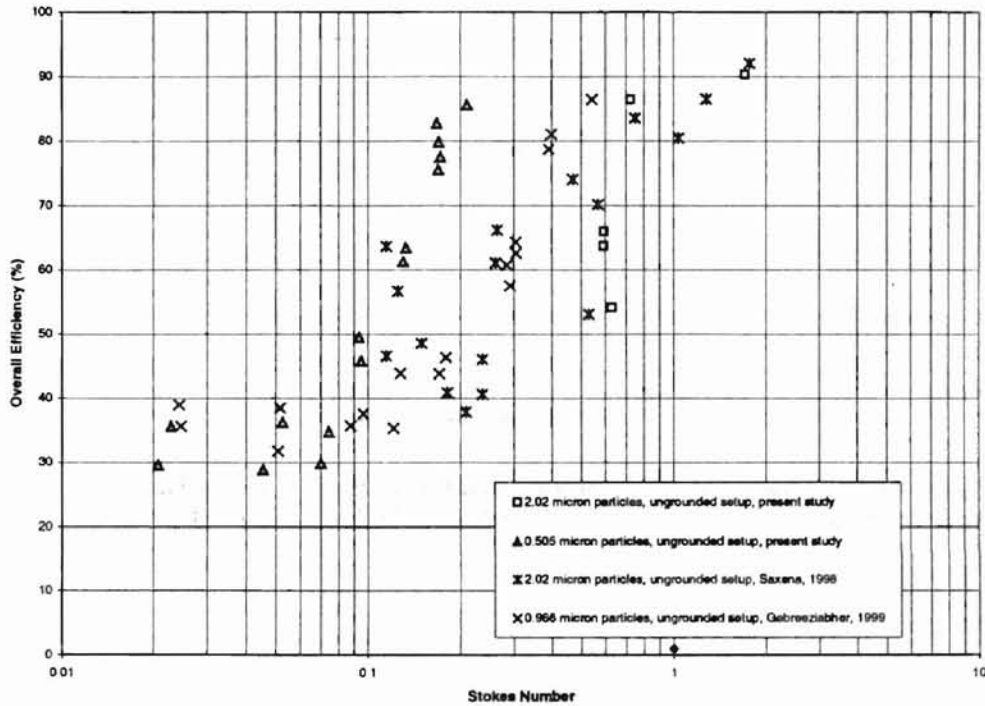


Figure 5-27 Efficiency as a Function of Stokes Number for 2.02, 0.966 and 0.505 Micron Particle Diameters in the Charged Setup

5.8 Empirical Model for Inertial Interception Regime

It was seen in Section 5.7 that modeling overall efficiency with Stokes number for different particle sizes did not yield one single curve as desired and expected.

In an attempt to model fibrous filter efficiency in the inertial impaction and interception regime, it is assumed that, since single fiber efficiencies are not only dependent upon Stokes number but also on the interception parameter, the abscissa must

take into account both of these factors. This is because Stokes number is purely an inertial number with no information on interception.

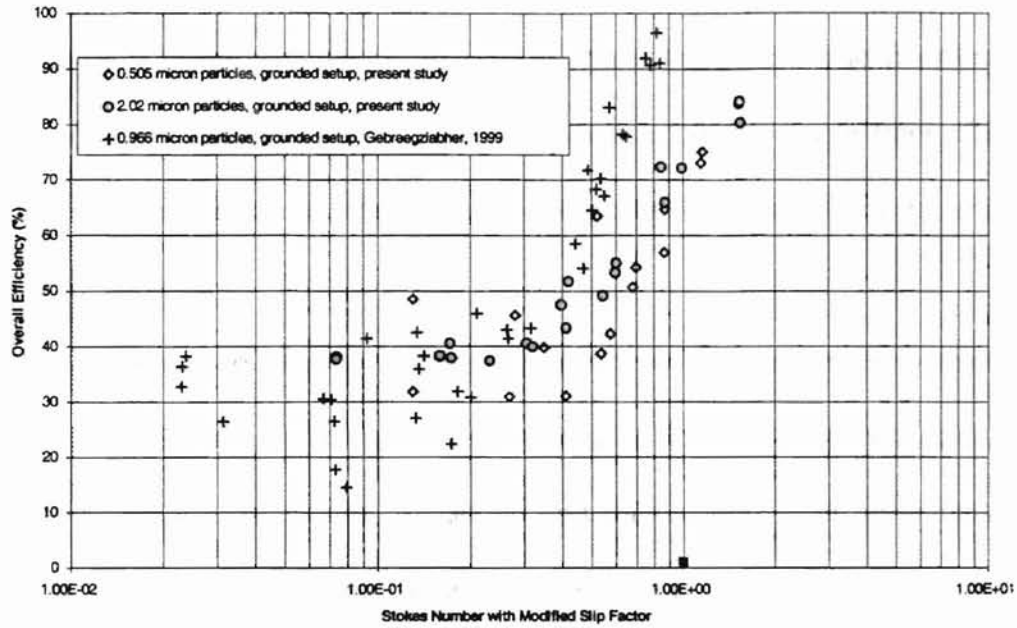


Figure 5-28 Efficiency as a Function of Stokes Number with Modified Slip Factor ($Q' = 2000$) for 2.02, 0.966 and 0.505 Micron Particle Diameters in the Charge Neutralized Setup

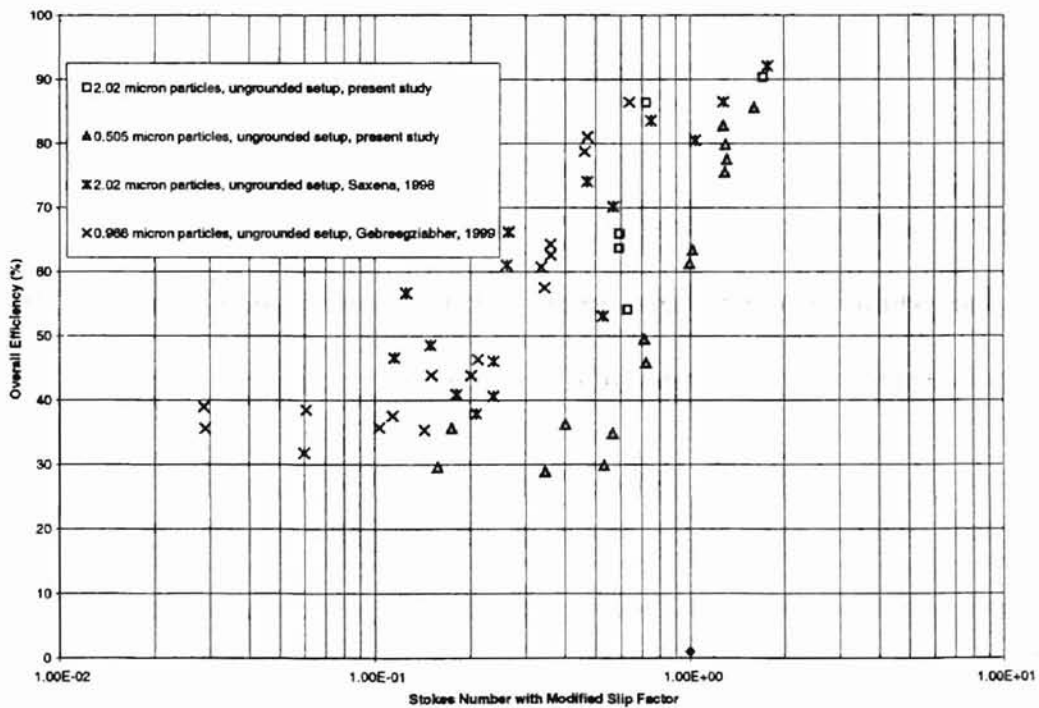


Figure 5-29 Efficiency as a Function of Stokes Number with Modified Slip Factor ($Q' = 2000$) for 2.02, 0.966 and 0.505 Micron Particle Diameters in the Charged Setup

If the combined effect of inertial impaction and interception is to be plotted, it's not sufficient to plot using Stokes number alone and an interception parameter (D_p/D_f) must be taken into account. Results expressed as a function of St cannot be compared unless three of the parameters, air velocity, particle diameter and fiber diameter are the same (Lastow and Podgorski, 1998). In Section 5.6, the single fiber efficiencies were plotted against Stokes number for only one particle size in each of the graphs (see Figs. 5-19 to 5-21).

In order to determine the appropriate plotting factor, it is assumed that the product of St and D_p/D_f raised to empirically determined powers can represent the combined affects of inertial impaction and interception when efficiency results from different particle sizes are plotted on the same graph. After trying out various combinations of the product of St and D_p/D_f , the author found that modeling $\eta\alpha/(1-\alpha)$ with $St^{0.73}(D_p/D_f)^{-1}$ fitted a 3rd order polynomial with a correlation coefficient of 0.89 using monodisperse particles with diameters of 2.02 microns, 0.966 micron and 0.505 micron (see Fig. 5-30).

In comparison, a plot of $\eta\alpha/(1-\alpha)$ for monodisperse particles with diameters of 2.02 microns, 0.966 micron and 0.505 micron against Stokes number only as shown in Fig. 5-31 gives a rather poor curve fit to a third degree polynomial equation with a curve coefficient of 0.55.

Only the tests involving the grounded setup were used so that the effect of electrostatic charge is reduced. Thus since all of the results were based on zero or low charge, inertial impaction and interception were primarily assumed dominant in this regime.

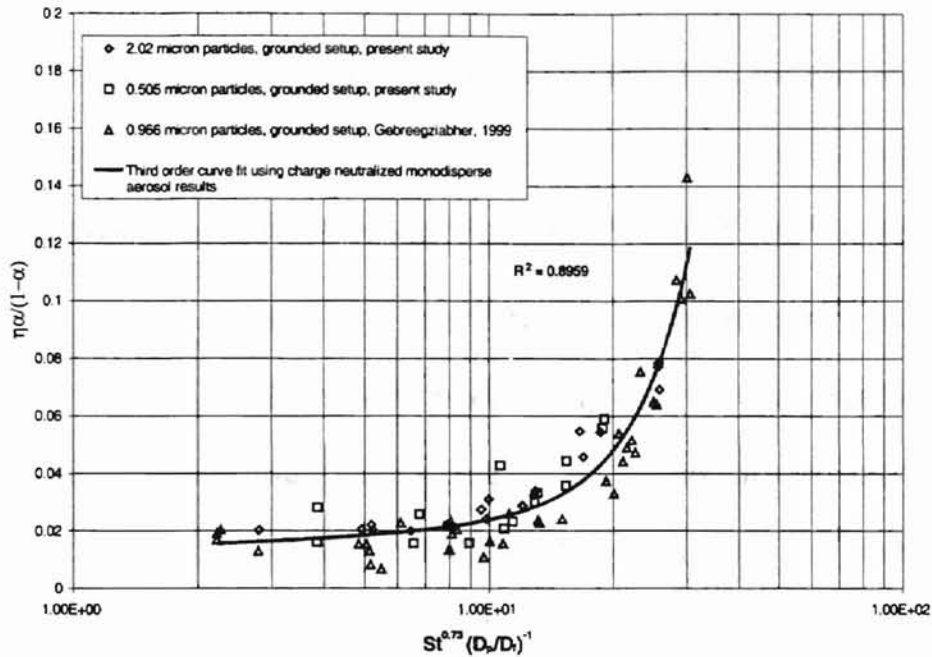


Figure 5-30 Efficiency ($\eta\alpha/(1-\alpha)$) vs. an Inertial Interception Parameter ($St^{0.73}(D_p/D_p)^{-1}$) for 2.02, 0.966 and 0.505 Micron Diameter PSL Particles in the Grounded Setup of the Small Angle Diffuser Housing

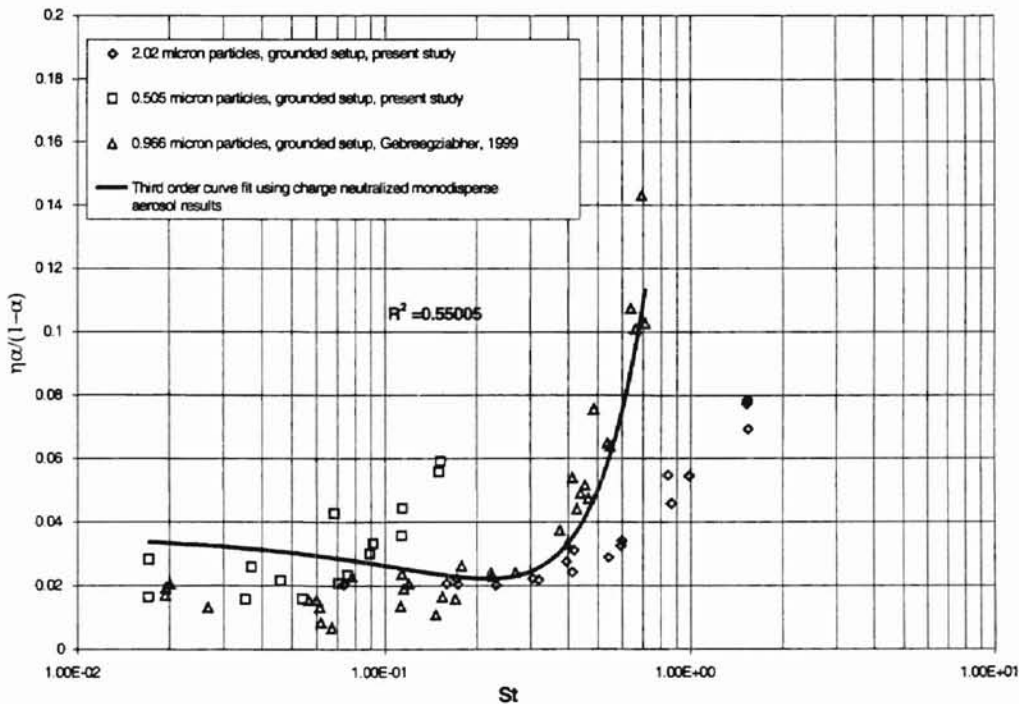


Figure 5-31 Efficiency ($\eta\alpha/(1-\alpha)$) vs. Stokes Number (St) for 2.02, 0.966 and 0.505 Micron Diameter PSL Particles in the Grounded Setup of the Small Angle Diffuser Housing

The polynomial curve fit equation formed from the data of Fig. 5-30 is shown below.

$$\begin{aligned} \eta\alpha/(1-\alpha) = & 4.5360 \times 10^{-06} \times (\text{St}^{0.73}(\text{D}_p/\text{D}_f)^{-1})^3 - 6.9463 \times 10^{-05} \times (\text{St}^{0.73}(\text{D}_p/\text{D}_f)^{-1})^2 \\ & + 1.3186 \times 10^{-03} \times \text{St}^{0.73}(\text{D}_p/\text{D}_f)^{-1} + 1.3200 \times 10^{-02} \end{aligned} \quad (5-4)$$

The polynomial equation shown in Eq. (5-4) was formulated on the basis of 66 data points with a correlation coefficient of 0.89. This curve fit equation was formulated with a value of St ranging from 0.017 to 1.541, and a value of D_p/D_f ranging from 0.013 to 0.053. Equation (5-4) may be used in the inertial interception regime when more than two of the three parameters, particle diameter (D_p), fiber diameter (D_f), and air velocity (V) are varied.

CHAPTER 6

SUMMARY AND RECOMMENDATIONS

6.1 Summary

The results and conclusions of the experiments in this study are summarized below.

- The initial pressure drop measurement across the filter was proportional to the average upstream velocity across the filter surface as measured by the LDV system (see Fig. 5-3). The correlation coefficient for a second order regression curve fit for a plot of initial pressure drop vs. the average upstream velocity was found to be 0.95.
- In order to avoid incorrect measurements using the LDV system, it was explained in Section 3.4 that the value of the high voltage amplification supplied to the PMTs must be carefully chosen. Region II (the region of decreasing validity) was found to be the most suitable region to carry out measurements for number density and efficiency in the present study.
- The local upstream velocities and number densities across the filter showed flat profiles as expected for the small angle diffuser housing. The local downstream velocities and number densities did not show flat profiles (see Section 5.4).
- Local efficiency profiles for the small angle diffuser housing are spread over a larger bandwidth at lower flow rates as compared to local efficiency profiles at higher flow rates (see Section 5.4).

- Overall efficiencies for the 2.02 micron and 0.505 micron diameter PSL particles showed an increasing trend with increasing flow rate in the small angle diffuser housing (see Section 5.5).
- For the 2.02 micron diameter particles, the tests conducted in the charge neutralized setup showed lower values of overall efficiency as compared to the tests conducted in the charged setup, for the entire range of flow as seen in Figs. 5-15 and 5-16. At lower flow rates, the difference in efficiencies between the charged and uncharged setup for the 2.02 micron diameter particles was more prominent, as compared to the efficiency difference at high flow rates.
- For the 0.505 micron diameter particles, electrostatic charge did not apparently show any effect on overall efficiency (see Figs. 5-17 and 5-18).
- Since the value of packing density (α) for the filter used in the present study is not exactly known, single fiber efficiency was represented by the expression $\eta\alpha/(1-\alpha)$ (see Section 5.5).
- Modeling $\eta\alpha/(1-\alpha)$ with the parameter $St^{0.73}(D_p/D_f)$ was able to collapse the efficiency curves for the PSL particles having diameters of 2.02 microns, 0.966 micron and 0.505 micron better than modeling $\eta\alpha/(1-\alpha)$ with Stokes number (St) (see Section 5.7). A reason for this might be because Stokes number being a purely inertial parameter does not correctly model single fiber efficiencies in the inertial and interception regime. Hence, the combined effect of inertial impaction and interception is needed to correctly model single fiber efficiencies within the inertial interception regime.
- The percentage of valid signals in a test run measured by the LDV system is a

characteristic function of PMT high voltage. Other LDV parameters remaining constant, signal-to-noise ratio is a function of particle size and the high voltage supplied to the PMTs (see Section 3.4).

- The bidisperse mixtures containing 2.02 microns and 0.966 micron; and 2.02 microns and 0.505 micron diameter PSL particles showed an increase in fractional efficiency with increasing flow rate. For both the mixtures, the lower particle size showed lower efficiency. For the bidisperse mixture containing 0.966 micron and 0.505 micron, no consistent trend was seen for the measured fractional efficiencies (see Section 5.6).

6.2 Recommendations

The author would like to suggest the following recommendations for future work in fibrous filtration efficiency measurements

- The empirical model, Eq. (5-5) in Section 5.7, can be further improved by conducting more tests in the inertial interception regime. This may be done by using more particle sizes in between 0.5 and 2 microns for the same flow rates examined in this study.
- For the present study, the author used the Purolator Products, Inc. A13192 filters for conducting all measurements. Filters with different properties (eg., fiber diameter) may be used to carry out measurements for filtration efficiency.
- The electrostatic charge on the surface filters can increase adhesion of particles on the fiber surface (Schmidt et al., 1998). Hence, electrostatic charge at the surface of the filter needs to be measured and regulated if possible. Brown (1998b) has proposed a technique to measure and eliminate electrostatic charge on the filter fiber

by providing ionizing radiation to a filter. According to Brown, a radiation dose of 1 R from an X-ray beam that produces 3.33×10^{-4} C of charge (in the form of positive and negative ions) in 1 m^3 of air, if applied to a filter, can neutralize the charge on filter fibers. In order to verify neutralization of the charge on the fiber using ionizing radiation, the following technique can be used. By measuring efficiency as a function of increased radiation dosage, the efficiency should eventually become independent of the radiation dose supplied, and hence should be related to the purely mechanical aspects of filtration. The value of radiation dosage at this efficiency can be used to infer the charge on the filter fiber (Brown, 1998b).

- Fractional efficiency measurements should be carried out for mixtures containing more than two particle sizes using the technique described in Section 3.5. This technique can then be used to study the effect of filtration efficiency dust, which is composed of particles of different sizes.
- To measure correct volume flow rates using the TSI flow meter, temperature at the location of the TSI flow meter sensor must be measured along with the flow rate.

REFERENCES

- Adrian, R.J. (1978), "Estimation of LDA Signal Strength and Signal-to-Noise Ratio," **TSI Quarterly**, Volume IV, Issue 1, February/March, pp. 3-9.
- Aerometrics Inc., a Division of TSI Inc. (1992), Doppler Signal Analyzer for Phase Doppler Particle Applications User's Manual, Sunnyvale, CA, draft 2.
- Aerometrics Inc. (1999), www.aerometrics.com (reference does not exist as of date).
- Agarwal, J. and Keady, P. (1980), "Theoretical Calculation and Experimental Observation of Laser Velocimeter Signal Quality," **TSI Quarterly**, Volume VI, Issue 1, February/March, pp. 3-9.
- Al-Sarkhi, A. (1999), "Filters Optimization Techniques for Design of Automotive Air Filter Housing with Improved Fluid Dynamics Performance," Ph.D. Thesis, School of Mechanical and Aerospace Engineering, Oklahoma State University, Stillwater, Oklahoma.
- Anand, S. (1997), "Filtration Efficiency Measurements on Pleated Filters," M. S. Thesis, School of Mechanical and Aerospace Engineering, Oklahoma State University, Stillwater, Oklahoma.
- Boulaud, D. and Renoux, A. (1998), "Stationary and Non-Stationary Filtration of Liquid Aerosols by Fibrous Filters," Advances in Aerosol Filtration, K. Spurny (ed.), pp. 13-25, CRC Press LLC, Boca Raton, Florida.
- Burroughs, H.E. (1995), <http://facilitiesnet.com/NS/NS3filtr.html>, Trade Press Publishing Corporation. (Also see Appendix G.)
- Brown, R.C. (1998a), "Air Flow Through Filters – Beyond Single Fiber Theory,"

- Advances in Aerosol Filtration, K. Spurny (ed.), pp. 153-172, CRC Press LLC, Boca Raton, Florida.
- Brown, R.C. (1998b), "Nature, Stability, and Effectiveness of Electric Charge in Filters," Advances in Aerosol Filtration, K. Spurny (ed.), pp. 219-240, CRC Press LLC, Boca Raton, Florida.
- Coherent Inc. (1991), Innova 70 Series Ion Laser Operator's Manual, Palo Alto, CA
- Davies, C. N. (1973), Air Filtration, Academic Press, New York, N. Y.
- Duran, R. (1995), "Improvement of Flow Uniformity and Modeling of Filtration Efficiencies for Automotive Air Filter Test Housings," M.S. Thesis, School of Mechanical and Aerospace Engineering, Oklahoma State University, Stillwater, Oklahoma.
- Eurovent (1988), "Eurovent 4/5 Method of Testing Air Filters used in General Ventilation," Eurovent/Cecomaf, Frankfurt, Germany.
- Flagan, R.C. and Seinfeld, J.H. (1988), Fundamentals of Air Pollution Engineering, Prentice Hall, Inc.
- Friedlander, S.K. (1998), "Aerosol Filtration by Fibrous Filters," Biochemical and Biological Engineering Science, N. Blakebrough (ed.), pp. 49-67, Academic Press Inc, New York, New York.
- Fuchs, N. A. (1964), The Mechanics of Aerosols, Pergamon Press, Oxford, England.
- Gebreegziabher, T. (1999), "Comparison of Filtration Efficiency of Pleated Filters for Different Particles," M.S. Thesis, School of Mechanical and Aerospace Engineering, Oklahoma State University, Stillwater, Oklahoma.
- Gougeon, R., Boulad, D., Fissan, H., Lange, R., and Renoux, A. (1994), "Filter Surfaces

- Loading with Liquid Aerosols by Confocal Microscopy," **Journal of Aerosol Science**, Vol.25, Suppl. 1, pp. S209-S210
- Hinds, W. C. (1982), Aerosol Technology: Properties, Behaviour and Measurement of Airborne Particles, John Wiley & Sons Inc., New York, New York.
- Jadbabaei, F. M. (1997), "Filtration Efficiency Measurements on Pleated Filters," M.S. Thesis, School of Mechanical and Aerospace Engineering, Oklahoma State University, Stillwater, Oklahoma.
- Kline, S. J. and McClintock, F. A. (1953), "Describing Uncertainties in Single-Sample Experiments," **Mechanical Engineering**, January, Vol. 75, pt. 2, pp. 3-8.
- Landahl, H. D. and Hermann, R. G. (1949), "Sampling of Liquid Aerosols by Wires, Cylinders, and Slides, and the Efficiency of Impaction of the Droplets," **Journal of Colloidal Science**, Vol. 4, pp. 103-136.
- Lastow, O. and Podgorski, A. (1998), "Single Fiber Collection Efficiency," Advances in Aerosol Filtration, K. Spurny (ed.), pp. 25-52, CRC Press LLC, Boca Raton, Florida.
- Lee, K.W. and Liu, B.Y.H. (1982), "Theoretical Study of Aerosol Filtration by Fibrous Filters," **Aerosol Science and Technology**, Vol. 1, pp. 147-161.
- Liang, F. (1997), "Particle Counting and Sizing with LDV for Automotive Air Filters," Ph.D. Thesis, School of Mechanical and Aerospace Engineering, Oklahoma State University, Stillwater, Oklahoma.
- Liang, F., Natarajan, B., Tian, Y. and Dougherty, R. L. (1994), "Local Efficiency Measurements Applicable to Both Automotive Engine and Cabin Filtration," **Particulate Science and Technology**, Vol. 12, No. 4, Oct-Dec, pp. 333-350.

- Maus, R. and Umhauer, H. (1996), "Determination of the Fractional Efficiencies of Fibrous Filter Media by Optical In-Situ Measurements," **Aerosol Science and Technology**, Vol. 24, April, pp. 161-173.
- Pastuszka, J. (1998), "Inertial Impaction," Advances in Aerosol Filtration, K. Spurny (ed.), pp. 437-453, CRC Press LLC, Boca Raton, Florida.
- Ptak, T. J. and Jaroszczyk, T. (1990), "Theoretical-Experimental Aerosol Filtration Model for Fibrous Filters at Intermediate Reynolds Numbers," **Proceedings of the Fifth World Filtration Congress**, Nice, France, pp. 566-572.
- Saffman, M. (1987), "Automatic Calibration of LDA Measurement Volume Size," **Applied Optics**, Vol. 26, No. 13, July.
- Saxena, P. (1998), "Comparison of Filtration Efficiency of Pleated Filters for Different Particles," M.S. Thesis, School of Mechanical and Aerospace Engineering, Oklahoma State University, Stillwater, Oklahoma.
- Schmidt, E., Gutsch, A., and Maus, R. (1998), "Filter Efficiency Modeling, Electrically Stimulated Agglomeration and Separation of Bioaerosols - Some Recent Trends in Aerosol Research," Advances in Aerosol Filtration, K. Spurny (ed.), pp. 361-380, CRC Press LLC, Boca Raton, Florida.
- Schweers, E. and Loffler, F. (1994), "Realistic Modelling of the Behaviour of Fibrous Filter through Consideration of Filter Structure," **Powder Technology**, 80, pp-191-206.
- Society of Automotive Engineers (1993), "SAE J1669 Passenger Compartment Air Filter Test Code - SAE Recommended Practice," Proposed Draft, SAE, Inc., Warrendale, PA.

Society of Automotive Engineers (1987), "SAE J726 Air Cleaner Test Code - SAE Recommended Practice," Society of Automotive Engineers Handbook, SAE, Inc., Warrendale, PA.

Spurny, K. (1998), "Aerosol Filtration at the End of the 20th Century," Advances in Aerosol Filtration, K. Spurny (ed.), pp. 13-24, CRC Press LLC, Boca Raton, Florida.

Suneja, S.K., and Lee, C.H. (1974), "Aerosol Filtration by Fibrous Filters at Intermediate Reynolds Numbers (≤ 100), **Atmospheric Environment**, Vol. 8, pp. 1081-1094.

APPENDICES

APPENDIX A

RESULTS FOR MONODISPERSE AEROSOLS CONTAINING 2.02 MICRON DIAMETER PSL PARTICLES IN THE SMALL ANGLE DIFFUSER HOUSING

Some of the test results using 2.02 micron particles were discussed in Chapter 5. All of these test results are presented in this appendix. Each of the tests presented in this appendix shows the local efficiency, local upstream number density, local downstream number density, local upstream velocity, and local downstream velocity respectively.

The average values of the efficiency, upstream and downstream number density, upstream velocity and downstream velocity for the tests are tabulated in Table A-1. These average values can be correlated with the figures in this appendix using the test code indicated at the bottom right hand corner of each figure and indicated for each test in Table A-1. The alphanumeric code for each test is designated as indicated Section 5.5.

Table A-1 Test Conditions and Average Values over the Filter Surface of Efficiency, Upstream and Downstream Velocities, and Upstream and Downstream Number Densities for 2.02 Micron Particles in the Small Angle Diffuser Housing

No.	Test Code	Test Date	Corrected Flow Rate	Overall Average Efficiency of the Filter	Upstream Number Density	Upstream Velocity	Downstream Number Density	Downstream Velocity	Pressure Drop (mm Water Column)			PSL Solution Strength	Temp. Deg. C	RH %	Electrostatic Charge
			m ³ /hr	(%)	(m ⁻³)	m/s	(m ⁻³)	m/s	Initial	Final	Rise	m ³ /m ³	At Mixing Box	(V)	
1	125-2ag	1/6/99	340.06	83.71	5.13E+07	4.38	8.31E+06	7.07	38.1	40.6	2.5	7.5/1500	30	45	0
2	125-2bg	12/30/98	340.06	80.31	9.40E+07	4.42	1.67E+07	6.80	38.1	43	4.9	7.5/1500	36	36	-100
3	125-2cg	2/17/99	340.06	84.19	9.35E+07	4.40	1.47E+07	6.82	40.6	43.2	2.5	11/1100	33	43	-100
4	75-2ag	12/29/98	204.04	65.92	1.89E+08	2.49	6.43E+07	4.03	10.2	12.7	2.5	15/1500	40	36	-100
5	75-2bg	1/7/99	204.04	72.35	1.17E+08	2.42	3.23E+07	3.81	10.2	12.7	2.5	7.5/1500	24	47	0
6	75-2cg	2/16/99	204.04	72.15	1.15E+08	2.84	3.18E+07	4.54	12.7	12.7	0	11/1100	24	47	0
7	50-2ag	1/1/99	136.03	49.15	1.96E+08	1.56	9.95E+07	2.76	7.6	7.6	0	7.5/3000	27	24	0
8	50-2bg	2/3/99	136.03	53.35	8.15E+07	1.71	3.77E+07	2.74	7.6	7.6	0	15/3000	32	37	0
9	50-2cg	2/3/99	136.03	54.98	2.69E+08	1.72	1.20E+08	2.73	7.6	7.6	0	15/1400	31	45	0
10	50-2dg	2/22/99	136.03	60.28	2.76E+08	1.34	1.09E+08	2.08	7.6	7.6	0	11/1100	33	43	0
11	35-2ag	1/27/99	95.22	52.89	2.19E+08	1.12	1.02E+08	1.77	7.6	10.2	2.5	15/1400	35	47	0
12	35-2bg	1/28/99	95.22	55.75	1.94E+08	1.07	8.55E+07	1.68	7.6	7.6	0	15/1400	30	47	0
13	35-2cg	2/1/99	95.22	47.56	2.89E+08	1.14	1.52E+08	1.88	7.6	7.6	0	15/1400	31	47	0
14	35-2dg	2/2/99	95.22	43.35	3.17E+08	1.18	1.79E+08	2.04	7.6	7.6	0	15/1400	31	43	0
15	35-2eg	2/15/99	95.22	51.71	2.25E+08	1.20	1.08E+08	1.93	5.1	5.1	0	11/1100	32	48	0
16	25-2ag	1/2/99	68.01	30	2.89E+08	0.77	2.02E+08	1.29	3.8	5.1	1.3	2/1000	25	45	0
17	25-2bg	1/9/99	68.01	32	2.91E+08	0.72	1.98E+08	1.06	3.8	3.8	0	7.5/1500	27	45	0
18	25-2cg	2/6/99	68.01	40.66	3.60E+08	0.88	2.13E+08	1.36	3.8	5.1	1.3	2/1000	32	58	0

Table A-1 (continued)

Test No.	Test Code	Test Date	Corrected Flow Rate	Overall Average Efficiency of the Filter	Upstream Number Density	Upstream Velocity	Downstream Number Density	Downstream Velocity	Pressure Drop (mm Water Column)			PSL Solution Strength	Temp. Deg. C	RH %	Electrostatic Charge
			m ³ /hr	(%)	(m ⁻³)	m/s	(m ⁻³)	m/s	Initial	Final	Rise	m ³ /m ³	At Mixing Box	(V)	
19	25-2dg	2/8/99	68.01	39.98	2.90E+08	0.92	1.73E+08	1.50	5.1	5.1	0	5/1000	32	60	0
20	25-2eg	2/19/99	68.01	37.43	2.71E+08	0.67	1.69E+08	0.98	5.1	6.4	1.3	11/1100	32	45	0
21	15-2ag	1/3/99	40.81	25	8.60E+08	0.40	6.45E+08	0.65	2.5	2.5	0	2/1000	30	60	0
22	15-2bg	1/4/99	40.81	26	9.15E+08	0.43	6.79E+08	0.68	2.5	2.5	0	2/1000	20	60	0
23	15-2cg	2/7/99	40.81	38.32	7.96E+08	0.46	4.88E+08	0.83	2.5	3.8	1.3	15/3000	36	46	0
24	15-2dg	2/9/99	40.81	37.98	5.39E+08	0.50	3.33E+08	0.81	2.5	3.8	1.3	7.5/3000	32	52	0
25	15-2eg	2/14/99	40.81	40.59	3.62E+08	0.49	2.14E+08	0.74	2.5	3.8	1.3	11/1100	32	45	0
26	10-2ag	2/20/99	27.21	38.13	1.01E+09	0.21	6.19E+08	0.31	2.5	2.5	0	2/1000	30	50	0
27	10-2bg	2/22/99	27.21	37.81	9.49E+08	0.21	5.84E+08	0.30	2.5	2.5	0	2/1000	32	45	0
28	125-2au	10/15/98	340.0	90.32	1.04E+08	4.91	1.01E+07	7.36	45.7	50.8	5.1	15/750	35	55	NA
29	75-2au	8/30/98	204.0	86.4	1.82E+08	2.07	2.44E+07	3.46	10.2	NA	NA	15/750	45	38	-500
30	75-2bu	8/29/98	204.0	55.85	2.13E+08	2.39	9.42E+07	3.28	10.2	NA	NA	15/750	36	49	-500
31	50-2au	10/16/98	136.03	63.69	2.34E+08	1.70	8.46E+07	2.59	10.2	10.2	0.0	15/750	35	55	NA
32	50-2bu	10/24/98	136.03	65.94	2.86E+08	1.70	9.65E+07	2.58	7.6	10.2	2.5	15/750	39	39	NA
33	50-2cu	10/16/98	136.03	54.13	5.91E+07	1.81	6.29E+07	2.98	10.2	10.2	0.0	16/800	NA	54.9	NA

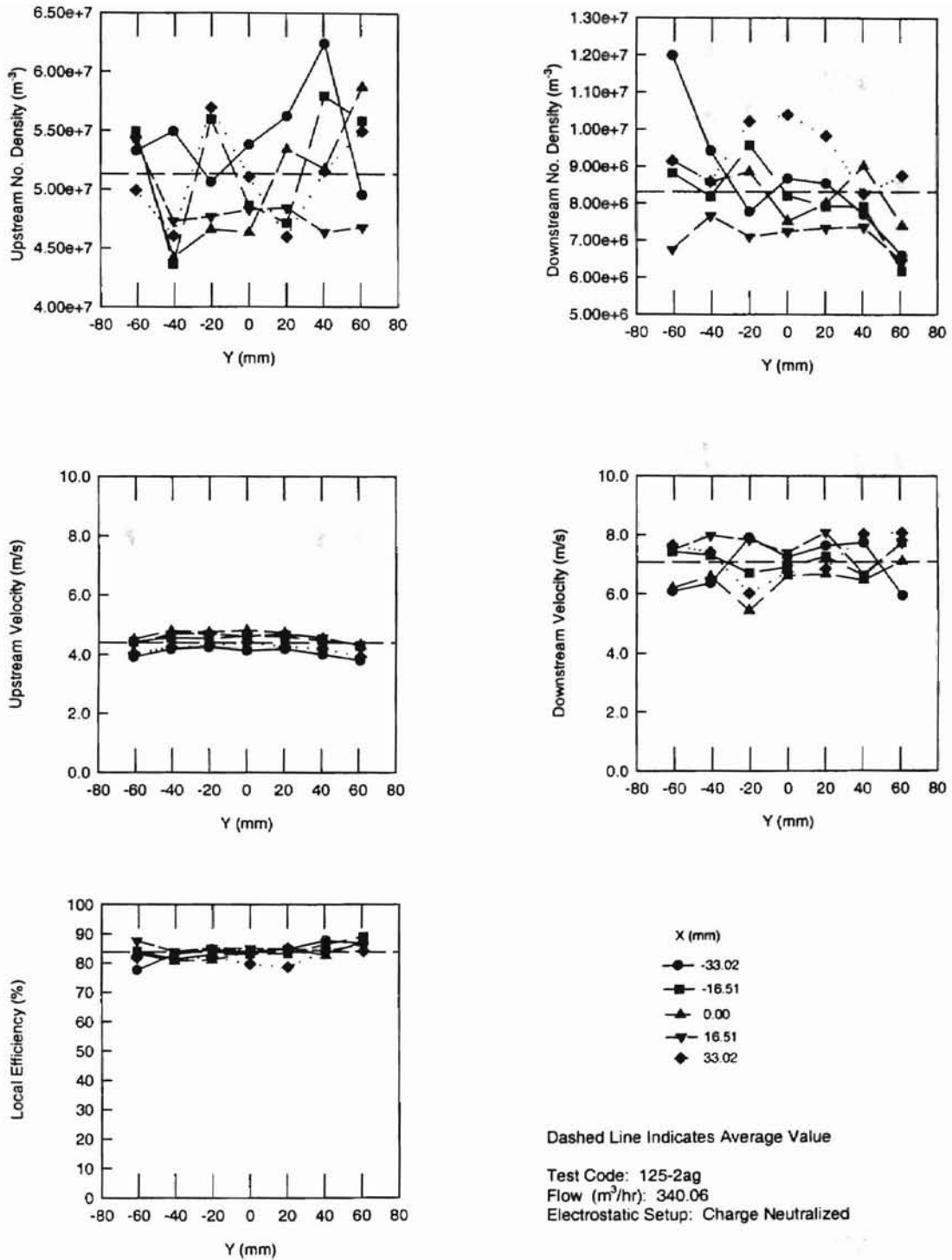


Figure A-1 Results for 2.02 Micron Diameter Monodisperse Aerosols using a Charge Neutralized Setup for a Flow Rate of 340.06 m³/hr in the Small Angle Diffuser Housing (125-2ag)

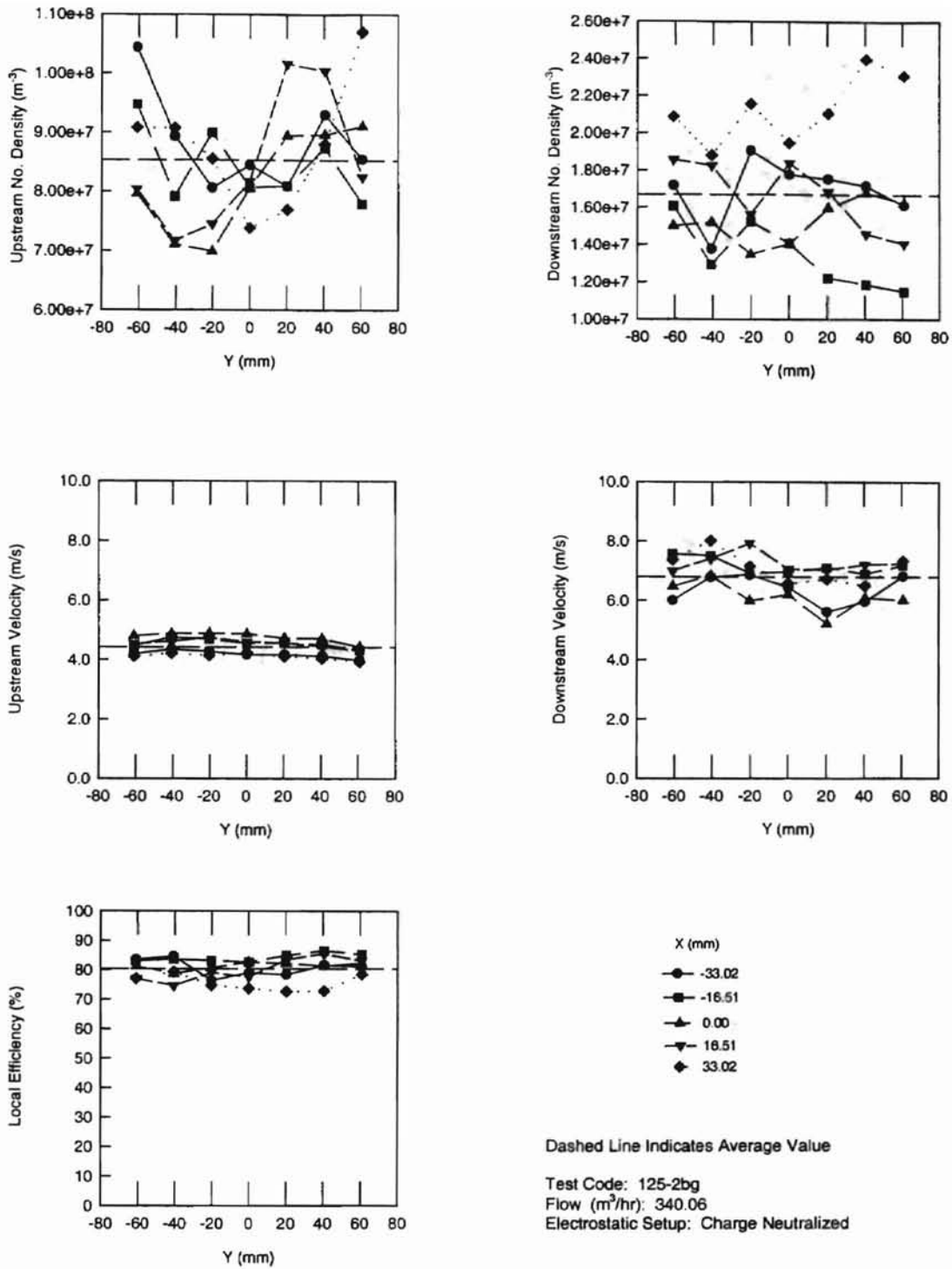


Figure A-2 Results for 2.02 Micron Diameter Aerosols using a Charge Neutralized Setup for a Flow Rate of 340.06 m³/hr in the Small Angle Diffuser Housing (125-2bg)

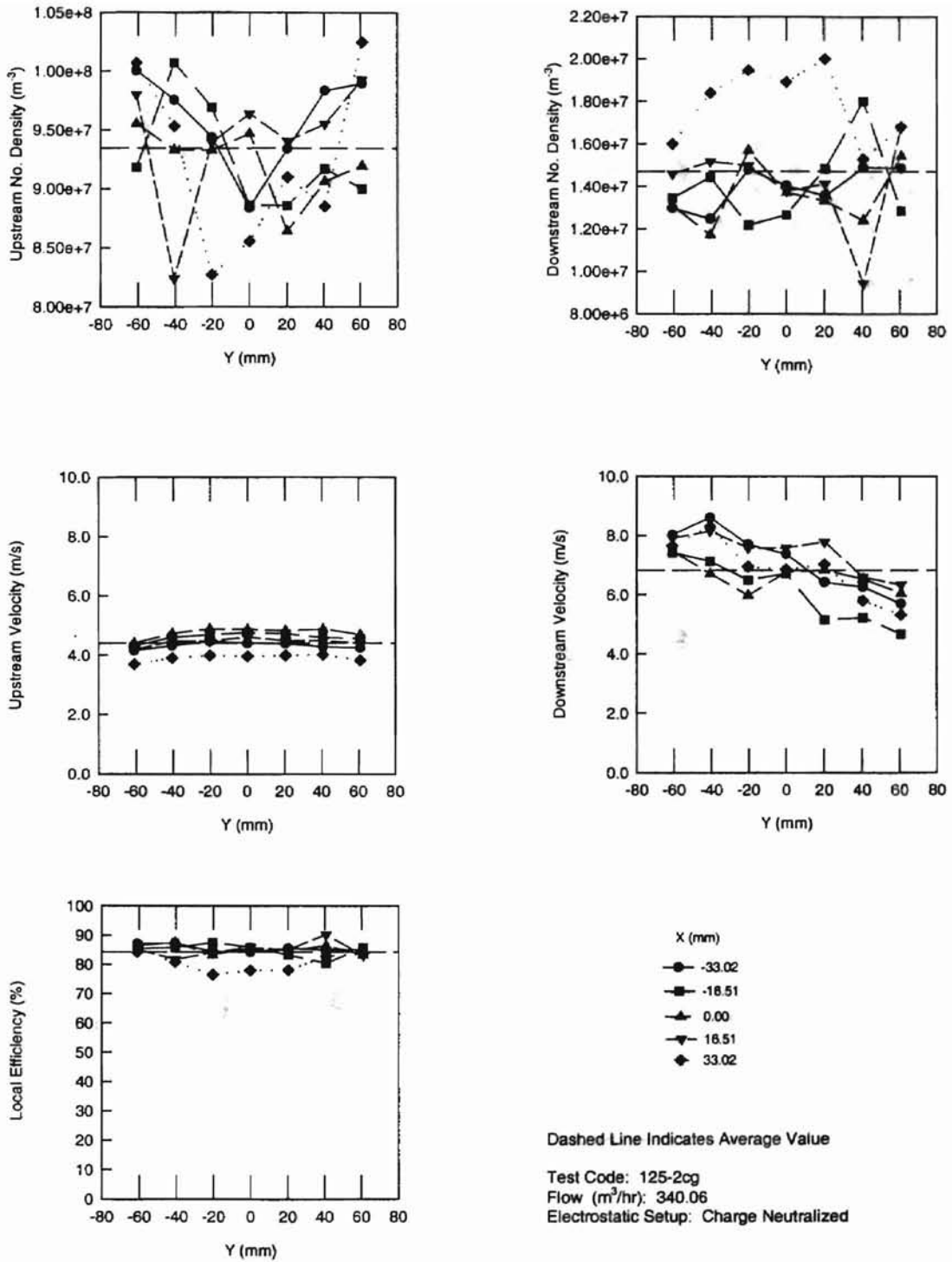


Figure A-3 Results for 2.02 Micron Diameter Aerosols using a Charge Neutralized Setup for a Flow Rate of 340.06 m³/hr in the Small Angle Diffuser Housing (125-2cg)

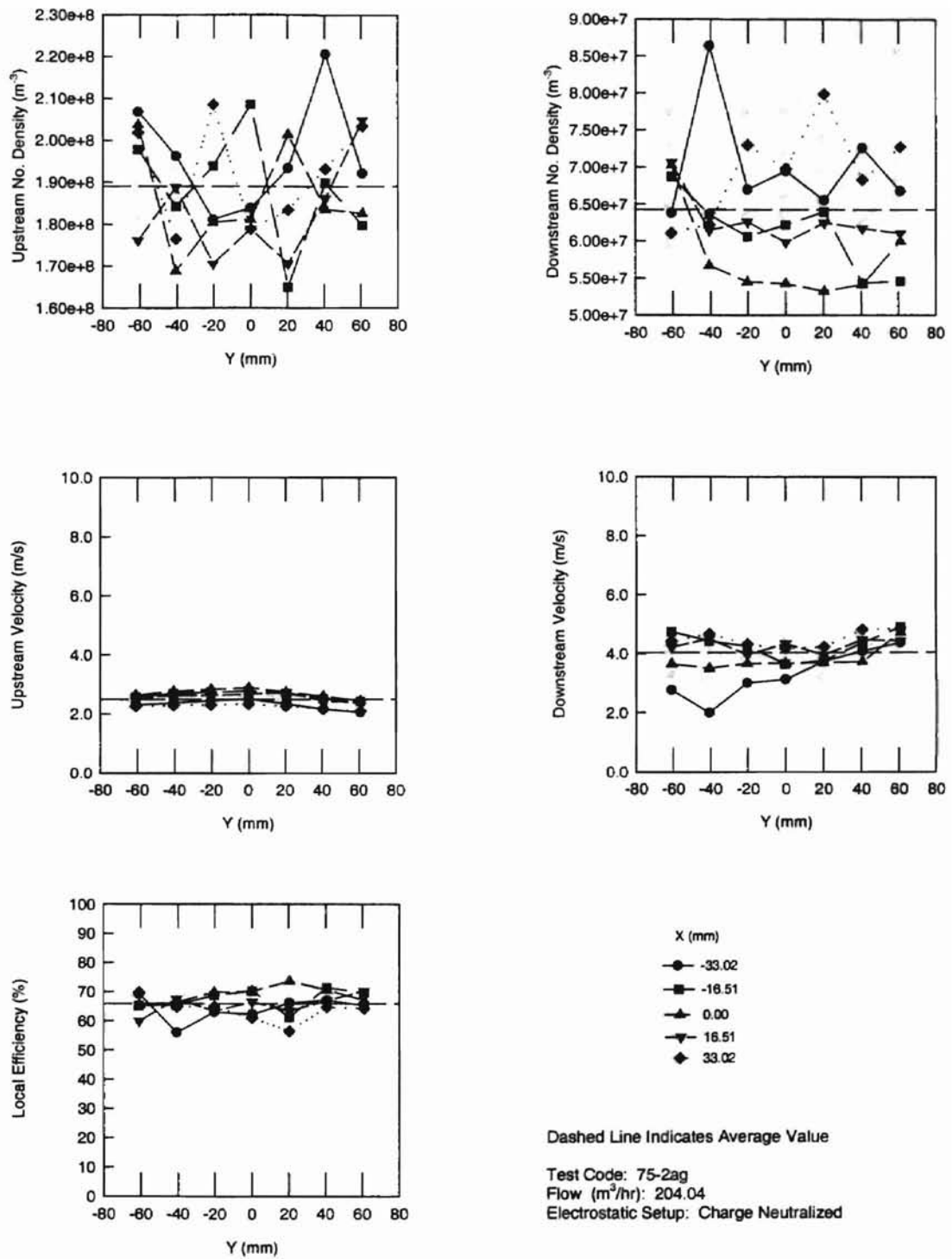


Figure A-4 Results for 2.02 Micron Diameter Aerosols using a Charge Neutralized Setup for a Flow Rate of 204.04 m^3/hr in the Small Angle Diffuser Housing (75-2ag)

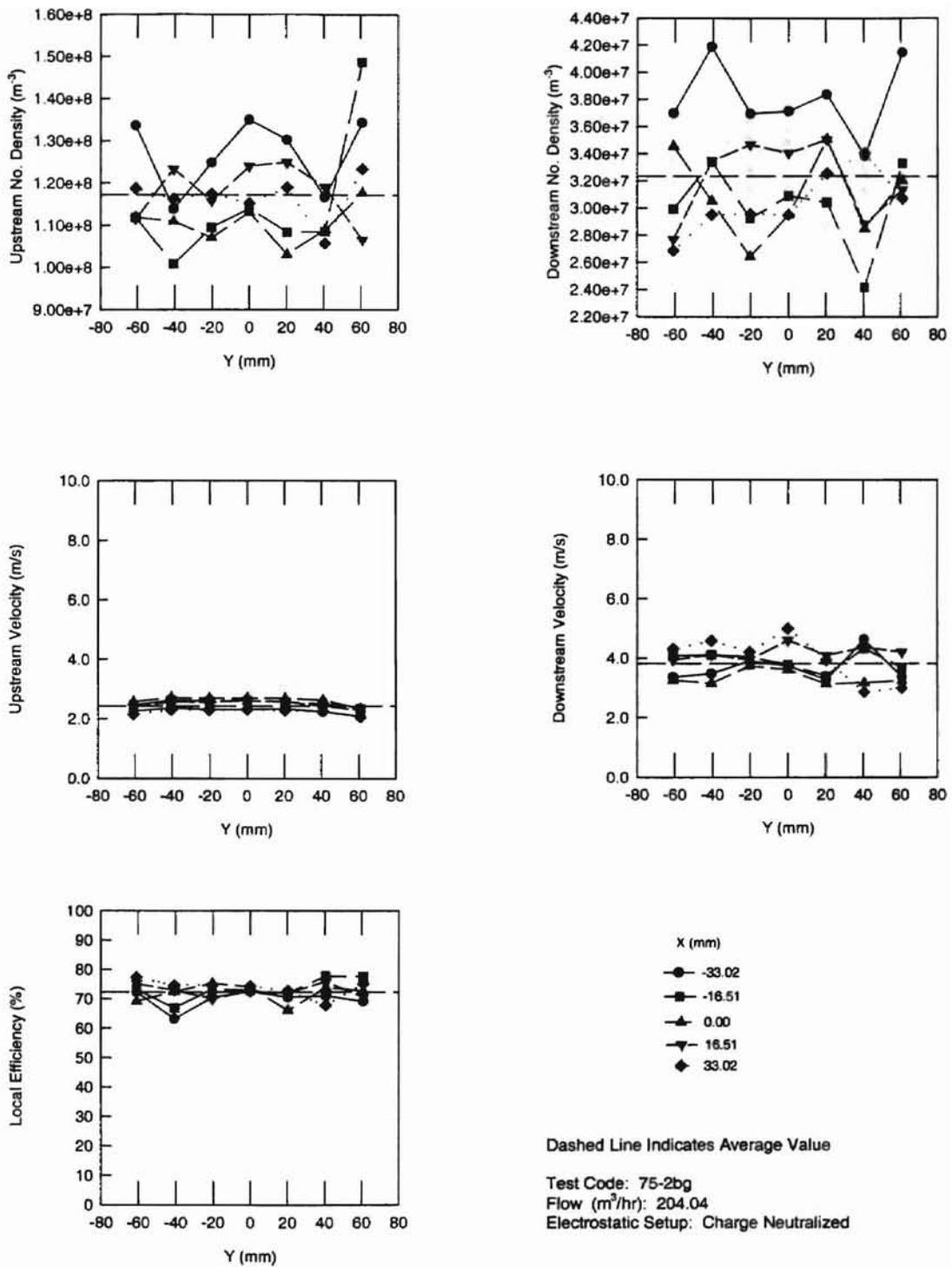


Figure A-5 Results for 2.02 Micron Diameter Aerosols using a Charge Neutralized Setup for a Flow Rate of 204.04 m^3/hr in the Small Angle Diffuser Housing (75-2bg)

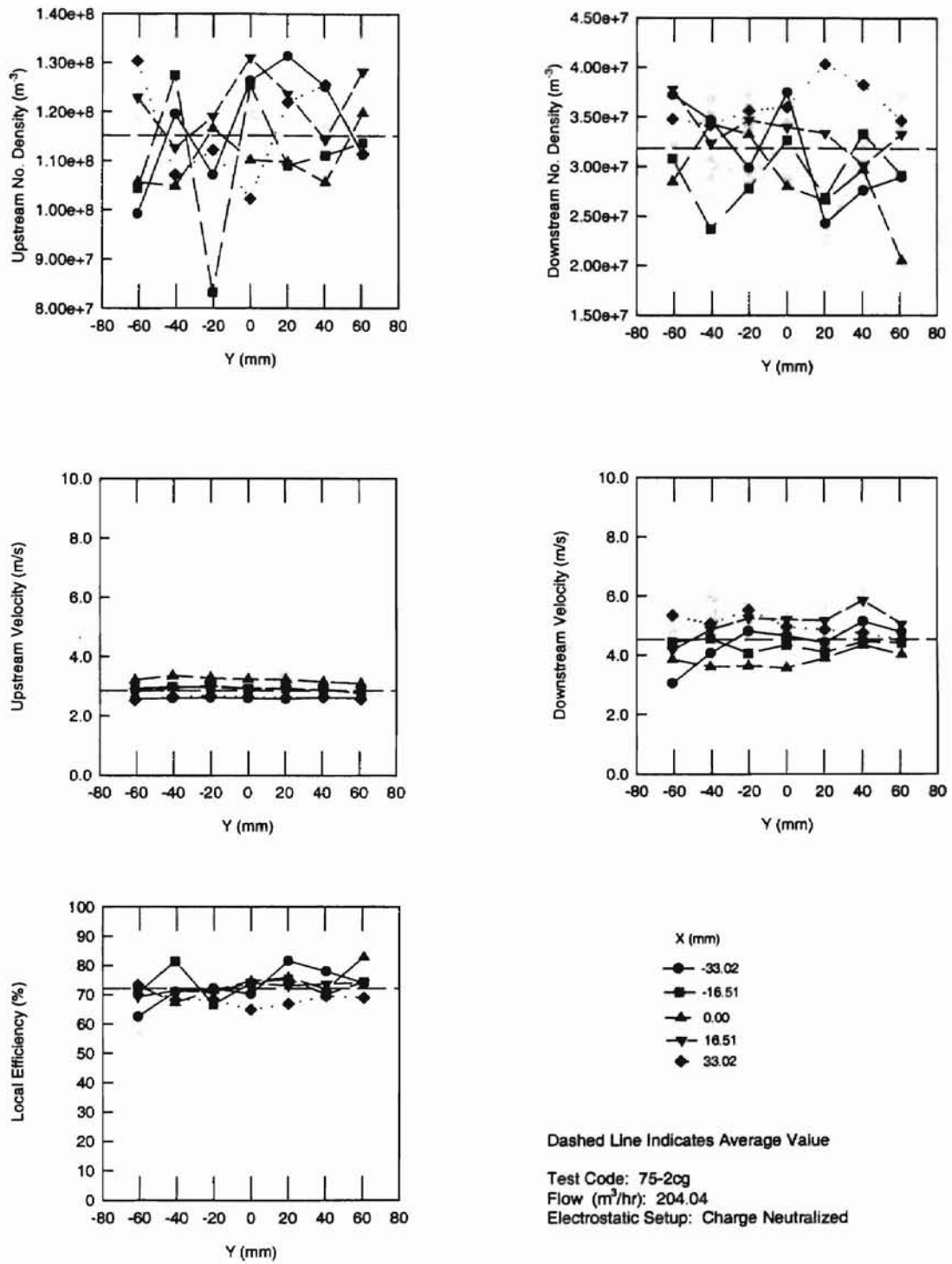


Figure A-6 Results for 2.02 Micron Diameter Aerosols using a Charge Neutralized Setup for a Flow Rate of $136.02 m^3/hr$ in the Small Angle Diffuser Housing (75-2cg)

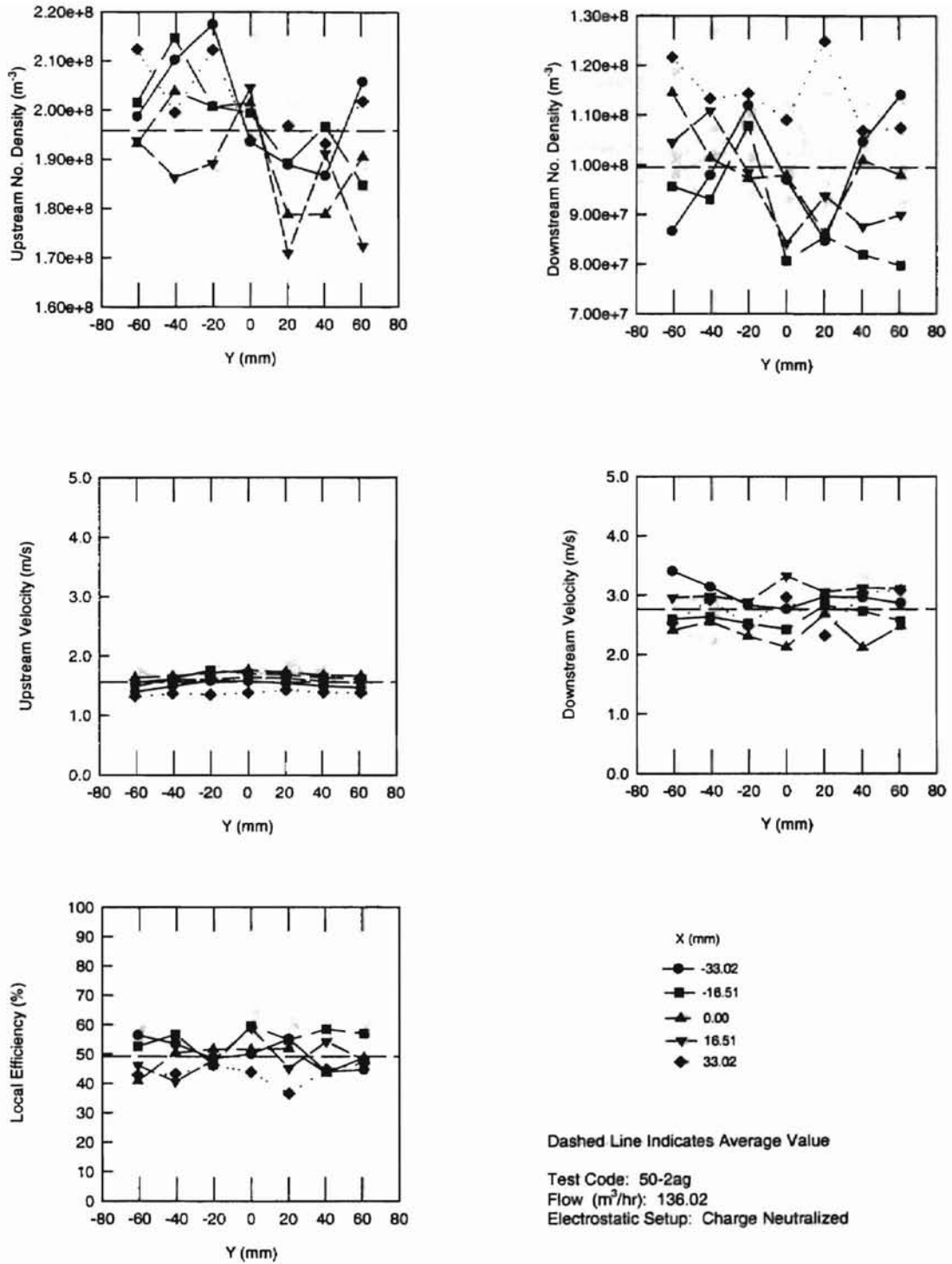


Figure A-7 Results for 2.02 Micron Diameter Aerosols using a Charge Neutralized Setup for a Flow Rate of 136.02 m³/hr in the Small Angle Diffuser Housing (50-2ag)

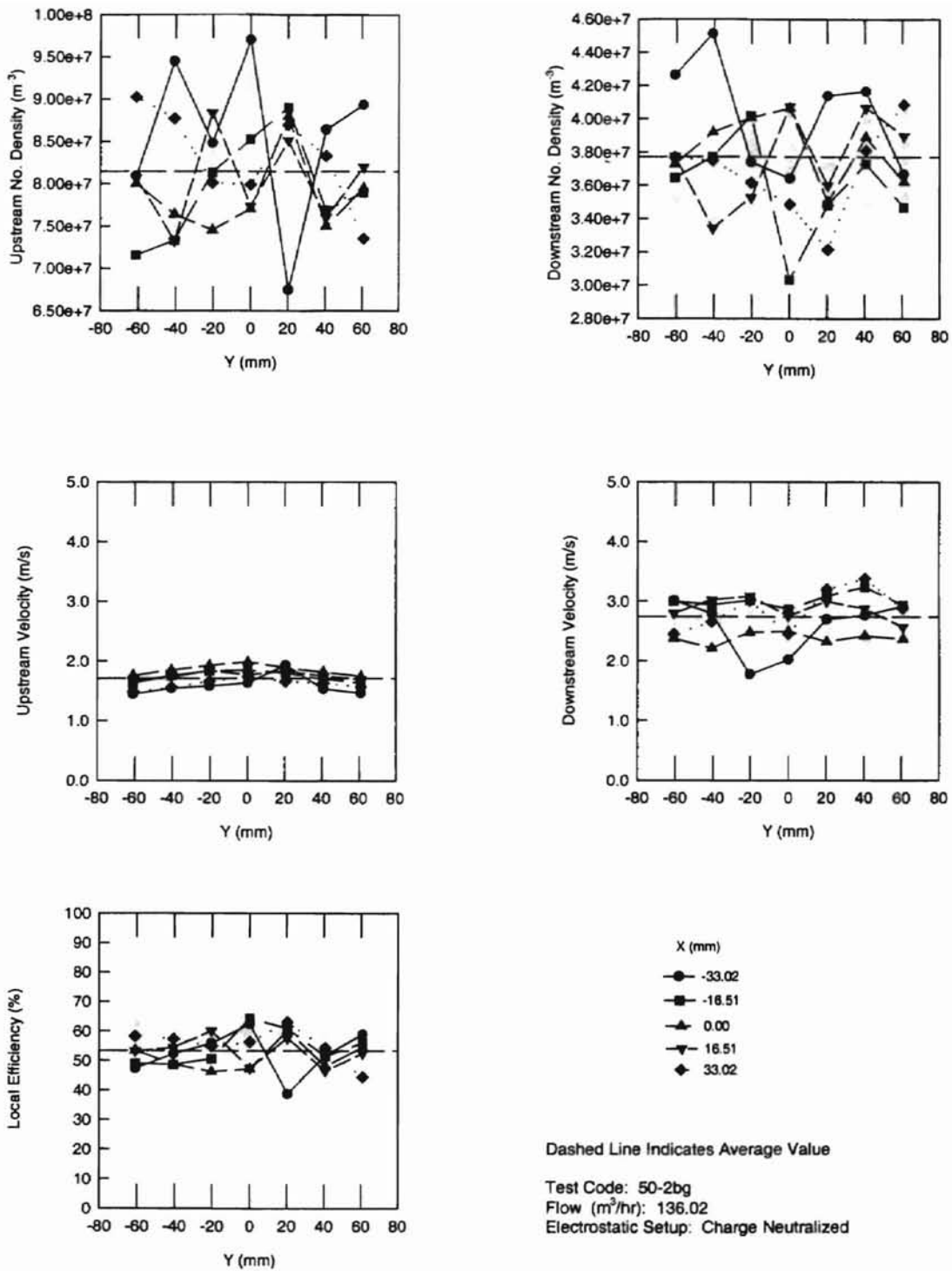


Figure A-8 Results for 2.02 Micron Diameter Aerosols using a Charge Neutralized Setup for a Flow Rate of 136.02 m^3/hr in the Small Angle Diffuser Housing (50-2bg)

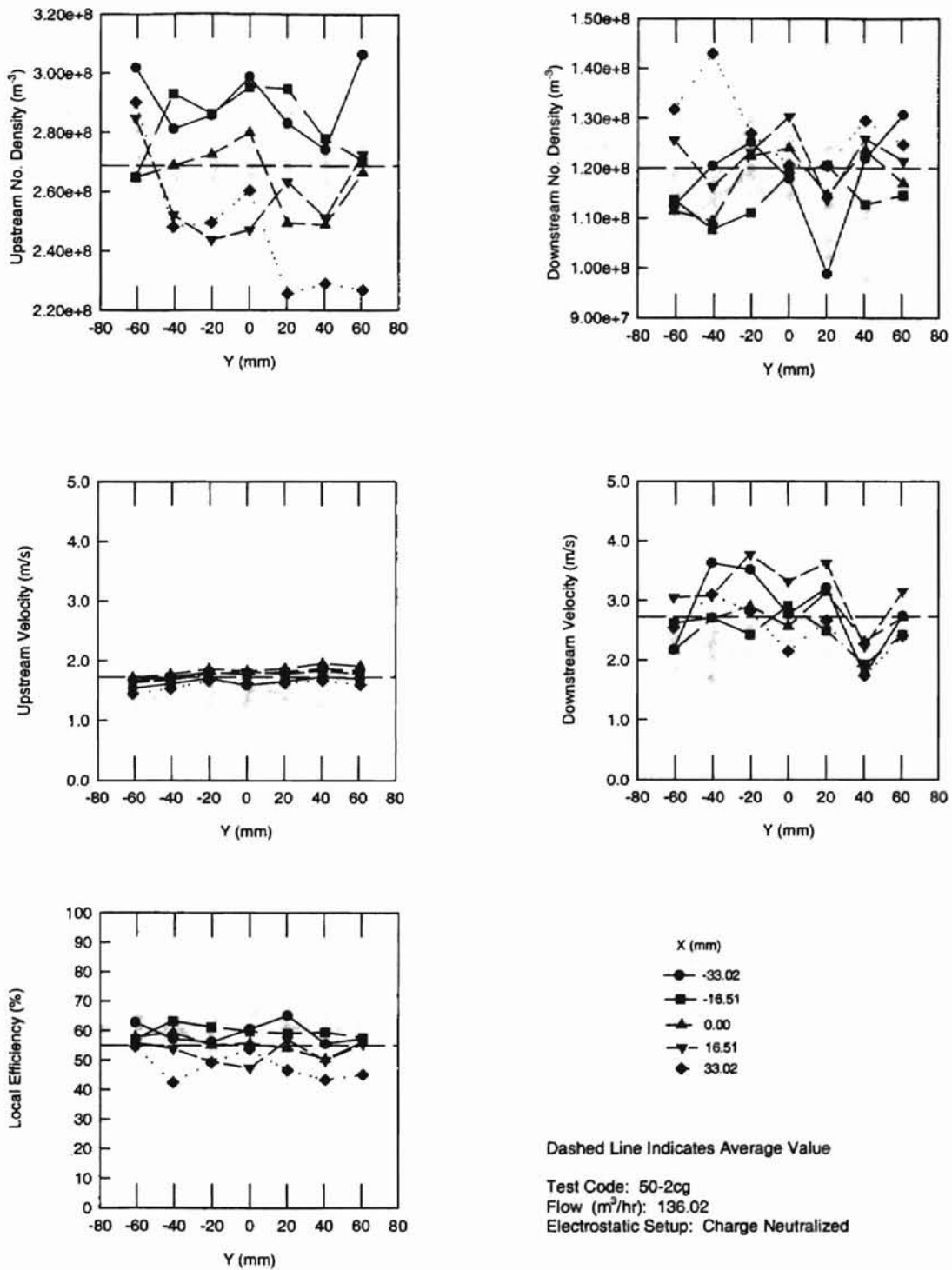


Figure A-9 Results for 2.02 Micron Diameter Aerosols using a Charge Neutralized Setup for a Flow Rate of 136.02 m³/hr in the Small Angle Diffuser Housing (50-2cg)

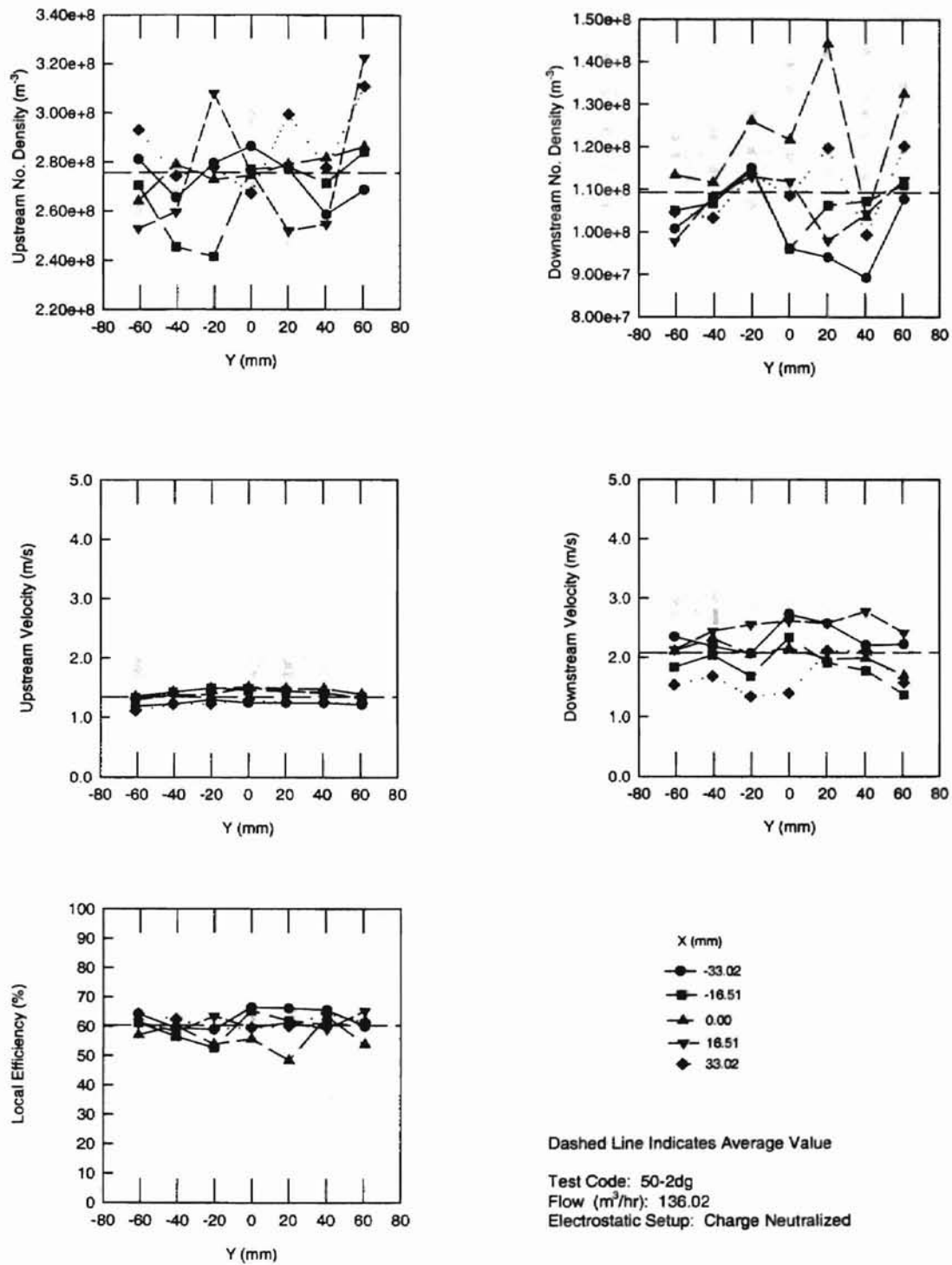


Figure A-10 Results for 2.02 Micron Diameter Aerosols using a Charge Neutralized Setup for a Flow Rate of $136.02 m^3/hr$ in the Small Angle Diffuser Housing (50-2dg)

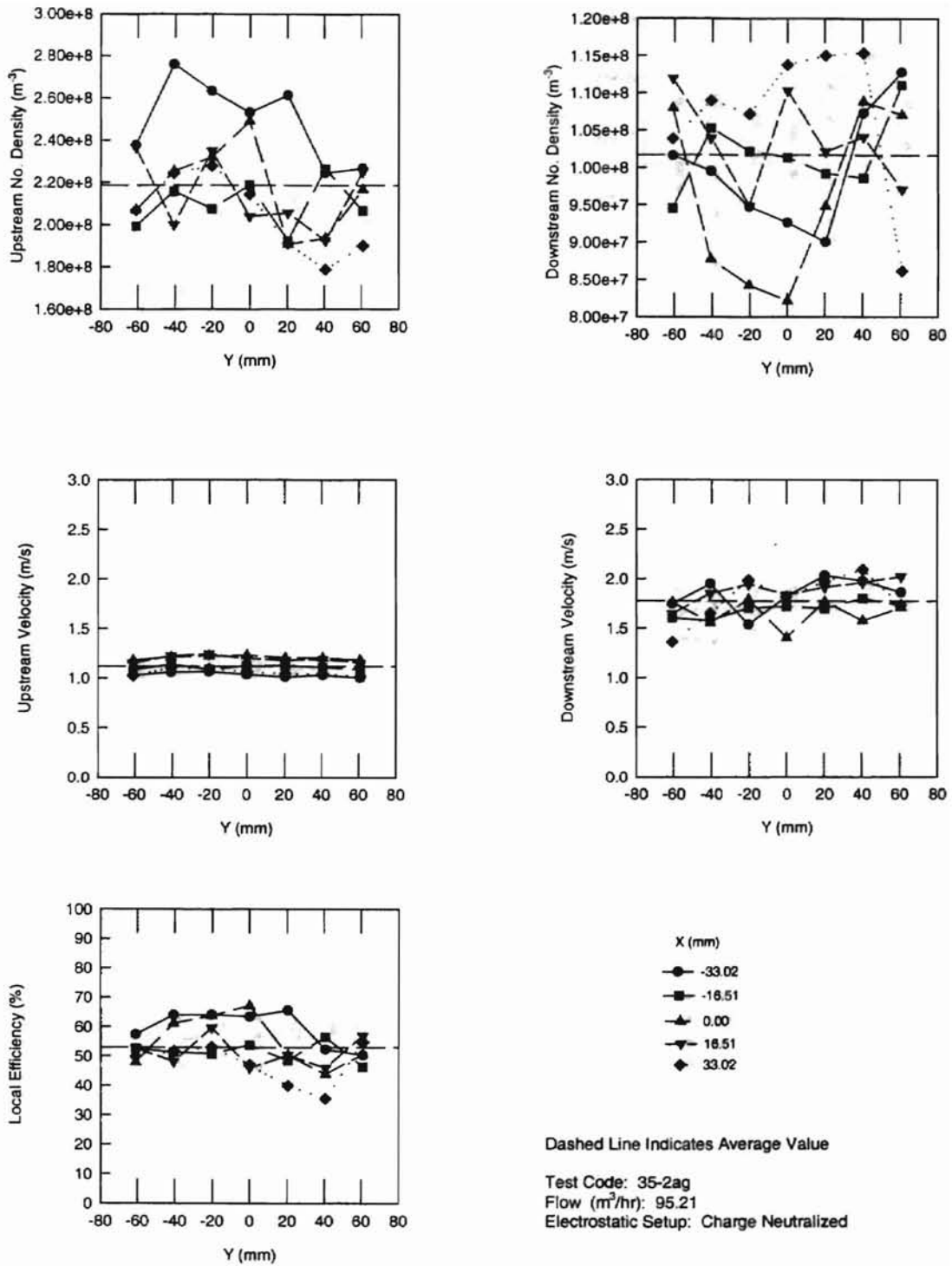


Figure A-11 Results for 2.02 Micron Diameter Aerosols using a Charge Neutralized Setup for a Flow Rate of 95.21 m³/hr in the Small Angle Diffuser Housing (35-2ag)

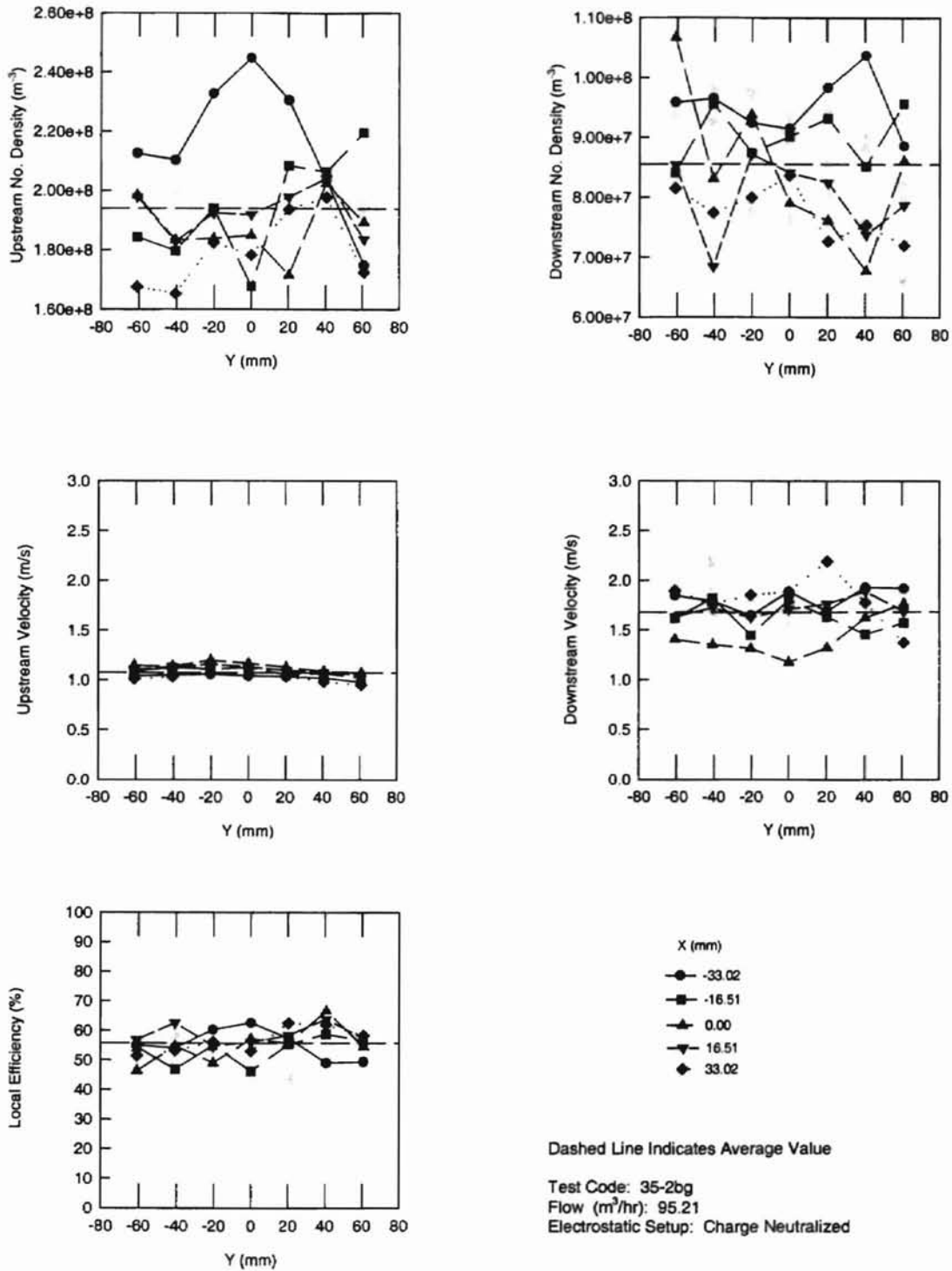


Figure A-12 Results for 2.02 Micron Diameter Aerosols using a Charge Neutralized Setup for a Flow Rate of 95.21 m^3/hr in the Small Angle Diffuser Housing (35-2bg)

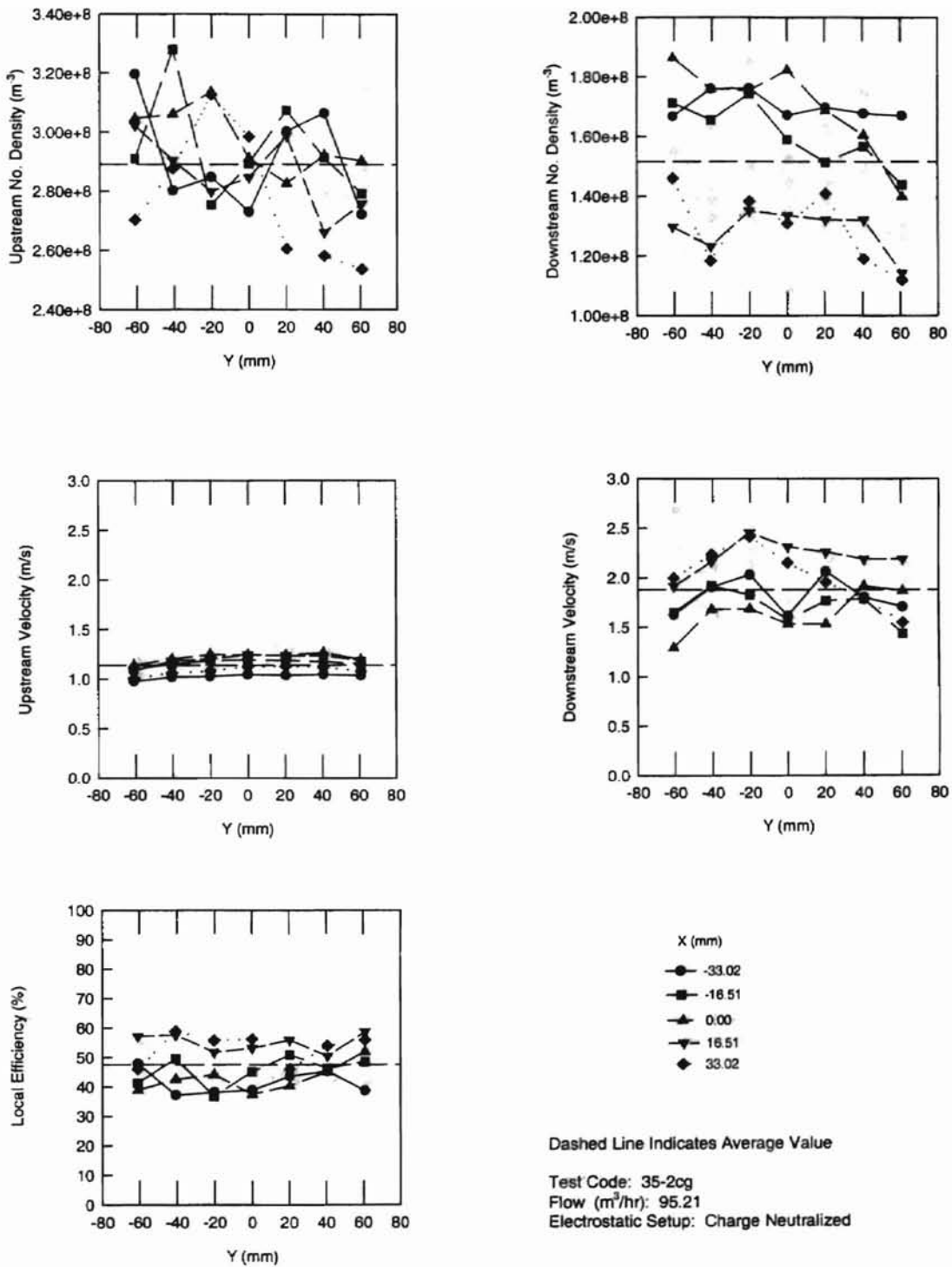


Figure A-13 Results for 2.02 Micron Diameter Aerosols using a Charge Neutralized Setup for a Flow Rate of $95.21 m^3/hr$ in the Small Angle Diffuser Housing (35-2cg)

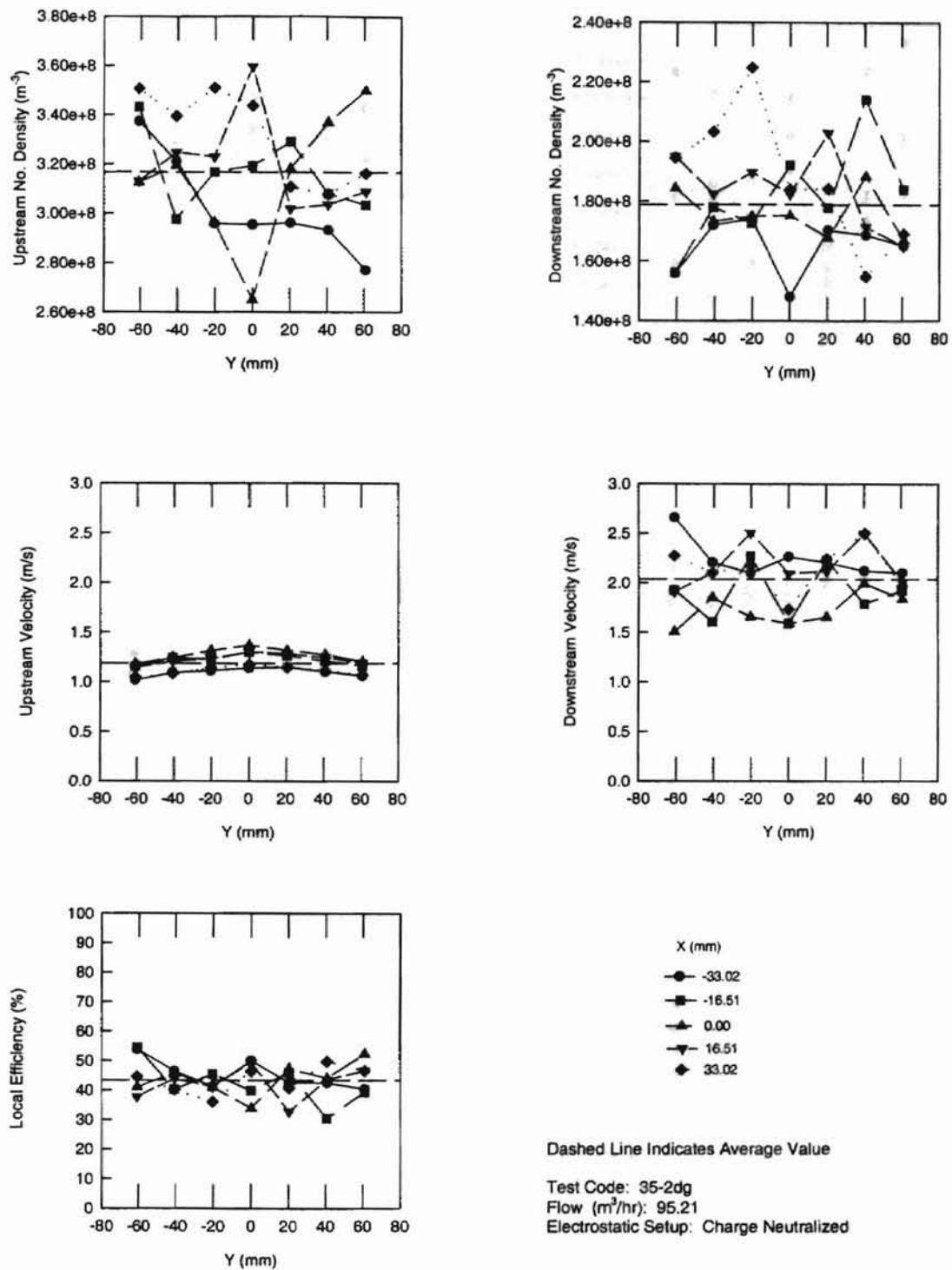


Figure A-14 Results for 2.02 Micron Diameter Aerosols using a Charge Neutralized Setup for a Flow Rate of 95.21 m³/hr in the Small Angle Diffuser Housing (35-2dg)

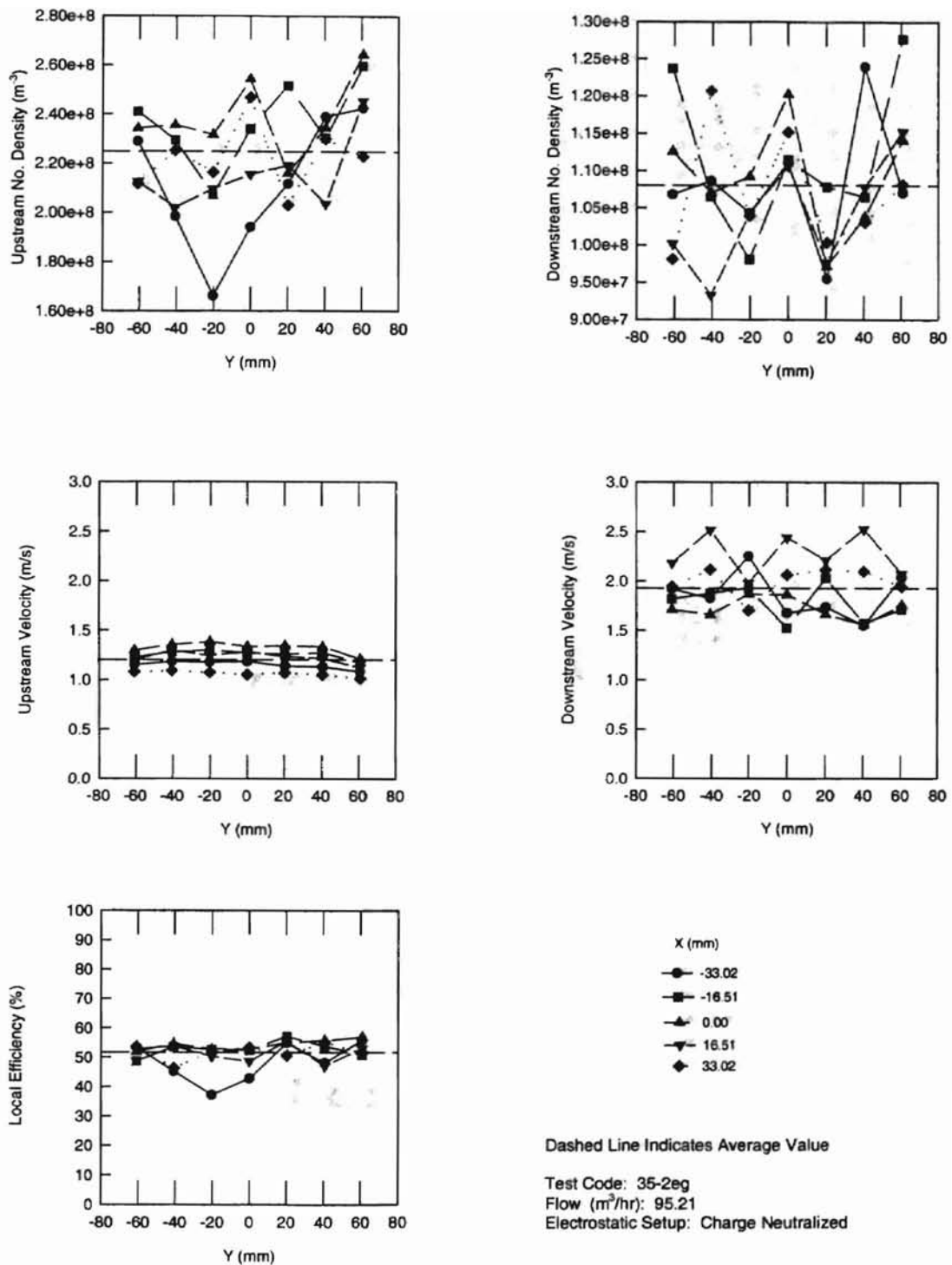


Figure A-15 Results for 2.02 Micron Diameter Aerosols using a Charge Neutralized Setup for a Flow Rate of 95.21 m³/hr in the Small Angle Diffuser Housing (35-2eg)

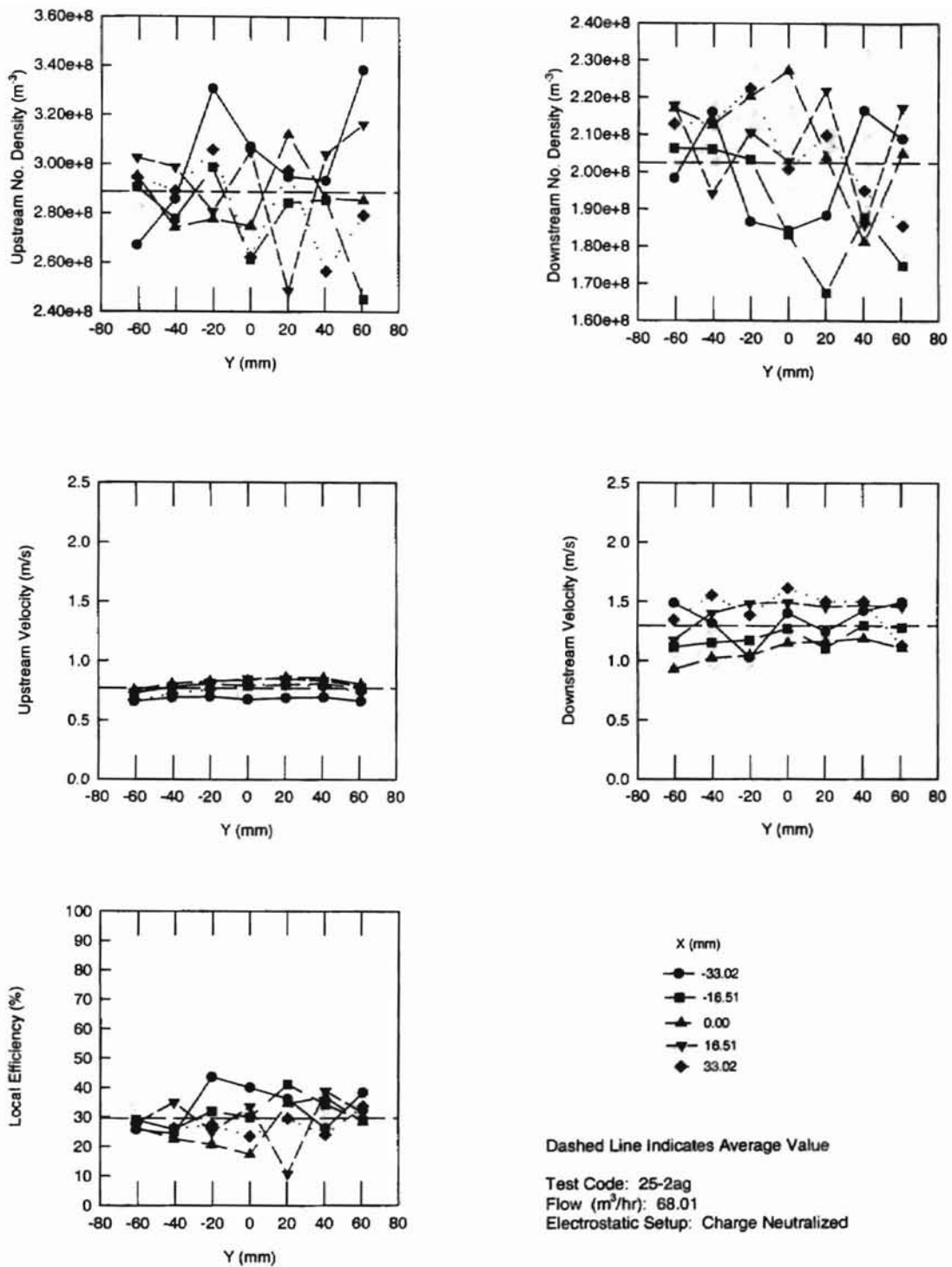
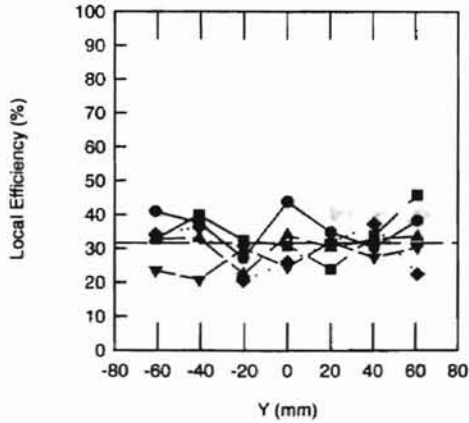
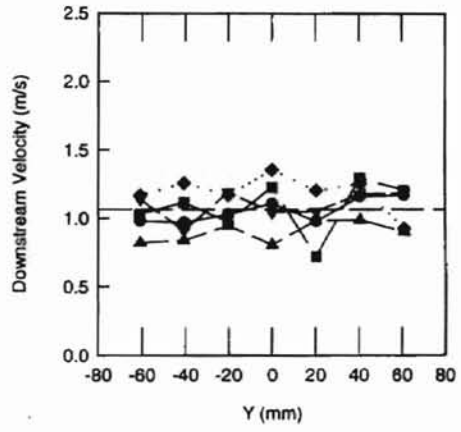
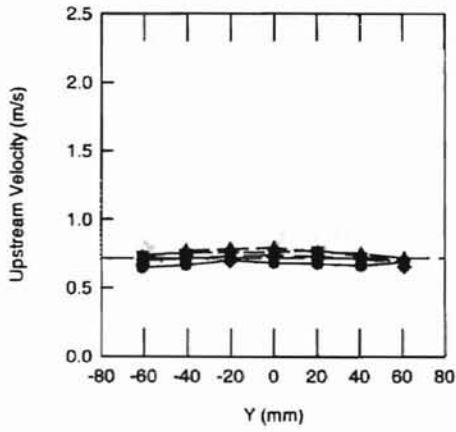
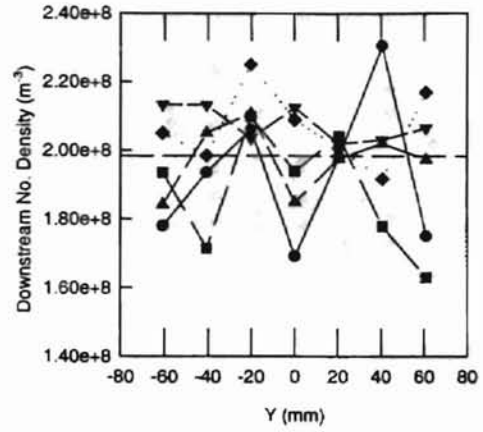
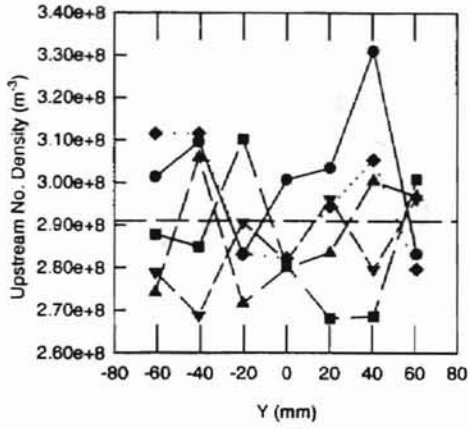


Figure A-16 Results for 2.02 Micron Diameter Aerosols using a Charge Neutralized Setup for a Flow Rate of 68.01 m³/hr in the Small Angle Diffuser Housing (25-2ag)



- X (mm)
- -33.02
 - -16.51
 - ▲ 0.00
 - ▼ 16.51
 - ◆ 33.02

Dashed Line Indicates Average Value
 Test Code: 25-2bg
 Flow (m³/hr): 68.01
 Electrostatic Setup: Charge Neutralized

Figure A-17 Results for 2.02 Micron Diameter Aerosols using a Charge Neutralized Setup for a Flow Rate of 68.01 m³/hr in the Small Angle Diffuser Housing (25-2bg)

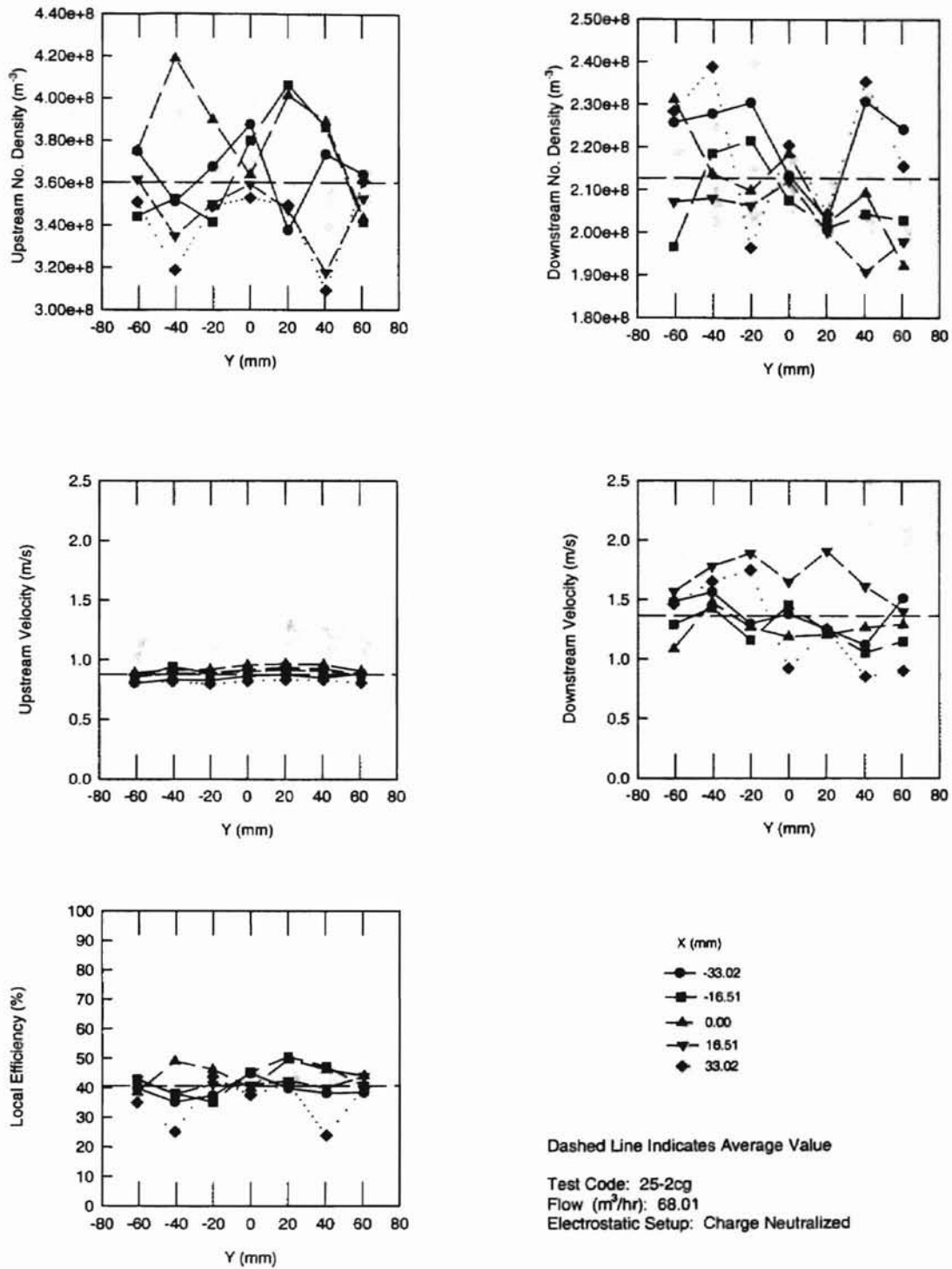


Figure A-18 Results for 2.02 Micron Diameter Aerosols using a Charge Neutralized Setup for a Flow Rate of 68.01 m³/hr in the Small Angle Diffuser Housing (25-2cg)

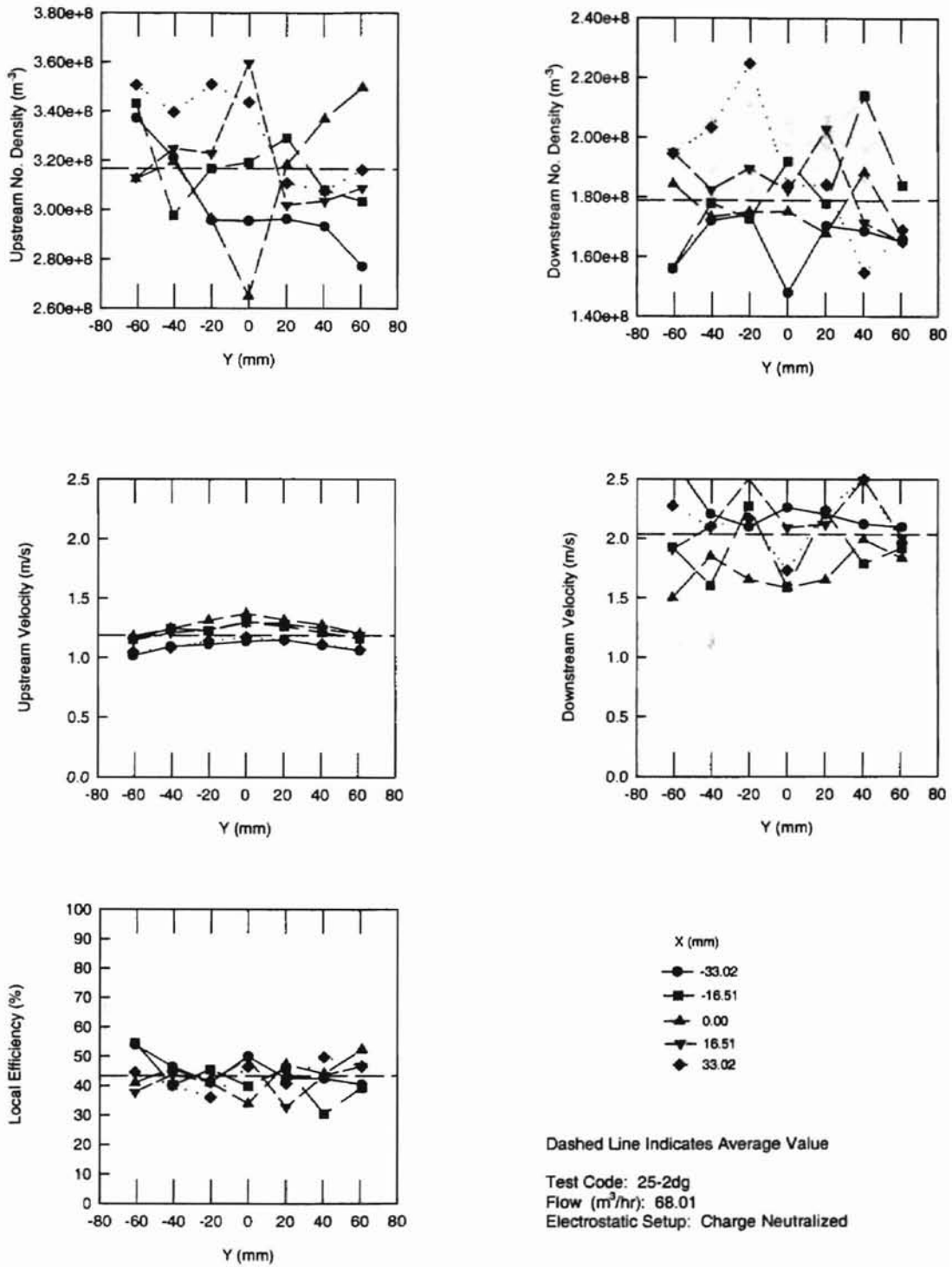


Figure A-19 Results for 2.02 Micron Diameter Aerosols using a Charge Neutralized Setup for a Flow Rate of 68.01 m³/hr in the Small Angle Diffuser Housing (25-2dg)

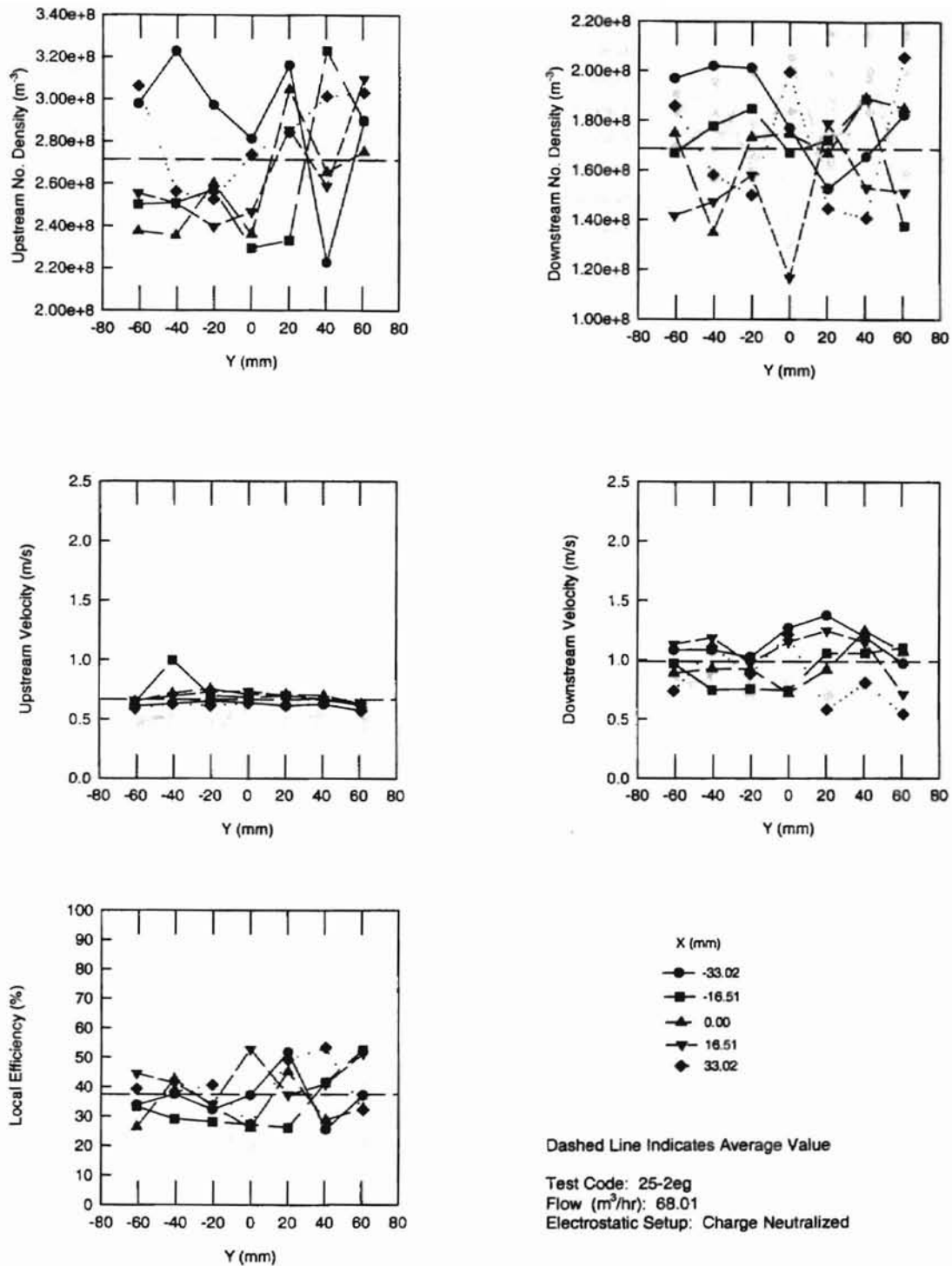


Figure A-20 Results for 2.02 Micron Diameter Aerosols using a Charge Neutralized Setup for a Flow Rate of 68.01 m³/hr in the Small Angle Diffuser Housing (25-2eg)

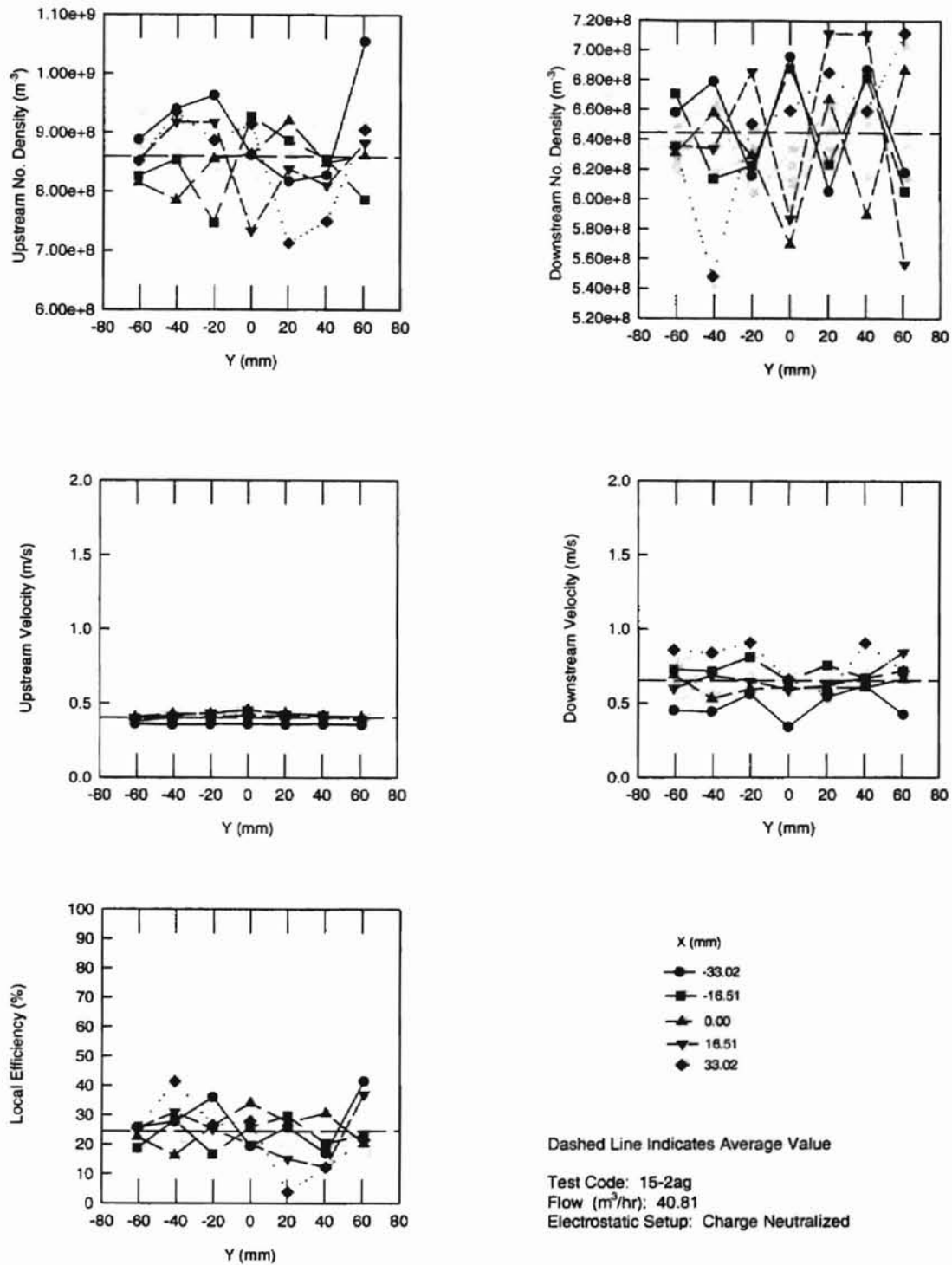


Figure A-21 Results for 2.02 Micron Diameter Aerosols using a Charge Neutralized Setup for a Flow Rate of 40.81 m^3/hr in the Small Angle Diffuser Housing (15-2ag)

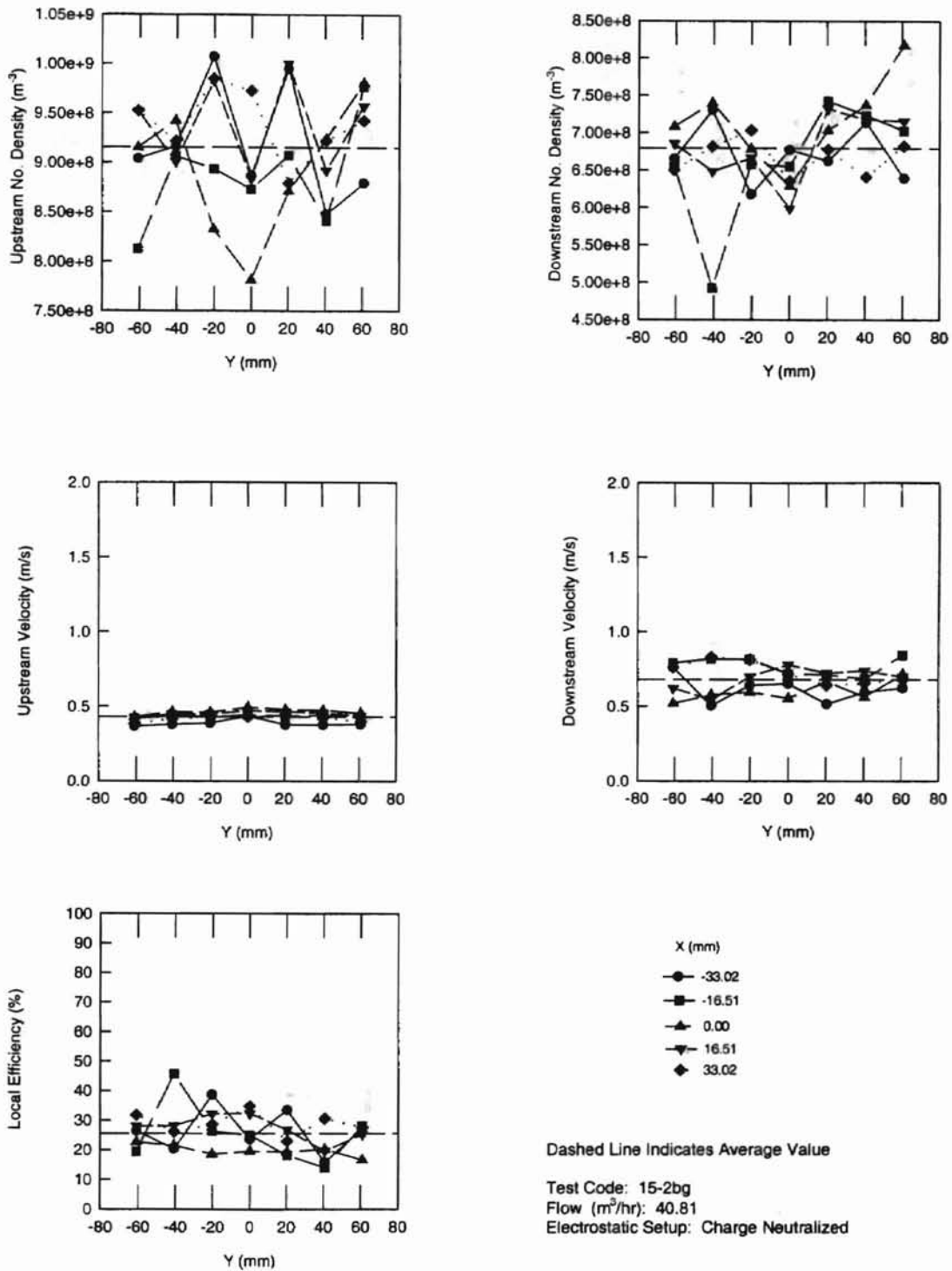


Figure A-22 Results for 2.02 Micron Diameter Aerosols using a Charge Neutralized Setup for a Flow Rate of 40.81 m^3/hr in the Small Angle Diffuser Housing (15-2bg)

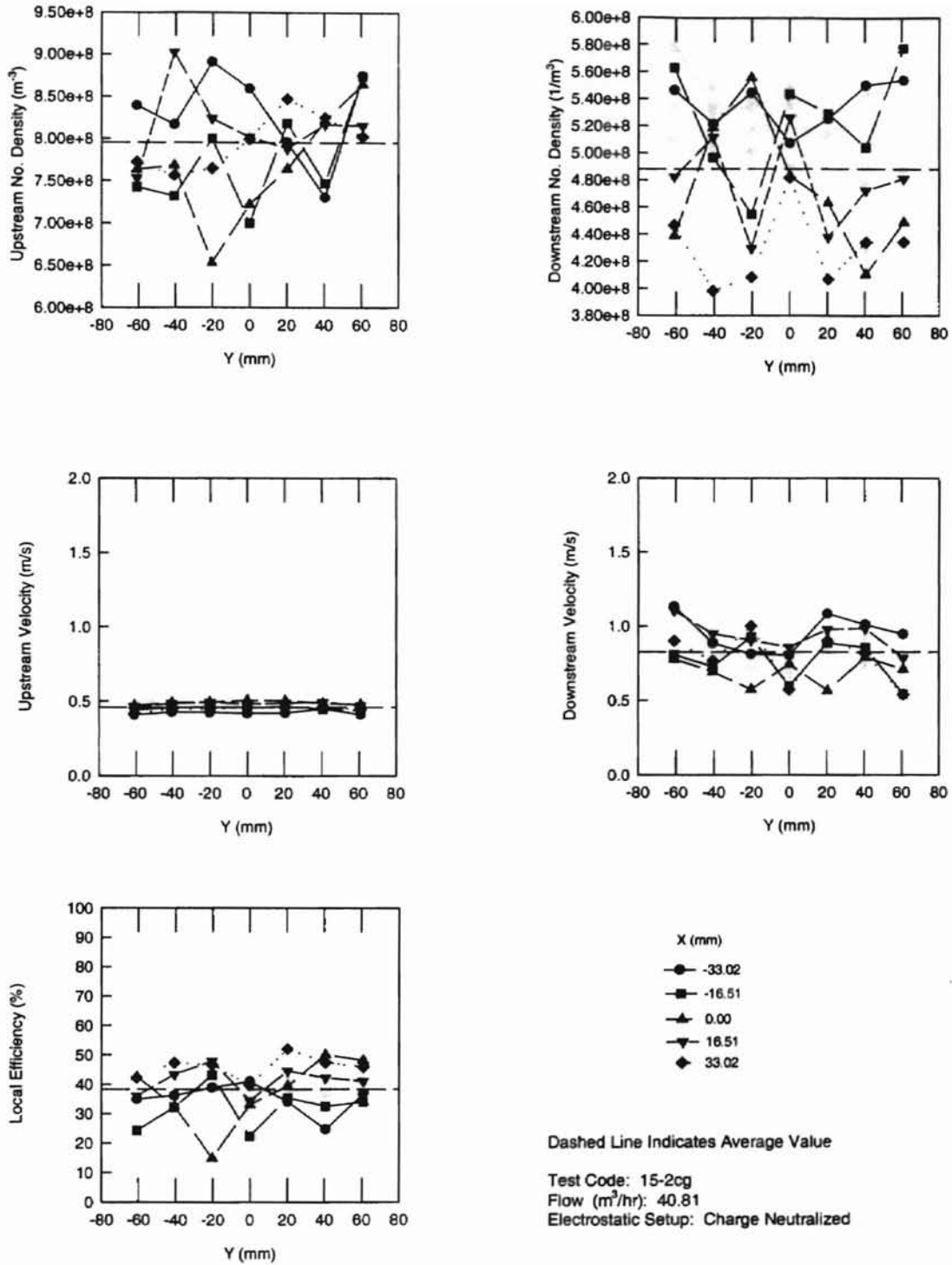


Figure A-23 Results for 2.02 Micron Diameter Aerosols using a Charge Neutralized Setup for a Flow Rate of $40.81 m^3/hr$ in the Small Angle Diffuser Housing (15-2cg)

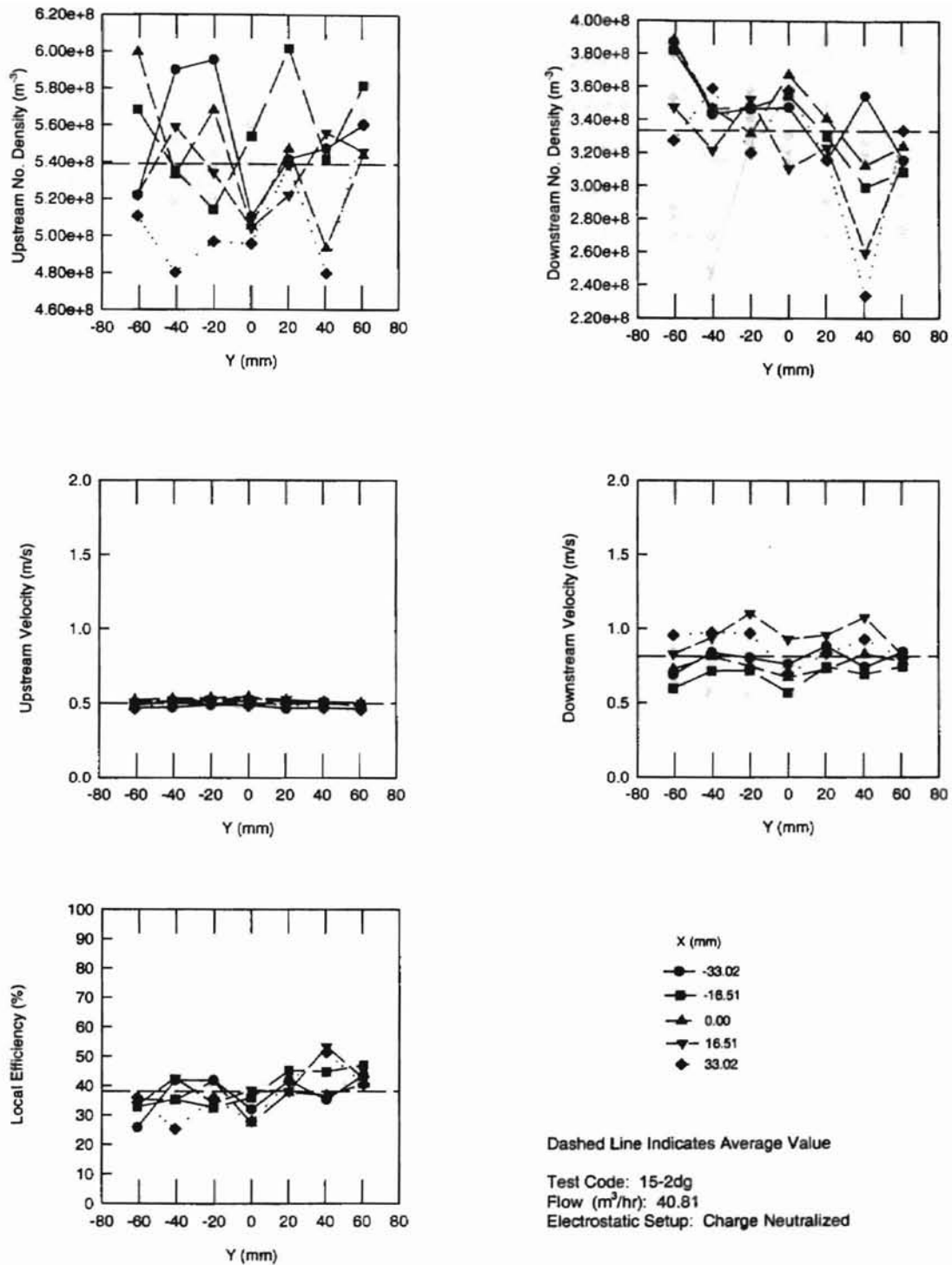


Figure A-24 Results for 2.02 Micron Diameter Aerosols using a Charge Neutralized Setup for a Flow Rate of $40.81 m^3/hr$ in the Small Angle Diffuser Housing (15-2dg)

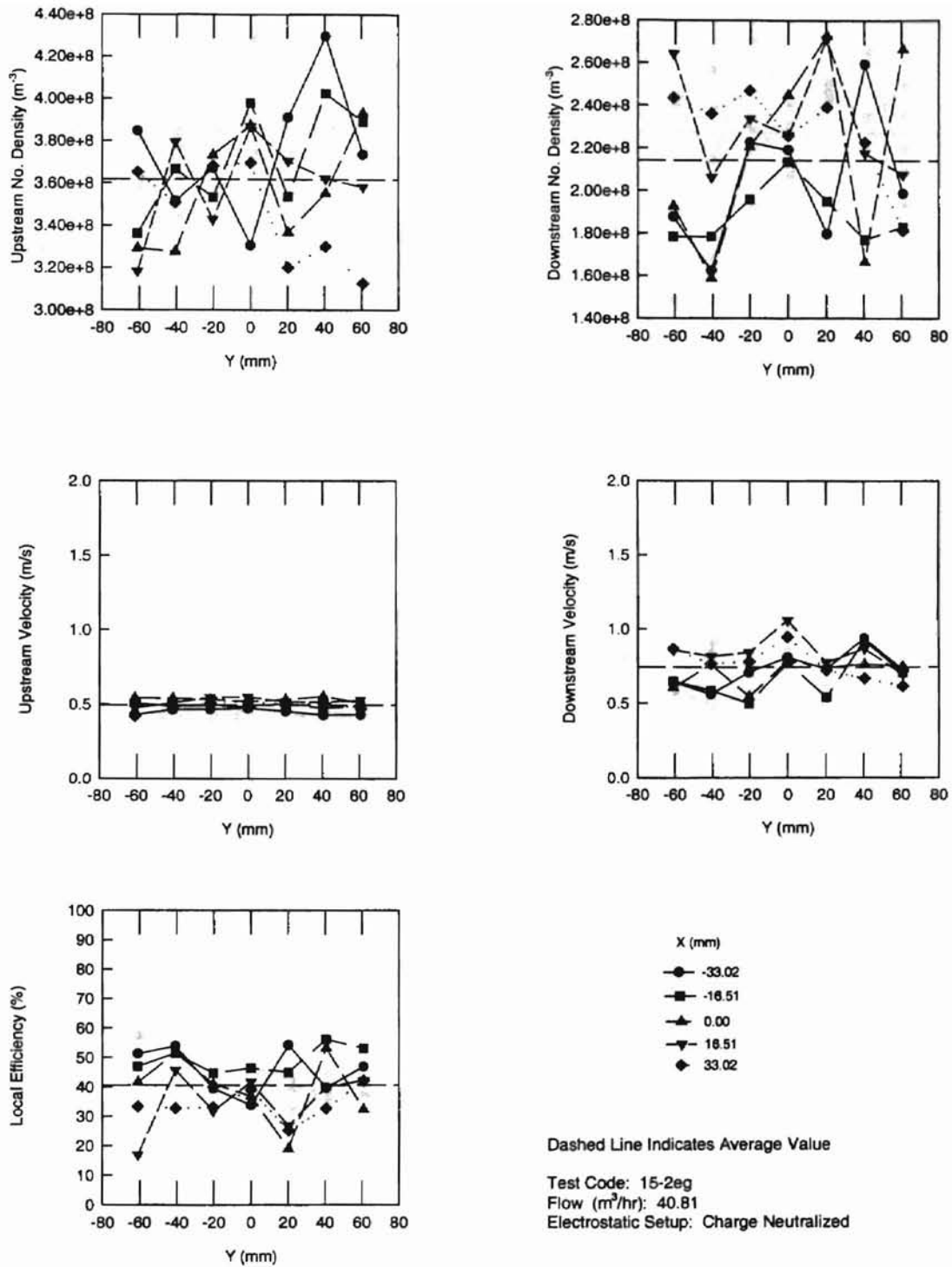
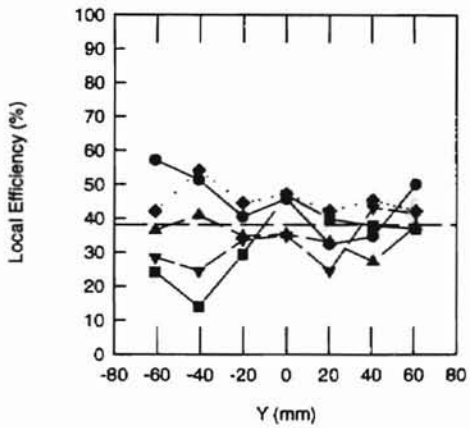
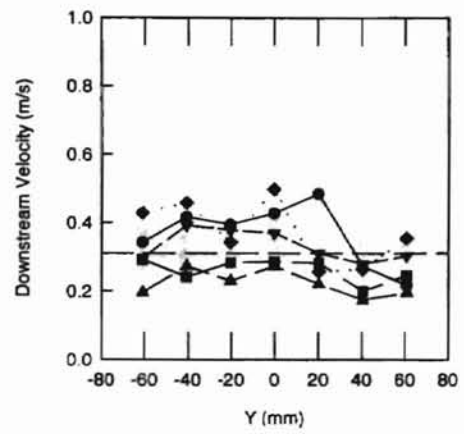
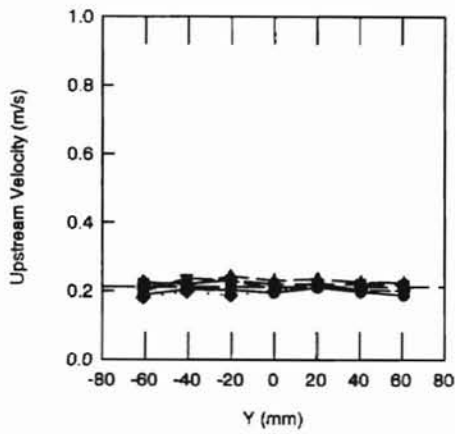
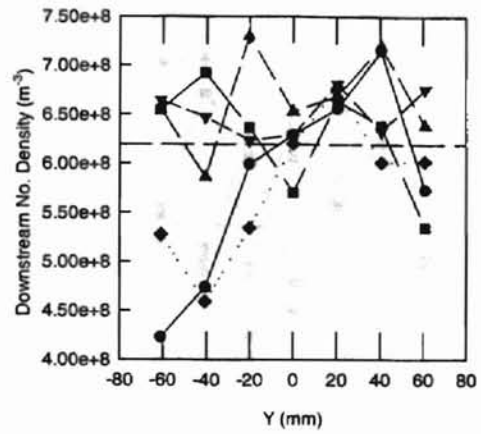
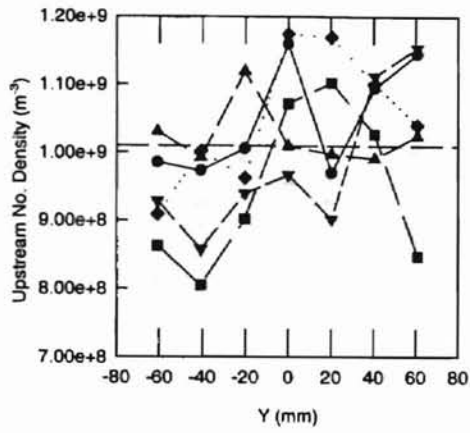


Figure A-25 Results for 2.02 Micron Diameter Aerosols using a Charge Neutralized Setup for a Flow Rate of 40.81 m³/hr in the Small Angle Diffuser Housing (15-2eg)



- X (mm)
- -33.02
 - -18.51
 - ▲ 0.00
 - ▼ 16.51
 - ◆ 33.02

Dashed Line Indicates Average Value

Test Code: 10-2ag

Flow (m^3/hr): 27.20

Electrostatic Setup: Charge Neutralized

Figure A-26 Results for 2.02 Micron Diameter Aerosols using a Charge Neutralized Setup for a Flow Rate of $27.2 m^3/hr$ in the Small Angle Diffuser Housing (10-2ag)

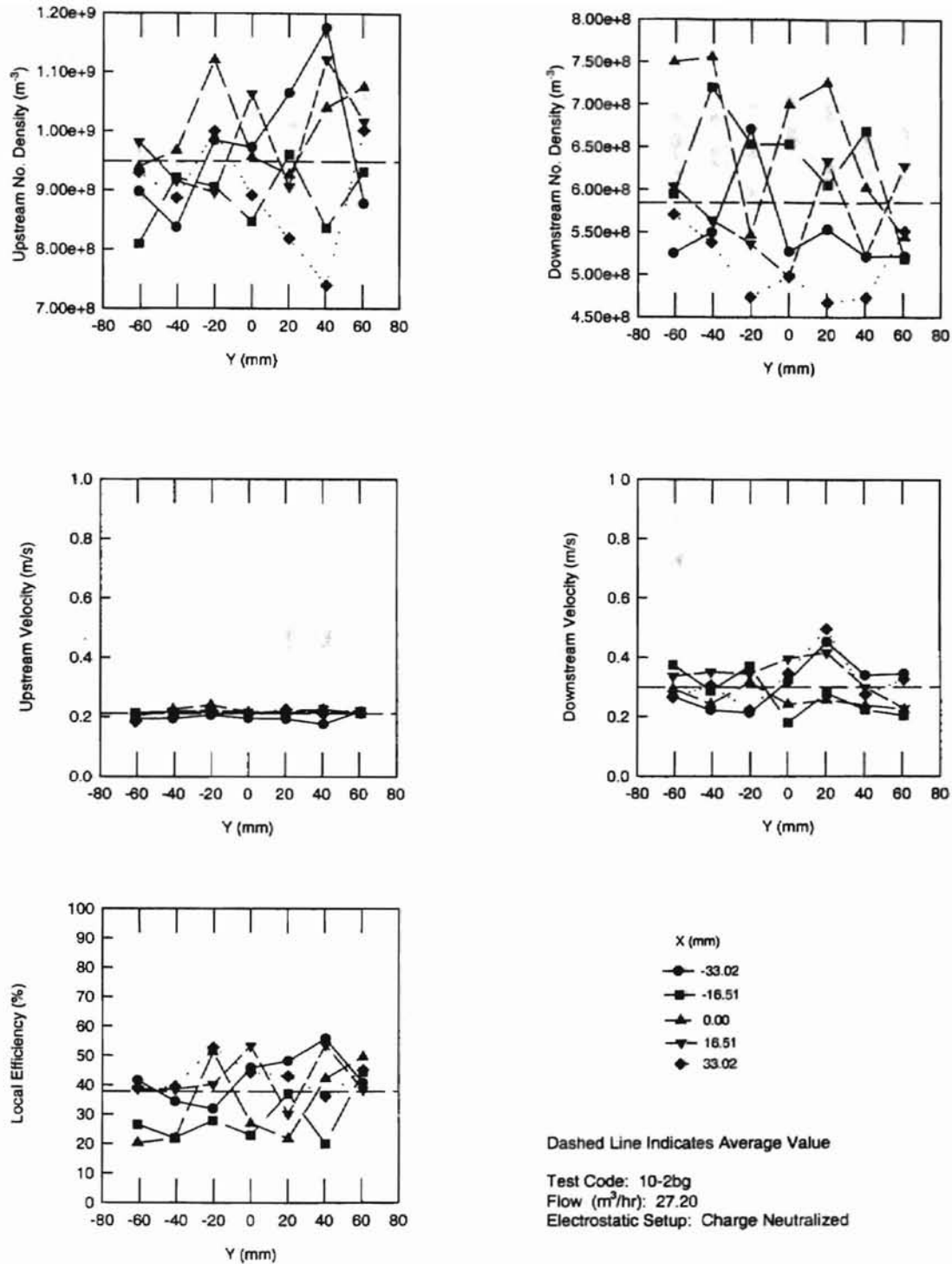


Figure A-27 Results for 2.02 Micron Diameter Aerosols using a Charge Neutralized Setup for a Flow Rate of $27.2 m^3/hr$ in the Small Angle Diffuser Housing (10-2bg)

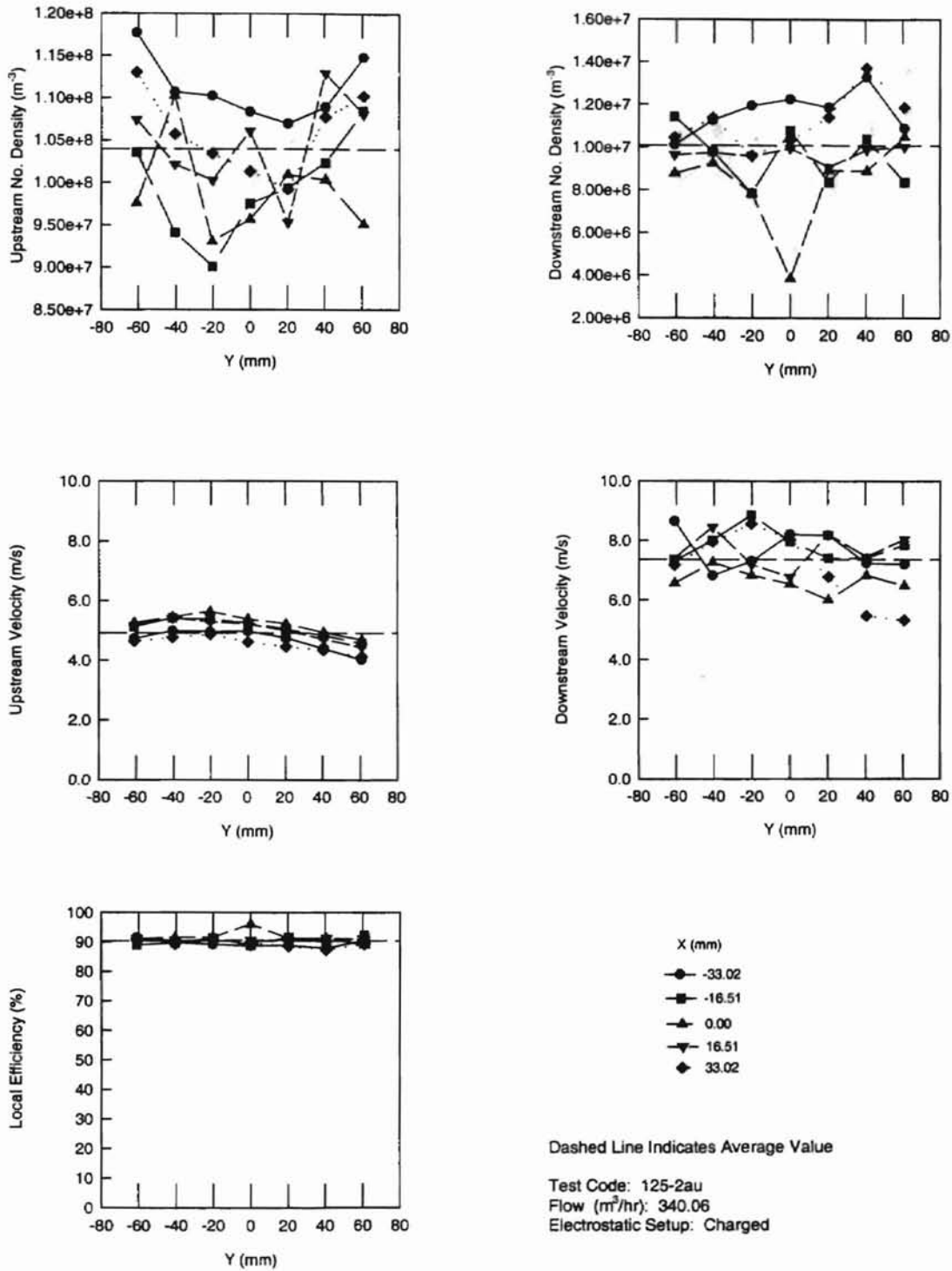


Figure A-28 Results for 2.02 Micron Diameter Aerosols using a Charged Setup for a Flow Rate of $340.06 m^3/hr$ in the Small Angle Diffuser Housing (125-2au)

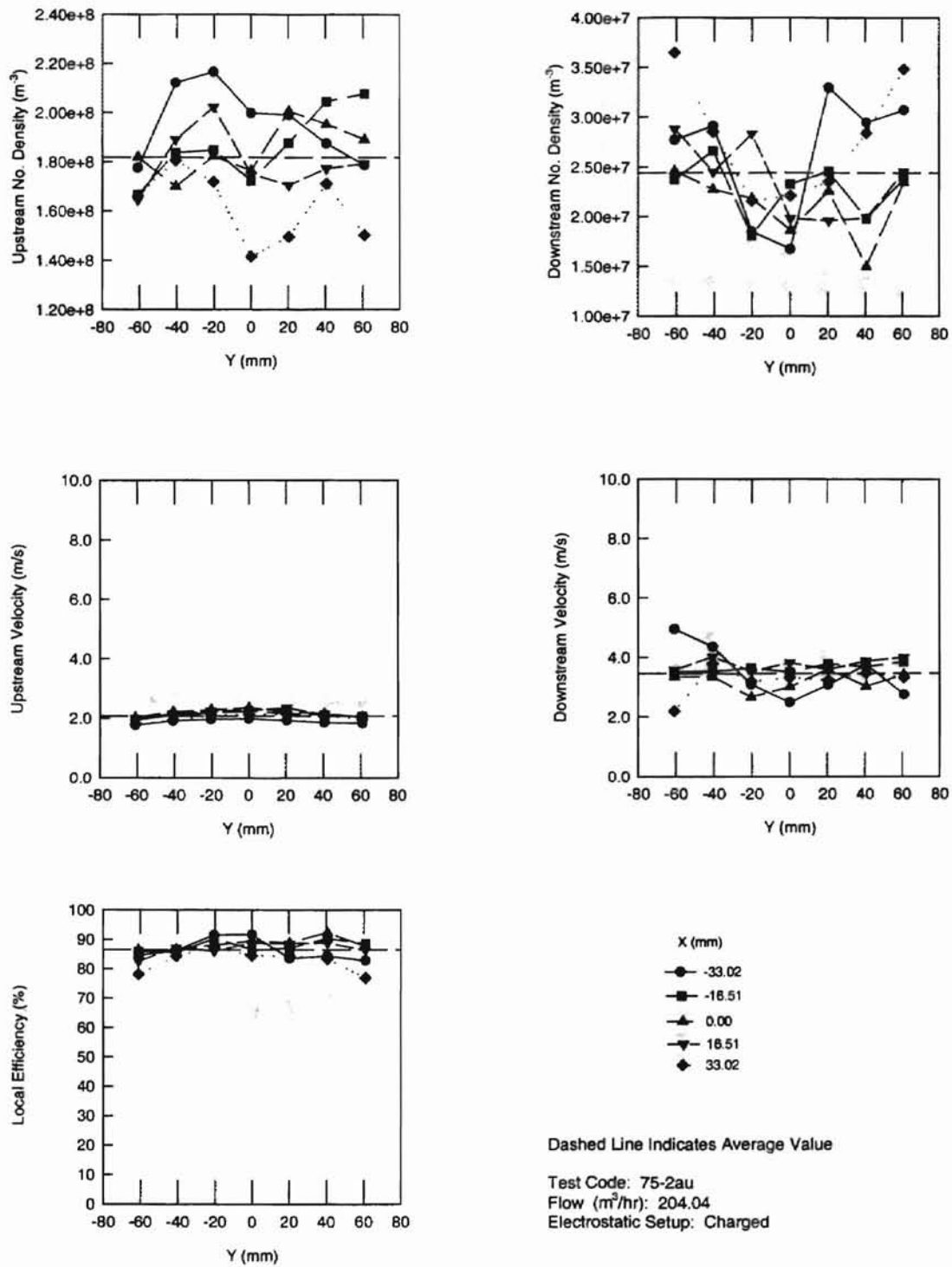


Figure A-29 Results for 2.02 Micron Diameter Aerosols using a Charged Setup for a Flow Rate of 204.04 m^3/hr in the Small Angle Diffuser Housing (75-2au)

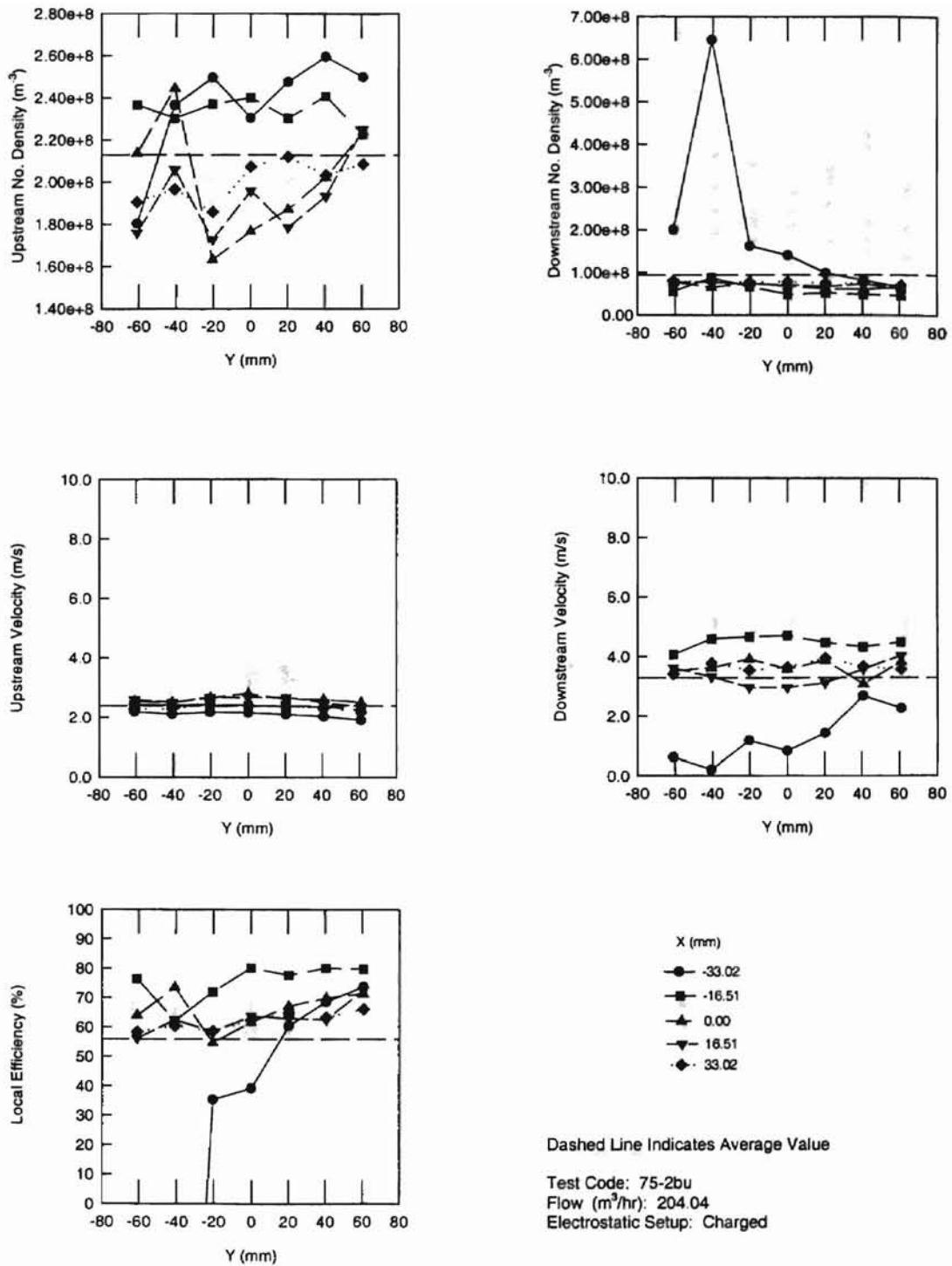


Figure A-30 Results for 2.02 Micron Diameter Aerosols using a Charged Setup for a Flow Rate of $204.04 m^3/hr$ in the Small Angle Diffuser Housing (75-2bu)

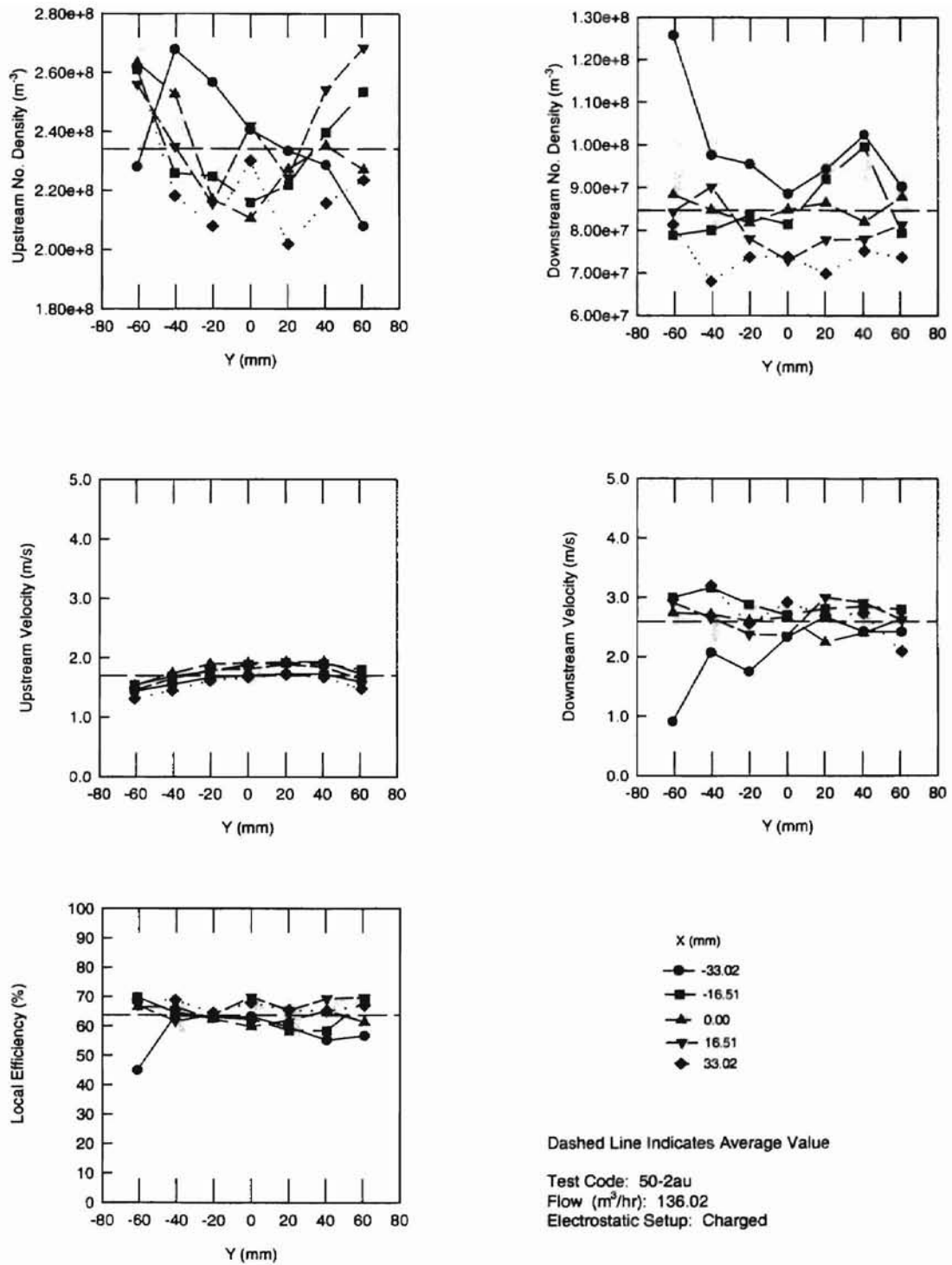


Figure A-31 Results for 2.02 Micron Diameter Aerosols using a Charged Setup for a Flow Rate of 136.02 m³/hr in the Small Angle Diffuser Housing (50-2au)

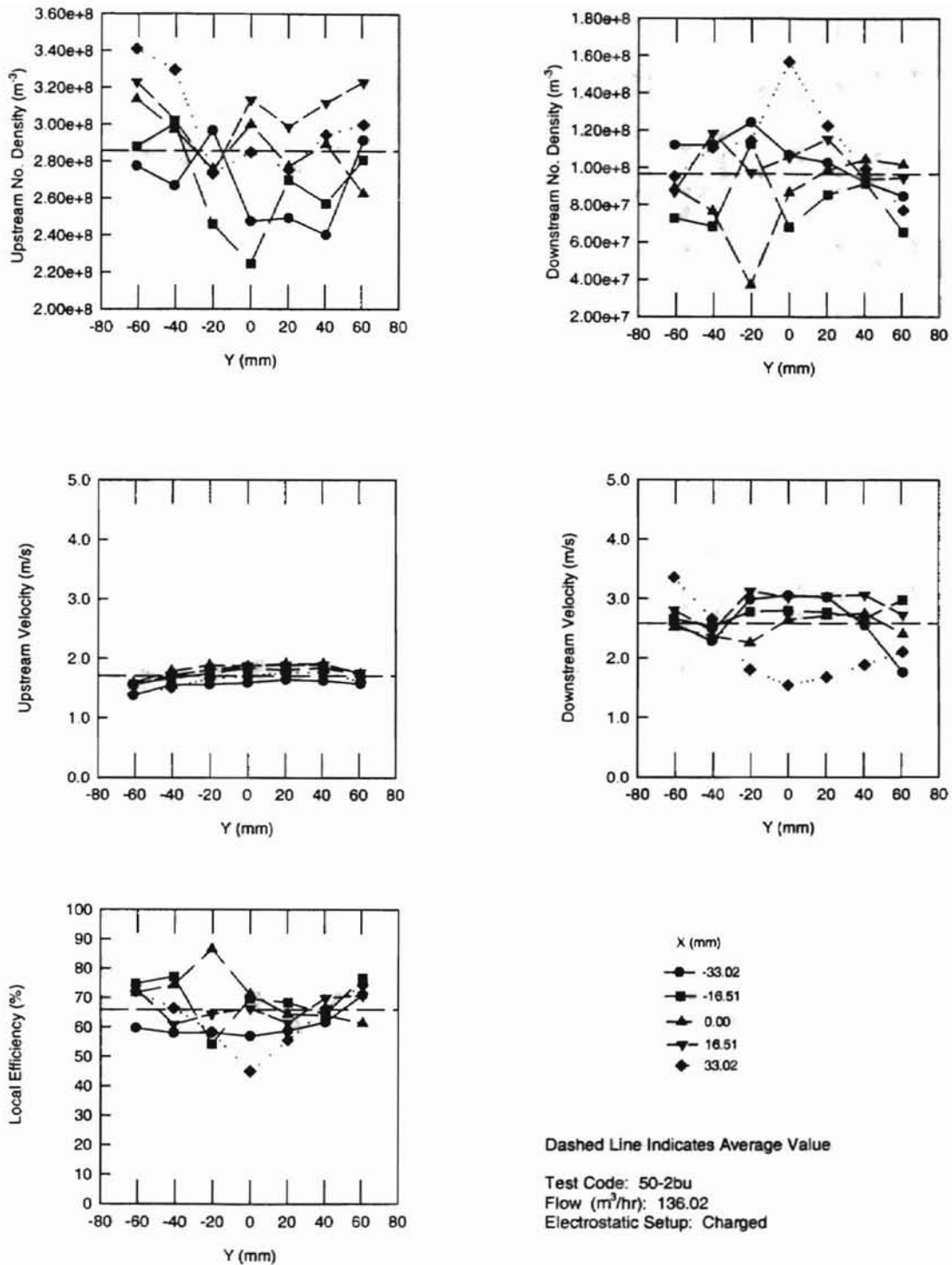
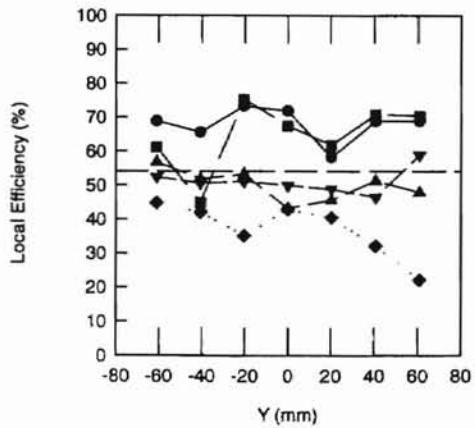
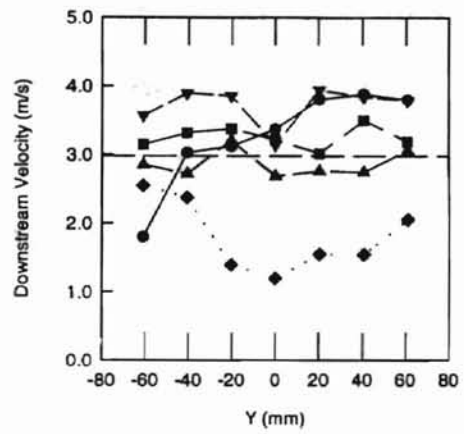
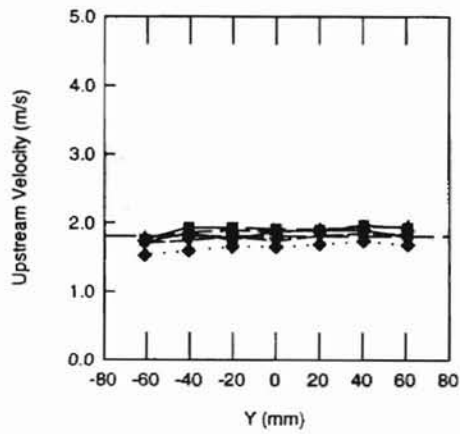
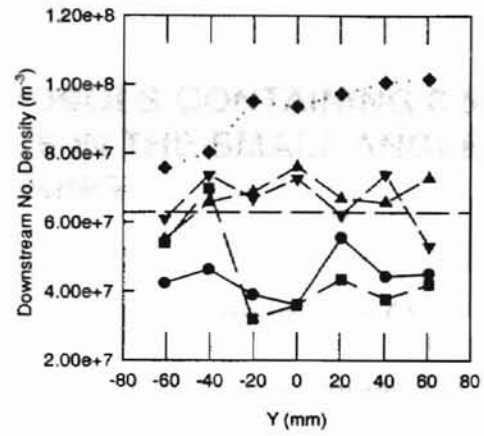
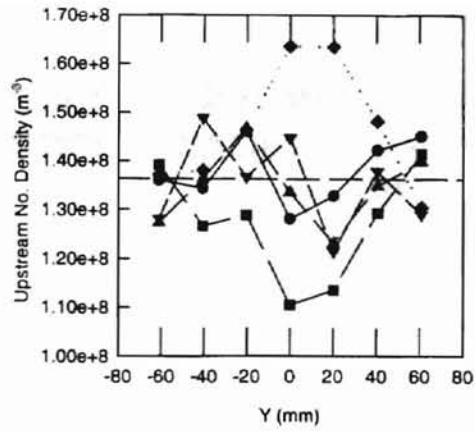


Figure A-32 Results for 2.02 Micron Diameter Aerosols using a Charged Setup for a Flow Rate of 136.02 m³/hr in the Small Angle Diffuser Housing (50-2bu)



X (mm)
 ● -33.02
 ■ -16.51
 ▲ 0.00
 ▼ 16.51
 ◆ 33.02

Dashed Line Indicates Average Value

Test Code: 50-2cu
 Flow (m^3/hr): 136.02
 Electrostatic Setup: Charged

Figure A-33 Results for 2.02 Micron Diameter Aerosols using a Charged Setup for a Flow Rate of $136.02 m^3/hr$ in the Small Angle Diffuser Housing (50-2cu)

APPENDIX B

RESULTS FOR MONODISPERSE AEROSOLS CONTAINING 0.505 MICRON DIAMETER PSL PARTICLES IN THE SMALL ANGLE DIFFUSER HOUSING

Some of the test results using 0.505 micron particles were discussed in Chapter 5. All of these test results are presented in this appendix. Each of the tests presented in this appendix shows the local efficiency, local upstream number density, local downstream number density, local upstream velocity, and local downstream velocity, respectively.

The average values of the efficiency, upstream and downstream number density, upstream velocity and downstream velocity for the tests are tabulated in Table B-1. These average values can be correlated with the figures in this appendix using the test code indicated at the bottom right hand corner of each figure and indicated for each test in Table B-1. The alphanumeric code for each test is designated as indicated Section 5.5.

Table B-1 Test Conditions and Average Values over the Filter Surface of Efficiency, Upstream and Downstream Velocities, and Upstream and Downstream Number Densities for 0.505 Micron Particles in the Small Angle Diffuser Housing

No.	Test Code	Test Date	Corrected Flow Rate	Overall Average Efficiency of the Filter	Upstream Number Density	Upstream Velocity	Downstream Number Density	Downstream Velocity	Pressure Drop (mm Water Column)			PSL Solution Strength	Temp. Deg. C	RH %	Electrostatic Charge
			m ³ /hr	(%)	(m ⁻³)	m/s	(m ⁻³)	m/s	Initial	Final	Rise	m ³ /m ³	At Mixing Box	(V)	
1	200-05ag	3/19/99	340.06	75.04	7.90E+07	5.69	1.96E+07	8.78	53.3	58.4	5.1	8/1000	37	42	0
2	200-05bg	3/24/99	340.06	73.06	7.83E+07	5.63	2.09E+07	8.51	53.3	58.4	5.1	8/1000	36	45	0
3	150-05ag	3/19/99	255.05	64.72	9.44E+07	4.27	3.30E+07	7.17	35.6	38.1	2.5	8/1000	36	42	0
4	150-05bg	3/26/99	255.05	56.89	1.36E+08	4.25	5.80E+07	6.62	33.0	35.6	2.5	8/1000	35	36	0
5	125-05ag	3/17/99	212.54	50.67	7.03E+07	3.35	6.04E+07	5.67	40.6	43.2	2.5	5/1000	33	50	0
6	125-05bg	3/17/99	212.54	54.24	1.33E+08	3.43	6.04E+07	5.67	27.9	27.9	0.0	5/1000	36	40	0
7	100-05ag	3/17/99	170.03	63.41428	1.59E+08	2.57	5.81E+07	4.50	17.8	20.3	2.5	5/1000	33	50	0
8	100-05bg	3/27/99	170.03	38.69	1.30E+08	2.64	7.94E+07	4.71	15.2	17.8	2.5	5/1000	35	40	0
9	100-05cg	3/27/99	170.03	42.25	1.65E+08	2.83	9.50E+07	4.26	15.2	17.8	2.5	5/1000	33	55	0
10	75-05ag	3/13/99	127.52	31.09	9.82E+07	2.02	6.72E+07	3.13	10.2	12.7	2.5	5/1000	35	42	0
11	75-05bg	4/1/99	127.52	39.84	2.56E+08	1.72	1.52E+08	3.11	7.6	10.2	2.5	5/1000	33	55	0
12	50-05ag	3/18/99	85.02	45.62	2.49E+08	1.38	1.34E+08	2.37	7.6	7.6	0.0	5/2000	35	40	0
13	50-05bg	3/31/99	85.02	30.96	3.10E+08	1.32	2.13E+08	2.18	6.4	6.4	0.0	5/2000	33	51	0
14	25-05ag	3/18/99	42.51	48.53	5.85E+08	0.64	2.98E+08	1.02	5.1	5.1	0.0	5/2000	35	42	0
15	25-05bg	3/30/99	42.51	31.84	7.52E+08	0.64	5.10E+08	1.19	2.5	3.8	1.3	5/2000	33	50	0
16	200-05au	12/11/98	544.10	85.6	2.03E+07	7.90	2.74E+06	11.45	68.6	76.2	7.6	3.5/1400	35	40	-150
17	175-05au	12/10/98	476.09	79.8	3.10E+07	6.39	6.23E+06	9.50	63.5	71.1	7.6	5/2000	36	37	-100
18	175-05bu	12/11/98	476.09	77.5	3.77E+07	6.45	7.54E+06	9.82	63.5	71.1	7.6	36647	40	35	-100

Table B-1 (continued)

No.	Test Code	Test Date	Corrected Flow Rate	Overall Average Efficiency of the Filter	Upstream Number Density	Upstream Velocity	Downstream Number Density	Downstream Velocity	Pressure Drop (mm Water Column)			PSL Solution Strength	Temp. Deg. C	RH %	Electrostatic Charge
									Initial	Final	Rise				
			m ³ /hr	(%)	(m ⁻³)	m/s	(m ⁻³)	m/s				m ³ /m ³	At Mixing Box	(V)	
19	150-05au	10/29/98	408.08	82.75	4.56E+07	6.28	7.99E+06	9.01	58.4	63.5	5.1	5/1000	NA	51.3	NA
20	150-05bu	11/5/98	408.08	75.51	5.40E+07	6.36	1.31E+07	10.10	53.3	61.0	7.6	5/1000	NA	51.3	NA
21	125-05au	11/4/98	340.06	63.4	9.94E+06	5.00	1.83E+07	7.51	45.7	50.8	5.1	5/1000	NA	47	NA
22	125-05bu	11/6/98	340.06	61.29149	6.10E+07	4.89	2.35E+07	7.67	45.7	50.8	5.1	2.5/1000	31	47	NA
23	100-05au	12/15/98	272.05	45.82	6.25E+07	3.55	3.37E+07	6.11	25.4	27.9	2.5	1.25/1000	40	37	-100
24	100-05bu	12/15/98	272.05	49.51	5.80E+07	3.50	2.90E+07	5.64	25.4	27.9	2.5	1.25/1000	41	37	-500
25	75-05au	28/10/98	204.04	23.55	7.90E+07	2.68	5.94E+07	4.49	17.8	17.8	0.0	5/1000	NA	51	NA
26	75-05bu	10/29/98	204.04	34.81	1.47E+08	2.79	7.56E+07	4.49	17.8	22.9	5.1	5/1000	NA	51	NA
27	75-05cu	12/16/98	204.04	29.84	8.97E+07	2.63	6.25E+07	4.01	12.7	22.9	10.2	1.25/1000	40	37	NA
28	50-05au	10/30/98	136.03	28.86	1.07E+08	1.70	7.53E+07	2.80	8.9	10.2	1.3	5/1000	32	55	NA
29	50-05bu	11/5/98	136.03	36.24	1.58E+08	1.97	1.00E+08	3.00	8.9	10.2	1.3	5/2000	32	55	NA
30	25-05au	11/4/98	68.01	35.64	3.17E+08	0.86	2.01E+08	1.34	5.1	5.1	0.0	5/2000	39	40	NA
31	25-05bu	11/6/98	68.01	8.58	1.96E+08	0.88	1.73E+08	1.41	5.1	5.1	0.0	5/2000	39	40	NA
32	25-05cu	12/16/98	68.01	29.54686	2.12E+08	0.78	1.45E+08	1.29	5.1	5.1	0.0	5/2000	37	40	-50

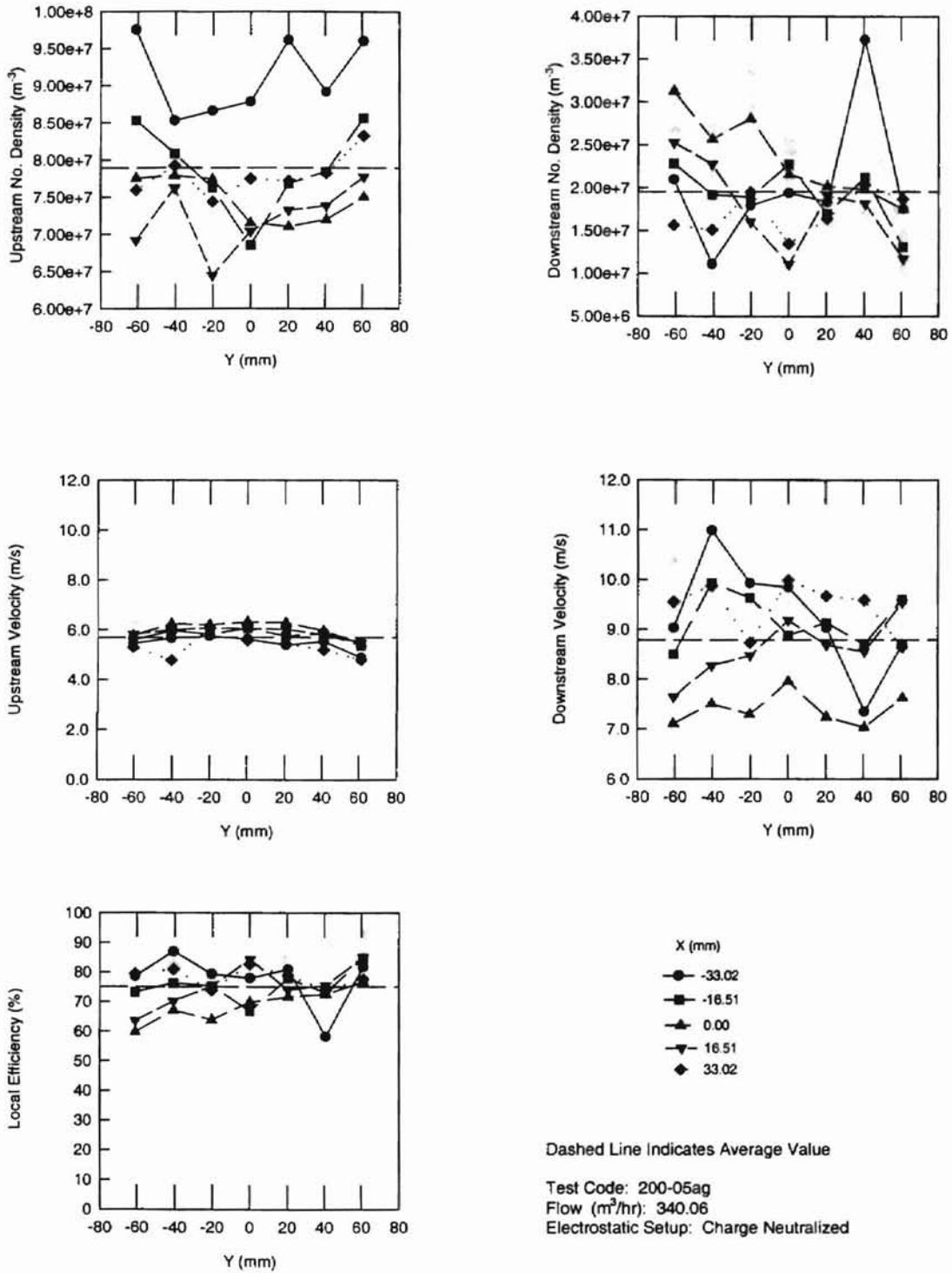


Figure B-1 Results for 0.505 Micron Diameter Aerosols using a Charge Neutralized Setup for a Flow Rate of 340.06 m³/hr in the Small Angle Diffuser Housing (200-05ag)

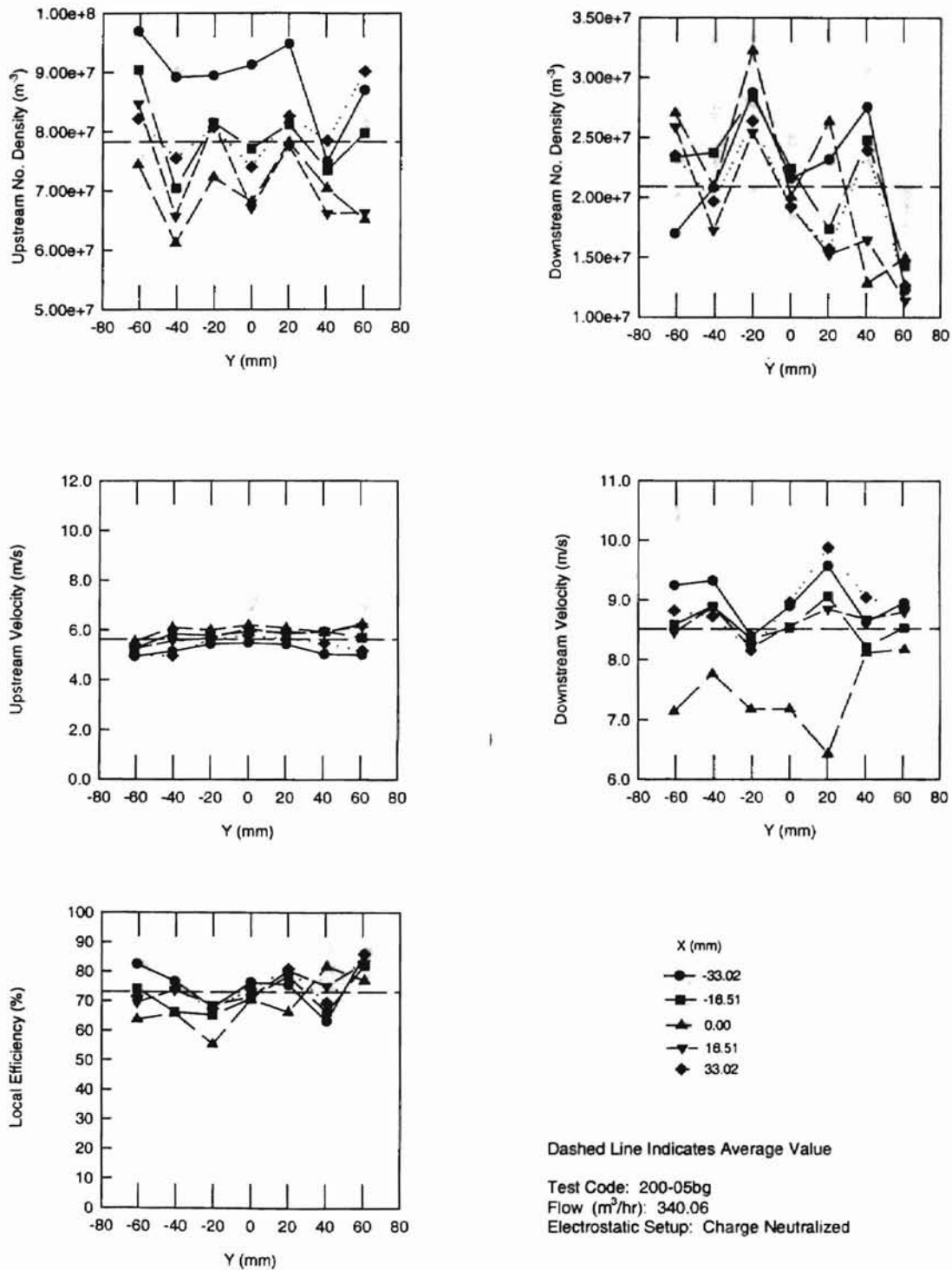


Figure B-2 Results for 0.505 Micron Diameter Aerosols using a Charge Neutralized Setup for a Flow Rate of 340.06 m^3/hr in the Small Angle Diffuser Housing (200-05bg)

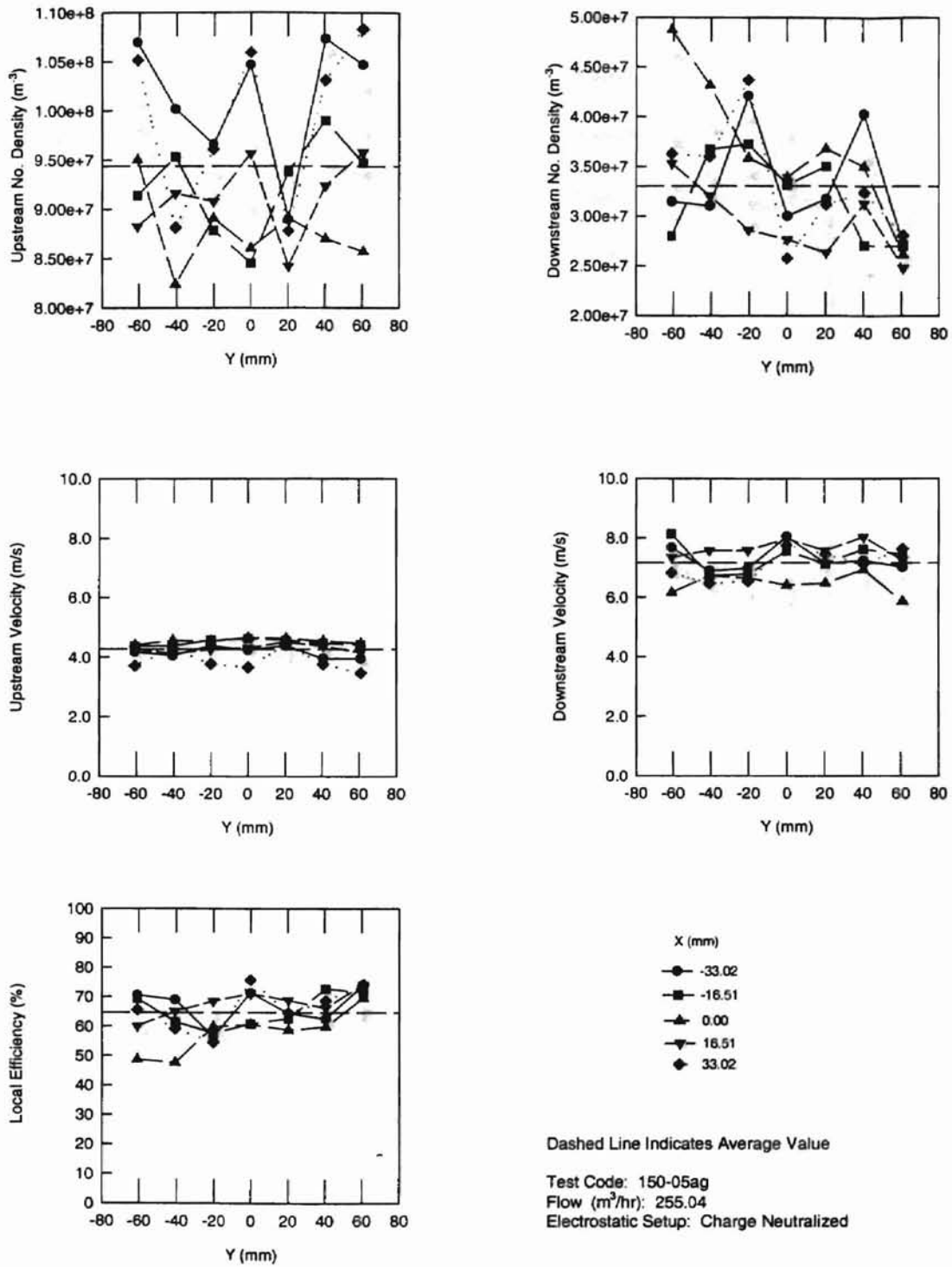


Figure B-3 Results for 0.505 Micron Diameter Aerosols using a Charge Neutralized Setup for a Flow Rate of 255.04 m³/hr in the Small Angle Diffuser Housing (150-05ag)

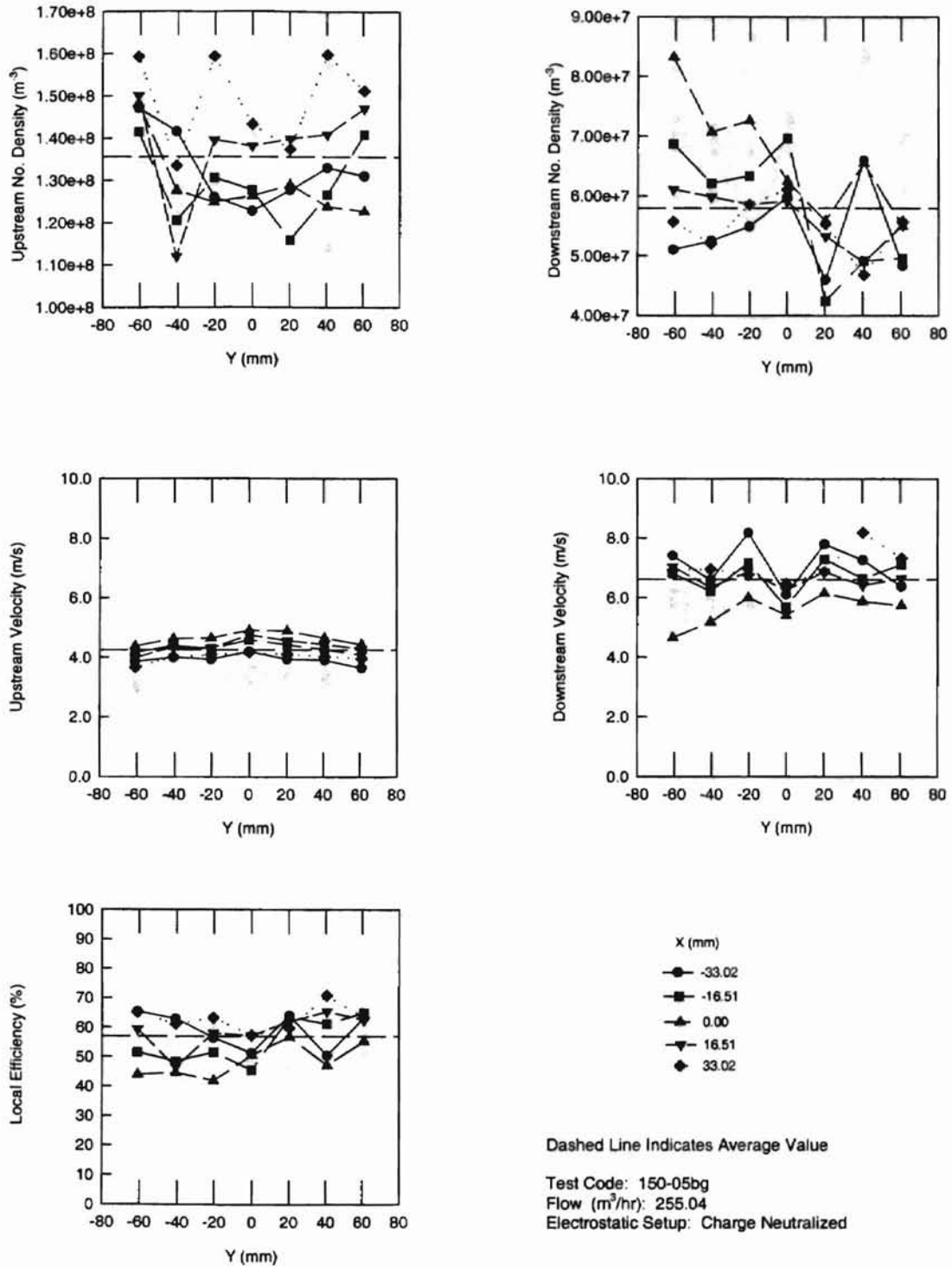


Figure B-4 Results for 0.505 Micron Diameter Aerosols using a Charge Neutralized Setup for a Flow Rate of $255.04 m^3/hr$ in the Small Angle Diffuser Housing (150-05bg)

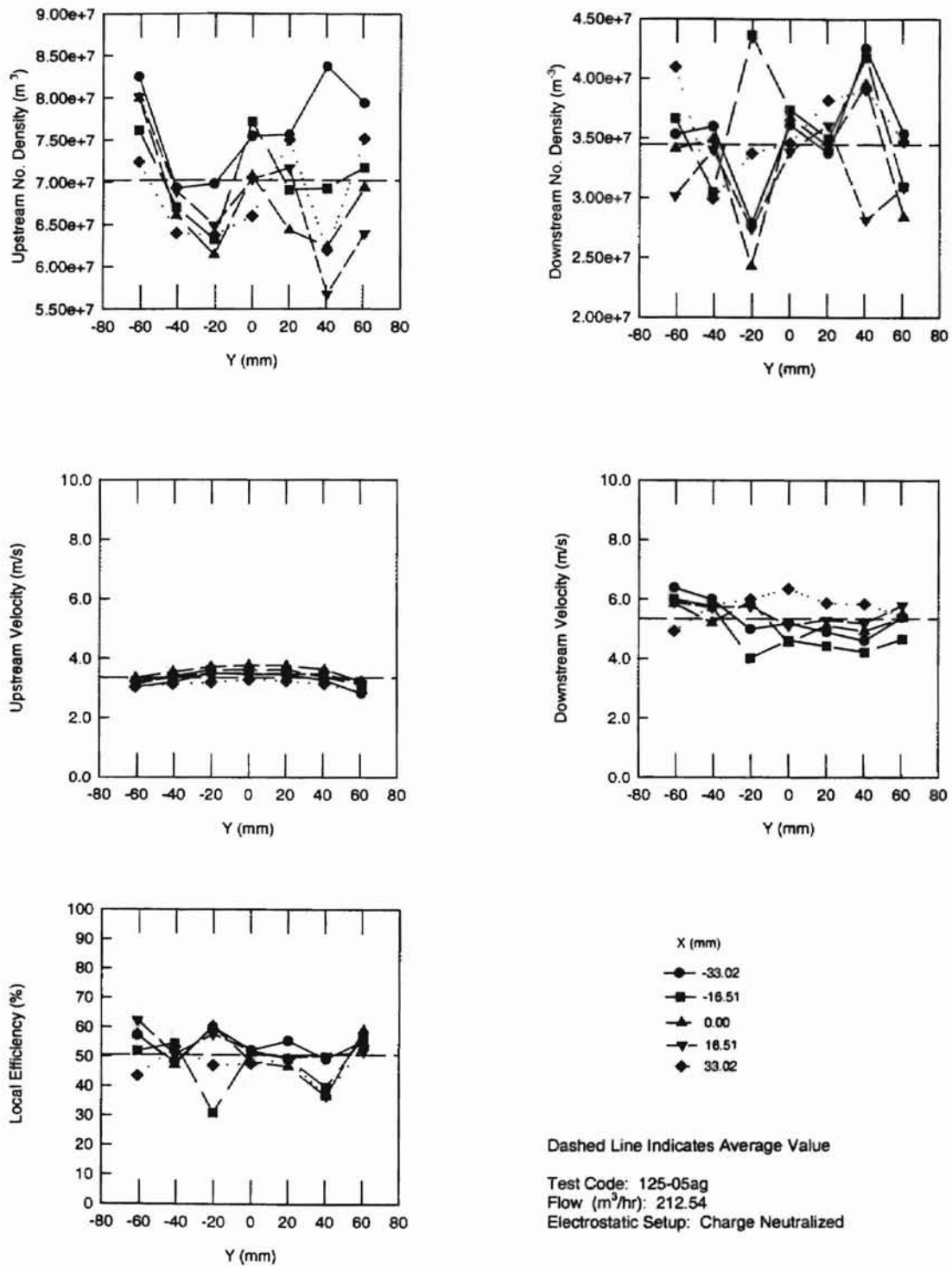


Figure B-5 Results for 0.505 Micron Diameter Aerosols using a Charge Neutralized Setup for a Flow Rate of $212.54 m^3/hr$ in the Small Angle Diffuser Housing (125-05ag)

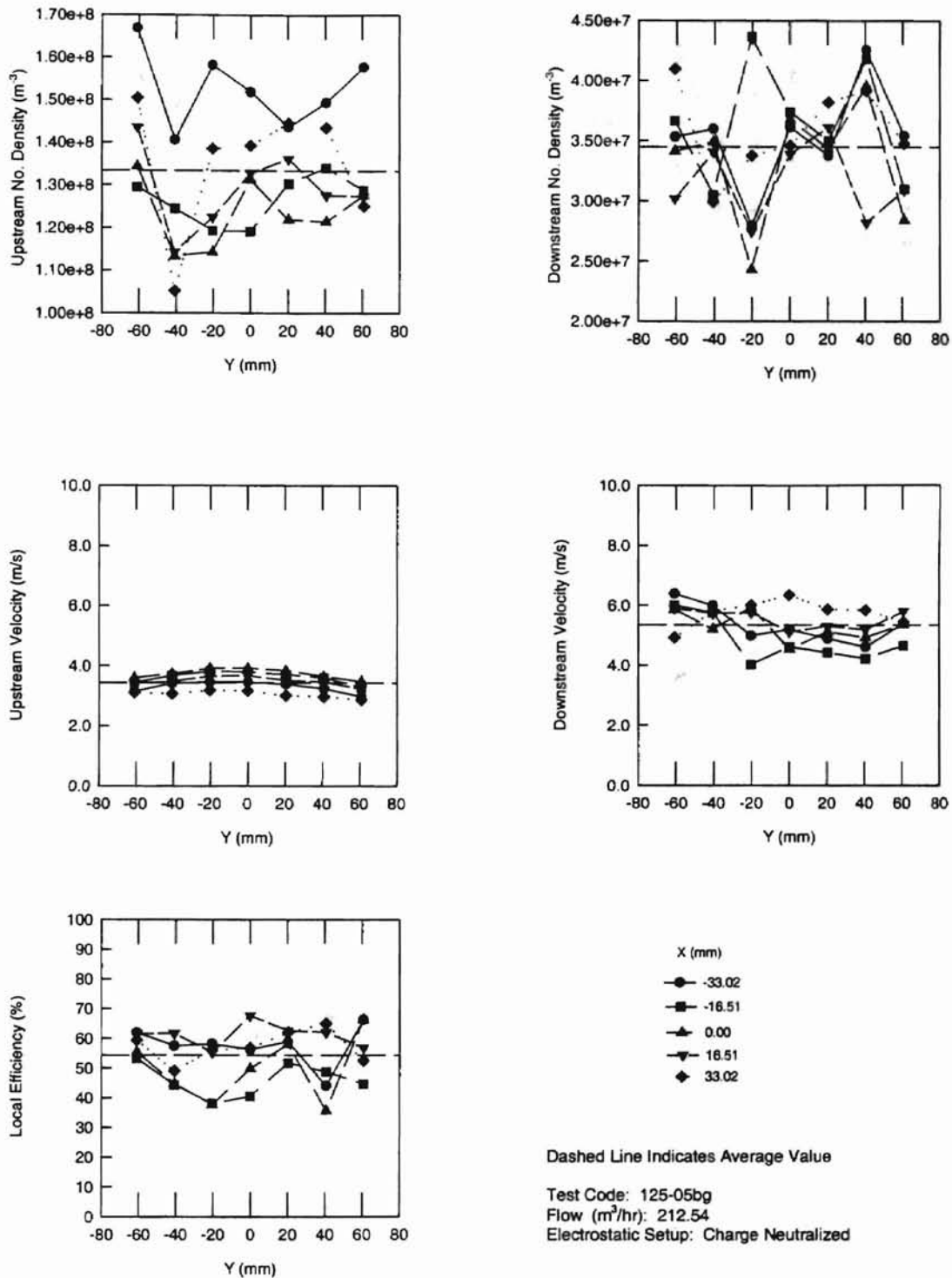


Figure B-6 Results for 0.505 Micron Diameter Aerosols using a Charge Neutralized Setup for a Flow Rate of 212.54 m^3/hr in the Small Angle Diffuser Housing (125-05bg)

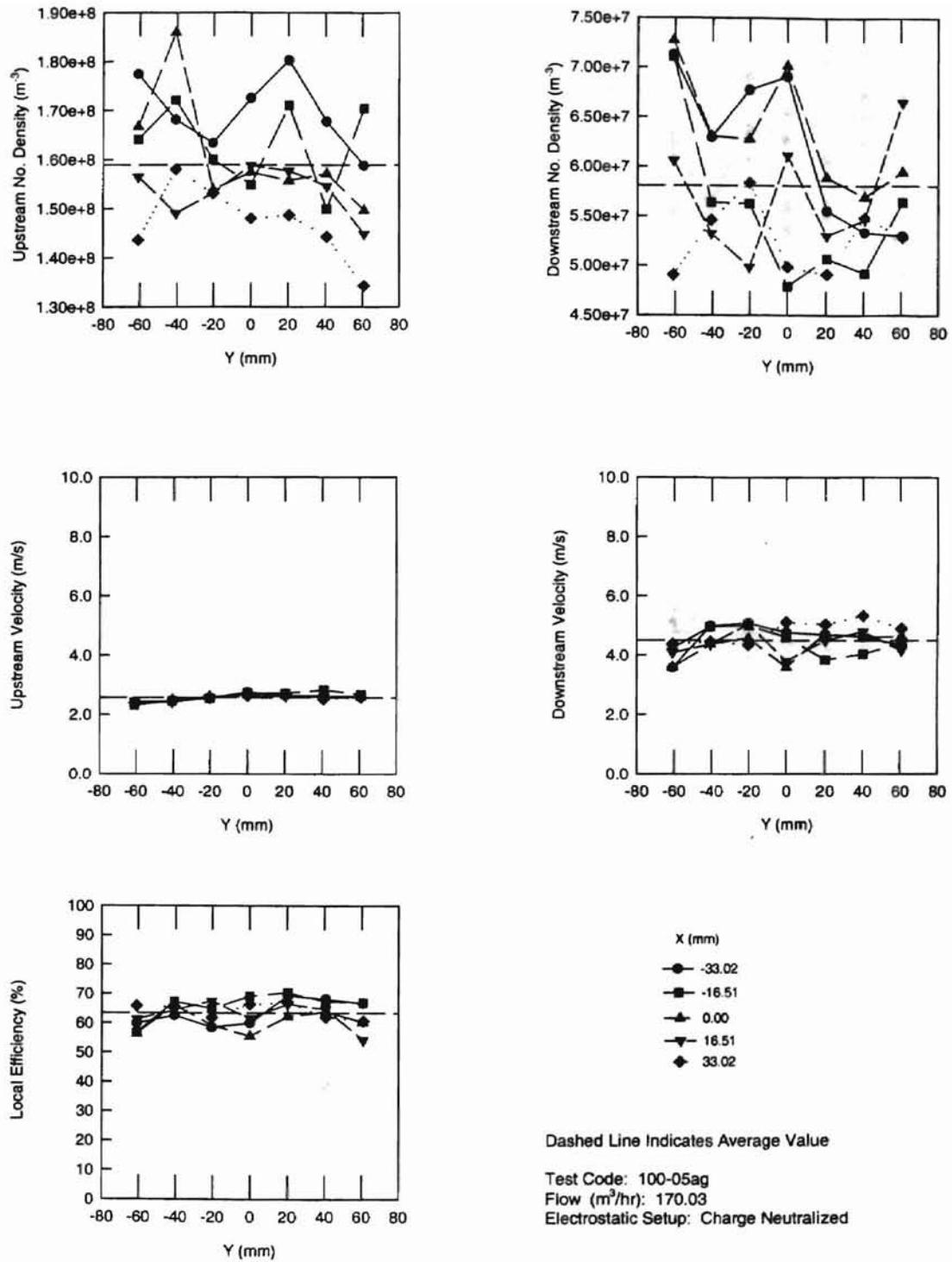
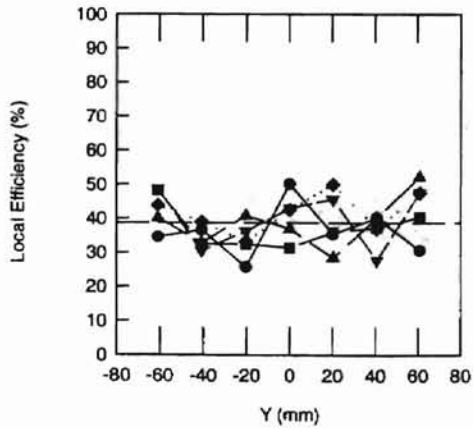
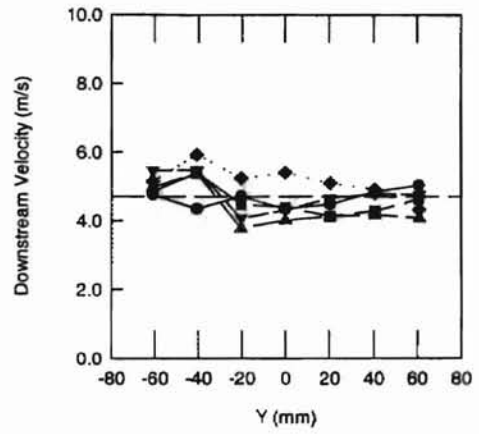
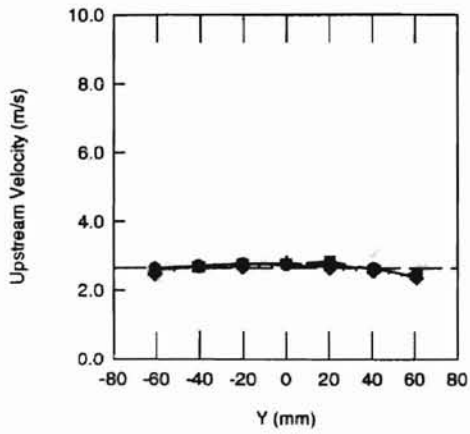
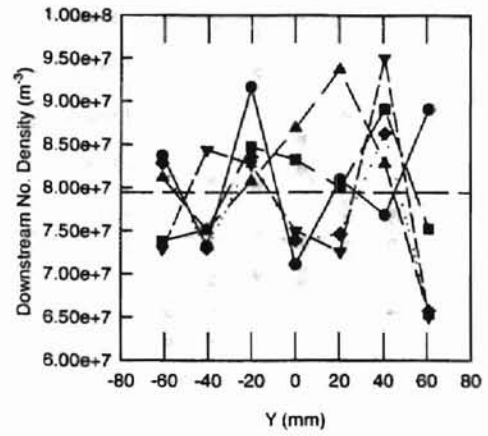
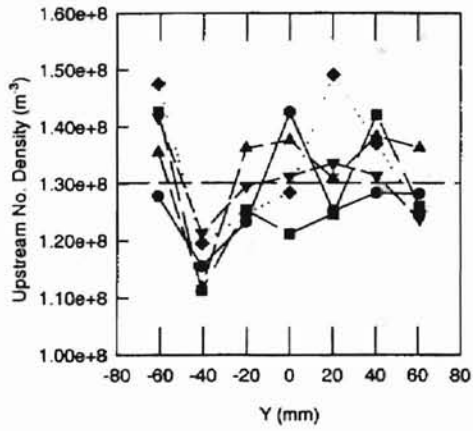


Figure B-7 Results for 0.505 Micron Diameter Aerosols using a Charge Neutralized Setup for a Flow Rate of 170.03 m^3/hr in the Small Angle Diffuser Housing (100-05ag)



X (mm)
 ● -33.02
 ■ -16.51
 ▲ 0.00
 ▼ 16.51
 ◆ 33.02

Dashed Line Indicates Average Value
 Test Code: 100-05bg
 Flow (m³/hr): 170.03
 Electrostatic Setup: Charge Neutralized

Figure B-8 Results for 0.505 Micron Diameter Aerosols using a Charge Neutralized Setup for a Flow Rate of 170.03 m³/hr in the Small Angle Diffuser Housing (100-05bg)

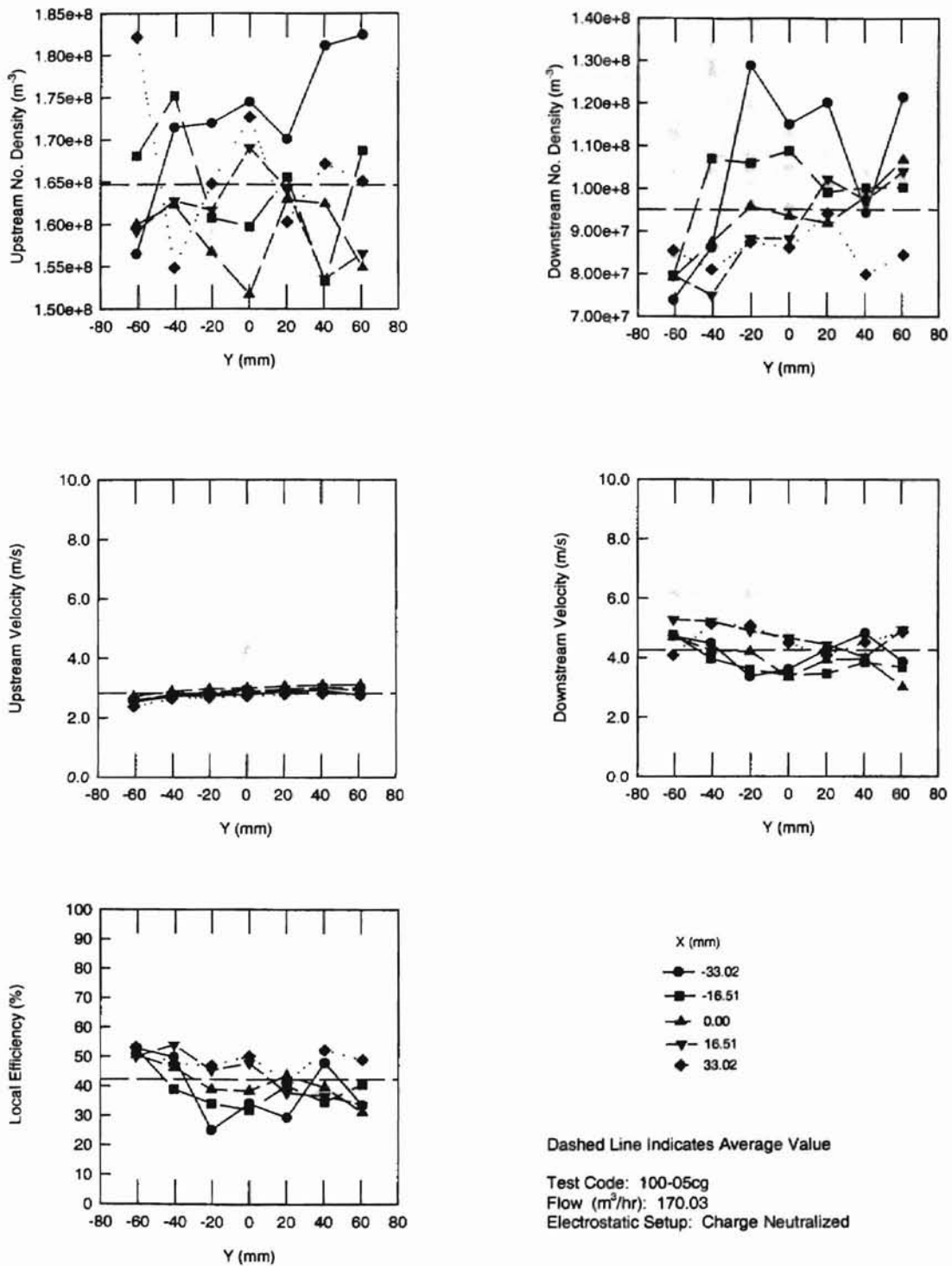
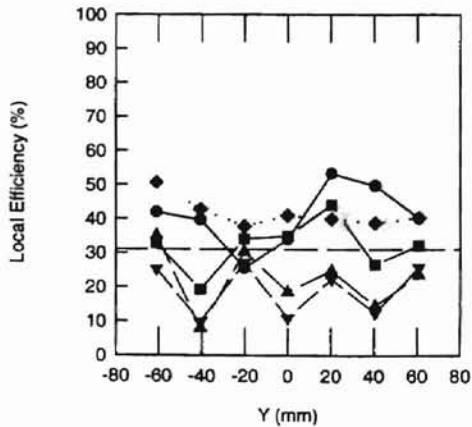
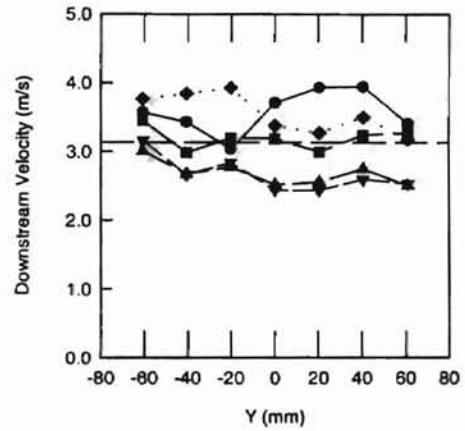
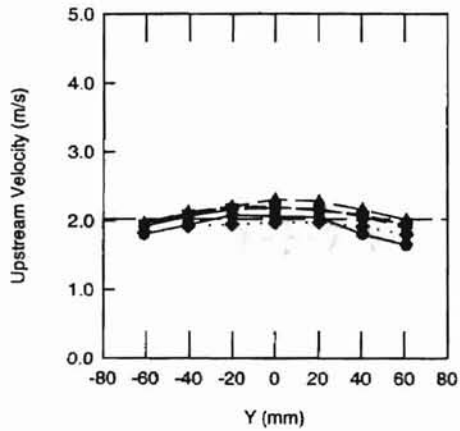
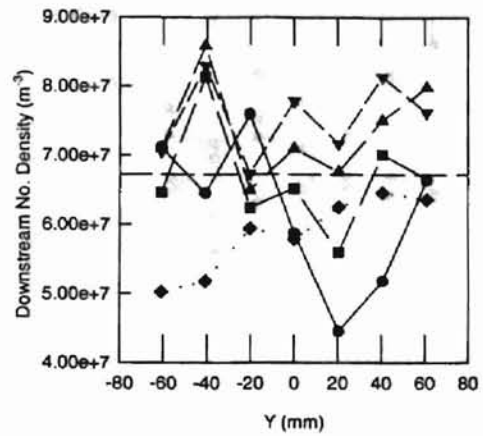
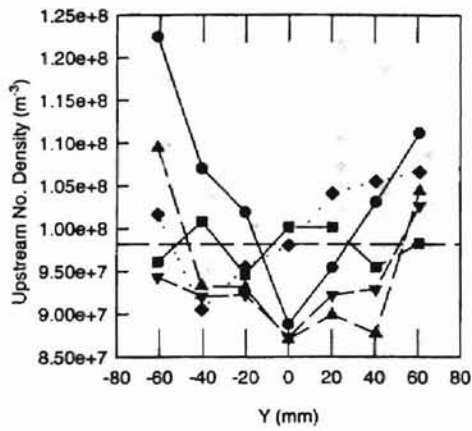


Figure B-9 Results for 0.505 Micron Diameter Aerosols using a Charge Neutralized Setup for a Flow Rate of $170.03 m^3/hr$ in the Small Angle Diffuser Housing (100-05cg)



X (mm)

- -33.02
- -16.51
- ▲ 0.00
- ▼ 16.51
- ◆ 33.02

Dashed Line Indicates Average Value

Test Code: 75-05ag

Flow (m³/hr): 127.52

Electrostatic Setup: Charge Neutralized

Figure B-10 Results for 0.505 Micron Diameter Aerosols using a Charge Neutralized Setup for a Flow Rate of 127.52 m³/hr in the Small Angle Diffuser Housing (75-05ag)

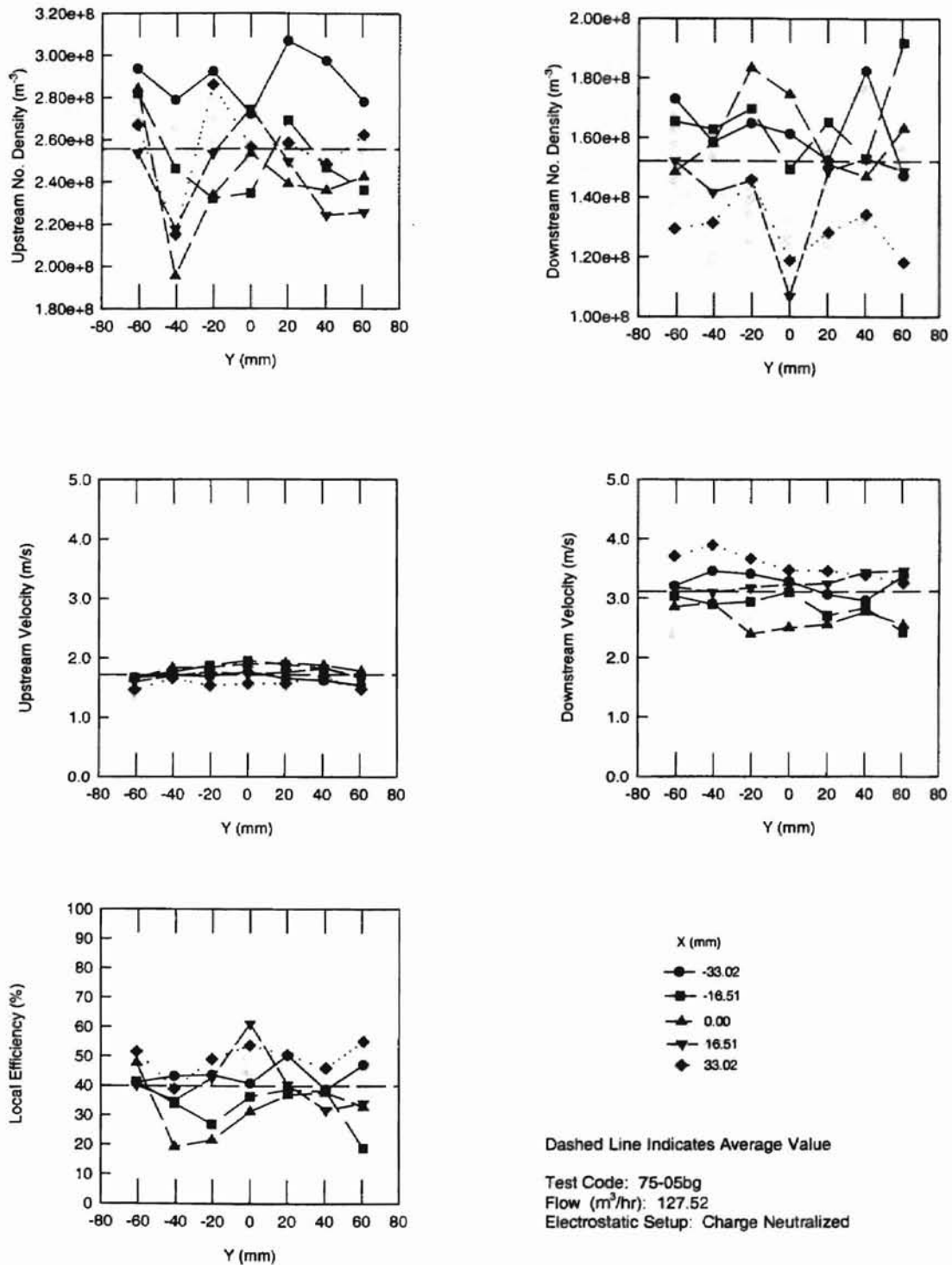
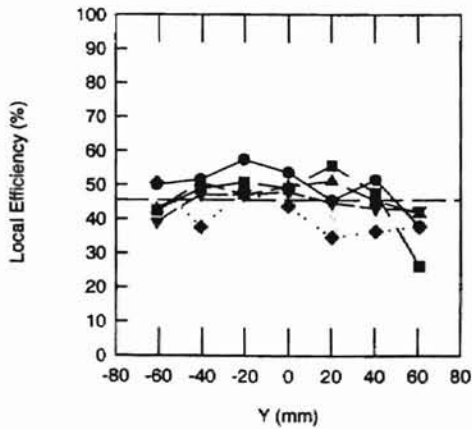
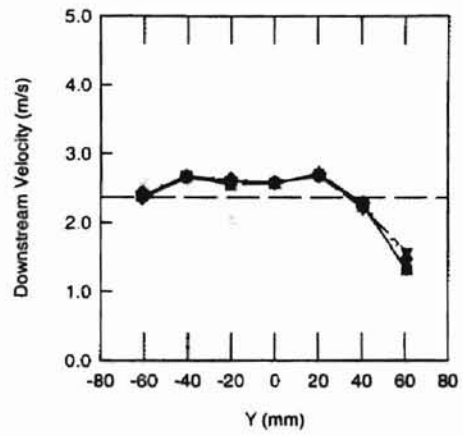
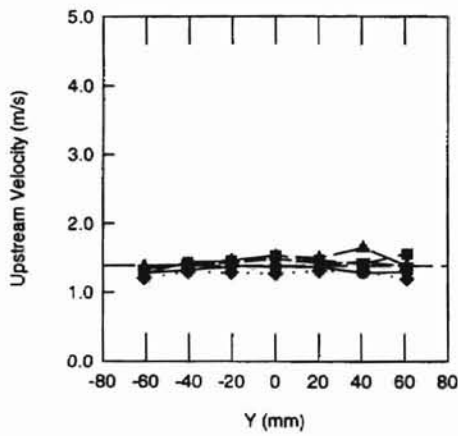
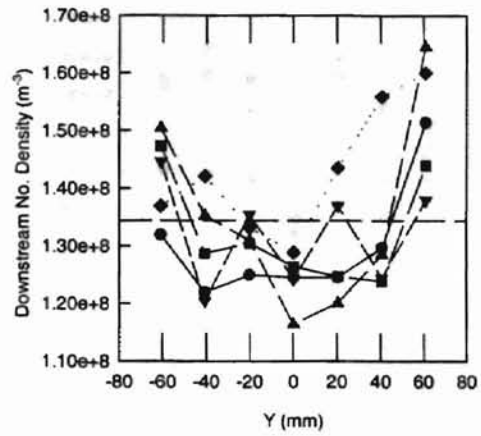
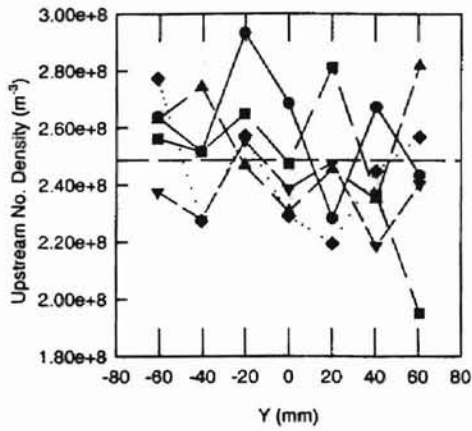


Figure B-11 Results for 0.505 Micron Diameter Aerosols using a Charge Neutralized Setup for a Flow Rate of 127.52 m³/hr in the Small Angle Diffuser Housing (75-05bg)

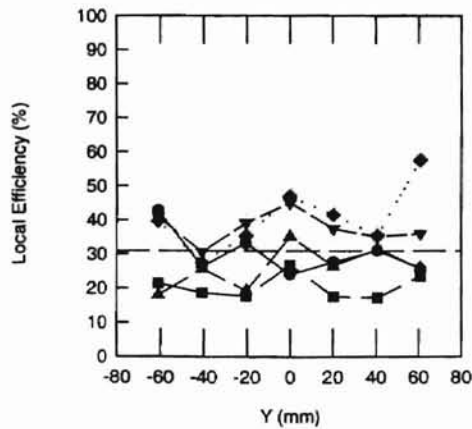
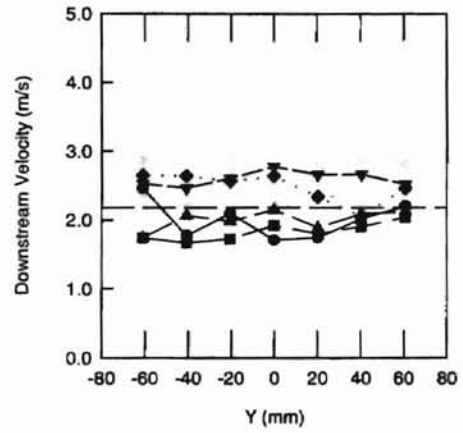
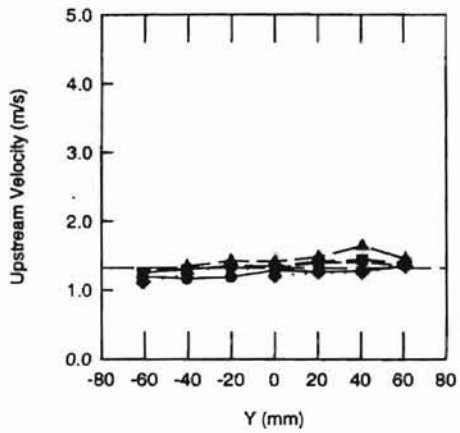
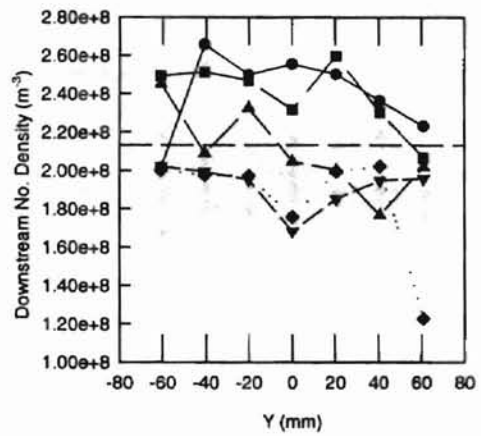
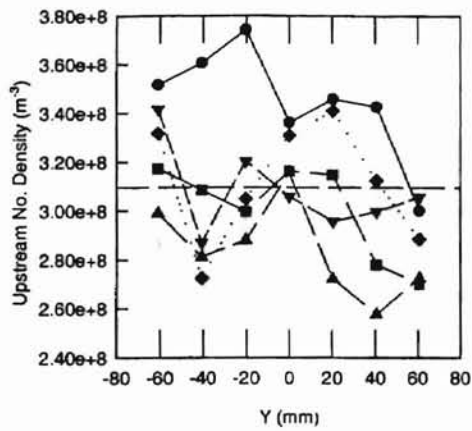


X (mm)
 ● -33.02
 ■ -16.51
 ▲ 0.00
 ▼ 16.51
 ◆ 33.02

Dashed Line Indicates Average Value

Test Code: 50-05ag
 Flow (m³/hr): 85.02
 Electrostatic Setup: Charge Neutralized

Figure B-12 Results for 0.505 Micron Diameter Aerosols using a Charge Neutralized Setup for a Flow Rate of 85.02 m³/hr in the Small Angle Diffuser Housing (50-05ag)



- X (mm)
- -33.02
 - -16.51
 - ▲ 0.00
 - ▼ 16.51
 - ◆ 33.02

Dashed Line Indicates Average Value

Test Code: 50-05bg

Flow (m³/hr): 85.02

Electrostatic Setup: Charge Neutralized

Figure B-13 Results for 0.505 Micron Diameter Aerosols using a Charge Neutralized Setup for a Flow Rate of 85.02 m³/hr in the Small Angle Diffuser Housing (50-05bg)

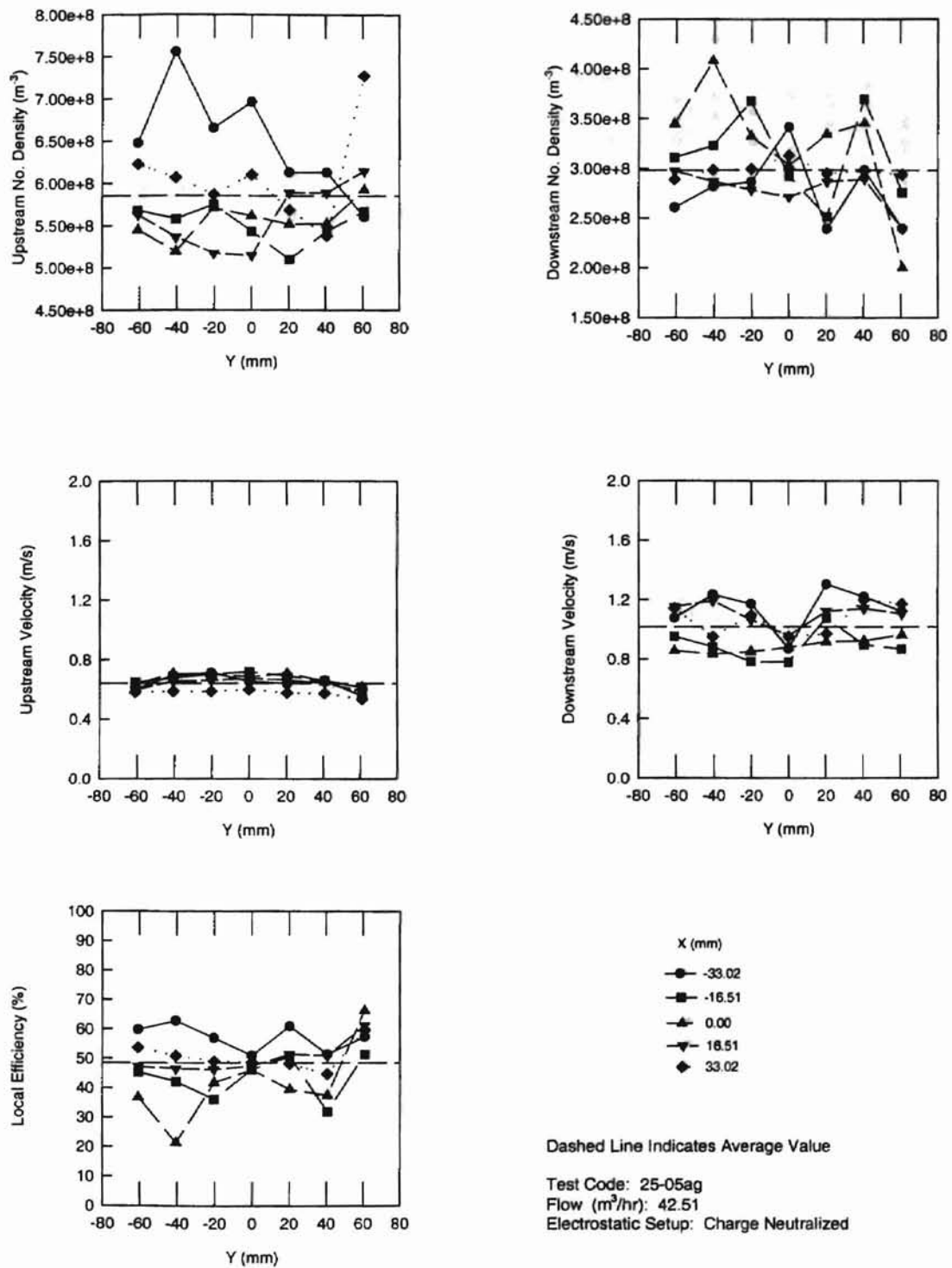
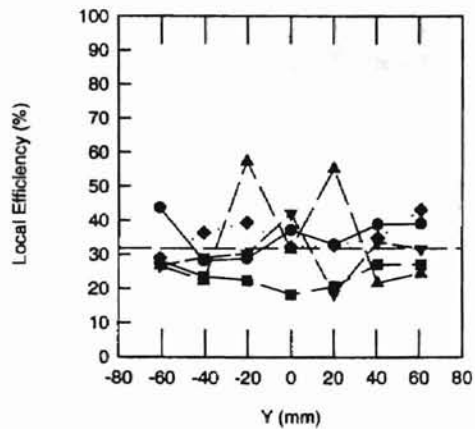
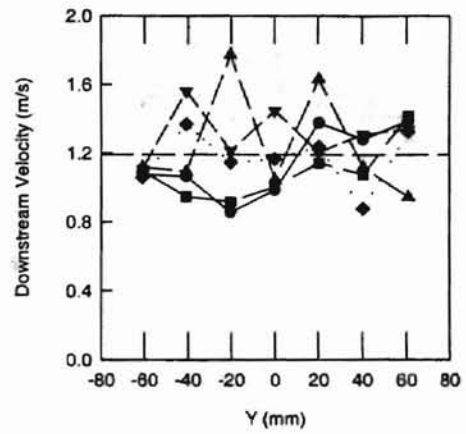
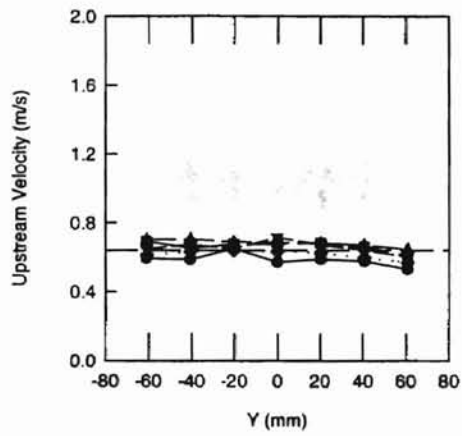
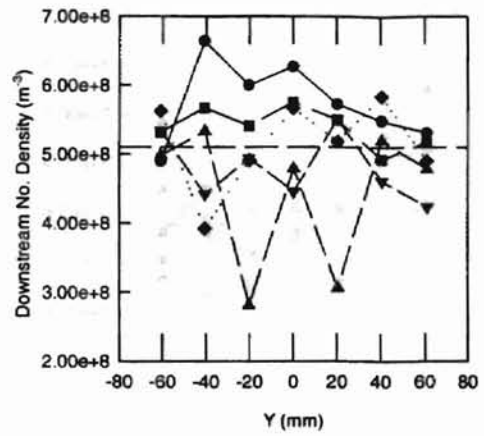
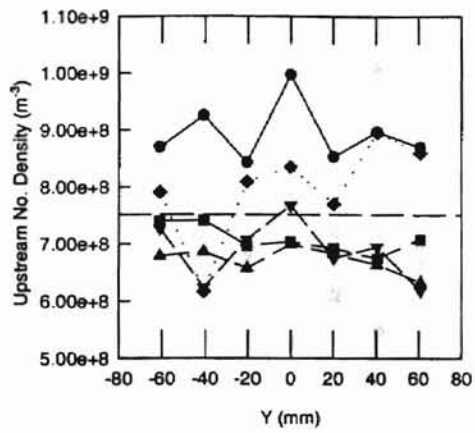


Figure B-14 Results for 0.505 Micron Diameter Aerosols using a Charge Neutralized Setup for a Flow Rate of 42.51 m^3/hr in the Small Angle Diffuser Housing (25-05ag)



X (mm)

- -33.02
- -18.51
- ▲ 0.00
- ▼ 18.51
- ◆ 33.02

Dashed Line Indicates Average Value

Test Code: 25-05bg

Flow (m^3/hr): 42.51

Electrostatic Setup: Charge Neutralized

Figure B-15 Results for 0.505 Micron Diameter Aerosols using a Charge Neutralized Setup for a Flow Rate of 42.51 m^3/hr in the Small Angle Diffuser Housing (25-05bg)

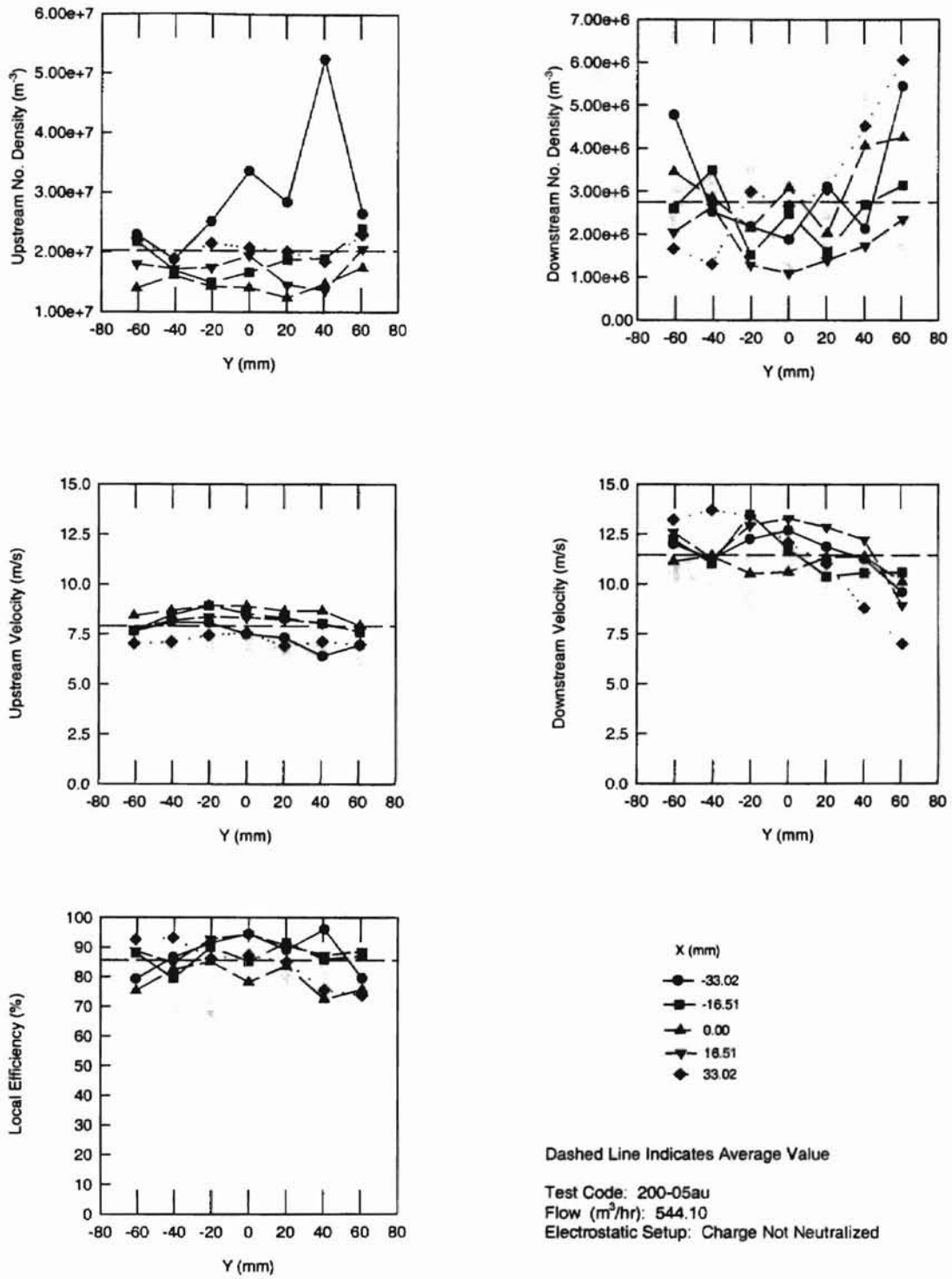
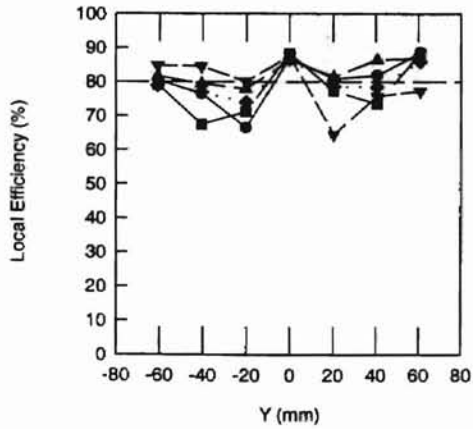
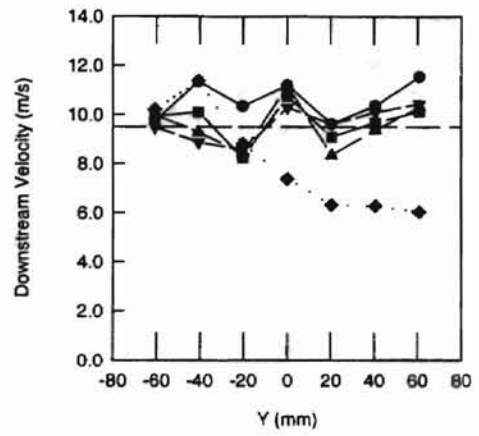
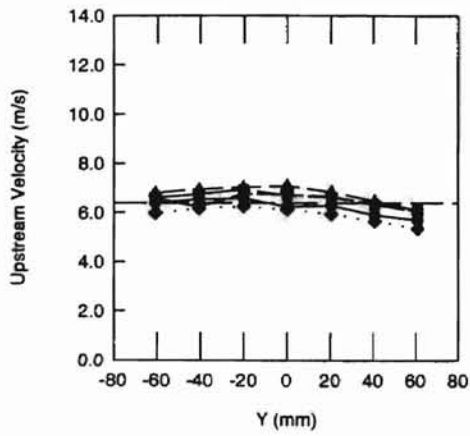
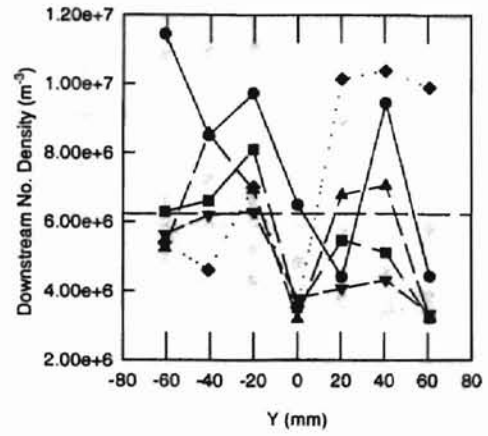
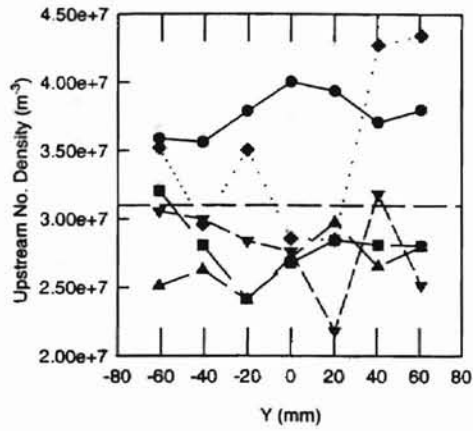


Figure B-16 Results for 0.505 Micron Diameter Aerosols using a Charged Setup for a Flow Rate of 544.10 m³/hr in the Small Angle Diffuser Housing (200-05au)



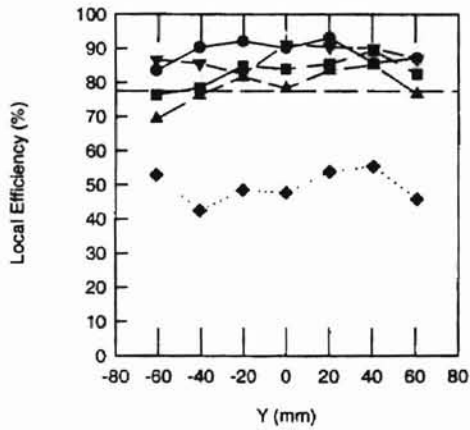
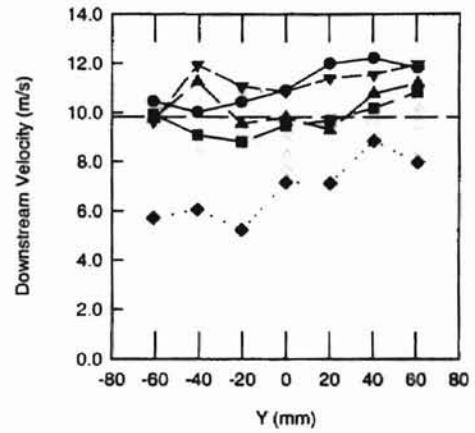
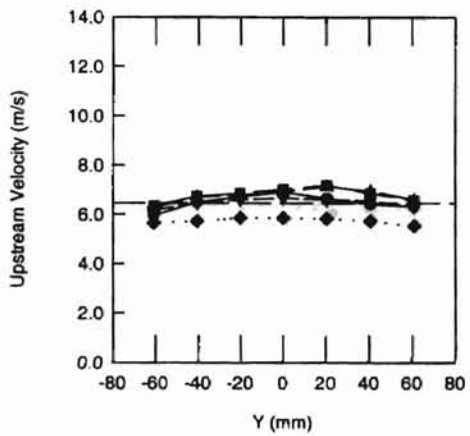
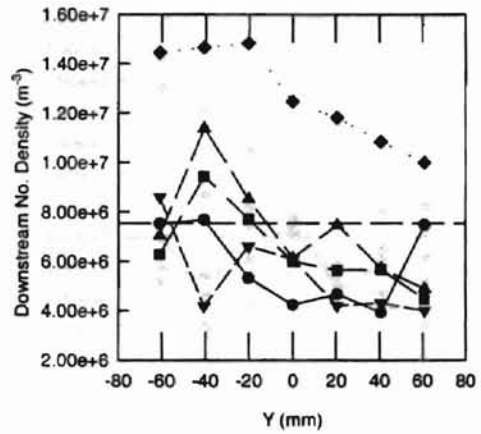
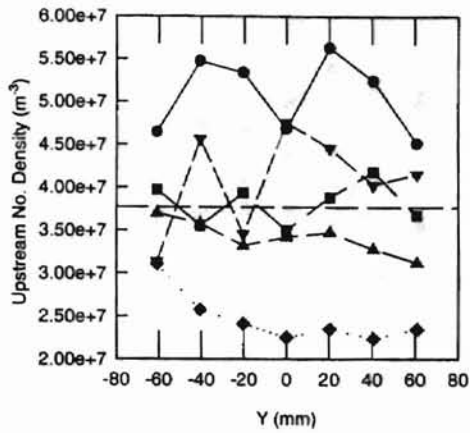
X (mm)

- -33.02
- -16.51
- ▲ 0.00
- ▼ 16.51
- ◆ 33.02

Dashed Line Indicates Average Value

Test Code: 175-05au
 Flow (m³/hr): 476.09
 Electrostatic Setup: Charged

Figure B-17 Results for 0.505 Micron Diameter Aerosols using a Charged Setup for a Flow Rate of 476.09 m³/hr in the Small Angle Diffuser Housing (175-05au)

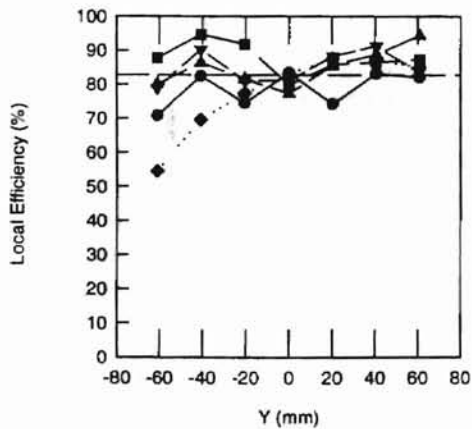
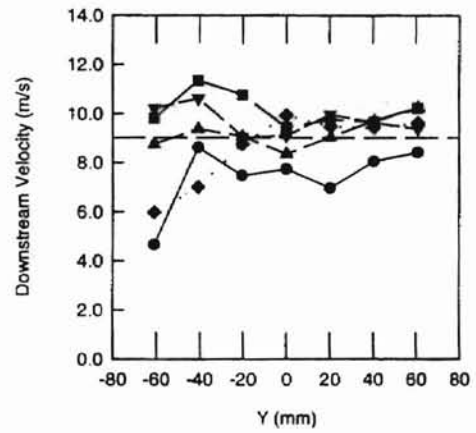
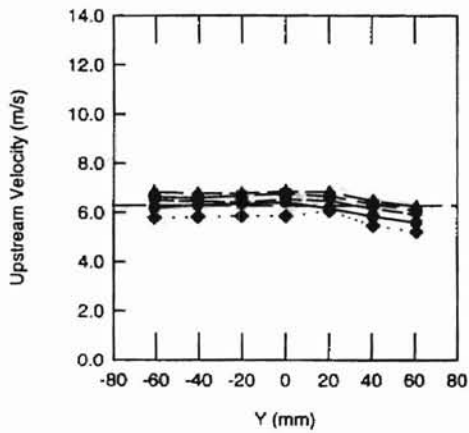
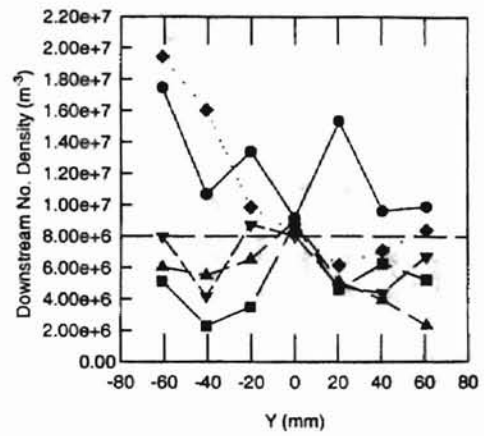
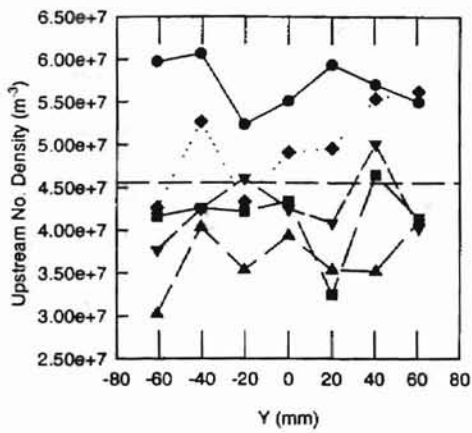


X (mm)
 ● -33.02
 ■ -16.51
 ▲ 0.00
 ▼ 16.51
 ◆ 33.02

Dashed Line Indicates Average Value

Test Code: 175-05bu
 Flow (m^3/hr): 476.09
 Electrostatic Setup: Charged

Figure B-18 Results for 0.505 Micron Diameter Aerosols using a Charged Setup for a Flow Rate of $476.09 m^3/hr$ in the Small Angle Diffuser Housing (175-05bu)



- X (mm)
- -33.02
 - -16.51
 - ▲ 0.00
 - ▼ 16.51
 - ◆ 33.02

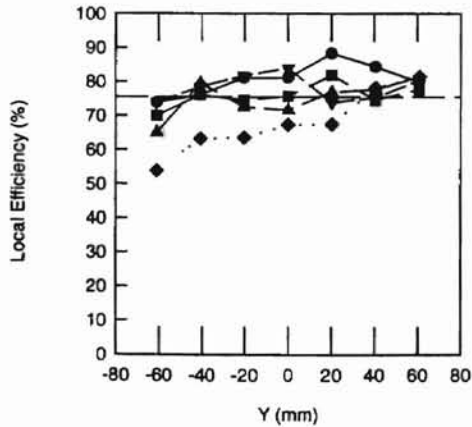
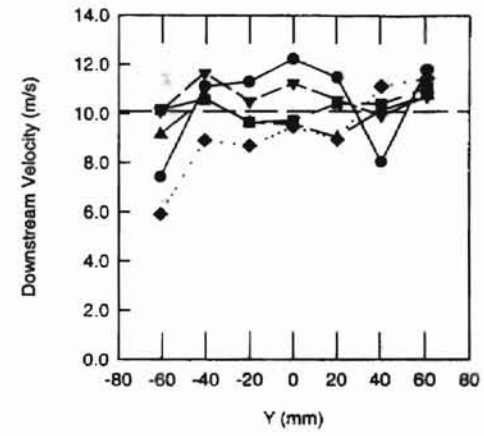
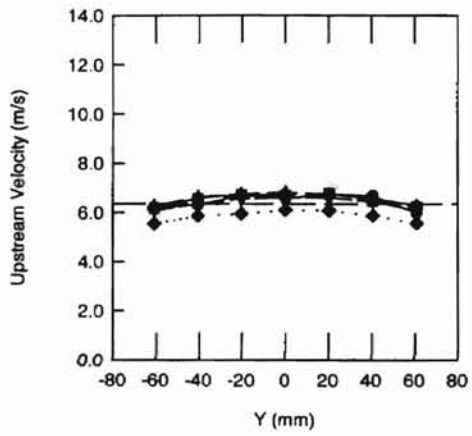
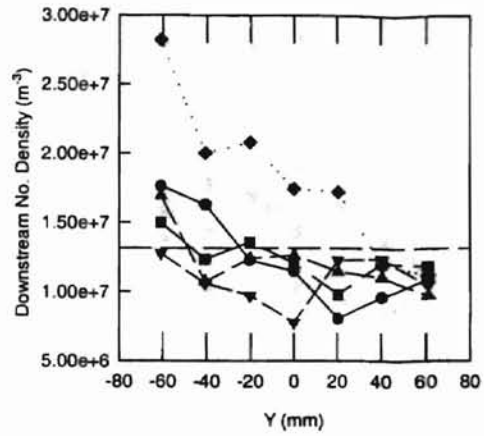
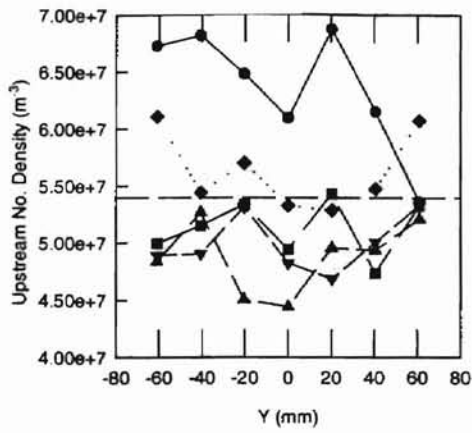
Dashed Line Indicates Average Value

Test Code: 150-05au

Flow (m^3/hr): 408.08

Electrostatic Setup: Charged

Figure B-19 Results for 0.505 Micron Diameter Aerosols using a Charged Setup for a Flow Rate of 408.08 m^3/hr in the Small Angle Diffuser Housing (150-05au)



X (mm)

- -33.02
- -18.51
- ▲ 0.00
- ▼ 16.51
- ◆ 33.02

Dashed Line Indicates Average Value

Test Code: 150-05bu
 Flow (m^3/hr): 408.08
 Electrostatic Setup: Charged

Figure B-20 Results for 0.505 Micron Diameter Aerosols using a Charged Setup for a Flow Rate of 408.08 m^3/hr in the Small Angle Diffuser Housing (150-05bu)

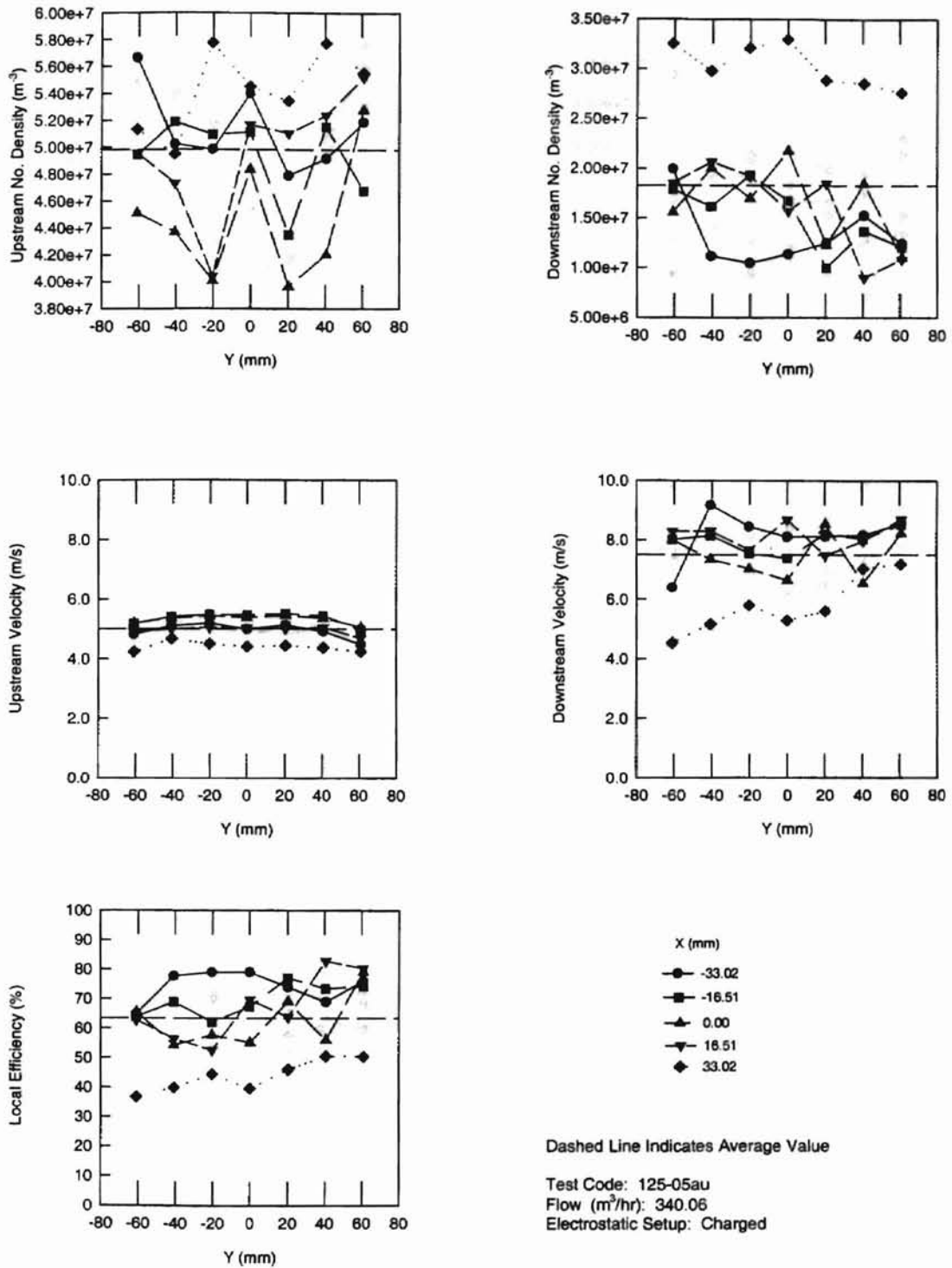


Figure B-21 Results for 0.505 Micron Diameter Aerosols using a Charged Setup for a Flow Rate of 340.05 m³/hr in the Small Angle Diffuser Housing (125-05au)

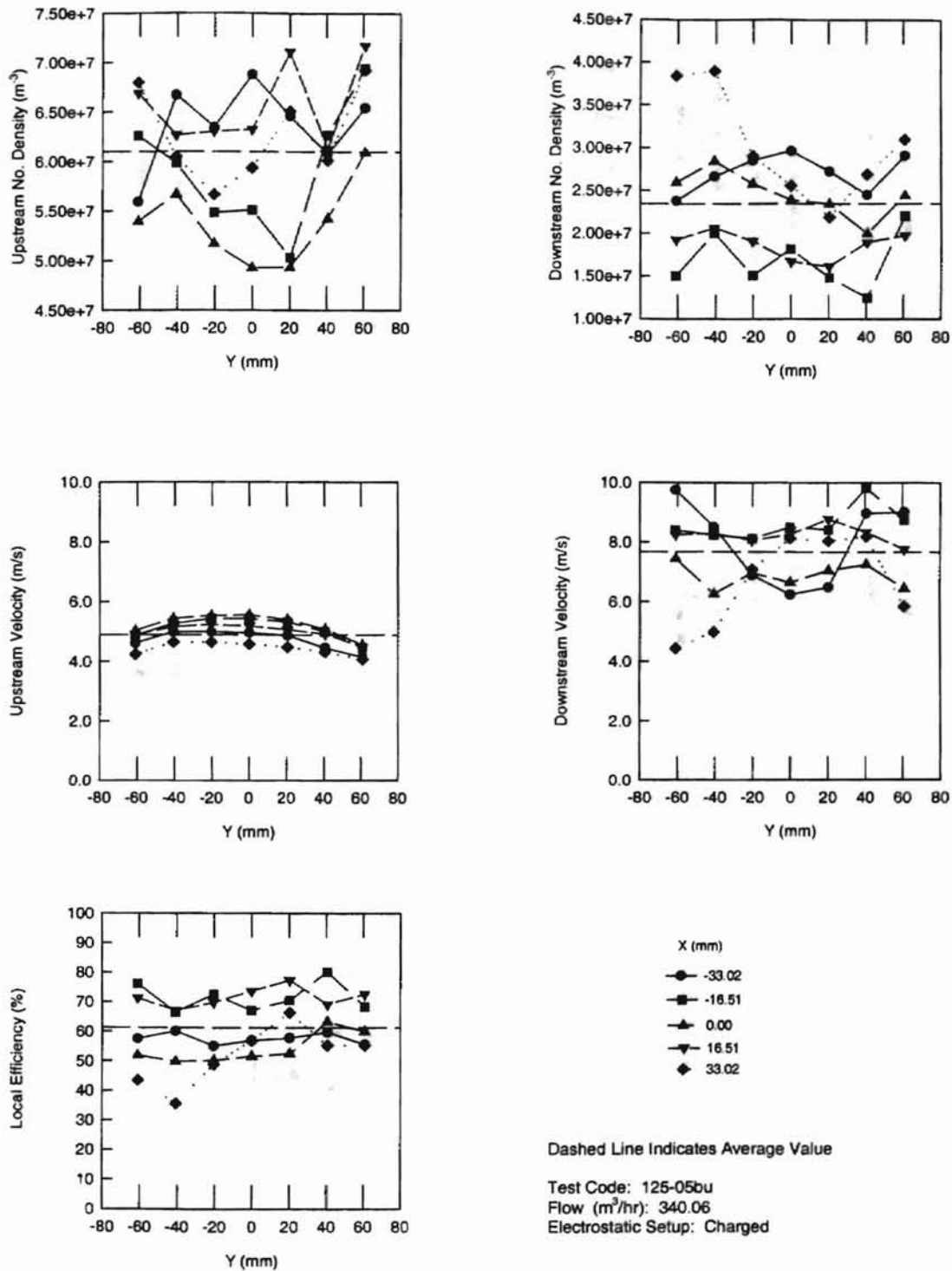
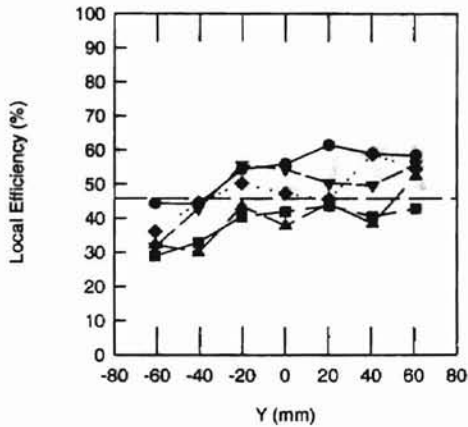
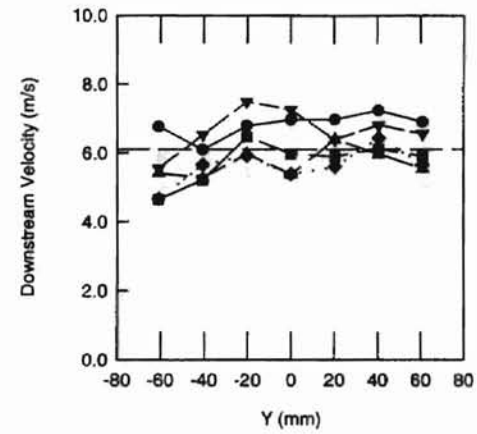
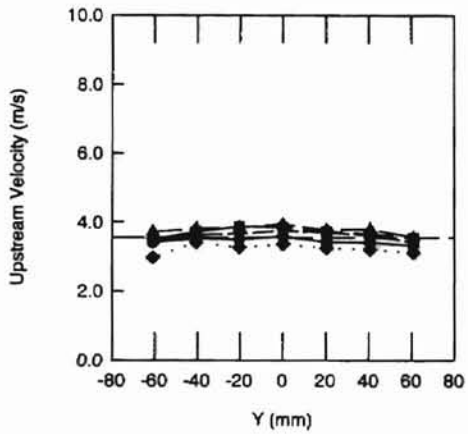
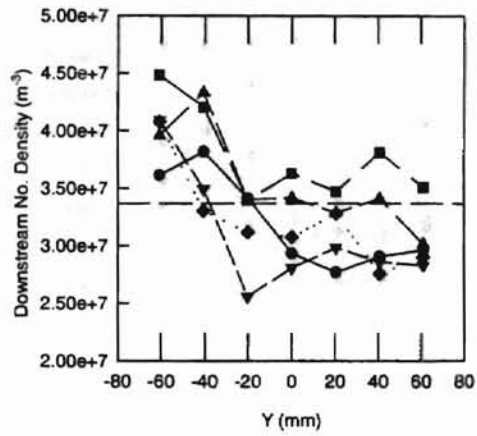
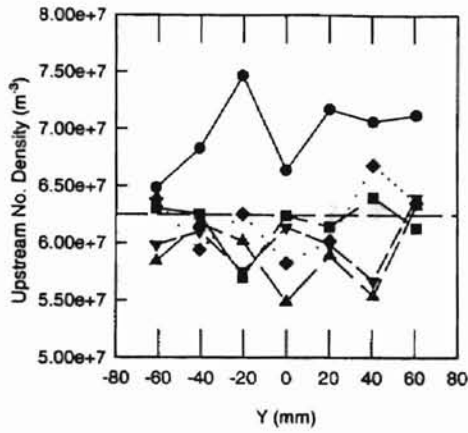


Figure B-22 Results for 0.505 Micron Diameter Aerosols using a Charged Setup for a Flow Rate of 340.05 m³/hr in the Small Angle Diffuser Housing (125-05bu)



- X (mm)
- -33.02
 - -18.51
 - ▲ 0.00
 - ▼ 16.51
 - ◆ 33.02

Dashed Line Indicates Average Value

Test Code: 100-05au
 Flow (m^3/hr): 272.05
 Electrostatic Setup: Charged

Figure B-23 Results for 0.505 Micron Diameter Aerosols using a Charged Setup for a Flow Rate of 272.05 m^3/hr in the Small Angle Diffuser Housing (100-05au)

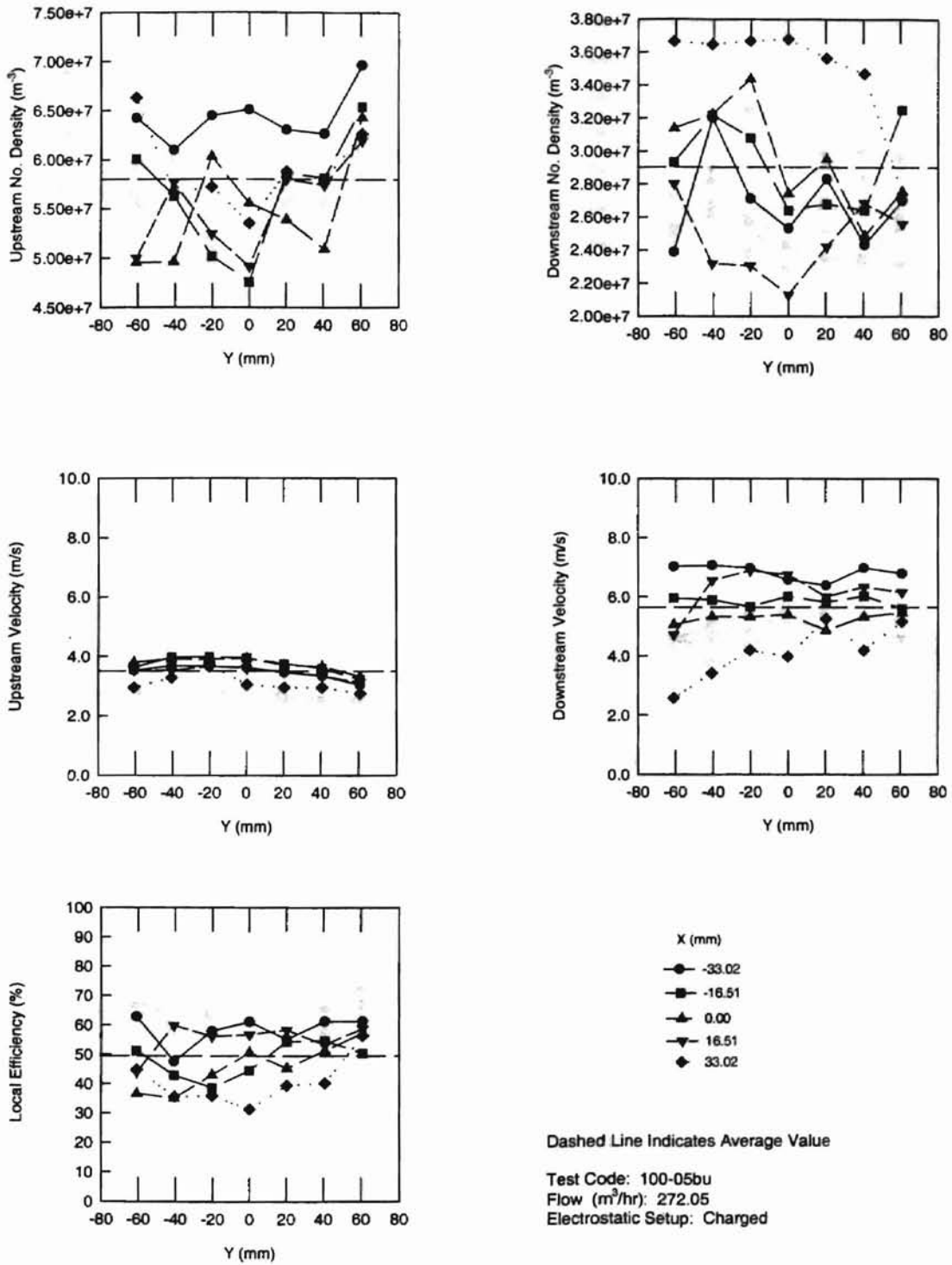


Figure B-24 Results for 0.505 Micron Diameter Aerosols using a Charged Setup for a Flow Rate of 272.05 m³/hr in the Small Angle Diffuser Housing (100-05bu)

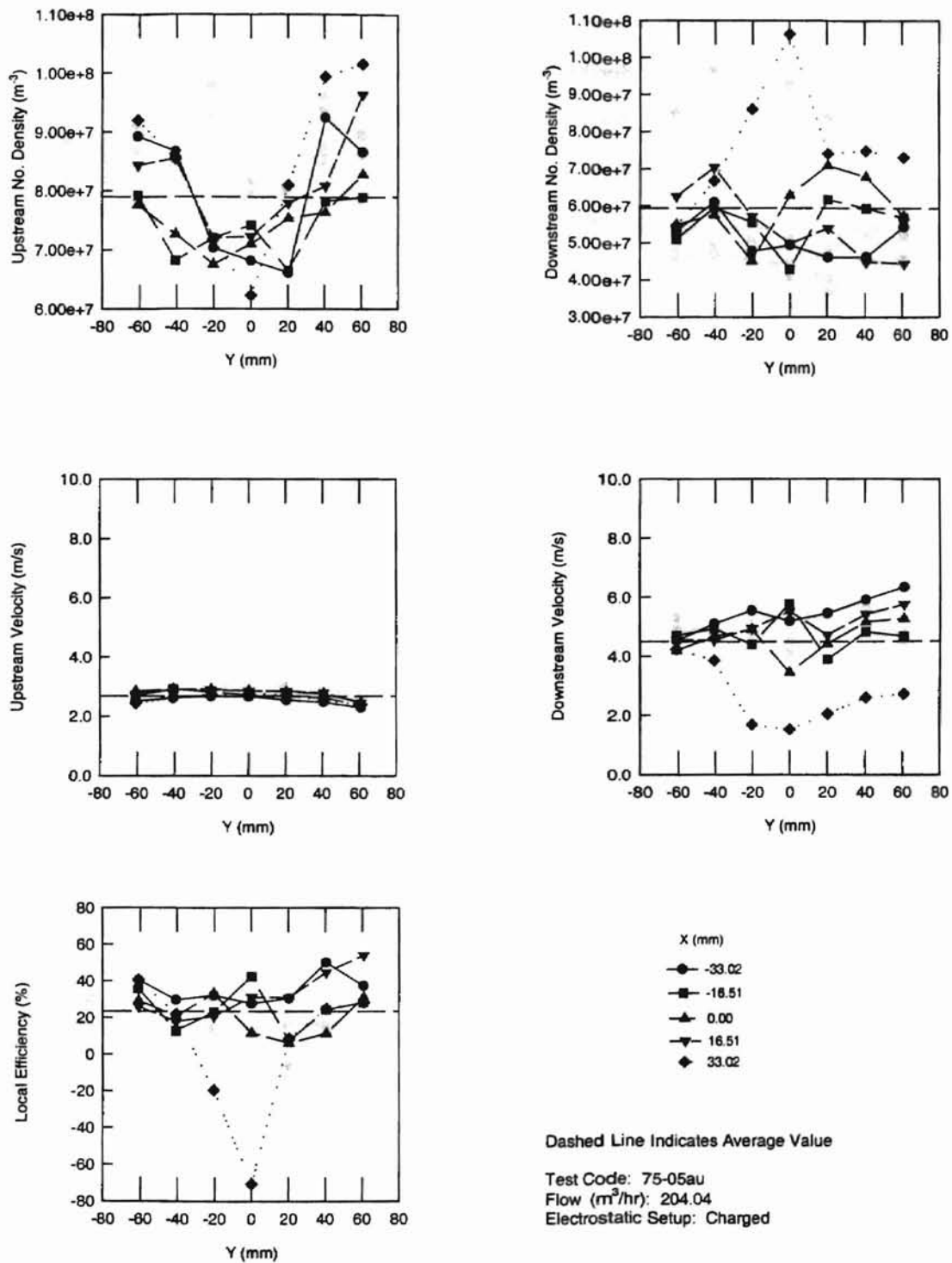


Figure B-25 Results for 0.505 Micron Diameter Aerosols using a Charged Setup for a Flow Rate of 204.04 m³/hr in the Small Angle Diffuser Housing (75-05au)

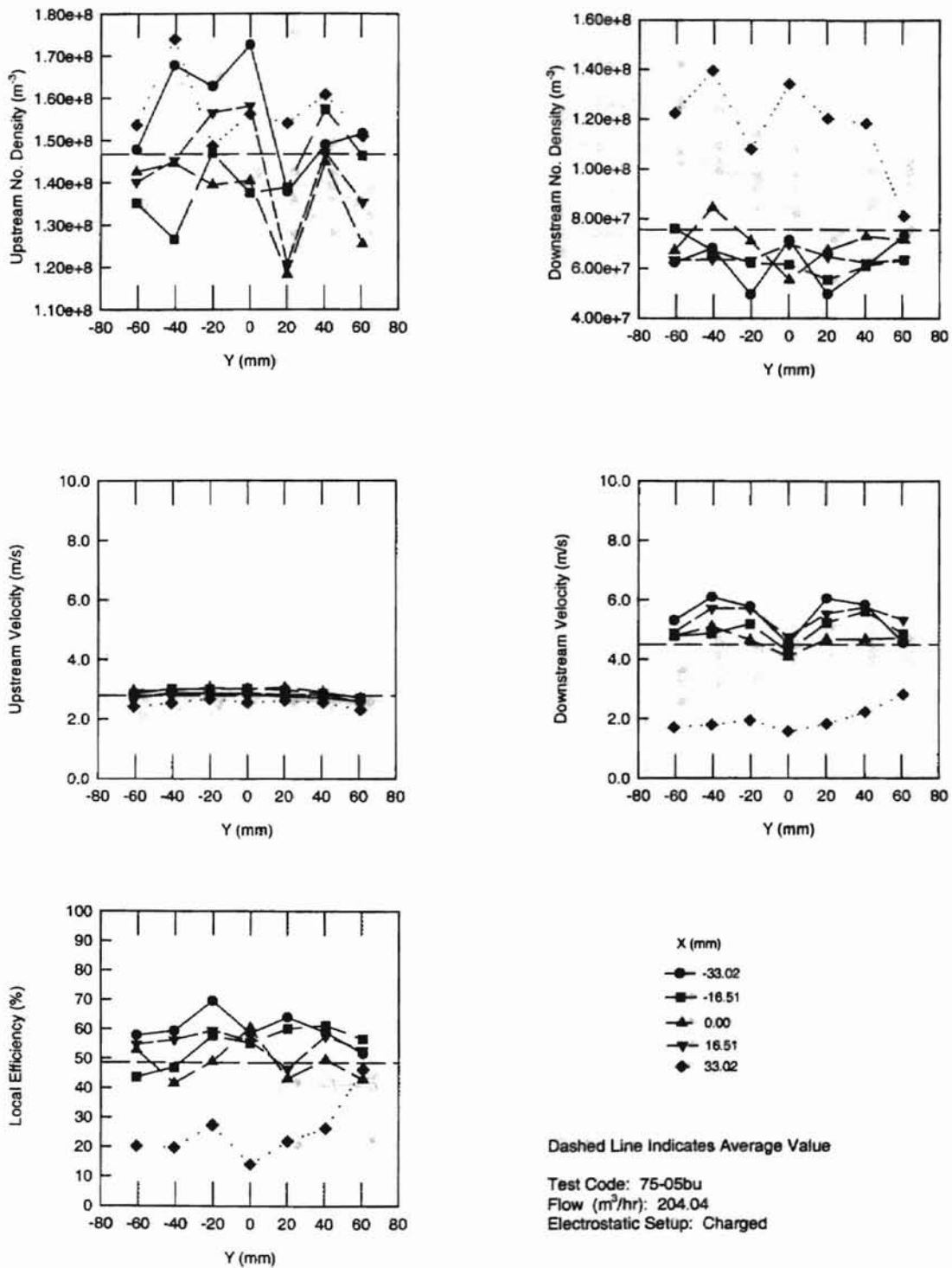


Figure B-26 Results for 0.505 Micron Diameter Aerosols using a Charged Setup for a Flow Rate of 204.04 m^3/hr in the Small Angle Diffuser Housing (75-05bu)

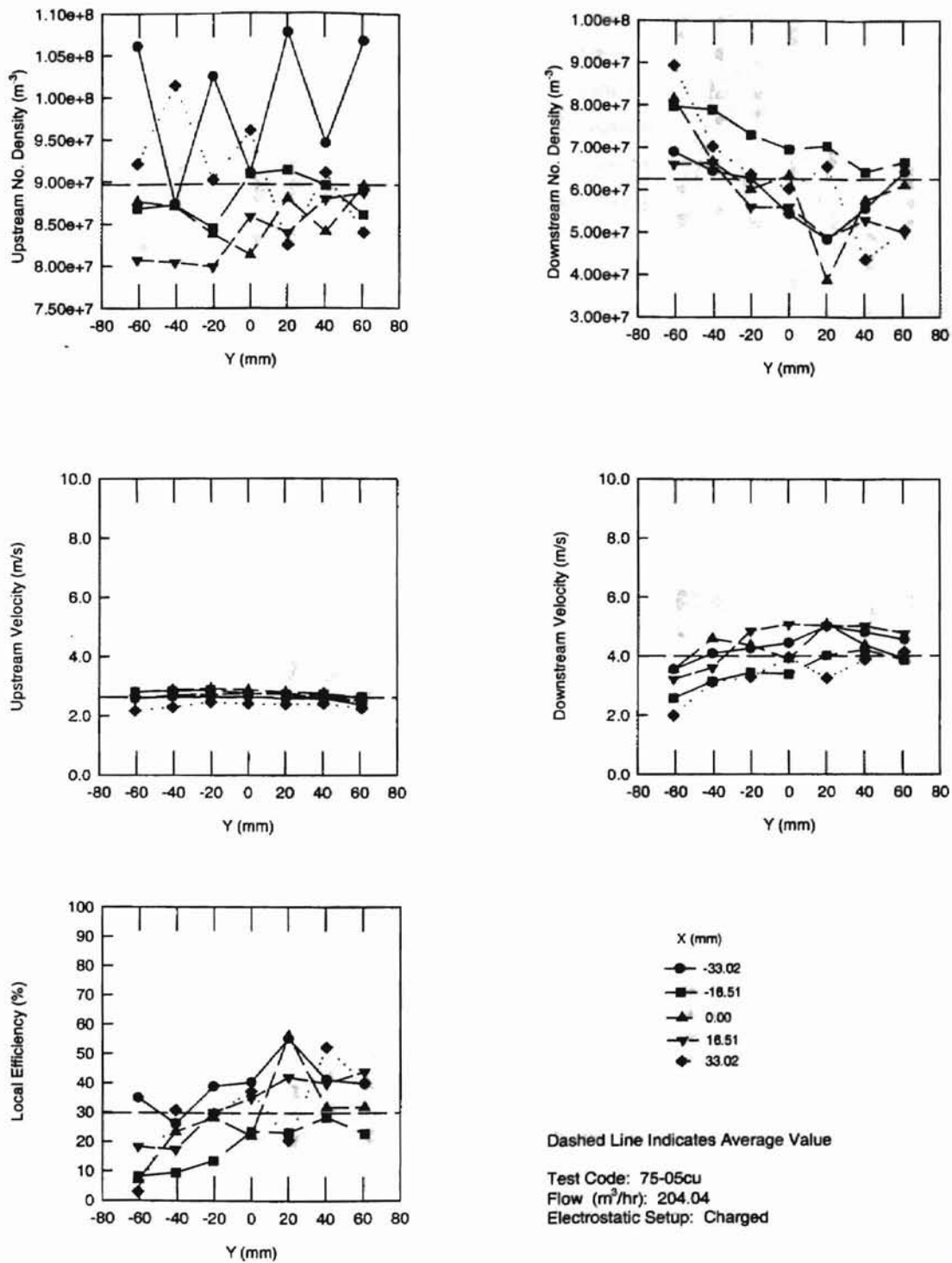
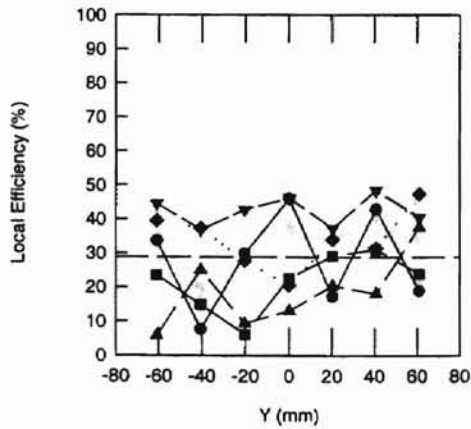
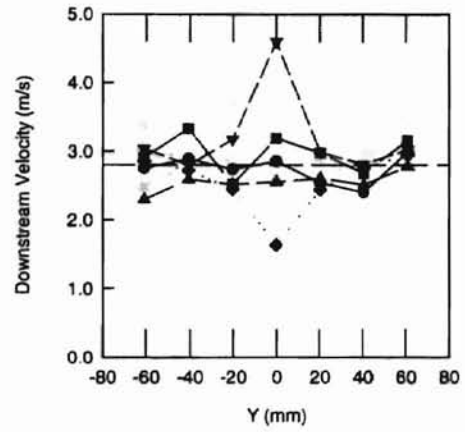
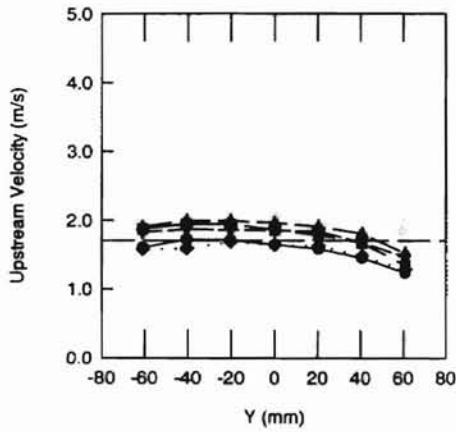
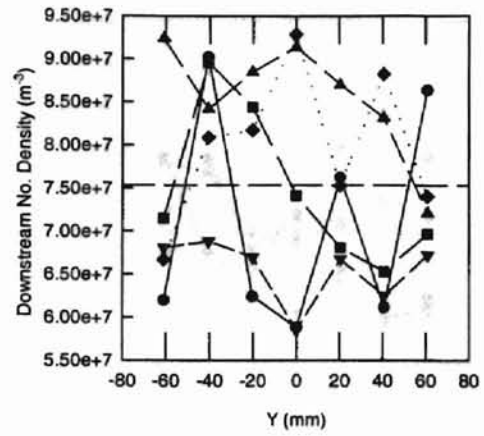
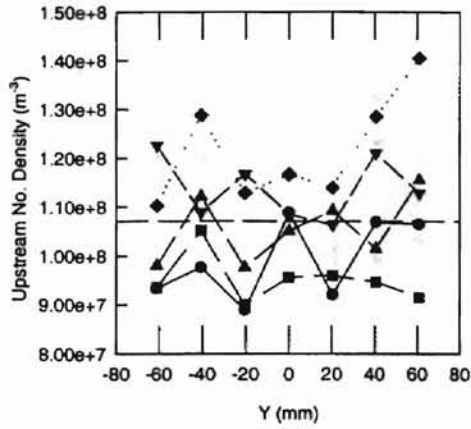


Figure B-27 Results for 0.505 Micron Diameter Aerosols using a Charged Setup for a Flow Rate of 204.04 m^3/hr in the Small Angle Diffuser Housing (75-05cu)



X (mm)
 ● -33.02
 ■ -18.51
 ▲ 0.00
 ▼ 18.51
 ◆ 33.02

Dashed Line Indicates Average Value

Test Code: 50-05au
 Flow (m^3/hr): 136.02
 Electrostatic Setup: Charged

Figure B-28 Results for 0.505 Micron Diameter Aerosols using a Charged Setup for a Flow Rate of 136.02 m^3/hr in the Small Angle Diffuser Housing (50-05au)

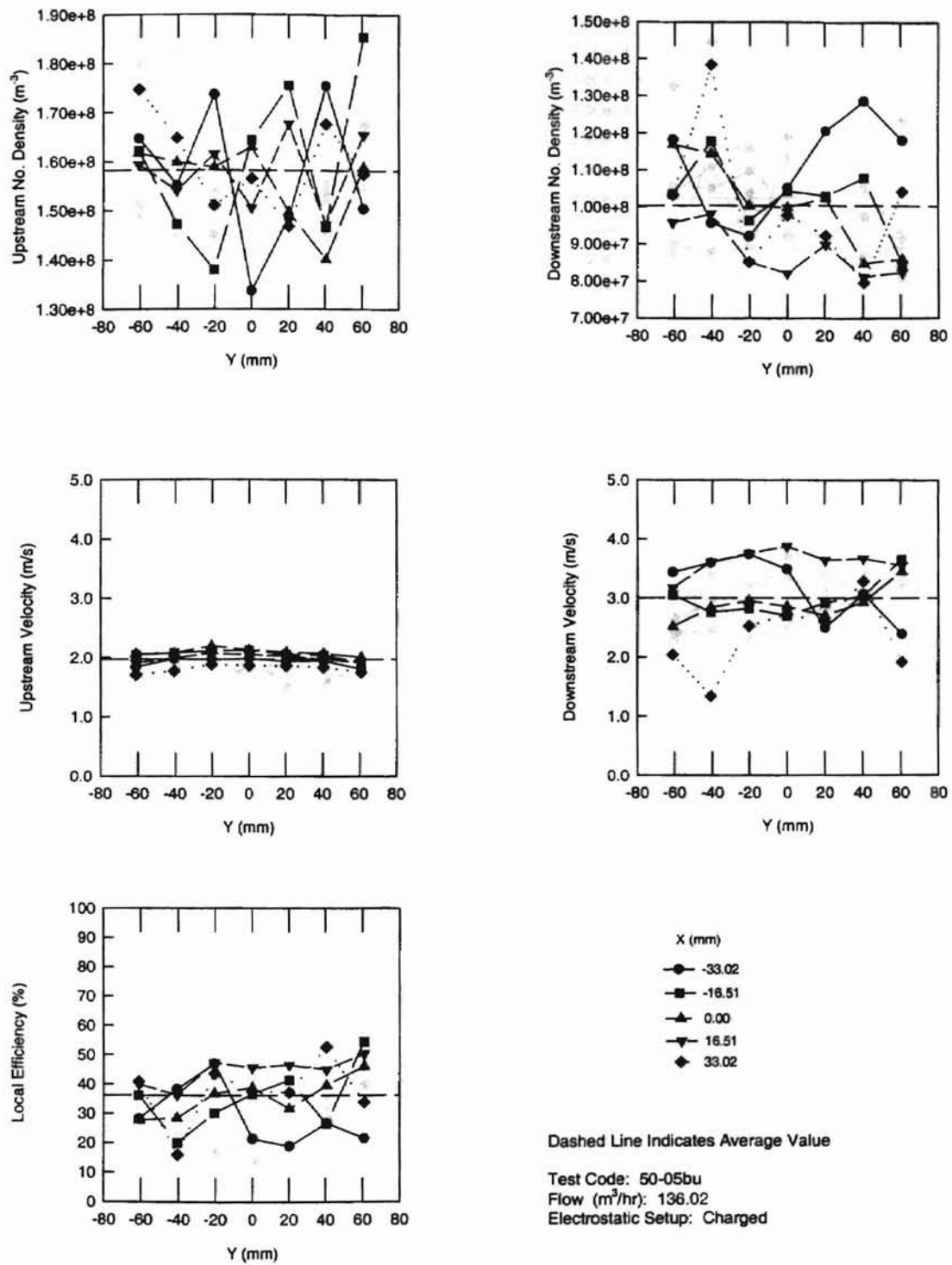


Figure B-29 Results for 0.505 Micron Diameter Aerosols using a Charged Setup for a Flow Rate of 136.02 m^3/hr in the Small Angle Diffuser Housing (50-05bu)

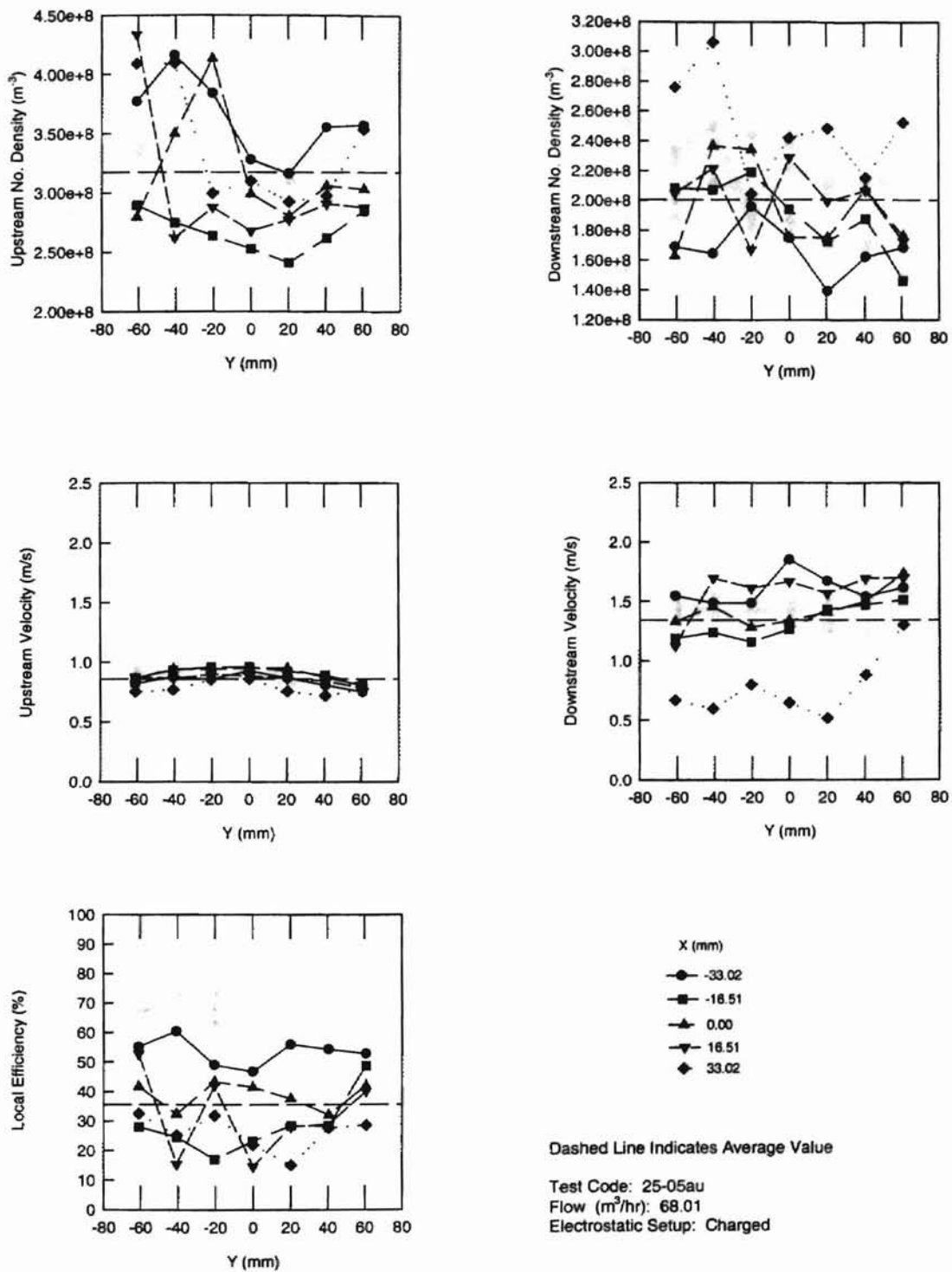


Figure B-30 Results for 0.505 Micron Diameter Aerosols using a Charged Setup for a Flow Rate of 68.01 m³/hr in the Small Angle Diffuser Housing (25-05au)

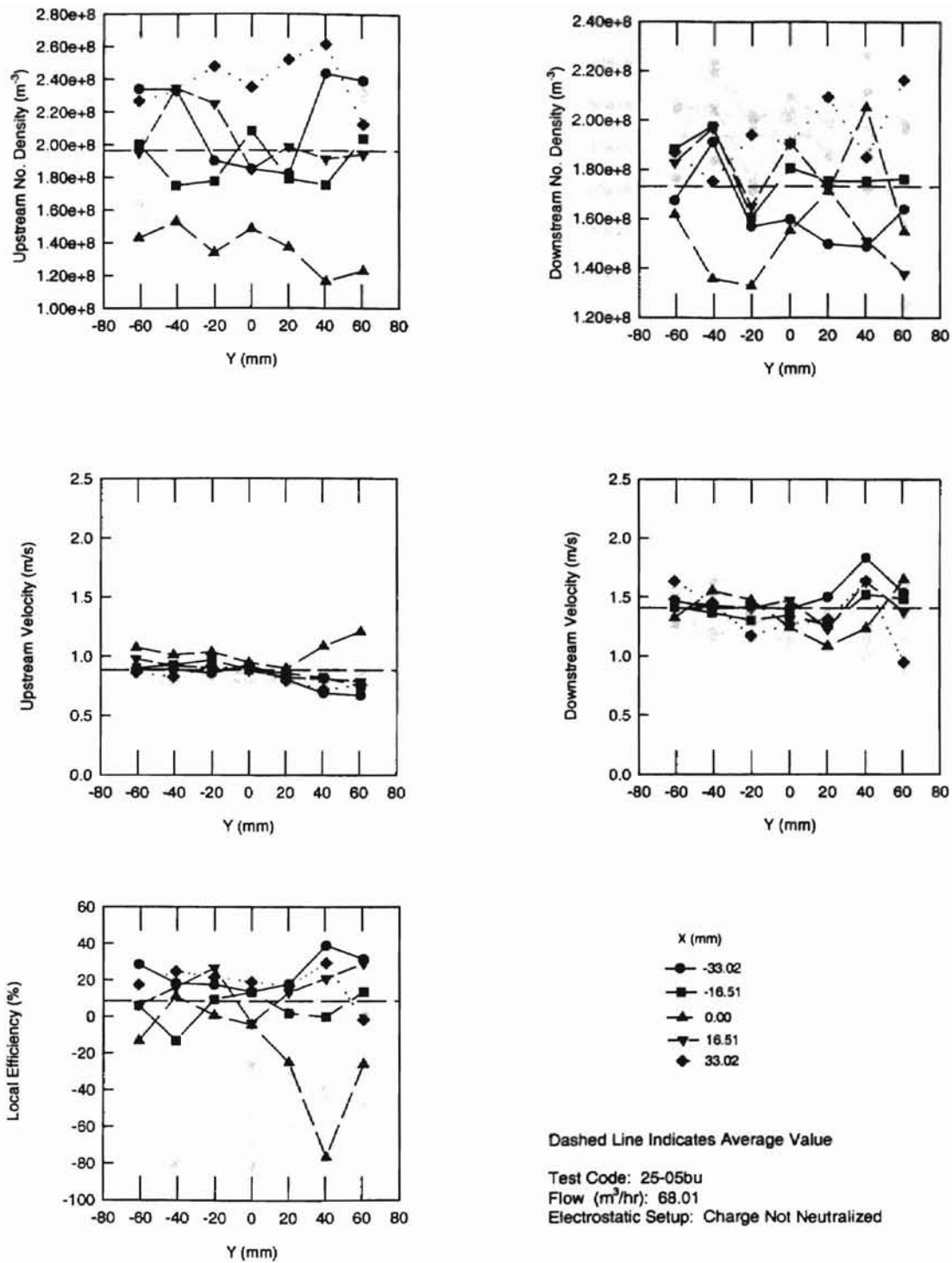


Figure B-31 Results for 0.505 Micron Diameter Aerosols using a Charged Setup for a Flow Rate of 68.01 m³/hr in the Small Angle Diffuser Housing (25-05bu)

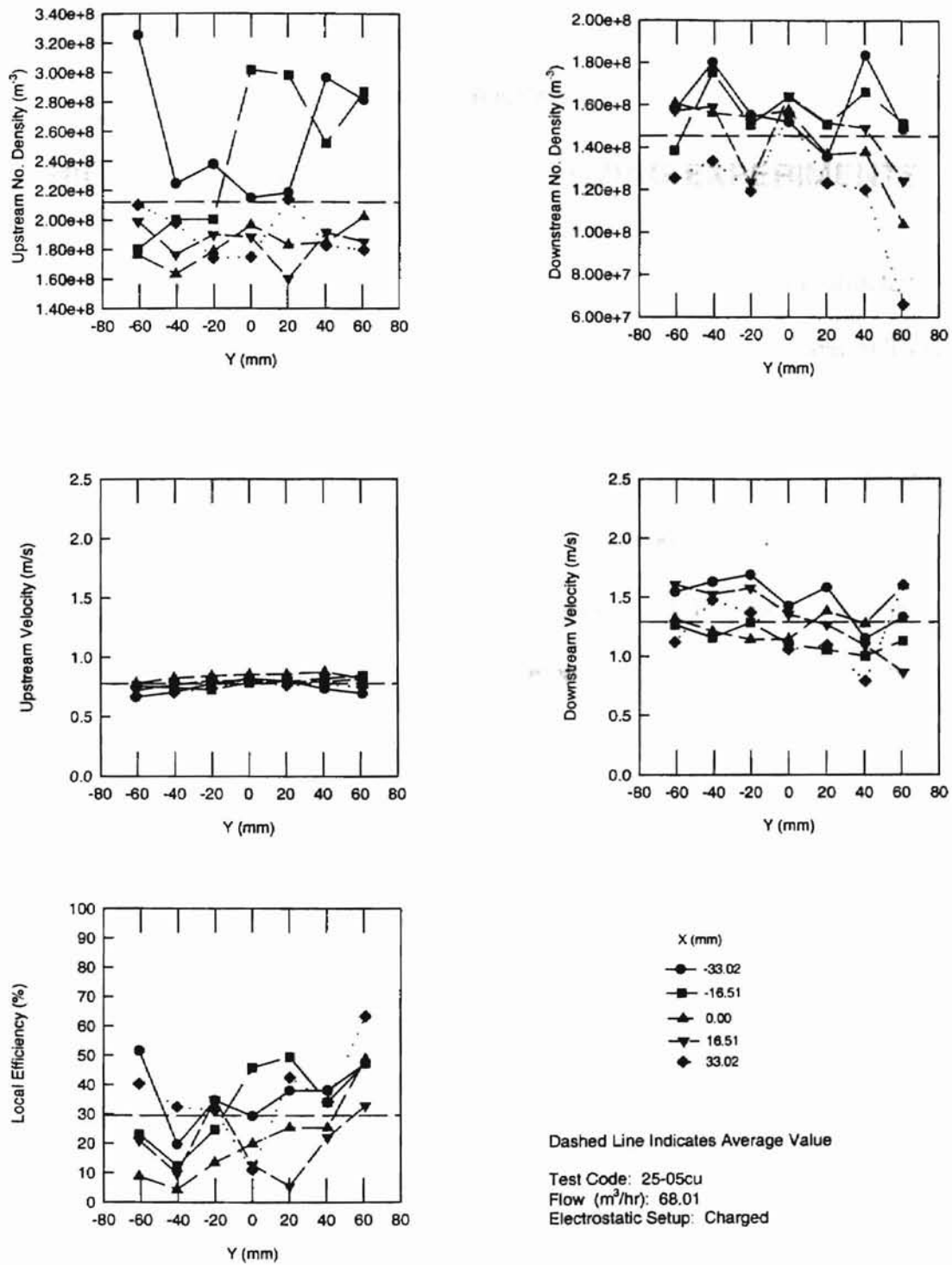


Figure B-32 Results for 0.505 Micron Diameter Aerosols using a Charged Setup for a Flow Rate of 68.01 m³/hr in the Small Angle Diffuser Housing (25-05cu)

APPENDIX C

HIGH VOLTAGE AND PARTICLE SIZING EXPERIMENTS

It was explained in Chapter 3 that efficiency measurement is not affected by the high voltage parameters used to carry out the experiments. The tests listed in Table 3-2 are presented in this Appendix as Figs. C-8 to C-16. The corresponding tests for the bidisperse mixtures listed in Also, as discussed in Chapter 5, the tests listed in Table 5-3, which were carried out in order to determine the measurability of particle fractions are presented in this thesis as Figs. C-1 to C-16. The tests listed in Table 3-3 also presented in this thesis as Figs. C-17 to C-28. The test numbers may be correlated with the above-mentioned tables to determine the parameters and configurations used to conduct the experiments. All tests were conducted at the central grid location of the filter.

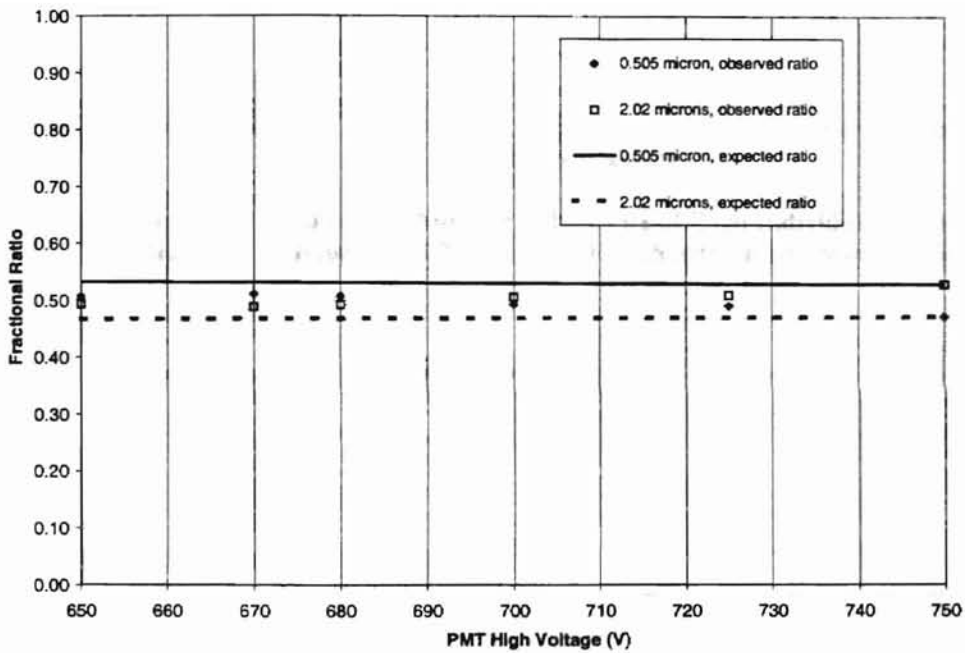


Figure C-1 Fractional Ratio of the Number of Particles of Each Individual Particle Size in a Bidisperse Mixture of 2.02 Micron and 0.505 Micron Diameter Particles (Test13)

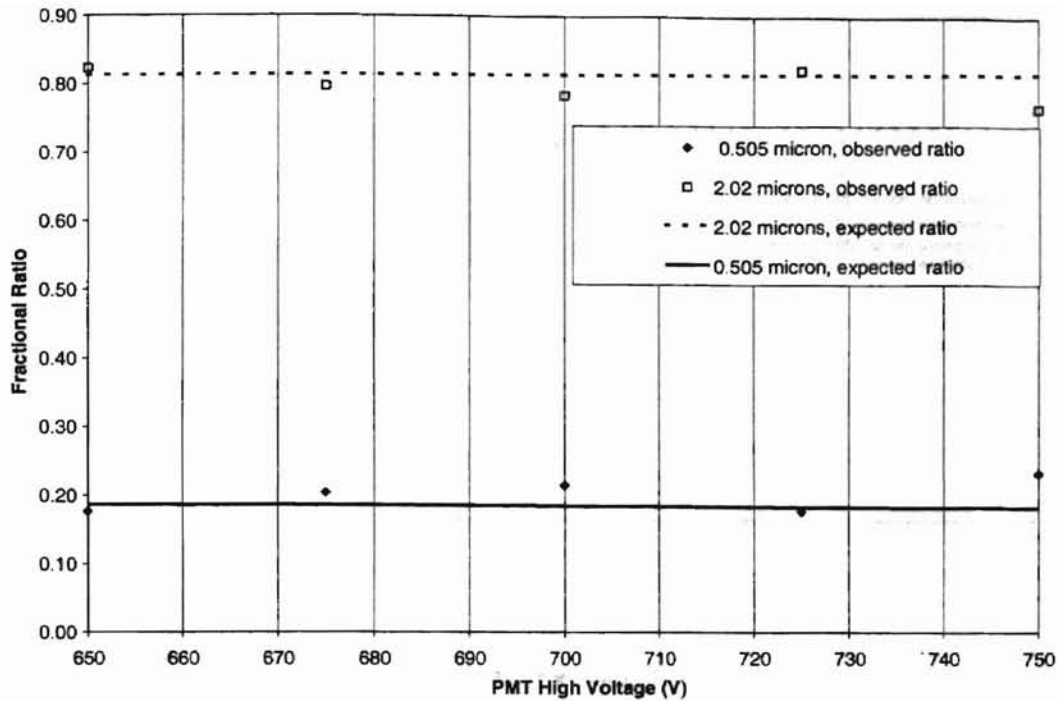


Figure C-2 Fractional Ratio of the Number of Particles of Each Individual Particle Size in a Bidisperse Mixture of 2.02 Micron and 0.505 Micron Diameter Particles (Test14)

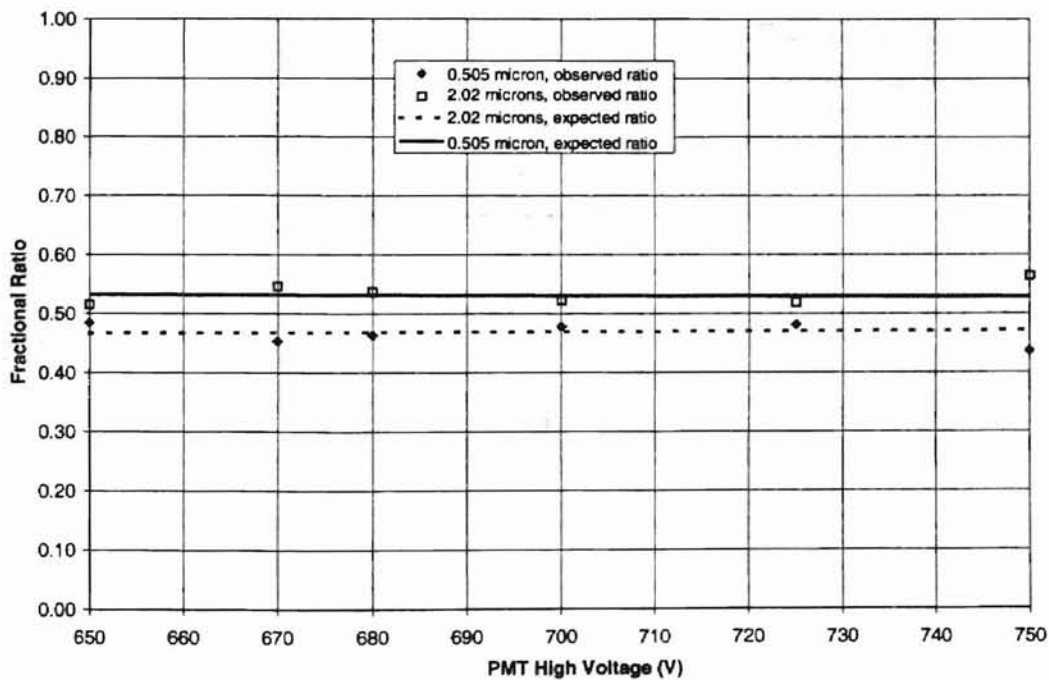


Figure C-3 Fractional Ratio of the Number of Particles of Each Individual Particle Size in a Bidisperse Mixture of 2.02 Micron and 0.505 Micron Diameter Particles (Test16)

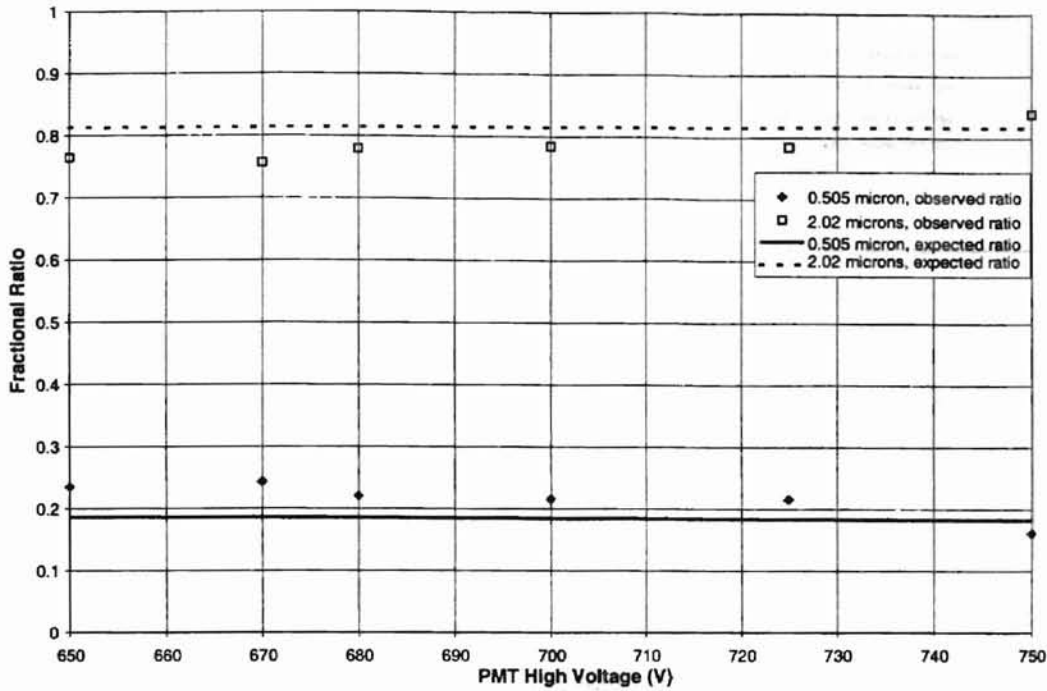


Figure C-4 Fractional Ratio of the Number of Particles of Each Individual Particle Size in a Bidisperse Mixture of 2.02 Micron and 0.505 Micron Diameter Particles (Test17)

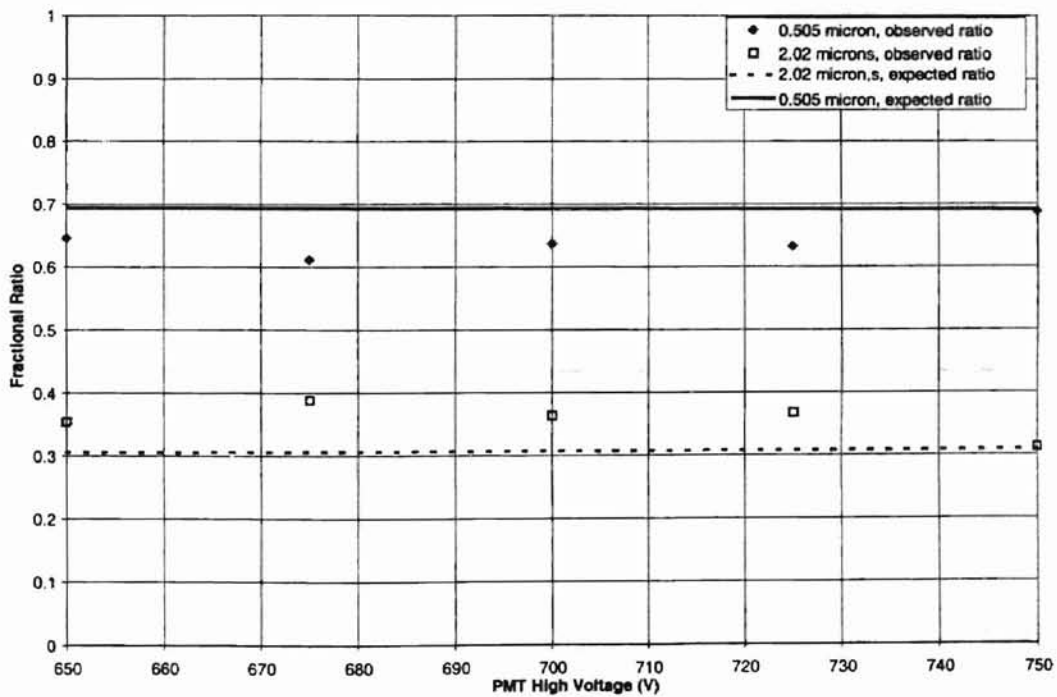


Figure C-5 Fractional Ratio of the Number of Particles of Each Individual Particle Size in a Bidisperse Mixture of 2.02 Micron and 0.505 Micron Diameter Particles (Test18)

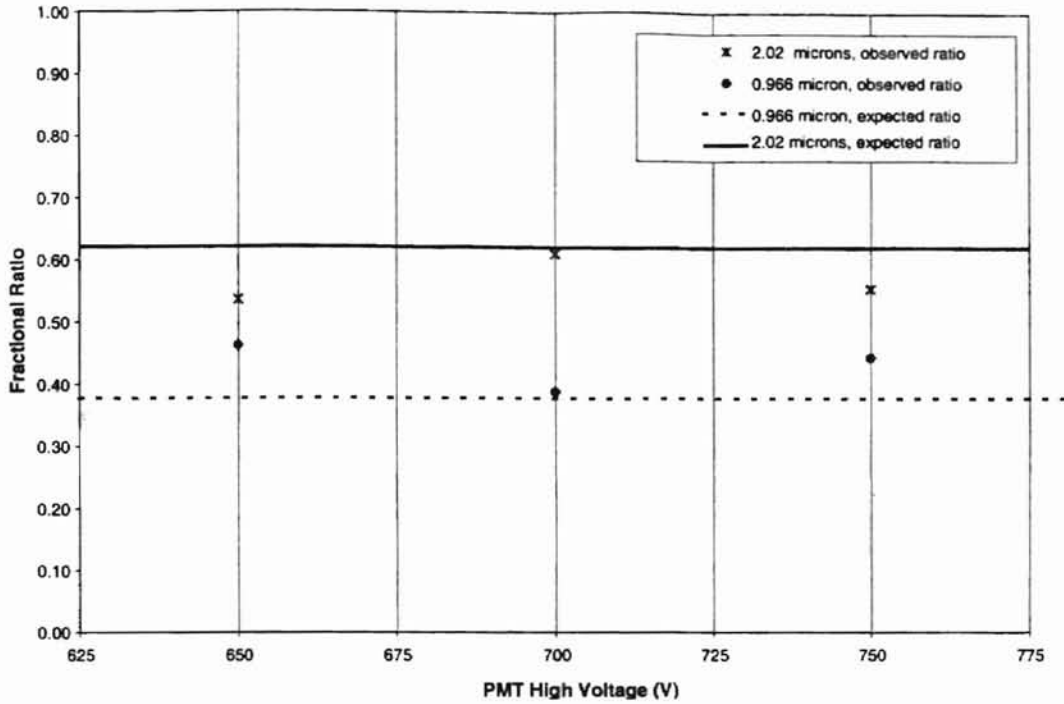


Figure C-6 Fractional Ratio of the Number of Particles of Each Individual Particle Size in a Bidisperse Mixture of 2.02 Micron and 0.505 Micron Diameter Particles (Test19)

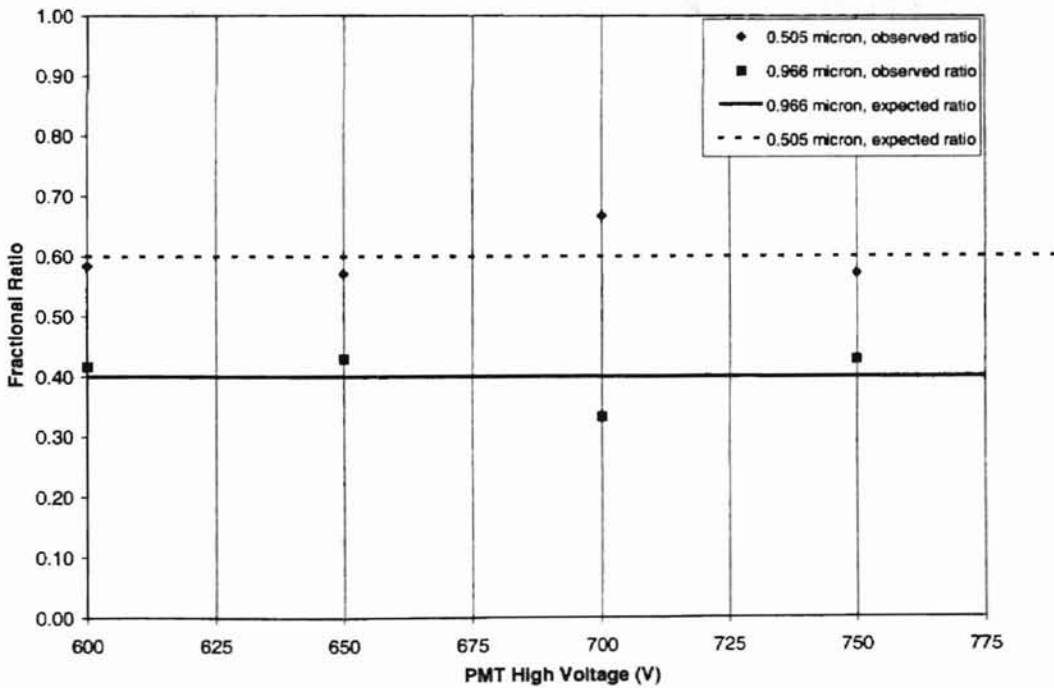


Figure C-7 Fractional Ratio of the Number of Particles of Each Individual Particle Size in a Bidisperse Mixture of 2.02 Micron and 0.505 Micron Diameter Particles (Test19)

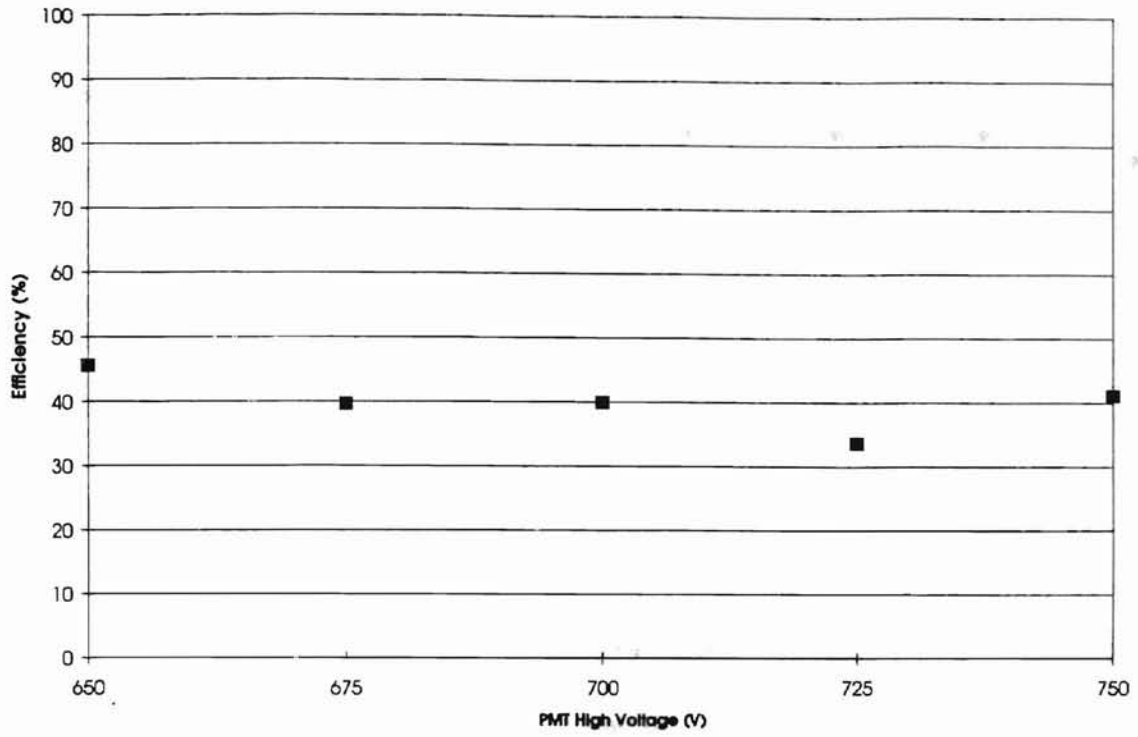


Figure C-8 Efficiency as a Function of High Voltage for 0.505 Micron Diameter Particles (Test23)

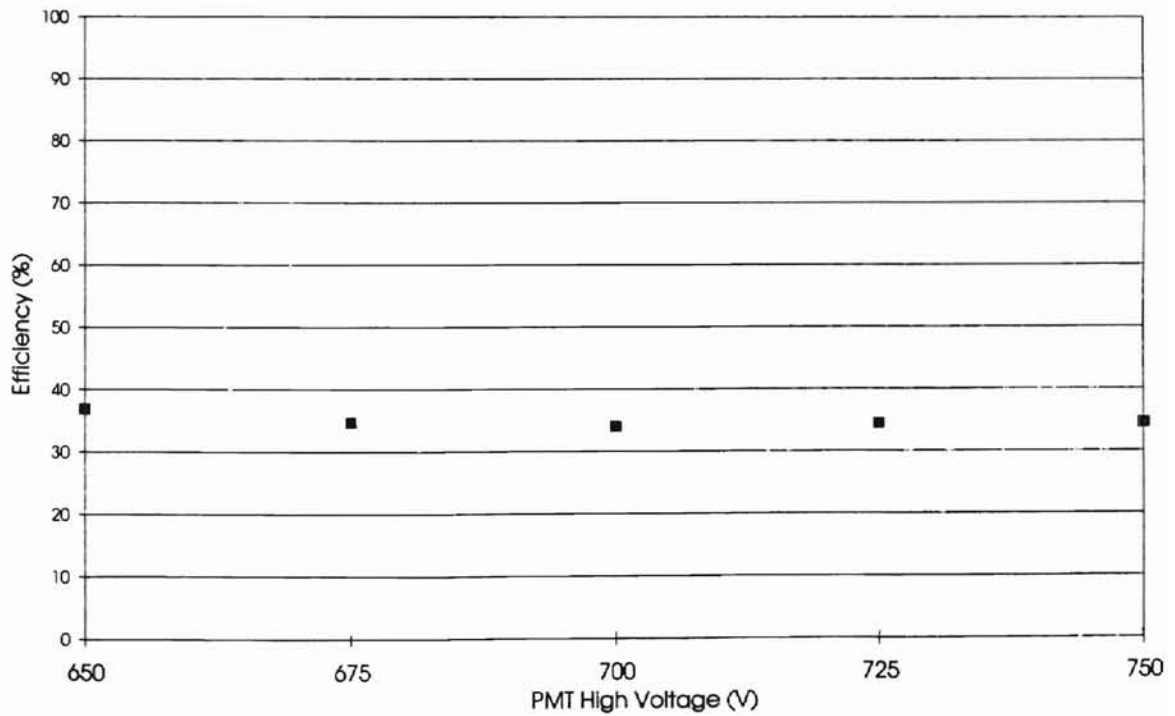


Figure C-9 Efficiency as a Function of High Voltage for 0.505 Micron Diameter Particles (Test24)

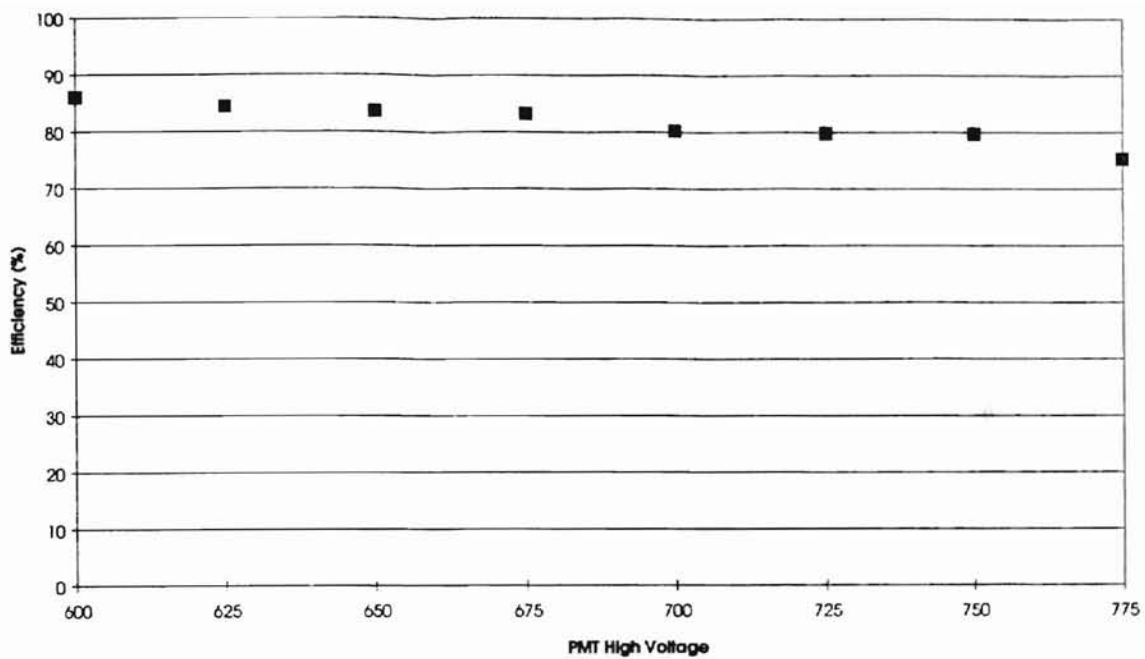


Figure C-10 Efficiency as a Function of High Voltage for 2.02 Micron Diameter Particles (Test25)

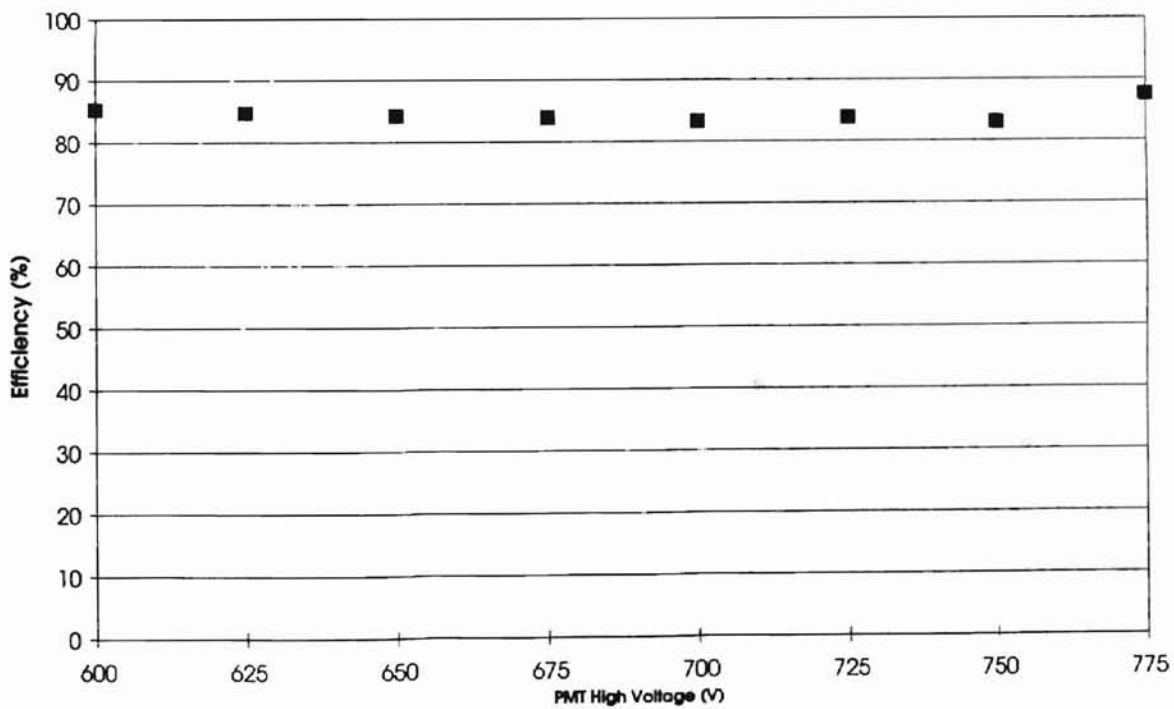


Figure C-11 Efficiency as a Function of High Voltage for 2.02 Micron Diameter Particles (Test26)

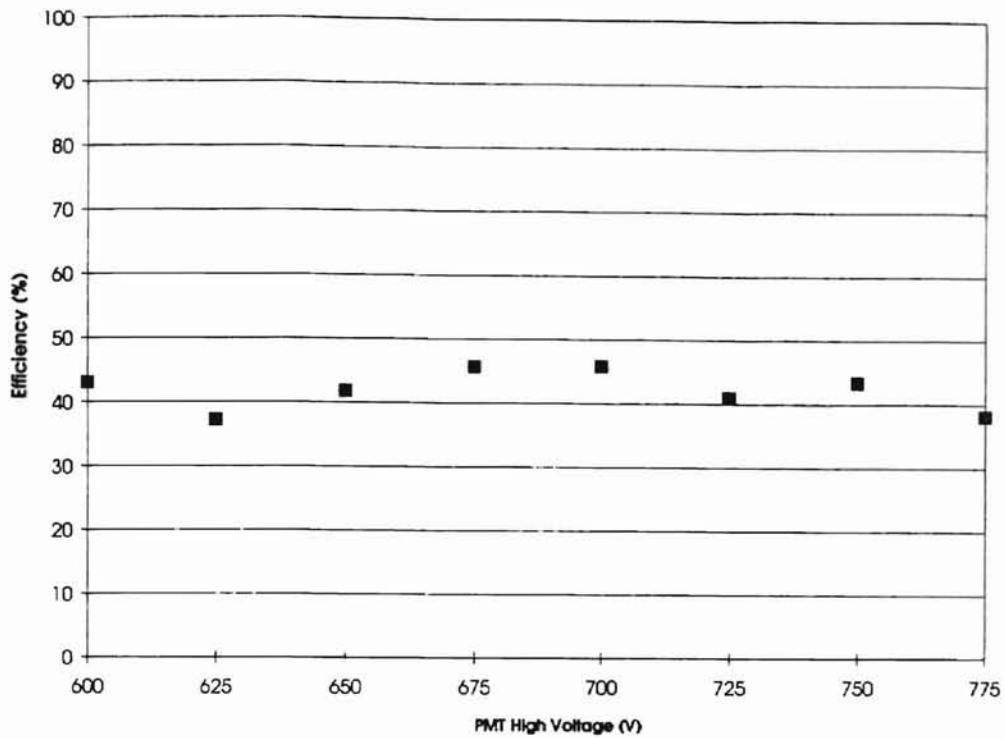


Figure C-12 Efficiency as a Function of High Voltage for 0.966 Micron Diameter Particles (Test27)

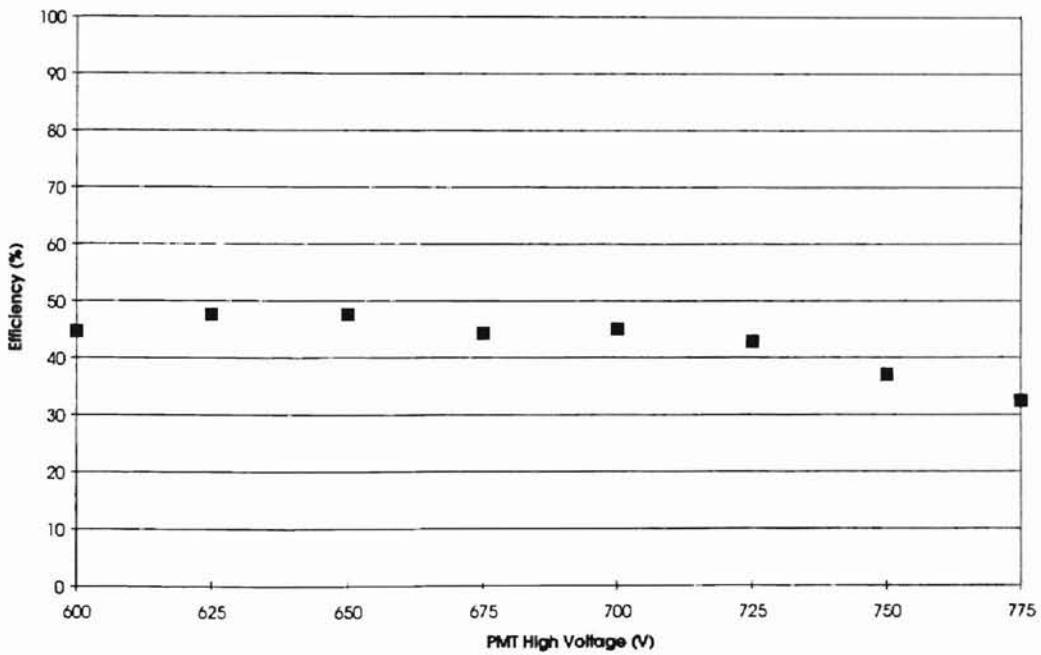


Figure C-13 Efficiency as a Function of High Voltage for 0.966 Micron Diameter Particles (Test28)

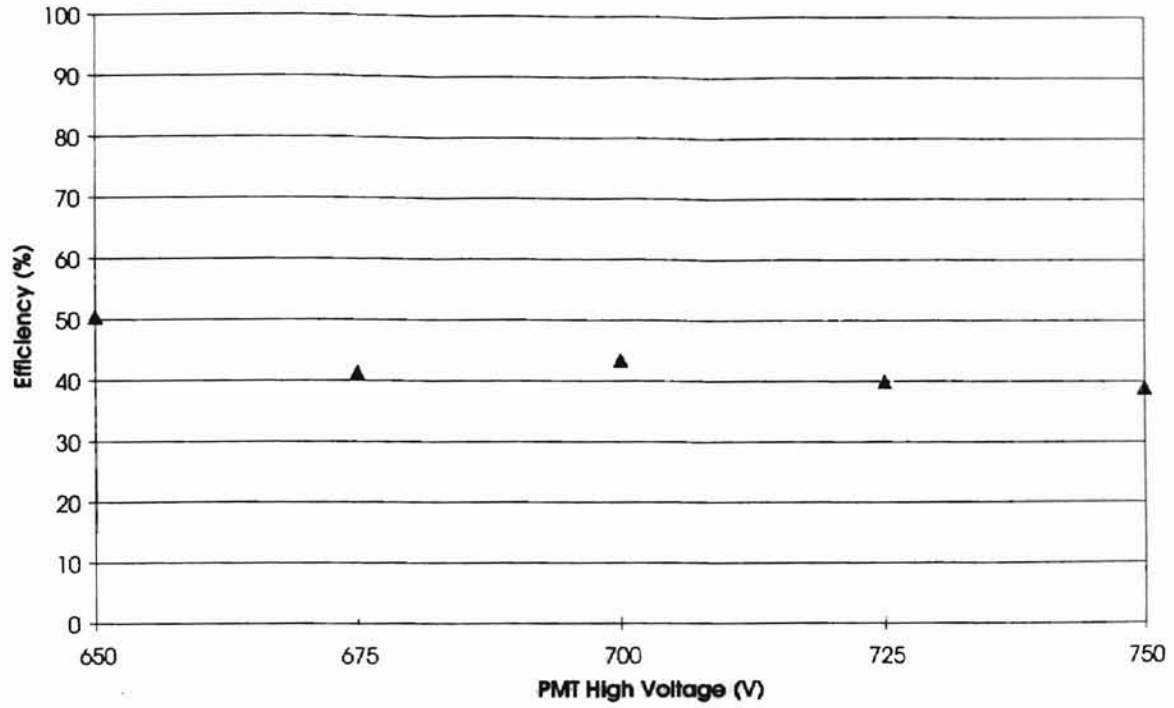


Figure C-14 Efficiency as a Function of High Voltage for 0.966 Micron Diameter Particles (Test33)

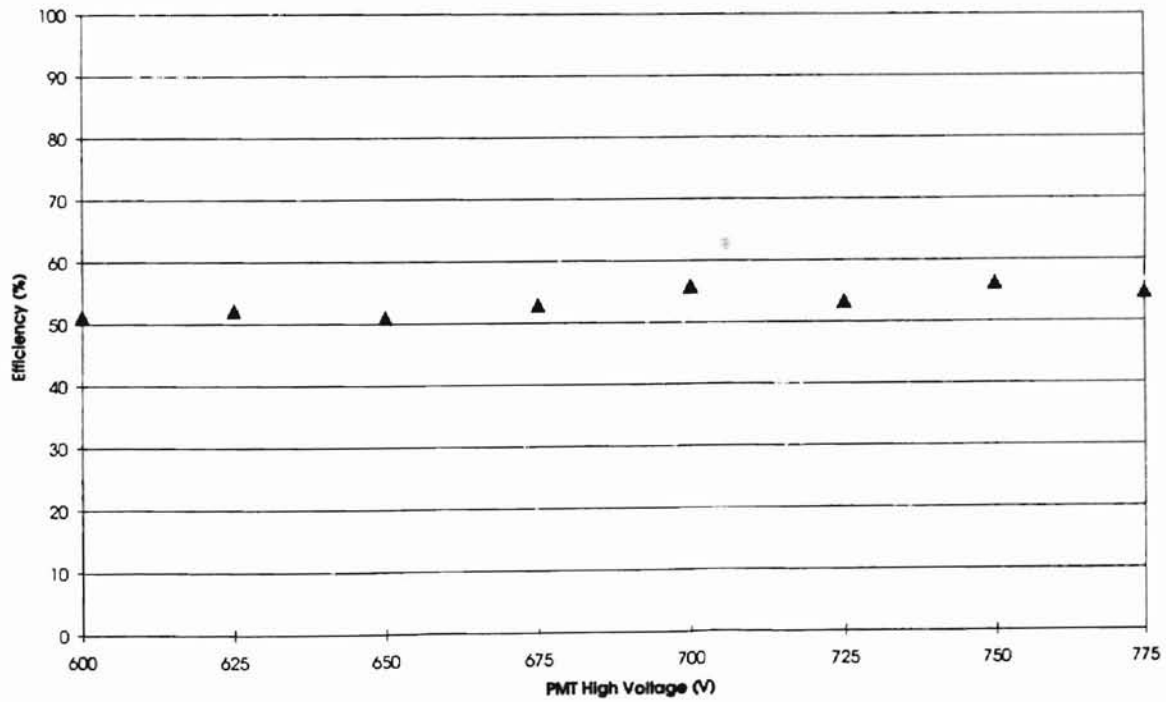


Figure C-15 Efficiency as a Function of High Voltage for 0.966 Micron Diameter Particles (Test34)

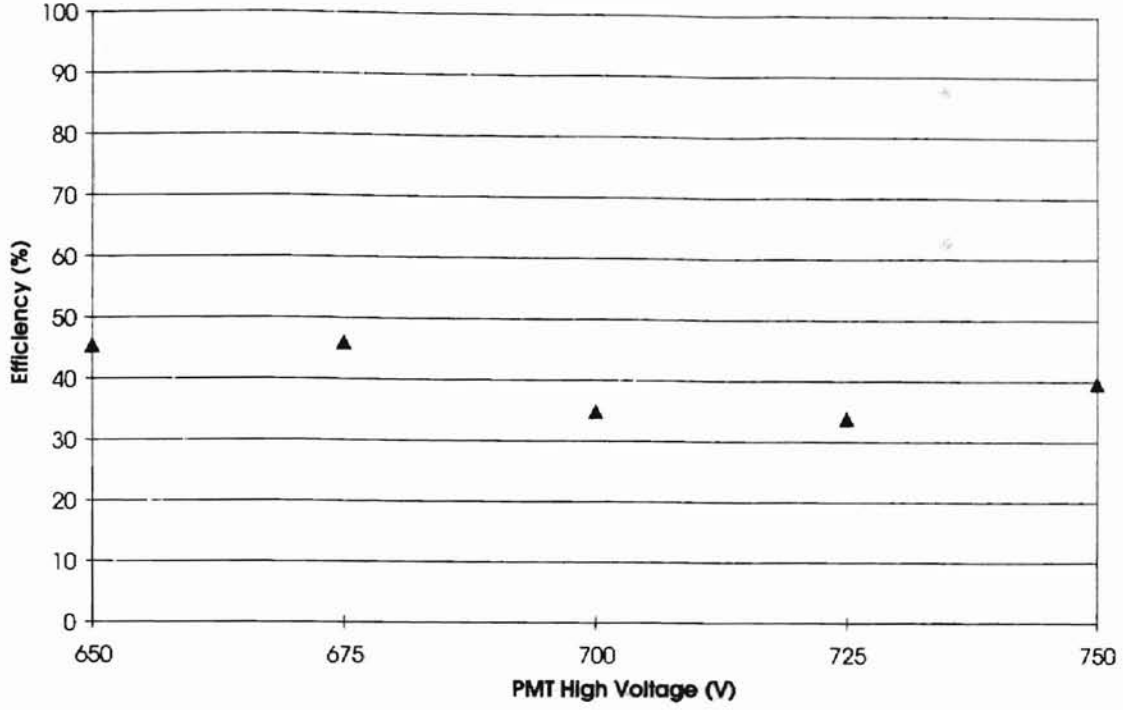


Figure C-16 Efficiency as a Function of High Voltage for 0.966 Micron Diameter Particles (Test38)

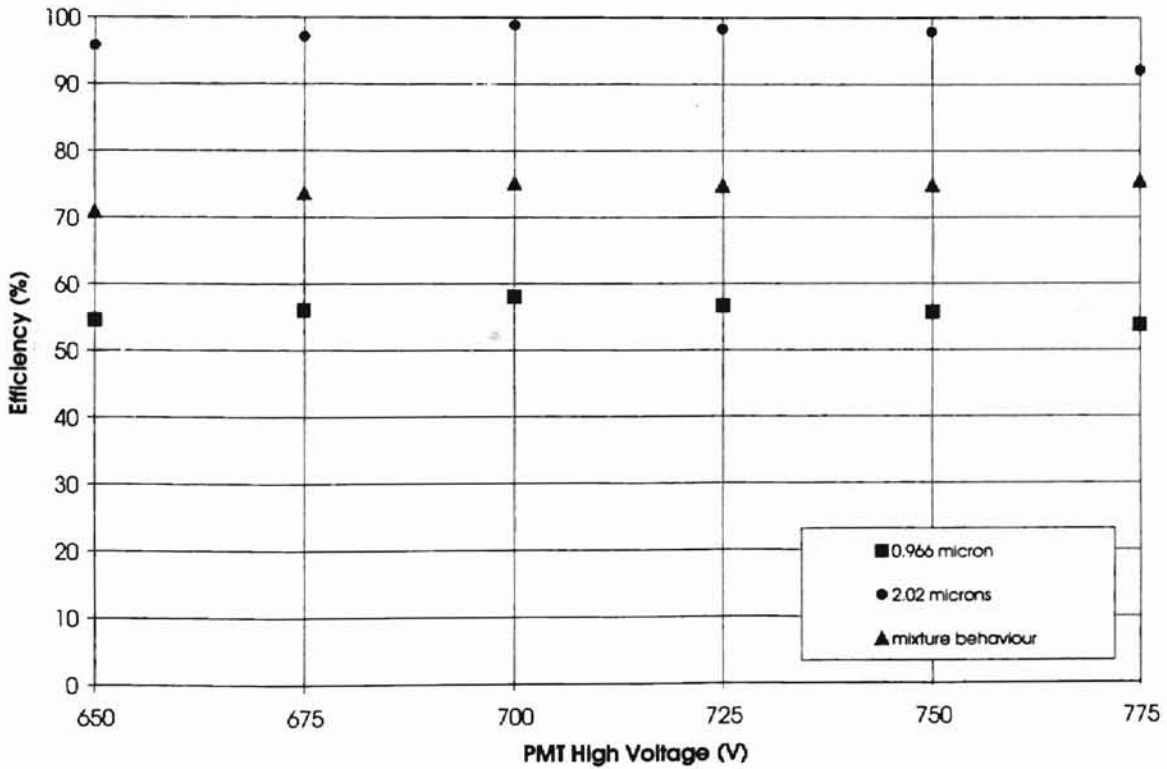


Figure C-17 Fractional Efficiency as a Function of High Voltage for a Mixture Containing Particles of Diameter 2.02 Microns and 0.966 Micron (Test29)

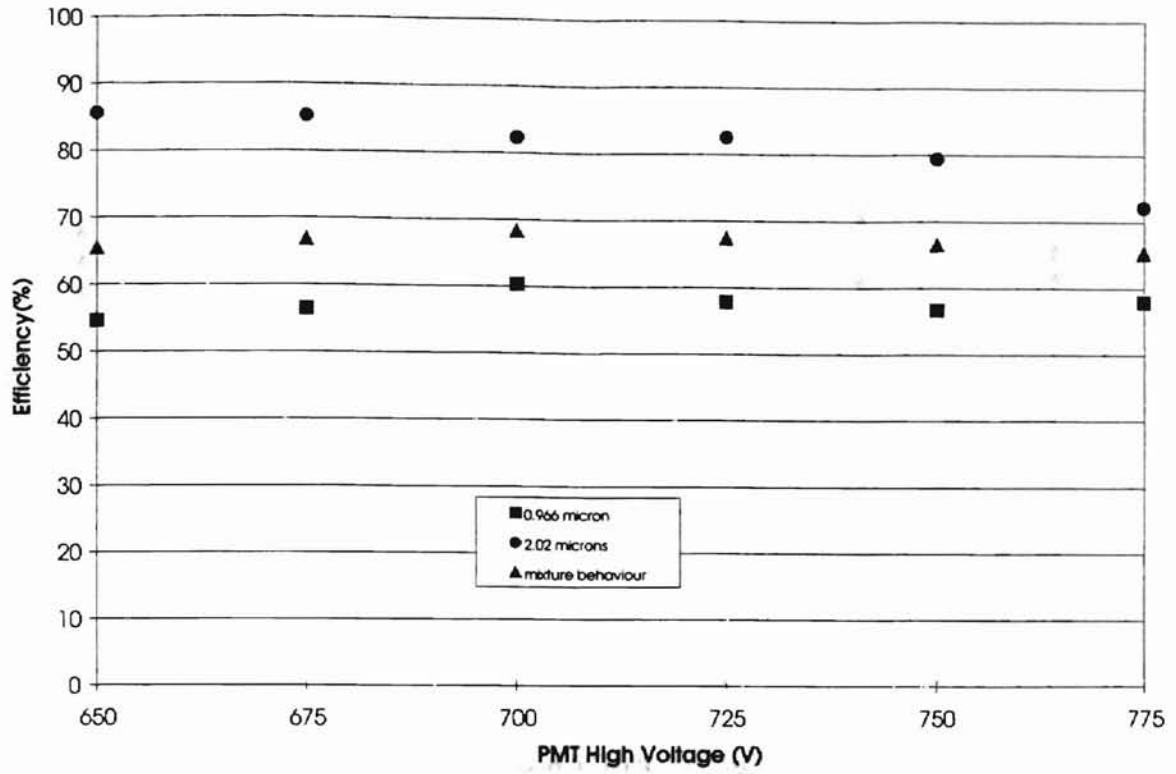


Figure C-18 Fractional Efficiency as a Function of High Voltage for a Mixture Containing Particles of Diameter 2.02 Microns and 0.966 Micron (Test30)

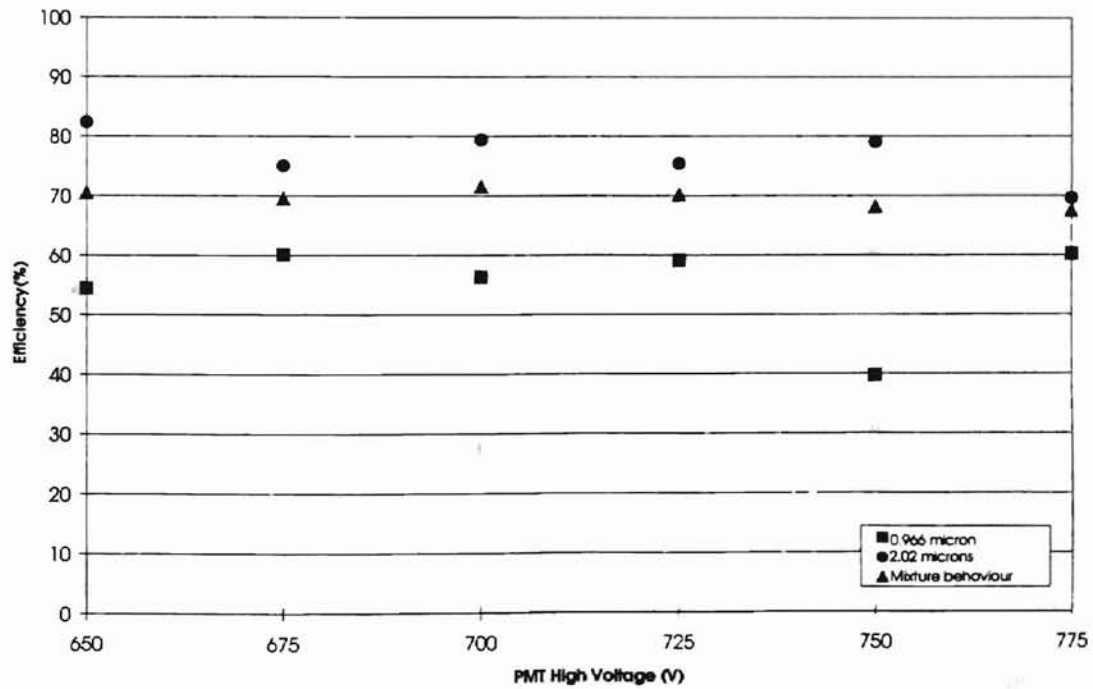


Figure C-19 Fractional Efficiency as a Function of High Voltage for a Mixture Containing Particles of Diameter 2.02 Microns and 0.966 Micron (Test40)

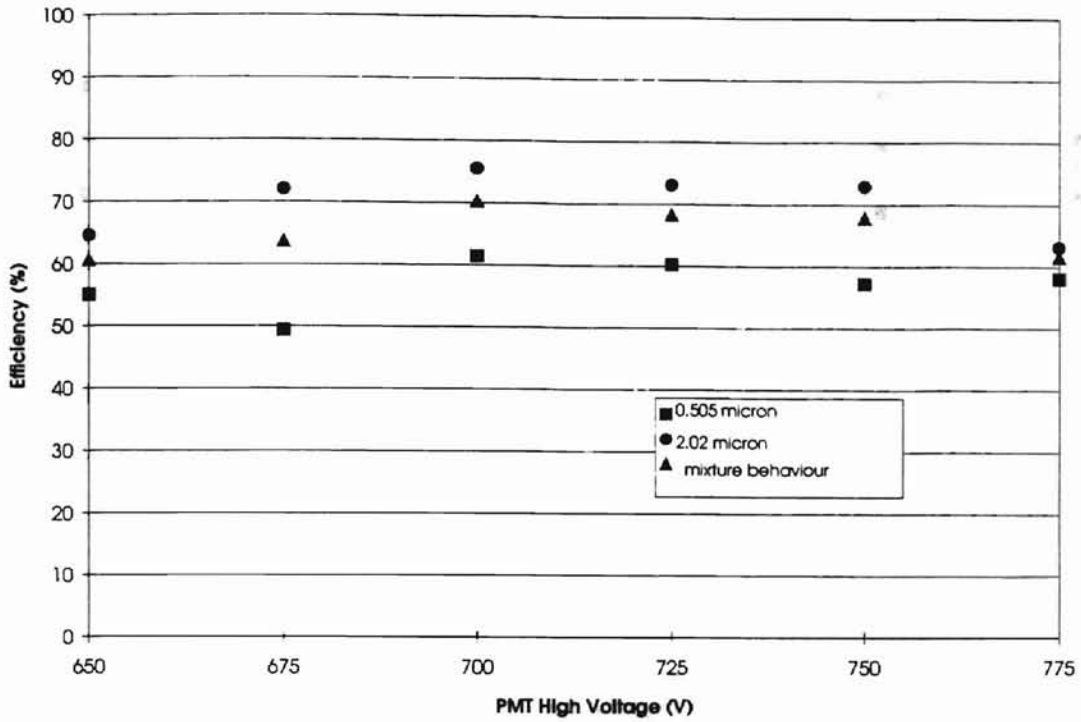


Figure C-20 Fractional Efficiency as a Function of High Voltage for a Mixture Containing Particles of Diameter 2.02 Microns and 0.505 Micron (Test21)

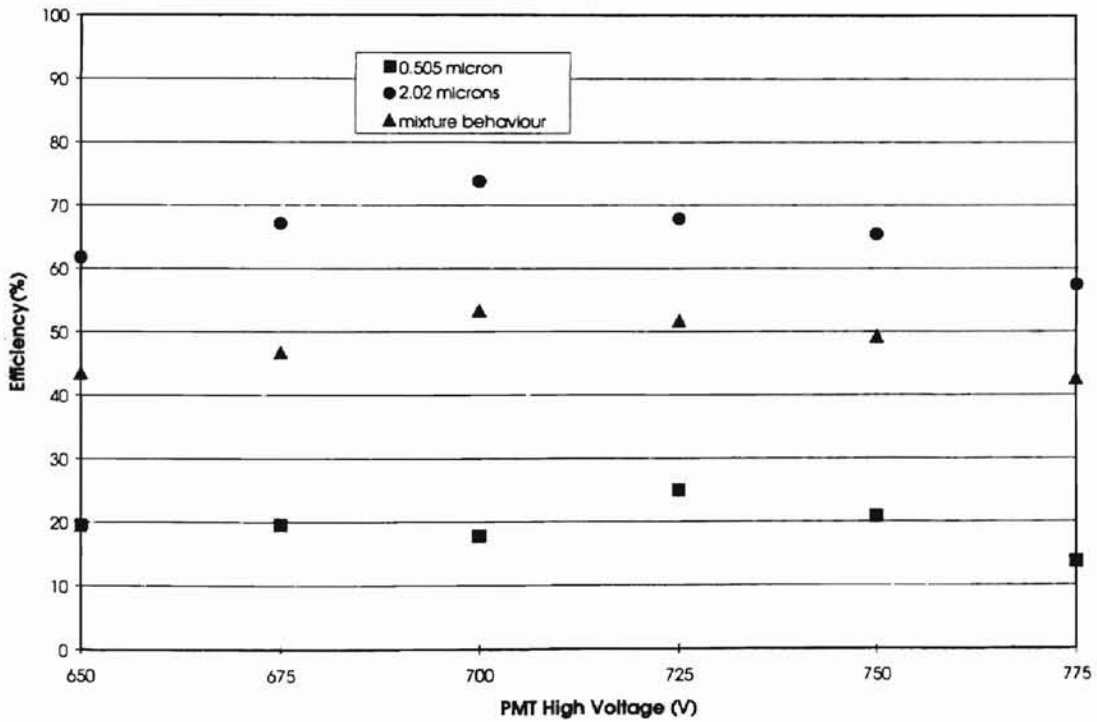


Figure C-21 Fractional Efficiency as a Function of High Voltage for a Mixture Containing Particles of Diameter 2.02 Microns and 0.505 Micron (Test22)

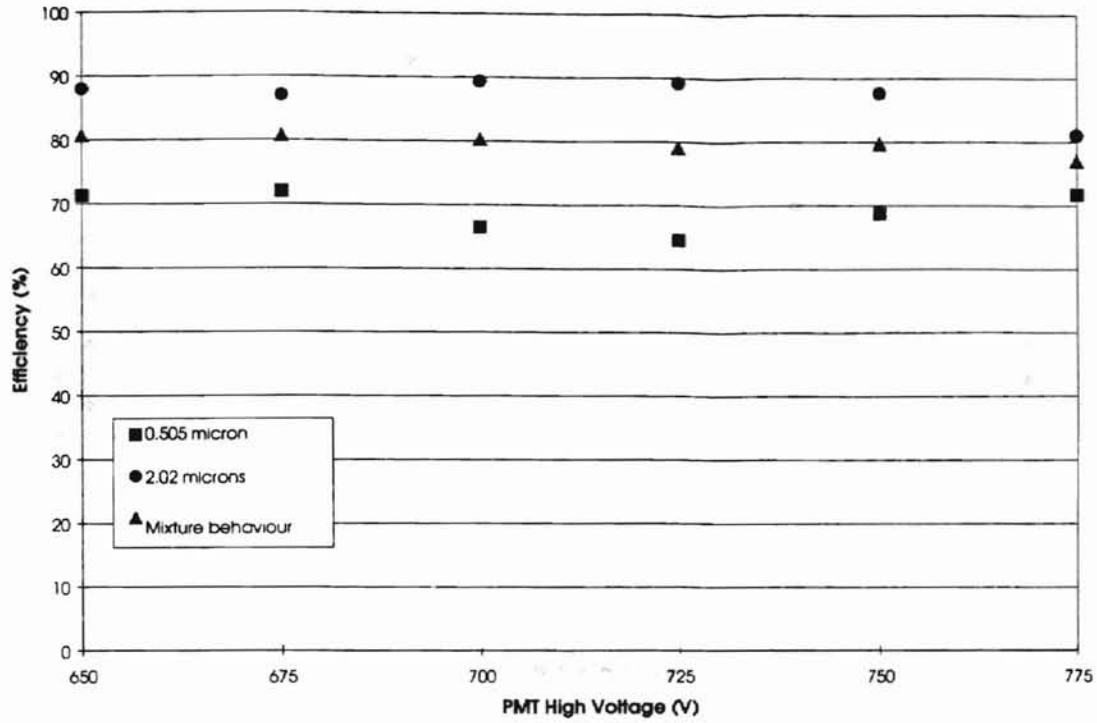


Figure C-22 Fractional Efficiency as a Function of High Voltage for a Mixture Containing Particles of Diameter 2.02 Microns and 0.505 Micron (Test35)

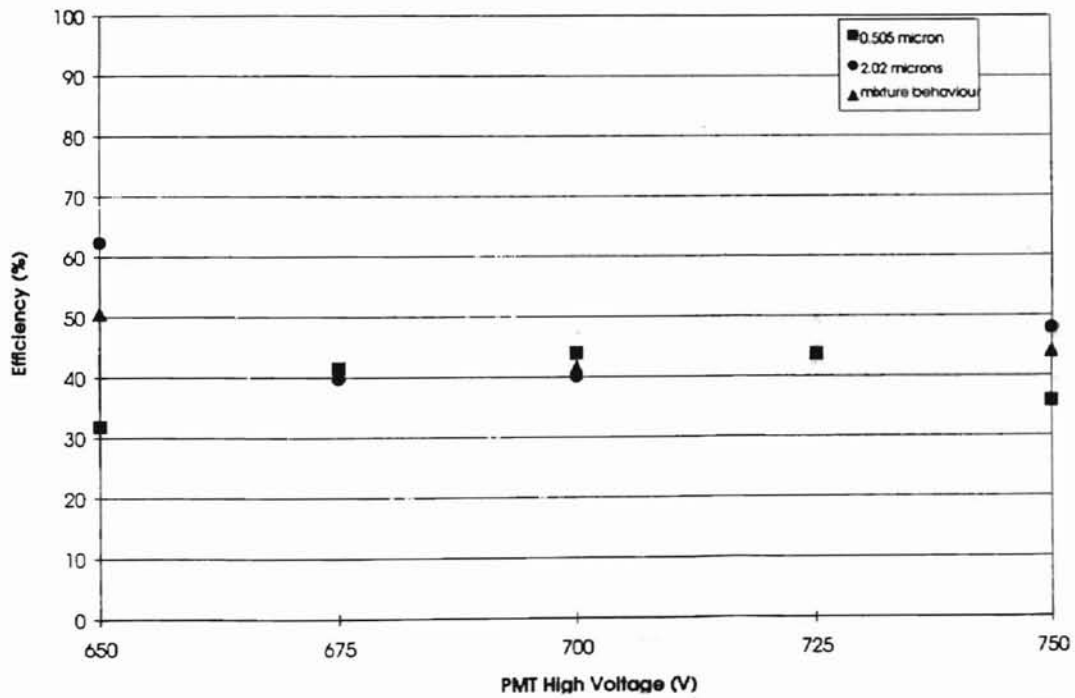


Figure C-23 Fractional Efficiency as a Function of High Voltage for a Mixture Containing Particles of Diameter 2.02 Microns and 0.505 Micron (Test39)

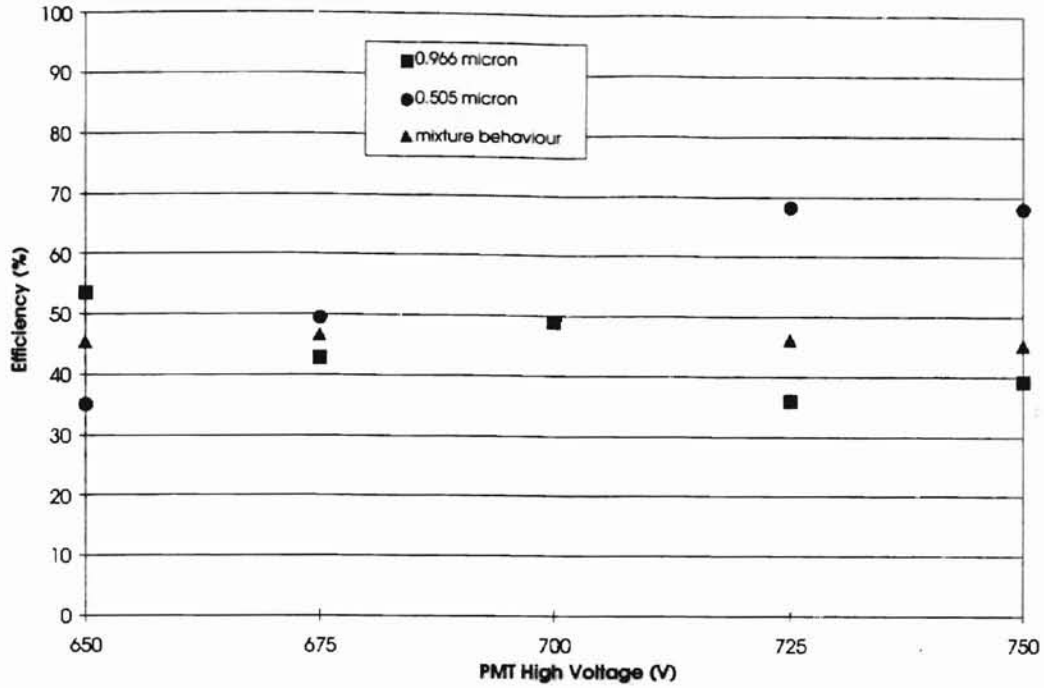


Figure C-24 Fractional Efficiency as a Function of High Voltage for a Mixture Containing Particles of Diameter 0.505 Micron and 0.966 Micron (Test31)

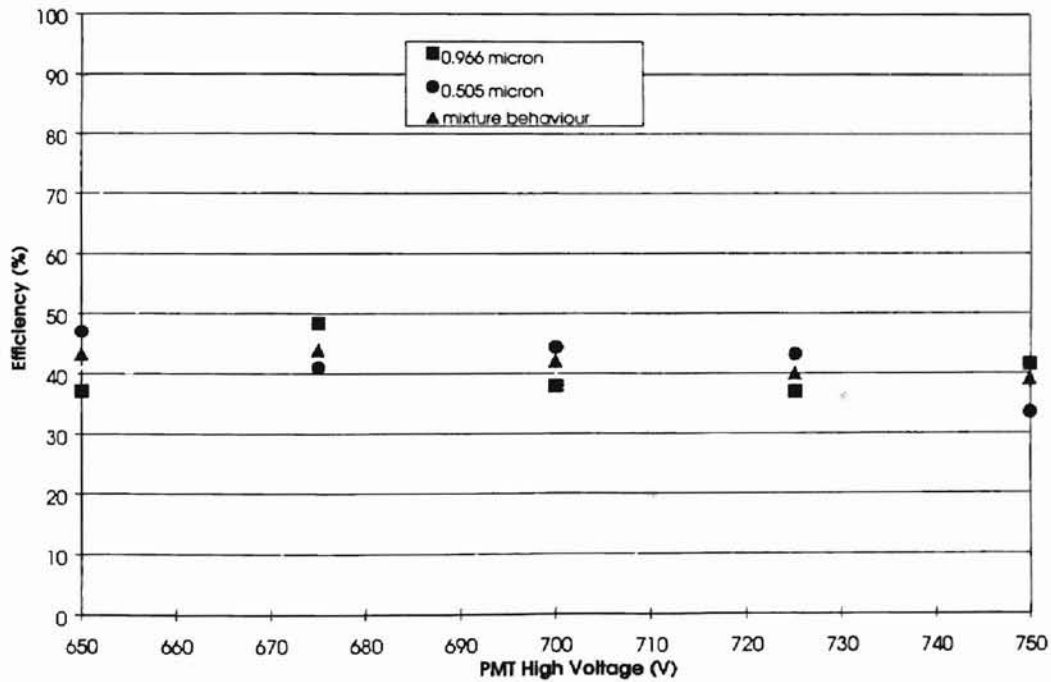


Figure C-25 Fractional Efficiency as a Function of High Voltage for a Mixture Containing Particles of Diameter 0.505 Micron and 0.966 Micron (Test32)

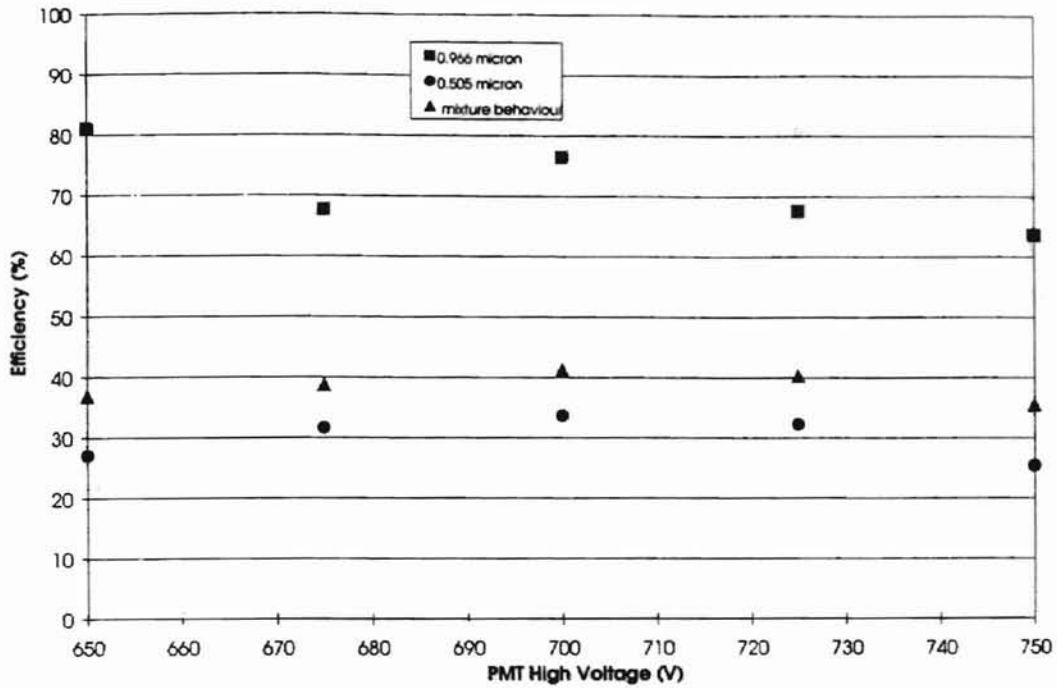


Figure C-26 Fractional Efficiency as a Function of High Voltage for a Mixture Containing Particles of Diameter 0.505 Micron and 0.966 Micron (Test36)

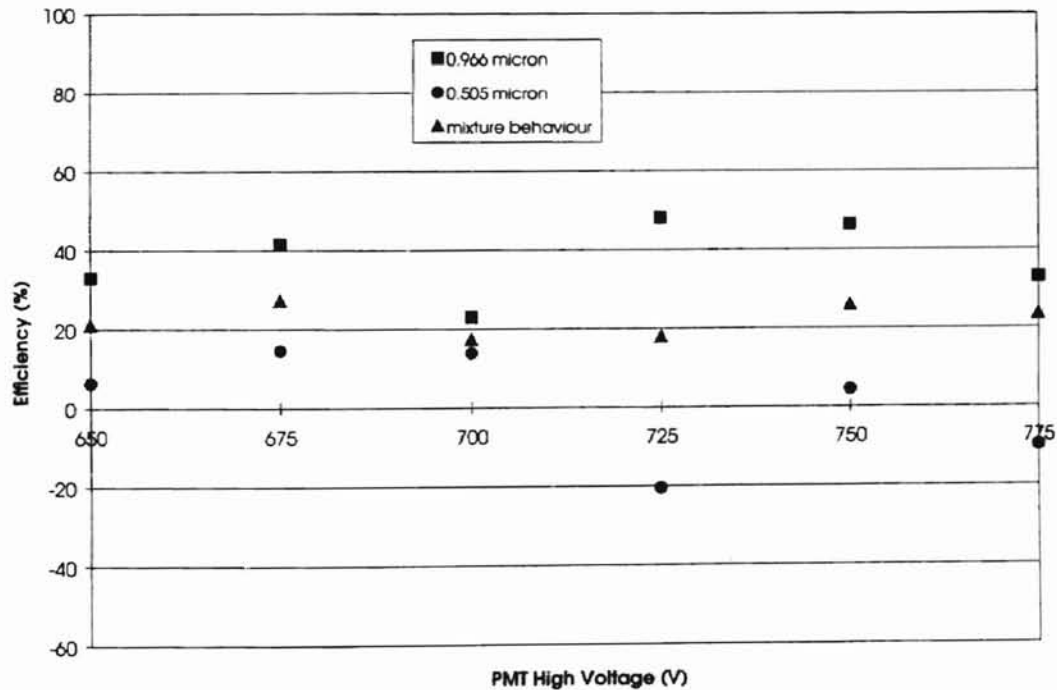


Figure C-27 Fractional Efficiency as a Function of High Voltage for a Mixture Containing Particles of Diameter 0.505 Micron and 0.966 Micron (Test37)

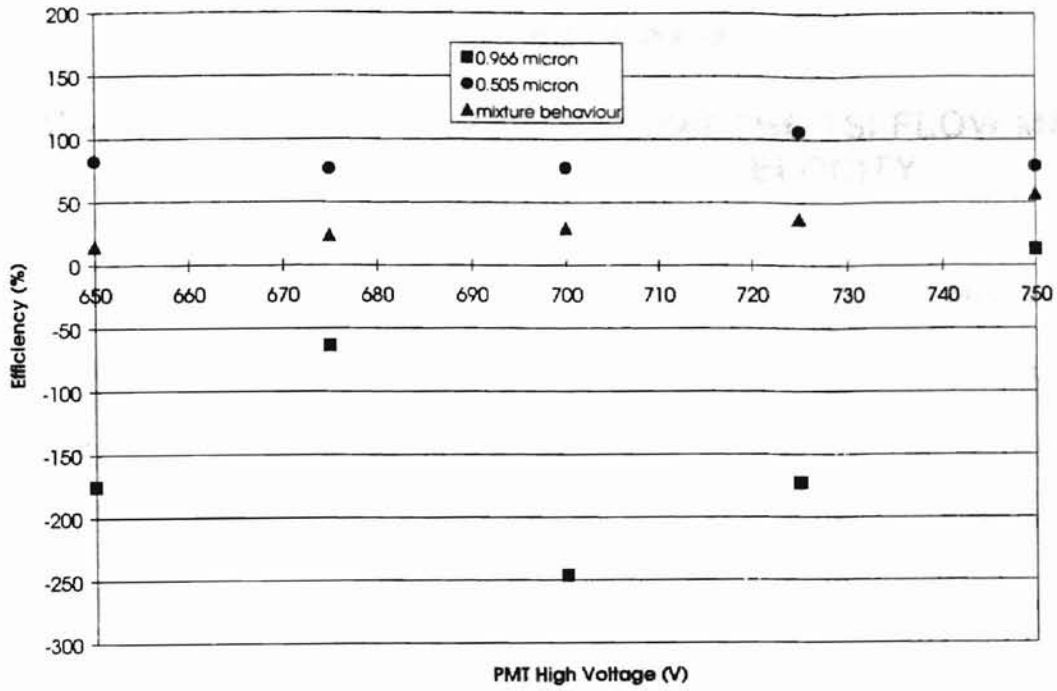


Figure C-28 Fractional Efficiency as a Function of High Voltage for a Mixture Containing Particles of Diameter 2.02 Microns and 0.966 Micron (Test41)

APPENDIX D

CALCULATION OF ERROR IN USING THE TSI FLOW METER FOR MEASURING DUCT VELOCITY

In this appendix, the error in the estimation of velocity and Stokes number is calculated if we use the TSI flow meter without information on the temperature and pressure known inside the flow nozzle.

The flowrate of a compressed gas at any pressure is inversely proportional to the absolute pressure and directly proportional to the absolute temperature from the universal gas law equation.

The TSI flow meter can be used to calculate the average velocity of air by measuring the total flow rate and dividing by the surface area of the conduit at the region of interest. The corrected velocity $V(T, P)$ can be given as

$$V(T, P) = \frac{\rho_{\text{air-standard}}}{\rho_{\text{air}}(T, P)} V_{\text{TSI}} \quad (\text{D-1})$$

where $\rho_{\text{air}}(T, P)$ is the density of air at temperature T and pressure P , V_{TSI} is the calculated velocity using the TSI flow meter without correcting for temperature and pressure and $\rho_{\text{air-standard}}$ is the density of air at standard conditions (15.55 °C and 1.013×10^5 Pa).

The corrected Stokes number $St(T, P)$ can be given as

$$St(T, P) = St_{\text{TSI}} \frac{1}{\left(\frac{\rho_{\text{air}}(T, P)}{\rho_{\text{air-standard}}} \right) \left(\frac{\mu_{\text{air}}(T, P)}{\mu_{\text{air-standard}}} \right)} \quad (\text{D-2})$$

where St_{TSI} is the value of velocity calculated using the TSI flow meter, $\mu_{\text{air}}(T, P)$ is the

dynamic viscosity of air at temperature T and pressure P, and $\mu_{\text{air-standard}}$ is the dynamic viscosity of air at standard conditions (15.55 °C and 1.013×10^5 Pa).

Table D-1 Tabulation of Calculated Error using the TSI Flow Meter

Temperature in (°C)	Absolute Temperature (°K)	Density (kg/m ³)	Viscosity (Pa-s)	Error in Velocity (%)	Error in Stokes Number (%)
0	273	1.2933	1.7231×10^{-05}	5.72	2.5416
5	278	1.2699	1.7478×10^{-05}	3.80	2.9553
10	283	1.2474	1.7722×10^{-05}	1.97	3.3693
15	288	1.2257	1.7965×10^{-05}	0.19	3.7764
20	293	1.2047	1.8205×10^{-05}	1.52	4.1934
25	298	1.1845	1.8444×10^{-05}	3.17	4.5971
30	303	1.1649	1.8680×10^{-05}	4.77	5.0133
35	308	1.1459	1.8915×10^{-05}	6.32	5.4282
40	313	1.1275	1.9148×10^{-05}	7.83	5.8449
45	318	1.1098	1.9379×10^{-05}	9.27	6.2512
50	323	1.0925	1.9608×10^{-05}	10.69	6.6731
55	328	1.0759	1.9835×10^{-05}	12.04	7.0794
60	333	1.0597	2.0061×10^{-05}	13.37	7.4916
65	338	1.0439	2.0285×10^{-05}	14.66	7.9135

Thus, if we assume that the temperature conditions inside the flow nozzle varied between 25 °C and 55 °C, the corresponding maximum error in measuring the velocity from the conditions described above would be 12.04% and hence the corresponding maximum error in calculating Stokes number would be 7.07%. Variation of pressure has been assumed to be negligible.

APPENDIX E

DSA RAW DATA LISTING

The author of this thesis was able to obtain an ASCII format listing of the data in a test run by modifying the code provided by Aerometrics Inc. Using this program, the author was able to study the quality of signals in a test run by extracting the LDV signal data from the raw file generated by the LDV system.

```
{ DSARAW.PAS 8-Apr-99,Ram Srinivasan read DSARDAT.006,create txt file)
(Reference 'Aming' Aerometrics DSARAW.PAS)

PROGRAM DSARaw;

USES Crt, R_DRDefs, R_SType, R_BadBin;

VAR
  RawDataRec      : raw_data_rec;           { record to hold raw data      }
  rHeader         : Raw_Data_Header;       { record to hold header info  }
  RawFile         : file;
  FPath           : str79;                 { raw data run                }
  DPath           : string[10];           {raw data test}
  Samp_Sta,
  comment1,
  comment2        : string[30];           {error status}

  Sample_Number  : longint;               { which sample we are displaying}
  Vel_On         : vel_switch_array;     { velocity enabled, ch1 - ch3  }
  Ext_On         : vel_switch_array;     { external inputs, ch1 - ch3  }
  Dia_On         : boolean;              { sizing enabled              }
  vFirstBin      : vel_array;            { velocity first bin value M/S }
  vBinInc        : vel_array;            { velocity bin increment M/S  }
  dFirstBin      : Single;               { size first bin value uM     }
  dBinInc        : Single;               { size bin increment uM      }
  eMinVal        : vel_array;            { value for ExtInp = 0        }
  eInc           : vel_array;            { Increment for ExtInp        }
  ReturnChar     : char;
  PageDown,
  Done           : boolean;
  Bin_Res        : Word;                 { Bin Resolution              }
  Intensity_Overlap : Vel_Array;         { save for version 00        }
  vel            : vel_array;            {final value of velocity}
  Int            : vel_array;            {final value of intensity}
  Transit        : vel_array;            {my file}
  outraw         : Text;                 {my file}
{*****
*
* Check_Measurement_Ranges
*
*****
```

```

*      Checks for old raw data files which are based on 50 bins *
*      with x4 resolution (200 bins) and extends the min/max *
*      values to 240 bins for use in the V4 software. *
*      Called after loading Raw Data File which sets the bin_inc*
*      to the proper value. *
*
*****}

PROCEDURE Check_Measurement_Ranges;
VAR
  ch : channel_type;
BEGIN
  IF Bin_Res <> 1 THEN BEGIN
    IF Dia_On
      THEN dBinInc := dBinInc/Bin_Res;
    FOR Ch := Ch1 TO Ch3 DO IF Vel_On[Ch]
      THEN vBinInc[ch] := vBinInc[ch]/Bin_Res;
    END;
  END;
END;

(*****}
*
*      Get_Raw_File *
*
*      Attempts to open a raw data file in the directory FPATH. *
*      FPATH is set to the command line parameter if available. *
*
*      After that the user is prompted for a PATH until a file *
*      is successfully opened or no path is given. *
*
*      Returns true if successful, sets the BadBin version for *
*      status processing and sets Sample_Number = 0. *
*
*****}

FUNCTION Get_Raw_File : Boolean;
VAR
  ok      : boolean;
BEGIN

  Get_Raw_File := False;
  ok           := False;
  Chdir('e:\dsadata\rampsize');

  IF paramcount > 0
    THEN FPath := paramstr(1)
    ELSE FPath := NULL_STR;
  REPEAT
    IF FPath = NULL_STR THEN BEGIN

      Write('Subdirectory of run (test)> '); readln(DPath);
      Chdir(DPath);
      Write('Run Directory (eg Run01 etc)> '); readln(FPath);
      Write('comments 1 of 2 '); readln(comment1);
      Write('comments 2 of 2 '); readln(comment2);
      IF FPath = NULL_STR THEN EXIT;
    END;
    Ok := Open_Raw_File(RawFile,FPath,rHeader);

  IF (NOT Ok) THEN BEGIN
    WriteLn;
    WriteLn('Unable to Open Raw Data File in ',FPath);
    Delay(1000);
  
```

```

        FPath := NULL_STR;
    END;
UNTIL ok;
Set_BadBin_Version(FPath);
Get_Raw_File := True;
Sample_Number := 0;
END;

{*****
*
*   Get_Header_Info
*
*   Copies header information from rHeader into the
*   appropriate global variables for easier access.
*
*   Performs any conversions which are necessary.
*
*****}

PROCEDURE Get_Header_Info;
VAR
    ch      : Channel_Type;
BEGIN
    WITH rHeader.swr DO BEGIN
        Dia_On := DiaOn;
        Vel_On := VelOn;
        Ext_On := ExtOn;
        Bin_Res:= BinRes;
    END;
    WITH rHeader.br DO BEGIN
        dFirstBin := DiaFB;
        dBinInc    := DiaBI;
        vFirstBin := VelFB;
        vBinInc    := VelBI;
    END;
    FOR ch := ch1 TO ch3 DO WITH rHeader.er[ch] DO BEGIN
        eMinVal[ch] := MinVal;
        eInc[ch]    := ExtInp_Increment(MinVal,MaxVal,NumBits);
    END;
    Check_Measurement_Ranges;
END;

{*****}
PROCEDURE Write_Heading;

VAR
    ch      : channel_type;
    row     : byte;
    tstr    : str4;

BEGIN
    Writeln(outraw,'DSA 4.18s Raw Data File Display');
    Writeln(outraw,'e:\dsadata\rampsize',FPath);
    Writeln(outraw,'Source code c:\temporar\dsa4\dsaraw\DSARAW.PAS 8-Apr-99
read DSARDAT.006 and create text file');
    Writeln(outraw,comment1);
    Writeln(outraw,comment2);

    Str(Raw_Data_File_Version_Loaded,tstr);

```



```

{Do_Top_Of_Screen;}
WITH rHeader.swr DO BEGIN

Writeln(outraw,'Number Of Pages   : ',Numpages);
Writeln(outraw,'Bin Resolution   : ',BinRes);

FOR ch := ch1 TO ch3 DO BEGIN
  Writeln(outraw,'Velocity '+ChStr(ch)+' ');
  IF Vel_On[ch] THEN BEGIN Writeln(outraw,'On');
  END ELSE BEGIN Writeln(outraw,'Off');
  END;
END;
WITH rHeader.mR DO BEGIN

  FOR ch := ch1 TO ch3 DO IF rChOn[ch] THEN BEGIN
    Writeln(outraw,'Fringe Spacing '+ChStr(ch)+' :
',FSpacing[ch]:7:5,'um');

    END;
  END;

END;

Writeln(outraw,'Sample':6,' ',' ','Status':7,' ',' ','Run
Time':12,' ',' ','velocity1':12,' ',' ','Intensity1':12,' ',' ','Transit':12,' ',' ','Fringe':1
2,' ',' ','velocity2':12,' ',' ','Intensity2':12,' ',' ','Transit':12,' ',' ','Fringe':12,' ',' ','
Sample Status':26);
Writeln(outraw,'Number':6,' ',' ','
':7,' ',' ','seconds':12,' ',' ','m/s':12,' ',' ','mV':12,' ',' ','us ch1':12,' ',' ','Count
ch1':12,' ',' ','m/s':12,' ',' ','mV':12,' ',' ','us ch2':12,' ',' ','Count ch2':12,' ',' ','
':30);

END;

{*****
*
*   Get_Next_Sample
*
*   Reads the next sample from the data file.  If PageDown is*
*   true then RAW_SAMPLES_PER_PAGE are read first.
*
*   Returns FALSE if there is an error reading the file or
*   the end of data has been reached.
*
*   Returns TRUE if successful and calls Get_RawSample_ID().
*
*****}

FUNCTION Get_Next_Sample : Boolean;
VAR
  i : Word;
BEGIN
  Get_Next_Sample := False;
  IF PageDown THEN BEGIN
    PageDown := False;
    FOR i := 1 TO RAW_SAMPLES_PER_PAGE DO
BlockRead(RawFile,RawDataRec,SizeOf(RawDataRec));
    Inc(Sample_Number,RAW_SAMPLES_PER_PAGE);

```

```

END;
BlockRead(RawFile,RawDataRec,SizeOf(RawDataRec));
IF ioresult = 0 THEN BEGIN
  IF End_Of_RawData(RawDataRec)
    THEN Exit
  ELSE BEGIN
    Inc(Sample_Number);
    Get_RawSample_ID(RawDataRec);
    Get_Next_Sample := True;
  END;
END;
END;

{*****
*
* Write_Sample_Data
*
*
*****}

PROCEDURE Write_Sample_Data;
VAR
  Row, Col : Byte;
  ch : channel_type;
  j : byte;
  temp : integer;
BEGIN
  WITH RawDataRec.sr3 DO BEGIN
    Row := 6; Col := 29;
    WriteAt(Col,Row,1,NULL_STR); Write(Sample_Number:6);

    IF status = S_Ok THEN BEGIN

      Samp_sta:='OKAY';
    END ELSE BEGIN
      temp := Abs(ErrorCode_To_BadBin(Status));
      Samp_sta:= BAD_HIST_LABELS[temp];
      vel[ch1]:=0.0;
      Int[ch1]:=0;
      Transit[ch1]:=0;
      Fcount[ch1]:=0;
      vel[ch2]:=0;
      Int[ch2]:=0;
      Transit[ch2]:=0;
      Fcount[ch2]:=0;

    END;

    IF status = S_Ok THEN BEGIN
      IF Vel_On[ch1] OR Vel_On[ch2] OR Vel_On[ch3] THEN BEGIN

        FOR ch := ch1 TO ch3 DO BEGIN
          IF vel_on[ch] AND rChOn[ch]
            THEN BEGIN

              vel[ch] := vFirstBin[ch] + Vel_Bin[ch]*vBinInc[ch]/256;

            END ELSE BEGIN

```

```

        vel[ch] := 0;

    END;
    END;
    END;

BEGIN

    FOR ch := ch1 TO ch3 DO BEGIN
        IF Vel_On[ch] AND rChOn[ch]
            THEN BEGIN

                Int[ch] := RawSample_Intensity(RawDataRec,ch)*5/30;
                END
            ELSE BEGIN

                Int[ch]:=0;

                END;
            END;
        IF Raw_Data_File_Version_Loaded >= 2 THEN BEGIN

            FOR ch := ch1 TO ch3 DO BEGIN
                IF Vel_On[ch] AND rChOn[ch]
                    THEN BEGIN

                        Transit[ch]:=GateCount[ch]*0.025;           {clock ticks
conversion}
                    END
                ELSE BEGIN

                    Transit[ch]:=0;

                    END;
                END;
            END;
        END;
        IF Ext_On[ch1] OR Ext_On[Ch2] OR Ext_On[ch3] THEN BEGIN

            FOR ch := ch1 TO ch3 DO BEGIN
                IF Ext_On[ch] AND rExtOn
                    THEN Write(eMinVal[ch]+Ext[ch]*eInc[ch]:10:3)
                    ELSE Write(' ':10);
                Write(' ':2);
            END;
        END
    END;

    Writeln(outraw,Sample_Number:6,' ',HexByte(Status):7,' ',Run_time:12:4,' ',vel[
ch1] :12:4,' ',Int[ch1] :12:2,' ',Transit[ch1]:12:3,' ',
Fcount[ch1]:12,' ',vel[ch2]:12:4,' ',Int[ch2]:12:2,' ',Transit[ch2]:12:3,' ',Fc
ount[ch2]:12,' ',Samp_Sta:26);

    END;

    END;

```

```

(*****
*
* PROGRAM DSARaw
*
* Main program. Simple stuff, just calls everyone in the
* right order.
*
*****)

BEGIN
  TextMode(CO80);
  TextColor(White);

  PageDown := False;

  IF NOT Get_Raw_File THEN EXIT;

  Get_Header_Info;
  { Chdir(FPath);}

  Assign(outraw,concat(Fpath+'.txt'));
  Rewrite(outraw);

  Write_Heading;

  Done := False;

  While Not Done DO BEGIN
    Done := NOT Get_Next_Sample;
    IF NOT Done THEN BEGIN
      Write_Sample_Data;
      Prompt('Converting data Raw Signal Data to Text Format');
      ReturnChar := 'R';
      PageDown := (ReturnChar = 'P');
      Done := (ReturnChar = 'Q');
    END;
  END;

  clrscr;
  Close(RawFile);
  Close(outraw);

END.

```

Using this code, a sample output of a test run in Region II as described in Chapter 3 has been presented in this appendix. The column indicating code status gives information on the quality of the signal which is indicated in the column titled "Sample Status".

e:\dsadata\ramsizerun41

Source code c:\temporar\dsa4\dsaraw\DSARAW.PAS 8-Apr-99 read DSARDAT.006 and create text file

Number Of Pages: 1

Bin Resolution: 1

Velocity Ch1

On

Velocity Ch2

Off

Velocity Ch3

Off

Fringe Spacing Ch1: 2.84884um

No.	Status	Sample	Status	Run Time	Peak	velocity1	Intensity1	Transit	Fringe
	code			seconds	Detection	m/s	mV	us ch1	Ch1
2	0	OK		0.0777	243	3.3286	98	23.025	27
3	0	OK		0.089	151	3.3456	97	19.45	23
4	0	OK		0.0921	125	3.0155	122	14.3	15
5	0	OK		0.1761	231	3.4914	95	12.9	16
6	0	OK		0.3801	228	3.7108	114	18.375	24
7	0	OK		0.3833	158	3.8716	95	8.15	11
9	0	OK		0.4506	225	3.3692	87	13.95	16
11	0	OK		0.7253	88	2.8331	93	20.175	20
12	0	OK		0.7825	192	2.7988	185	28.275	28
13	0	OK		0.7992	14	3.4264	96	11.95	14
14	0	OK		1.0165	31	3.226	134	21.35	24
15	0	OK		1.2083	237	3.4117	126	12.55	15
16	0	OK		1.2736	31	3.2773	98	18.25	21
17	0	OK		1.2814	231	3.6925	119	9.2	12
20	0	OK		1.5378	244	2.1568	80	5.45	4
21	0	OK		1.5424	93	2.7491	107	15.35	15
22	0	OK		1.6768	188	2.9259	80	13.325	14
25	0	OK		1.9302	141	3.0096	127	7.625	8
26	0	OK		1.9975	109	2.7707	85	9.725	9
30	0	OK		2.1608	14	3.4581	91	5.025	6
32	0	OK		2.2196	249	3.5411	116	9.4	12
33	0	OK		2.2203	120	3.5228	89	13.05	16
36	0	OK		2.6149	224	2.9887	104	19.4	20
37	0	OK		2.6396	60	3.4493	95	19.175	23
40	0	OK		2.9071	248	3.2737	127	16.425	19
41	0	OK		2.9199	240	3.6075	114	21.05	27
42	0	OK		3.1472	225	3.0655	127	10.45	11
43	0	OK		3.3391	248	2.8311	194	38.325	38
44	0	OK		3.4801	97	3.1832	94	9.475	11
45	0	OK		3.6807	183	3.8425	89	9.4	13
46	0	OK		3.7399	76	3.5741	94	8.325	10
47	0	OK		3.7796	97	3.4548	84	16.725	20
49	0	OK		3.9077	142	3.5261	127	19.925	25
50	0	OK		3.9251	124	3.4359	123	19.425	23
51	0	OK		4.0503	199	4.1115	127	26.325	38
52	0	OK		4.0613	227	3.6879	113	5.675	7
55	0	OK		4.2147	130	4.0027	122	9.65	14

56	0	OK	4.2516	62	3.3074	255	23.15	27
57	0	OK	4.3232	226	2.7105	73	23.075	22
59	0	OK	4.6311	7	3.3607	118	28.5	34
60	0	OK	4.6883	14	3.227	95	13.675	15
61	0	OK	4.8028	7	3.1165	95	11.475	13
62	0	OK	4.8784	63	3.0635	96	9.7	10
63	0	OK	4.985	62	2.8073	94	18.425	18
64	0	OK	5.0903	228	3.1793	100	7.35	8
65	0	OK	5.1701	161	3.142	96	21.9	24
66	0	OK	5.19	115	3.3692	91	8.4	10
67	0	OK	5.3238	31	3.1914	87	7.325	8
68	0	OK	5.4207	28	3.3721	88	12.2	14
69	0	OK	5.5732	39	3.2146	96	18.825	21
70	0	OK	5.5948	135	3.5352	87	9.65	12
71	0	OK	5.6863	232	3.4123	71	8.275	10
72	0	OK	6.2776	234	3.0233	119	35.725	38
75	0	OK	6.4534	217	2.6598	127	15.7	15
77	0	OK	6.5703	135	2.7589	153	27.25	26
78	0	OK	6.6226	28	3.1832	107	14.625	16
79	0	OK	6.7781	69	2.8203	117	9.125	9
80	0	OK	6.8852	143	2.7141	237	28.175	27
83	0	OK	6.9791	135	3.834	126	16.225	22
84	0	OK	7.029	81	3.7124	127	14.2	19
87	0	OK	7.3373	135	3.8768	137	26.8	36
88	0	OK	7.502	184	3.5336	109	16.225	20
89	0	OK	7.5198	243	3.024	87	9.25	10
90	0	OK	7.5204	154	3.0819	99	9.6	10
91	0	OK	7.5266	15	3.1557	104	12.9	14
92	0	OK	7.6023	30	3.0917	223	29.525	32
93	0	OK	7.7026	159	3.7412	89	21.6	28
94	0	OK	7.7123	28	3.3845	102	15.175	18
95	0	OK	7.7782	31	3.5509	95	15.2	19
96	0	OK	8.0754	67	3.2692	255	16.725	19
97	0	OK	8.137	131	2.7036	114	22.375	21
98	0	OK	8.1646	29	2.8001	92	11.025	11
99	0	OK	8.1857	199	3.6326	94	18.25	23
101	0	OK	8.2407	94	3.3015	91	15.475	18
102	0	OK	8.2836	62	3.4689	95	8.025	10
103	0	OK	8.4724	30	3.7006	91	27.75	36
105	0	OK	8.5341	7	3.2701	102	7.2	8
108	0	OK	8.7812	133	3.4666	96	13.975	17
109	0	OK	8.8896	225	3.1734	95	14.3	16
110	0	OK	8.9056	56	2.974	120	18.425	19
111	0	OK	9.0196	224	3.0998	111	24.45	27
112	0	OK	9.103	190	3.0688	124	19.075	21
113	0	OK	9.1641	193	3.2652	126	34.325	39
115	0	OK	9.3612	152	3.6627	71	10.75	14
116	0	OK	9.5102	145	3.1835	87	8.875	10
117	0	OK	9.8458	62	3.3604	73	26.8	32
118	0	OK	9.9612	252	3.5307	95	9.65	12
119	0	OK	10.1041	58	3.1387	124	20.125	22
120	0	OK	10.1283	165	3.4793	150	20.325	25

122	0	OK	10.2149	197	3.2629	86	9.975	11
123	0	OK	10.2164	124	3.5003	107	17.4	21
124	0	OK	10.27	113	2.9652	96	9.8	10
125	0	OK	10.4973	248	2.7896	95	31.35	31
127	0	OK	10.5522	241	3.5107	95	13.7	17
129	0	OK	10.5811	9	3.1884	93	21.4	24
130	0	OK	10.6168	229	3.0086	127	13.125	14
131	0	OK	10.7125	225	3.1319	87	10.925	12
133	0	OK	10.8783	150	3.3993	86	20.125	24
136	0	OK	11.0718	3	3.2358	86	12.275	14
137	0	OK	11.1621	62	3.8419	87	13.375	18
139	0	OK	11.3249	196	3.4604	250	28.15	34
142	0	OK	11.4776	14	2.802	191	37.125	37
143	0	OK	11.6378	57	3.0727	122	14.95	16
144	0	OK	11.6624	10	2.7824	239	35.025	34
147	0	OK	11.8553	20	3.2224	111	21.3	24
149	0	OK	12.0985	248	2.3532	99	8.425	7
150	0	OK	12.193	49	3.1887	95	6.7	7
155	0	OK	12.498	135	3.091	250	40	43
156	0	OK	12.5067	250	3.292	99	14.15	16
157	0	OK	12.5849	15	3.2322	115	12.9	15
159	0	OK	12.7115	120	3.0665	95	21.525	23
161	0	OK	12.9027	193	3.8533	95	5.85	8
163	0	OK	13.0409	53	2.9776	103	10.875	11
165	0	OK	13.2713	33	2.6945	80	16.6	16
169	0	OK	13.333	224	2.8118	96	10.7	11
170	0	OK	13.3336	100	2.4791	96	23.675	21
171	0	OK	13.3772	249	3.1838	88	14.775	17
172	0	OK	13.5058	197	3.4323	85	10.775	13
174	0	OK	13.672	55	2.9413	127	19.925	21
175	0	OK	13.6776	224	2.9491	95	15.3	16
177	0	OK	14.0493	112	3.5362	111	19	24
178	0	OK	14.099	98	3.481	123	13.975	17
179	0	OK	14.1417	252	3.3231	108	19.825	23
180	0	OK	14.1716	52	3.9105	95	6.5	9
181	0	OK	14.201	15	2.7765	93	15.325	15
183	0	OK	14.3473	28	3.1266	88	17.35	19
184	0	OK	14.4193	120	3.3793	93	15.75	19
186	0	OK	14.5934	243	3.4699	87	7.375	9
187	0	OK	14.6244	44	3.0387	89	10.225	11
188	0	OK	14.6581	112	3.2433	94	11.95	14
189	0	OK	14.7219	125	3.1273	124	11.825	13
190	0	OK	14.8859	190	3.378	81	11.4	14
191	0	OK	14.8861	224	3.4346	127	13.825	17
192	0	OK	14.8868	56	3.5388	135	14.525	18
193	0	OK	14.9327	225	3.7402	91	8.875	12
194	0	OK	14.9662	243	2.7269	99	16.8	16
195	0	OK	15.1269	244	2.2937	127	31.425	25
196	0	OK	15.1438	127	2.8001	124	17	17
197	0	OK	15.1841	149	3.1848	87	11.825	13
198	0	OK	15.2257	224	3.2492	114	13.2	15
199	0	OK	15.2375	62	3.1855	96	11	12

201	0	OK	15.3201	165	3.2443	94	9.35	11
202	0	OK	15.4324	240	2.8449	105	25.85	26
203	0	OK	15.434	7	3.0766	99	14.3	15
204	0	OK	15.4429	232	3.1436	90	9.875	11
205	0	OK	15.6571	122	2.8655	114	22.325	22
206	0	OK	15.6818	79	3.2224	93	14.975	17
207	0	OK	15.6957	60	3.4686	97	16.975	21
208	0	OK	15.7049	63	3.2368	152	31.5	36
210	0	OK	15.7312	120	3.6428	95	11.525	15
211	0	OK	15.8647	167	3.1786	126	22.85	25
212	0	OK	15.9192	135	3.4362	89	9.025	11
213	0	OK	15.9249	113	2.8161	95	15.675	15
214	0	OK	15.9761	230	3.5254	94	8.4	10
215	0	OK	15.9963	185	2.8606	123	22.725	23
216	0	OK	16.1142	82	3.0632	106	15.275	16
218	0	OK	16.7707	15	3.3362	79	7.1	8
219	0	OK	16.7787	46	2.8733	91	17.15	17
220	0	OK	16.7906	27	3.2724	101	11.025	13
221	0	OK	16.8499	31	2.974	118	31.45	33
222	0	OK	16.8545	69	2.8266	111	11.075	11
223	0	OK	16.8583	184	3.2178	104	24.325	27
225	0	OK	16.928	31	3.4512	77	12.975	16
226	0	OK	16.9391	242	3.8298	87	11.625	16
228	0	OK	17.1964	209	4.3296	95	10.25	16
231	0	OK	17.3073	102	3.2956	87	2.65	3
233	0	OK	17.3596	7	3.1498	100	7.825	9
235	0	OK	17.4027	244	3.4496	167	20.675	25
236	0	OK	17.4256	163	3.6941	109	17.1	22
238	0	OK	17.6032	133	3.7598	121	9.625	13
239	0	OK	17.6596	14	2.9465	126	30.45	31
240	0	OK	17.6783	252	3.0714	125	9.7	10
241	0	OK	17.7838	175	3.6039	118	18.55	23
242	0	OK	17.8102	248	2.9936	112	17.15	18
243	0	OK	17.8493	177	2.7546	89	19.425	19
245	0	OK	17.9087	135	3.0465	98	19.25	21
246	0	OK	17.9137	201	3.2332	139	25.05	28
248	0	OK	18.0904	193	3.616	115	14.85	19
250	0	OK	18.1764	131	3.4715	192	23.2	28
251	0	OK	18.2296	60	3.346	82	11.95	14
253	0	OK	18.3337	84	2.6177	118	33.975	31
254	0	OK	18.5676	224	3.3947	99	11.825	14
255	0	OK	18.5981	248	3.3182	91	21.95	26
256	0	OK	18.5989	151	3.9406	102	7.475	10
257	0	OK	18.6456	241	2.92	125	20.925	21
258	0	OK	18.6528	193	3.1358	249	23.125	25
261	0	OK	18.8228	14	3.1632	111	12.45	14
263	0	OK	18.9566	147	3.1616	84	3.725	4
266	0	OK	19.1181	30	3.1328	126	17.85	20
267	0	OK	19.135	75	3.1541	89	6.2	7
268	0	OK	19.2061	131	2.5886	105	30.85	28
269	0	OK	19.2844	240	3.7382	143	25.2	33
270	0	OK	19.3651	119	2.6667	106	11.65	11

271	0	OK	19.4425	124	3.3172	95	11.45	13
272	0	OK	19.5187	56	2.6053	117	20.225	18
273	0	OK	19.5487	71	3.6398	116	16.225	21
274	0	OK	19.5752	108	3.057	107	17.175	18
276	0	OK	19.6735	137	4.4149	127	11.475	18
277	0	OK	19.7892	239	3.2031	115	17.525	20
278	0	OK	19.8099	60	3.2607	173	19.825	23
279	0	OK	19.8323	98	3.8441	69	7.875	11
281	0	OK	19.9166	129	3.5826	129	20.175	25
282	0	OK	19.927	113	3.6411	111	9.475	12
283	0	OK	20.0513	47	2.5435	90	15.675	14
284	0	OK	20.0781	13	2.6193	105	25.975	24
285	0	OK	20.0908	178	2.6899	106	11.625	11
287	0	OK	20.2787	7	2.2137	162	36.675	28
288	0	OK	20.4375	94	3.3117	97	12.05	14
289	0	OK	20.4382	240	3.1525	91	20.925	23
291	0	OK	20.6447	29	3.159	112	10.525	12
292	0	OK	20.6851	114	3.0521	127	14.175	15
294	0	OK	20.7728	124	3.1554	100	19.025	21
295	0	OK	20.8021	7	2.7899	91	15.5	15
296	0	OK	20.8167	240	3.327	72	14.25	17
297	0	OK	20.8574	191	3.4274	103	12.475	15
300	0	OK	21.0556	92	3.1247	83	3.125	3
301	0	OK	21.1456	136	3.5601	126	11.925	15
302	0	OK	21.2687	248	2.7324	92	12.275	12
303	0	OK	21.278	7	2.7514	97	17.925	17
304	0	OK	21.3152	224	2.5932	91	19.75	18
305	0	OK	21.3216	160	2.1718	158	41.35	32
306	0	OK	21.4501	126	2.8589	111	23.05	23
307	0	OK	21.5642	38	3.8945	109	10.5	14
308	0	OK	21.5775	60	3.2152	95	16.525	19
309	0	OK	21.5805	227	3.2316	179	29.325	33
310	0	OK	21.6142	44	3.5088	108	7.075	9
311	0	OK	21.7305	62	2.719	103	27.85	27
312	0	OK	21.7834	248	2.4856	87	7.425	6
314	0	OK	22.0006	139	2.9969	95	8.2	9
316	0	OK	22.3305	122	3.4944	80	5.175	6
317	0	OK	22.3624	131	3.6186	84	10.175	13
318	0	OK	22.4999	50	3.5908	100	25.325	32
319	0	OK	22.7597	131	3.63	121	19.575	25
320	0	OK	22.8973	240	2.9158	251	39.2	40
321	0	OK	22.9248	14	3.4025	133	19.725	24
323	0	OK	23.0081	215	3.9919	105	8.05	11
324	0	OK	23.0271	232	2.4676	123	22.35	19
325	0	OK	23.0436	56	3.4823	150	29.225	36
326	0	OK	23.1476	113	3.2391	85	8.775	10
327	0	OK	23.1845	120	3.6013	110	9.625	12
328	0	OK	23.2169	248	2.937	95	20.4	21
329	0	OK	23.2374	131	3.1338	112	21.875	24
331	0	OK	23.2529	198	3.4378	113	16.8	20
332	0	OK	23.3434	192	3.209	91	11.925	13
334	0	OK	23.5778	129	2.6736	94	10.2	10

335	0	OK	23.63	224	2.7141	86	19.9	19
336	0	OK	23.8015	124	3.2675	127	22.175	25
337	0	OK	24.2099	3	3.073	125	15.925	17
340	0	OK	24.3378	226	3.2708	86	8.4	10
342	0	OK	24.5798	70	3.4087	85	8.2	10
343	0	OK	24.6401	24	3.8294	105	2.725	4
344	0	OK	24.806	31	3.209	247	19.275	22
345	0	OK	24.8726	158	2.7422	98	20.5	20
346	0	OK	24.8821	112	3.3139	143	25.75	30
347	0	OK	25.0587	121	3.1655	107	13.55	15
348	0	OK	25.0825	61	3.0845	103	13.275	14
350	0	OK	25.1929	240	3.8229	109	18.475	25
351	0	OK	25.2036	241	3.7337	125	17.8	23
352	0	OK	25.3721	252	3.0874	95	11.4	12
353	0	OK	25.3752	80	2.9387	111	14.675	15
354	0	OK	25.5027	94	2.9655	125	22.5	23
355	0	OK	25.5141	122	3.414	139	19.7	24
356	0	OK	25.5675	240	3.2649	103	20.775	24
357	0	OK	25.666	10	3.1485	123	13.55	15
358	0	OK	25.6808	240	3.8226	119	16.95	23
359	0	OK	25.6962	71	3.3777	81	7.475	9
360	0	OK	25.7642	44	4.1511	111	17.275	25
361	0	OK	25.7917	240	2.7926	222	37.05	36
362	0	OK	25.8184	94	2.954	127	22.35	23
363	0	OK	25.8391	15	2.7527	91	13.975	14
364	0	OK	25.8769	159	3.2656	111	18.575	21
366	0	OK	26.0806	60	3.0152	95	19.225	20
367	0	OK	26.0827	177	2.9217	85	16.2	17
368	0	OK	26.1591	240	2.5974	103	17.35	16
369	0	OK	26.1719	209	3.0698	103	13.45	14
370	0	OK	26.2466	197	3.9968	87	13	18
371	0	OK	26.3322	215	3.4954	127	18.8	23
373	0	OK	26.4547	122	2.7814	117	17.7	17
374	0	OK	26.5846	18	3.9183	91	3.9	5
375	0	OK	26.6058	195	3.4787	88	12.025	15
377	0	OK	26.6947	31	3.1825	88	22.25	25
378	0	OK	26.8118	224	3.0217	127	19.55	21
379	0	OK	26.9954	121	4.1043	90	12.8	18
380	0	OK	27.2031	39	2.7406	102	15.65	15
381	0	OK	27.3318	30	3.0142	127	17.4	18
382	0	OK	27.4265	102	2.8158	96	16.725	17
383	0	OK	27.6291	193	2.5464	91	13.625	12
385	0	OK	27.8093	3	2.9433	123	21.025	22
387	0	OK	27.939	61	3.6366	102	11.975	15
388	0	OK	28.2774	175	3.3084	92	11.325	13
390	0	OK	28.4373	192	2.5905	99	23.875	22
391	0	OK	28.4538	127	3.4898	101	13.85	17
392	0	OK	28.5946	27	3.6461	93	13.4	17
395	0	OK	28.7476	3	3.4346	96	12.225	15
396	0	OK	28.7516	176	3.3953	83	9.3	11
397	0	OK	28.7794	240	3.5774	106	19.05	24
399	0	OK	28.857	1	3.0972	159	31.35	34

400	0	OK	29.2022	129	2.3261	155	28.925	24
401	0	OK	29.2276	143	3.6447	77	9.225	12
1	7	Signal/Noise Ch1	0.0198	7.375				
8	7	Signal/Noise Ch1	0.3899	14.8				
10	7	Signal/Noise Ch1	0.654	11.475				
18	7	Signal/Noise Ch1	1.3141	13.925				
19	7	Signal/Noise Ch1	1.3794	17.45				
23	7	Signal/Noise Ch1	1.7425	7.525				
24	7	Signal/Noise Ch1	1.7841	30.925				
27	7	Signal/Noise Ch1	2.0211	19.675				
28	7	Signal/Noise Ch1	2.0253	14.325				
29	7	Signal/Noise Ch1	2.0461	10.975				
31	7	Signal/Noise Ch1	2.2147	20.7				
34	7	Signal/Noise Ch1	2.2917	17.225				
35	7	Signal/Noise Ch1	2.5288	11.525				
38	7	Signal/Noise Ch1	2.8296	17				
39	7	Signal/Noise Ch1	2.8562	26.125				
48	7	Signal/Noise Ch1	3.8804	19.675				
53	7	Signal/Noise Ch1	4.0625	9.275				
54	7	Signal/Noise Ch1	4.067	13.6				
58	7	Signal/Noise Ch1	4.6002	11.95				
73	7	Signal/Noise Ch1	6.2931	8.45				
74	7	Signal/Noise Ch1	6.3233	14.125				
76	7	Signal/Noise Ch1	6.5118	11.7				
81	7	Signal/Noise Ch1	6.9137	6.025				
82	7	Signal/Noise Ch1	6.9177	26.975				
85	7	Signal/Noise Ch1	7.0443	6.15				
86	7	Signal/Noise Ch1	7.2212	16.325				
100	7	Signal/Noise Ch1	8.2169	7.25				
104	7	Signal/Noise Ch1	8.4838	18.05				
106	7	Signal/Noise Ch1	8.5974	12.575				
107	7	Signal/Noise Ch1	8.6814	10.95				
114	7	Signal/Noise Ch1	9.3245	13.975				
121	7	Signal/Noise Ch1	10.1556	15.425				
126	7	Signal/Noise Ch1	10.5187	21.9				
128	7	Signal/Noise Ch1	10.5788	3.925				
132	7	Signal/Noise Ch1	10.7633	10.925				
134	7	Signal/Noise Ch1	11.0236	7.4				
135	7	Signal/Noise Ch1	11.0601	31.75				
138	7	Signal/Noise Ch1	11.2267	6.55				
140	7	Signal/Noise Ch1	11.3855	13.175				
141	7	Signal/Noise Ch1	11.4062	33.65				
145	7	Signal/Noise Ch1	11.6858	12.75				
146	7	Signal/Noise Ch1	11.7829	6.1				
148	7	Signal/Noise Ch1	12.001	15.1				
151	7	Signal/Noise Ch1	12.3604	16.1				
152	7	Signal/Noise Ch1	12.4096	28.125				
153	7	Signal/Noise Ch1	12.4478	9.15				
154	7	Signal/Noise Ch1	12.4567	12.925				
158	7	Signal/Noise Ch1	12.6483	2.675				
160	7	Signal/Noise Ch1	12.8787	21.3				
162	7	Signal/Noise Ch1	12.9408	10.125				

164	7	Signal/Noise Ch1	13.2628	26.6
166	7	Signal/Noise Ch1	13.2798	5.575
167	7	Signal/Noise Ch1	13.3176	18
168	7	Signal/Noise Ch1	13.3182	18.025
173	7	Signal/Noise Ch1	13.5317	6.45
176	7	Signal/Noise Ch1	13.9596	16.85
182	7	Signal/Noise Ch1	14.3183	10.6
185	7	Signal/Noise Ch1	14.557	18.275
200	7	Signal/Noise Ch1	15.3126	10.8
209	7	Signal/Noise Ch1	15.7296	31.45
217	7	Signal/Noise Ch1	16.397	16.425
224	7	Signal/Noise Ch1	16.8822	6.7
227	7	Signal/Noise Ch1	17.1241	31.7
229	7	Signal/Noise Ch1	17.2219	27
230	7	Signal/Noise Ch1	17.2506	13.45
232	7	Signal/Noise Ch1	17.3249	27.5
234	7	Signal/Noise Ch1	17.3746	7.9
237	7	Signal/Noise Ch1	17.443	4.575
244	7	Signal/Noise Ch1	17.8834	7.55
247	7	Signal/Noise Ch1	18.0549	19.175
249	7	Signal/Noise Ch1	18.1502	12.975
252	7	Signal/Noise Ch1	18.3267	18.35
259	7	Signal/Noise Ch1	18.7083	26.45
260	7	Signal/Noise Ch1	18.7805	11.025
262	7	Signal/Noise Ch1	18.8247	17.65
264	7	Signal/Noise Ch1	18.9834	16.775
265	7	Signal/Noise Ch1	19.0029	30.975
275	7	Signal/Noise Ch1	19.5772	10.4
280	7	Signal/Noise Ch1	19.9107	24.025
286	7	Signal/Noise Ch1	20.1952	17.125
290	7	Signal/Noise Ch1	20.4747	12.325
293	7	Signal/Noise Ch1	20.6876	13.35
298	7	Signal/Noise Ch1	20.9376	9.1
299	7	Signal/Noise Ch1	20.9434	14.3
313	7	Signal/Noise Ch1	21.9294	22.3
315	7	Signal/Noise Ch1	22.0925	17.675
322	7	Signal/Noise Ch1	22.9454	8.475
330	7	Signal/Noise Ch1	23.2375	13.6
333	7	Signal/Noise Ch1	23.5073	30.35
338	7	Signal/Noise Ch1	24.244	14.55
339	7	Signal/Noise Ch1	24.2735	16.05
341	7	Signal/Noise Ch1	24.3982	18.625
349	7	Signal/Noise Ch1	25.1196	10.95
365	7	Signal/Noise Ch1	26.0268	10.8
372	7	Signal/Noise Ch1	26.4546	9.95
376	7	Signal/Noise Ch1	26.651	7.1
384	7	Signal/Noise Ch1	27.7935	17.4
386	7	Signal/Noise Ch1	27.9275	11.725
389	7	Signal/Noise Ch1	28.2818	17.675
393	7	Signal/Noise Ch1	28.6793	10.55
394	7	Signal/Noise Ch1	28.717	19.975
398	7	Signal/Noise Ch1	28.796	4.525

APPENDIX F

EFFECT OF PARTICLE SIZE ON PROBE VOLUME

The effect of particle size on probe volume are presented in Fig. F-1. The particle size of 5 microns shows the highest average transit length as compared to the particle sizes of 2.02 microns, 0.966 micron and 0.505 micron. The lower the particle size, the lower the transit length. Using the program in Appendix G, the author attempted to study the effect of particle size on the size of the probe volume (see Chapter 3 for a discussion on probe volume).

The author initially attempted to use this method in sizing the particles. However this method was not successful because the difference in transit lengths for these particle sizes is not significant. Also each particle size can have a varying trajectory, and thus a lower transit length could be attributed to any particle size. Hence this method did not yield useful results.

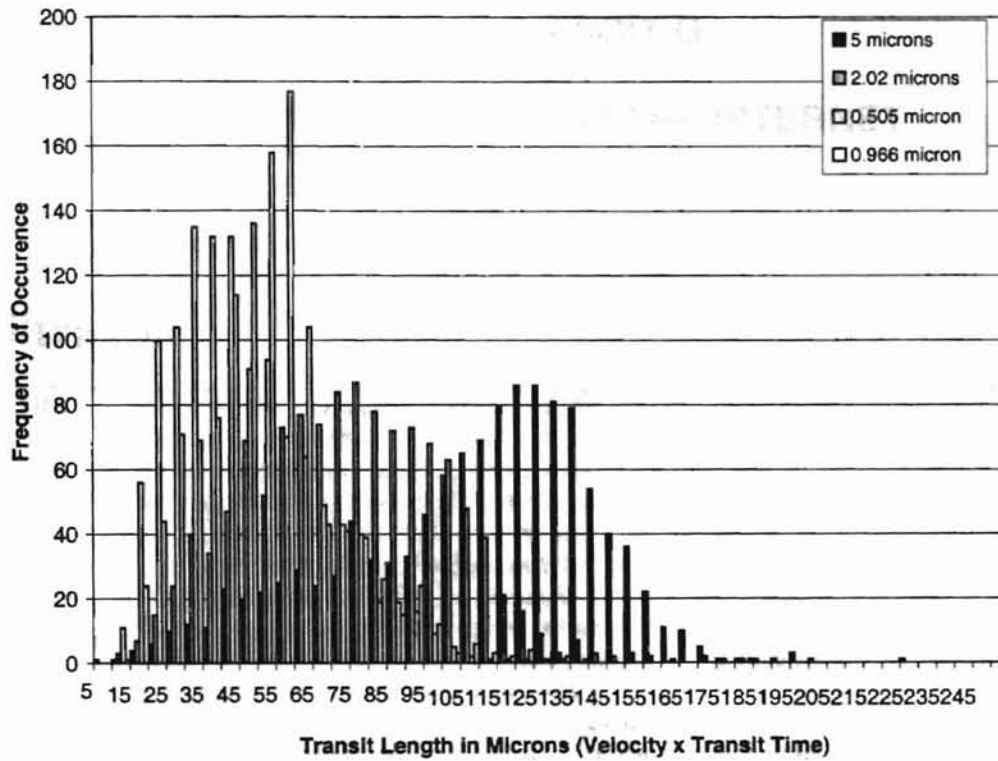


Figure F-1 Effect of Particle Size on the Transit Time of the LDV Signal

APPENDIX G

REFERENCES FROM THE INTERNET

1. Reference for <http://facilitiesnet.com/NS/NS3filtr.html>.

Filtration

FILTRATION IS A mystery to many designers and facility managers, perhaps misunderstood by others and probably underutilized by most. A better understanding of filtration technology can help facilities professionals prevent and mitigate indoor environmental quality problems.

Consider the basic objective: Facilities professionals need to know how to bring fresh air to a large group of people in an airtight environment. "What that means is putting 100 people in a 50-person space without complaints," said Wayne Robertson, a designer with Heery and Co.

The tactics and technologies available to accomplish this can be reduced to three basic principles: elimination, which is source control; extraction, which is filtration; and dilution, which is ventilation. These are the engineering principles for contaminant control in conditioned space. A truly healthy building depends upon a balance of usage of all three principles.

Filtration may appear to be an underutilized technology in commercial buildings. There's been a recent trend to grade filtration to medium efficiency pleats. Yet many aging buildings still use low-end filters. As testimony to the widespread usage of inadequate filtration, an entirely new industry of duct cleaning has been formed.

The following ASHRAE Standard 62-89 definitions set the stage for this discussion:

- **Air Cleaning System** is a device or combination of devices applied to reduce the concentration of airborne contaminants such as micro-organisms, dusts, fumes, respirable particles, other particulate matter, gases, and/or vapors in air. (Note: The critical factor is that the system provides the ability to control all of the referenced contaminants to attain acceptable air quality.)
- **Ventilation Air** is that portion of the supply air that is outdoor air, plus any recirculated air that has been treated for the purpose of maintaining acceptable indoor air quality. (Note: The key is that "ventilation air" can be defined as treated return air as a component of required ventilation rates.)
- **Air Conditioning** is the process of treating air to meet the requirements of a conditioned space by controlling its temperature, humidity, distribution and cleanliness. (Note: The operative word is "cleanliness" which usually is forgotten in the definition.)
- **Outdoor Air** is air taken from the external atmosphere; it hasn't been circulated through the system. (Note: This is not called "fresh air.")
- **Contamination** is an unwanted airborne constituent that may reduce acceptability of the air.
- **Filtration** (according to the author) is a device or system to treat air to remove those contaminants which cannot be seen. (The author's definition of "filtration" doesn't cover low-end panel filters and media which take out only large visible matter such as lint and hair.)

High-efficiency filtration is a relatively old and well-developed technology. However, specialized filtration has been predominantly focused on industry. Nevertheless, the products exist, they are proven and the application technology is well-developed. It is ready now to use in controlling contaminants in indoor air in commercial buildings.

Basic to an understanding of filtration is that airborne contaminants are both gaseous phase (chemicals in solution in air) and particulate (solid matter). This article focuses on particulate control.

The undergirding technologies of particulate control are impingement, straining and electromagnetic fields:

- **Impingement** means "collision." A particle will impinge, or collide, with a filter fiber and cling. This is the predominant mechanism for large particle filtration (such as paint booth filtration), as well as a range of low-efficiency prefilters.
- **Straining** acts very much like a screen. The filtration medium forms small holes or paths for airflow. Particles larger than the path will be withheld and retained within the medium.
- **Electromagnetic fields** are used to alter and manipulate the medium's electrostatic charge to capture the airborne particle, enabling it to "ground out" onto a collecting plate or media. The particles then are held into place with electromagnetic forces.

The media used for filtration include paper, usually in the form of a felt-like mat. Natural fibers such as cotton are used. Fabricated fibers such as superfine glass and a variety of synthetics also are used in the form of a lofted mat. Some of the latter synthetic fibers have an inherent surface charge or can be altered to enhance their natural charge. This allows the media to employ electromagnetic capture, in addition to simple straining. But charged media can lose their charge in an airstream and revert back into strainer filters, which can be detrimental to their anticipated efficacy.

Numerous factors can influence removal efficiency, or incoming particulate quantity compared with outgoing particulate quantity. For example, a highly efficient filter is a brick wall. Yet, because it won't allow air to flow easily, it's not an "effective" filtering device. Efficacy better describes performance because it includes consideration of the desired result.

To understand, evaluate and properly apply filtration equipment, other factors beyond efficiency must be considered. These include life and/or capacity, air flow characteristics, and total cost per unit time. A full evaluation of efficacy also includes life-cycle cost estimates. This includes raw material depletion; environmental impact from manufacturing, as well as disposal; and the inherent energy burden.

Specifically, "fractional efficiency" is defined as "In" minus "Out" divided by "In" multiplied by 100 -- that gives you an efficiency value. The more useful meaning of fractional efficiency refers to the efficiency of a particulate filter at specific particle "size fractions." This addresses more directly the issue of efficacy -- as in "What can I expect of this filter against a specific problem component of the air stream, such as mold spores?"

Factors affecting particle capture behaviour include particle size, mass and charge. A filter's efficiency is highly dependent upon particle size; a rating system that doesn't specify a precise size can be misleading. The type and loading characteristics of the filter media or device also will affect efficiency and performance. Strainer media such as those used in bag filters will increase in efficiency as it loads. Thus, a rating system that uses averaging over the filter's life cycle can provide misleading information about the efficiency of the filter during its early life. Conversely, electrostatic-type filters lose efficiency as the electromagnetic sites are filled with captured filtrate.

All filtration types have relatively high efficiency on larger particles. However, only the higher efficiency ASHRAE-rated filters maintain acceptable efficiencies at low and submicron size.

Evaluating performance

The filter test method most appropriate for commercial buildings is ASHRAE TM 52.1. Unfortunately, this test method has serious weaknesses. Its "Arrestance Values" show large numbers. However, this measures retention of predominantly large mass particles and does not indicate efficiency.

Also, its Atmospheric Dust Spot Method uses an undefined test aerosol -- ambient atmospheric air. The determination also is based upon discoloration, which is 1930s technology. The data also is presented as an average which distorts the actual performance, overstating it for much of the filter's life.

Fortunately, a new version of the ASHRAE Standard is being developed. Designated 52.2, the standard will use a defined test aerosol, will report fractional efficiency from 0.3 microns through 10 microns, and will report initial point data. In late summer 1995, ASHRAE expected a public review draft to be issued in fall.

Effective design

With this working knowledge, the following process will be an effective design model: First, identify the contaminant. Usually the air is a stew including many different contaminants. To develop the appropriate system and select the proper filtering media, you'll need to know the nature and content of the complete airstream. Next, establish control objectives or targets -- for example, no more than 10,000 particles per cubic foot of respirable size. Then, select the control strategy, starting with filtering device/system selection. This includes type, media and efficiency expectations.

Before deciding upon a specific system or device, perform a life-cycle cost analysis. A given system might perform adequately, but might have short life, or high energy or maintenance costs.

Finally, establish the airflow path. How will the air be delivered to and from the filtering device? How much air will be treated and how will it be delivered to the targeted zone? Should prefiltration be used? Anecdotal evidence indicates that only HEPA, gas phase sorbers, minipleat and electronic precipitators must be protected by prefiltration. Use of prefilters on other filter types usually drives up costs adds little in extended life or life-cycle value.

H.E. "Barney" Burroughs is a director and principal in Environmental Design International Ltd., Atlanta, and is president of IAQ/BWC Building Wellness Consultancy. From July 1994 Building Operating Management.

[/graphics/pgend.map/graphics/pgend.map](#)

© 1995 Trade Press Publishing Corporation

APPENDIX H

LIST OF EQUIPMENT

1. 5 Watt Argon-Ion Laser: Coherent, Model Innova 70-A, Serial No. P/S 92K-1758
2. Remote Control for the Laser: Coherent, Model I-70, Serial No. 92411171
3. Fiber Drive: Aerometrics, Inc., Model FBD1240, Serial No. 026
4. Bragg Cell: IntraAction, Inc., Model ME-40H, Serial No. 3247
5. Photomultiplier Tubes: Aerometrics, Inc., Model RCM2200L, Serial No. 029
6. Doppler Signal Analyzer: Aerometrics, Inc., Model DSA3220, Serial No. 044
7. Computer and Monitor: Impression 3, IBM Compatible 80486 DX2, 66 MHz
8. Computer for Traverse System and MS-Excel Data Acquisition Files: Gateway 2000, IBM Compatible, 80486, 33 MHz
9. Laser Transceiver: Aerometrics, Inc., Model XRV1212, Serial No. 001
10. Three Stepper Motors (Sanyo Denki, Type: 103-850-11)
11. Oscilloscope: Hewlett Packard, Model 54501A
12. Plexiglass Test Housings: Similar to SAE J1669 Small Angle Diffuser Housing
13. Pleated Test Filters: Purolator Products, Inc., Inc., A13192 (formerly AF3192)
14. TSI Mass Flow Sensor: TSI, Model 2018, Serial No. 30644
15. Atomizer: TSI Model 9306, Six-Jet Atomizer
16. SAE J726 Air Stand, Purolator Products, Inc.
17. Rival Compact Heater, Model T114 (1250 W)
18. Electric Heater [with 1300 W and 1500 W Capacity]

19. Stepper Motor Drives, Model CMD-40
20. 24 V DC - 6 A Power Supply (Acme Electronics)
21. Connector 3 for Digital Output, Model PCLD-780
22. Omega RH20/RH21 Digital Temperature and Humidity Meters
23. SunBeam Mechanical Thermometer-Hygrometer
24. Electro-Tech Systems, Inc., Model 210 Static Meter
25. Room Air Conditioner: Cooling Capacity 12600 Btu/hr
26. Polystyrene Latex (PSL) Particles: 0.497, 0.966, 2.04 μm Diameter, Duke Scientific

APPENDIX I

ERROR ANALYSIS

The errors or uncertainties in the overall efficiency of the filter can be calculated based on a simple analysis of the variation in the number density calculation. Anand (1997) and Saxena (1998) have presented the prediction of the uncertainties in their experimental filtration efficiency measurements using error analysis as proposed by Kline and McClintock (1953). This was based on the assumption of a random error in number density measurements. Thus the error in number density due to errors in particle count, n_{attempts} , velocity, V , time, t , and cross-sectional area of probe volume, A_p has been shown by Anand to be

$$\frac{dN}{N} = \left[\left(\frac{dn_{\text{attempts}}}{n_{\text{attempts}}} \right)^2 + \left(\frac{dV}{V} \right)^2 + \left(-\frac{dt}{t} \right)^2 + \left(-\frac{dA_p}{A_p} \right)^2 \right]^{1/2} \quad (\text{I-1})$$

where the number density is defined as follows:

$$N = \frac{n}{V t A_p} \quad (\text{I-2})$$

On the other hand, the filtration efficiency based on number density or particle count (concentration) is given as

$$\eta_i = \frac{N_{iup} - N_{idown}}{N_{iup}} = 1 - \frac{N_{idown}}{N_{iup}} = 1 - R_d \quad (\text{I-3})$$

where N_{iup} and N_{idown} are the upstream and downstream number densities, respectively.

Thus the error in the measured efficiencies will be predicted by the following equation

(for the derivation, refer to Anand, 1997):

$$\frac{d\eta_i}{\eta_i} = \sqrt{2}(c_e) \frac{N_{idown}}{N_{iup}} = \sqrt{2}(c_e)R_d \quad (I-4)$$

where c_e is the fractional error values for the upstream and downstream number densities assuming both fractional errors are of the same magnitude. It is defined as follows:

$$c_e = \frac{\Delta N_{iup}}{N_{iup}} = \frac{\Delta N_{idown}}{N_{idown}} = \frac{dN_i}{N_i} \quad (I-5)$$

where ΔN_{iup} and ΔN_{idown} are the deviations (errors) in the upstream and downstream number densities.

Anand (1997) assumed an error of 2% for the cross-sectional area of the probe volume of the LDA system. However, this might be more than 2% if one sees the errors in calculating the cross-sectional area of the probe volume by approximating it as a perfect ellipsoid and without any corrections to the variation in the cross-sectional area of the probe volume. Thus assuming a maximum error of 7.5% in the cross-sectional area of the probe volume would not be an exaggeration. Similarly the percentage errors in particle count (due to noise), time for data collection, and velocity can be assumed as 5%, 2%, and 2%, respectively. Following the above error assumptions, the error in number density becomes (from Eq. (I-1))

$$\frac{dN_i}{N_i} = \left[(0.05)^2 + (-0.02)^2 + (-0.02)^2 + (-0.075)^2 \right] = 0.0945, \text{ or } 9.45\% \quad (I-6)$$

Substituting this 9.45% number density error into the equation for efficiency error in Eq. (I-4), the general error equation for filtration efficiency measurement reduces to:

$$\frac{d\eta_i}{\eta_i} = \sqrt{2}(0.0945)R_d = (0.1262)R_d \quad (I-7)$$

Therefore it is possible to find the experimental overall and local filtration efficiency errors using Eq. (I-4).

APPENDIX J

RESULTS FOR MONODISPERSE AEROSOLS CONTAINING 0.505 MICRON DIAMETER AND 2.02 MICRON DIAMETER PSL PARTICLES IN THE SIMULATED AUTOMOTIVE FILTER HOUSING

The overall results for the tests conducted in the simulated automotive filter housing (Al-Sarkhi, 1999) are shown in Table J-1. Each test is assigned a unique identification number. This identification number indicates the test flow rate, the particle diameter, the setup used and the file name under which it is stored. For example, for test code 80-2ausaf,

“80” corresponds to the test flow rate of 136.0 m³/hr (80 scfm); “2” is the particle diameter of 2.02 microns (“05” would indicate 0.505 micron); “a” is the 1st test performed (“b” would correspond to 1st test repetition; “c” would correspond to 2nd test repetition, and so on); “u” indicates an ungrounded setup; saf indicates that the simulated automotive filter housing was used.

Table J-1 Test Conditions and Average Values over the Filter Surface of Efficiency, Upstream and Downstream Velocities, and Upstream and Downstream Number Densities in the Simulated Automotive Filter Housing

No.	Test Code	Test Date	Corrected Flow Rate	Overall Average Efficiency of the Filter	Upstream Number Density	Upstream Velocity	Downstream Number Density	Downstream Velocity	Pressure Drop (mm Water Column)			PSL Solution Strength	Electrostatic Charge
									Initial	Final	Rise		
			m ³ /hr	(%)	(m ⁻³)	m/s	(m ⁻³)	m/s				m ³ /m ³	(V)
1	80-2ausaf	11/17/99	136.03	10.21	1.08E+08	7.83	8.77E+07	4.08	10.16	12.7	2.54	15/750	-50
2	60-2ausaf	11/15/99	102.02	11.24	1.26E+08	5.64	9.38E+07	3.07	7.62	7.62	0	15/750	-50
3	45-2ausaf	11/12/99	76.51	49.16	2.23E+08	3.77	1.11E+08	2.04	2.54	5.08	2.54	15/750	-2000
4	35-2ausaf	11/16/99	59.51	17.24	3.04E+08	3.20	2.40E+08	1.89	2.54	5.08	2.54	15/750	-50
5	25-2ausaf	11/17/99	42.51	-7.09	2.25E+08	2.53	2.33E+08	1.47	2.54	2.54	0	15/750	-150
6	20-2ausaf	11/18/99	34.01	14.24	3.85E+08	1.72	3.23E+08	0.97	2.54	2.54	0	15/750	-250
7	80-05ausaf	11/20/99	136.03	-283.64	4.81E+07	8.22	1.26E+08	4.15	10.16	12.7	2.54	5/1000	-50
8	45-05ausaf	11/19/99	76.51	-190.26	1.38E+08	4.58	2.18E+08	2.61	2.54	5.08	2.54	5/1000	0
9	25-05ausaf	11/19/99	42.51	-190.26	7.77E+07	2.37	2.03E+08	1.45	2.54	2.54	0	5/1000	0

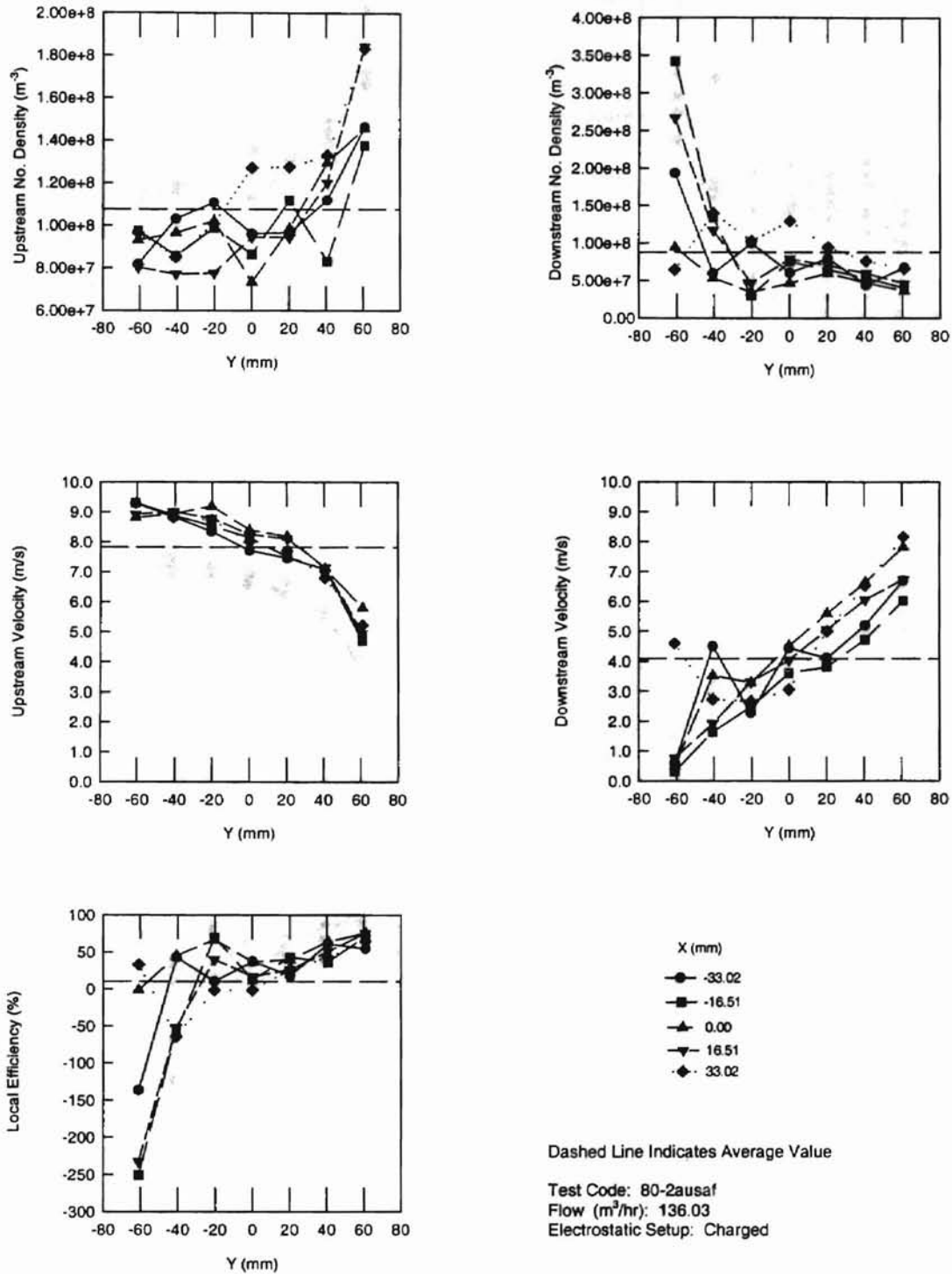


Figure J-1 Results for 2.02 Micron Diameter Aerosols using a Charged Setup for a Flow Rate of 136.03 m³/hr in the Simulated Automotive Filter Housing (80-2ausaf)

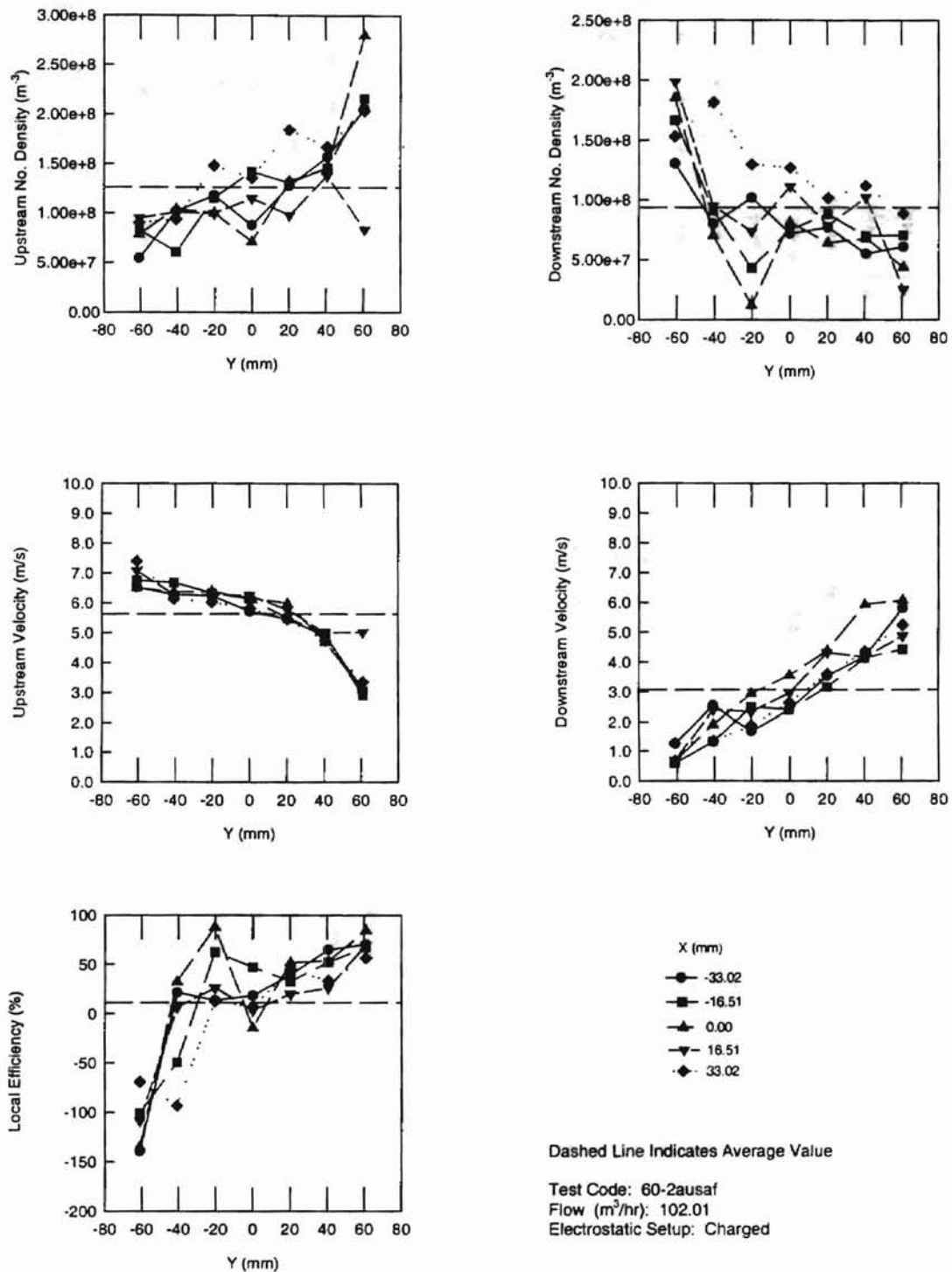


Figure J-2 Results for 2.02 Micron Diameter Aerosols using a Charged Setup for a Flow Rate of 102.01 m³/hr in the Simulated Automotive Filter Housing (60-2ausaf)

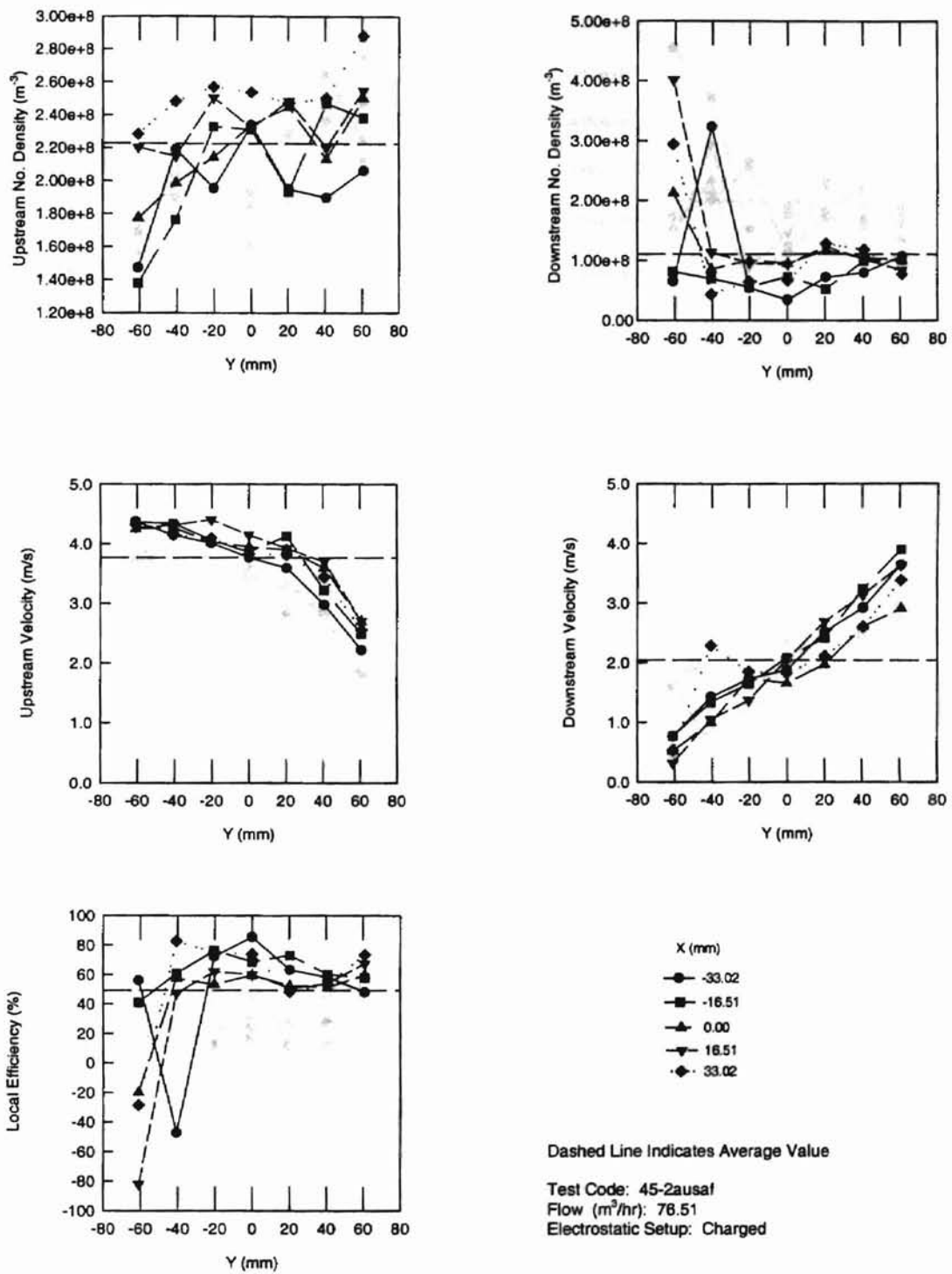


Figure J-3 Results for 2.02 Micron Diameter Aerosols using a Charged Setup for a Flow Rate of 76.51 m³/hr in the Simulated Automotive Filter Housing (45-2ausaf)

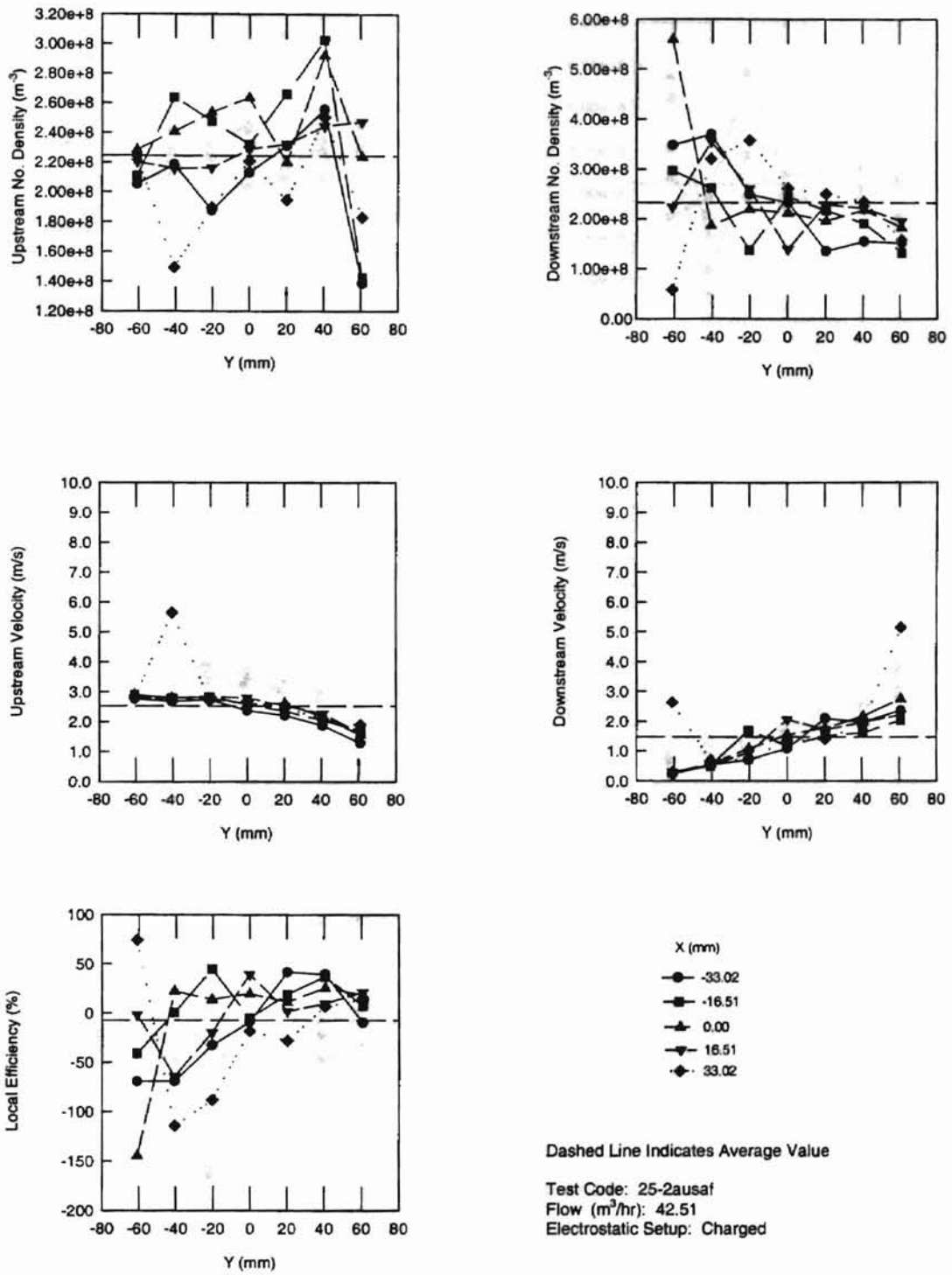


Figure J-5 Results for 2.02 Micron Diameter Aerosols using a Charged Setup for a Flow Rate of 42.51 m³/hr in the Simulated Automotive Filter Housing (25-2ausaf)

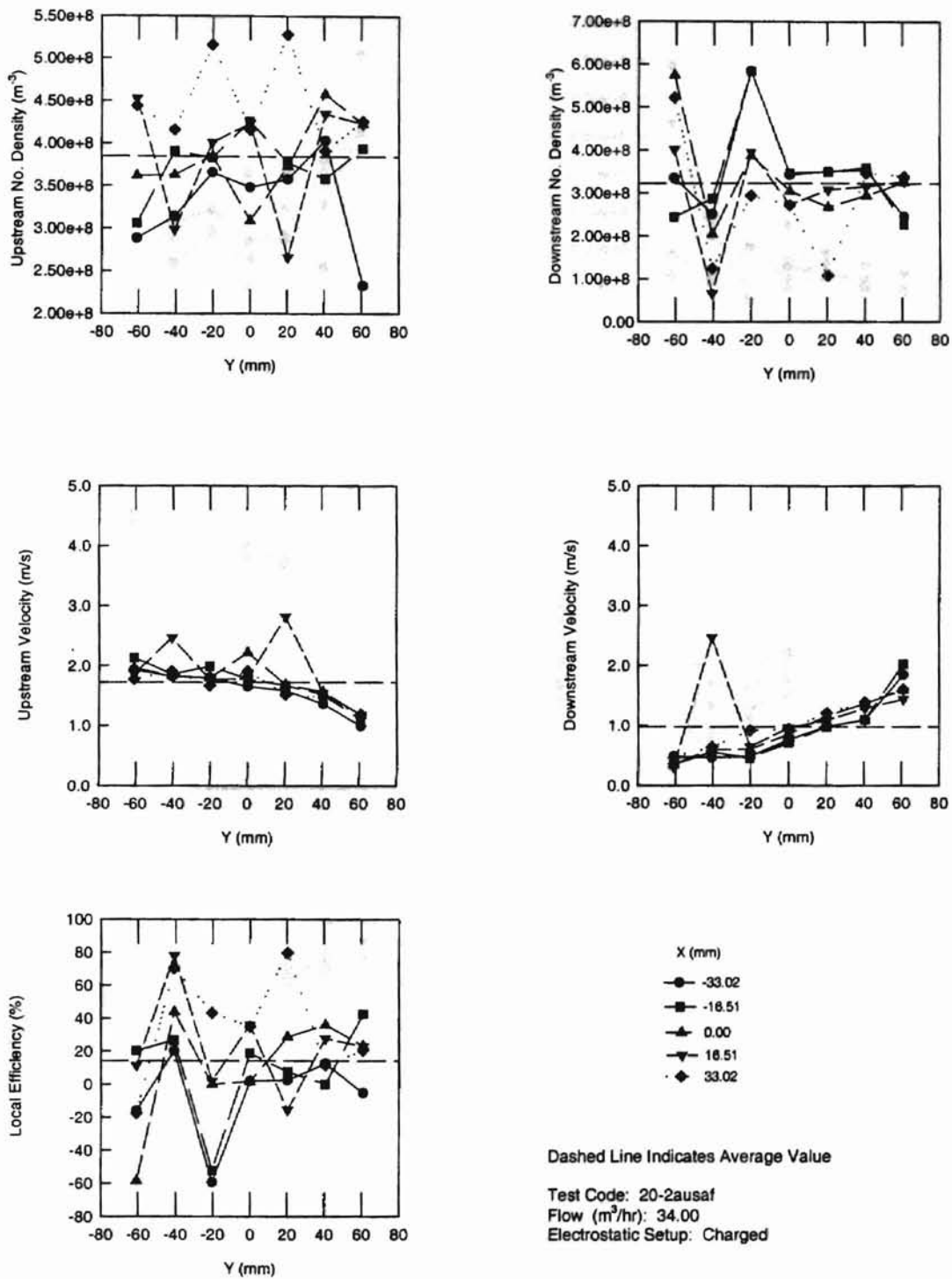


Figure J-6 Results for 2.02 Micron Diameter Aerosols using a Charged Setup for a Flow Rate of 34.00 m³/hr in the Simulated Automotive Filter Housing (20-2ausaf)

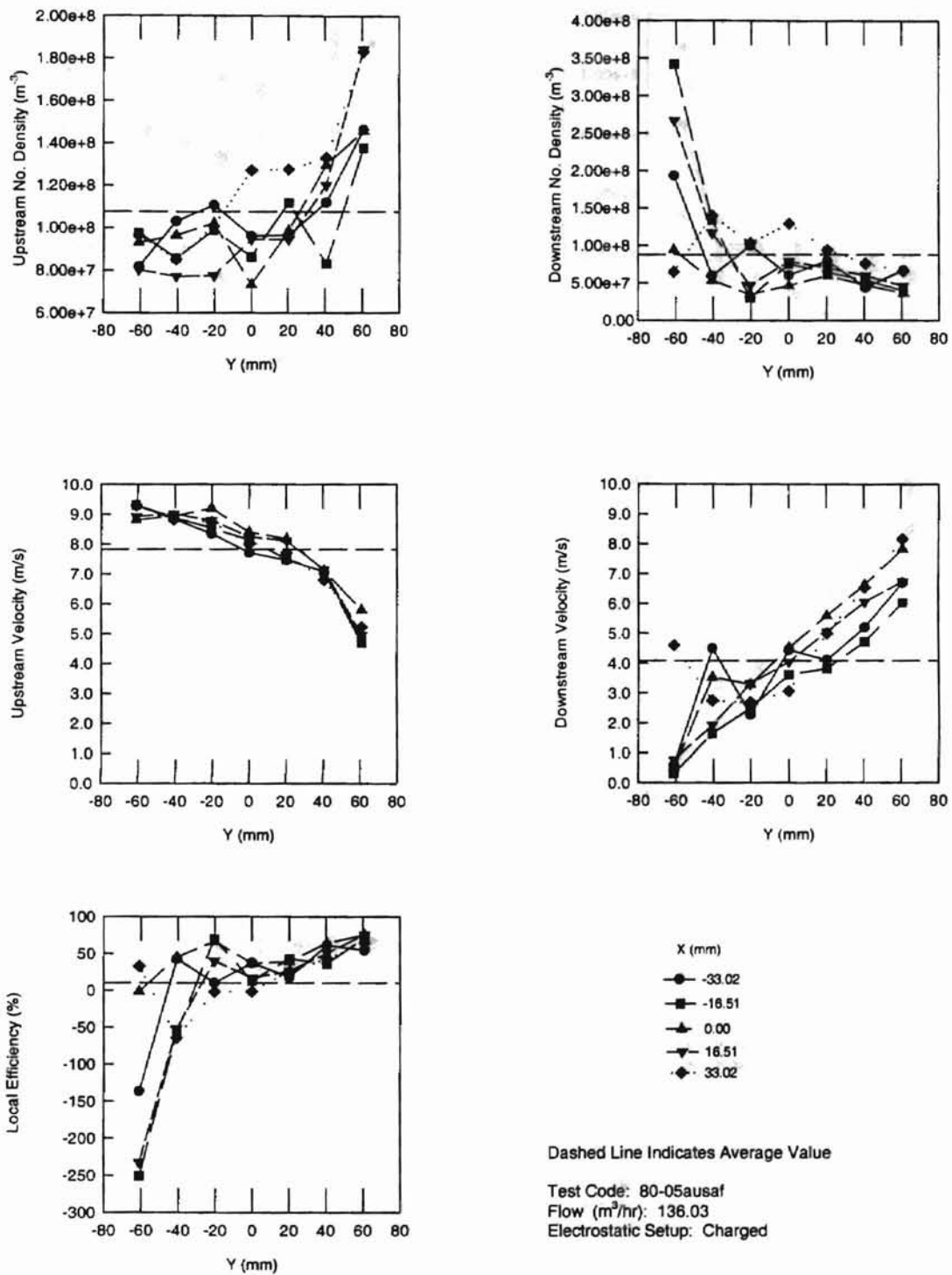


Figure J-7 Results for 0.505 Micron Diameter Aerosols using a Charged Setup for a Flow Rate of 136.03 m^3/hr in the Simulated Automotive Filter Housing (80-05ausaf)

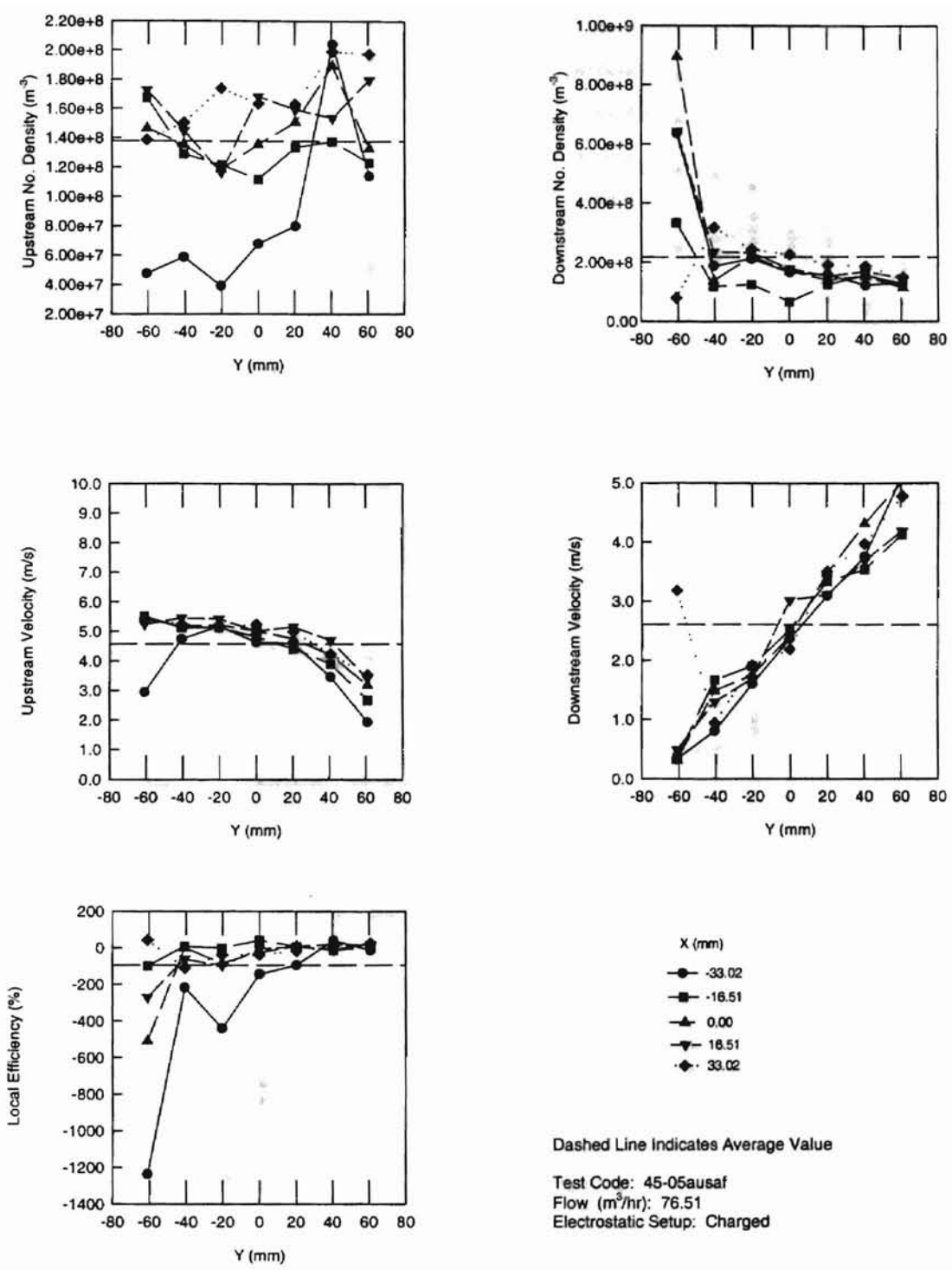


Figure J-8 Results for 0.505 Micron Diameter Aerosols using a Charged Setup for a Flow Rate of 76.51 m^3/hr in the Simulated Automotive Filter Housing (45-05ausaf)

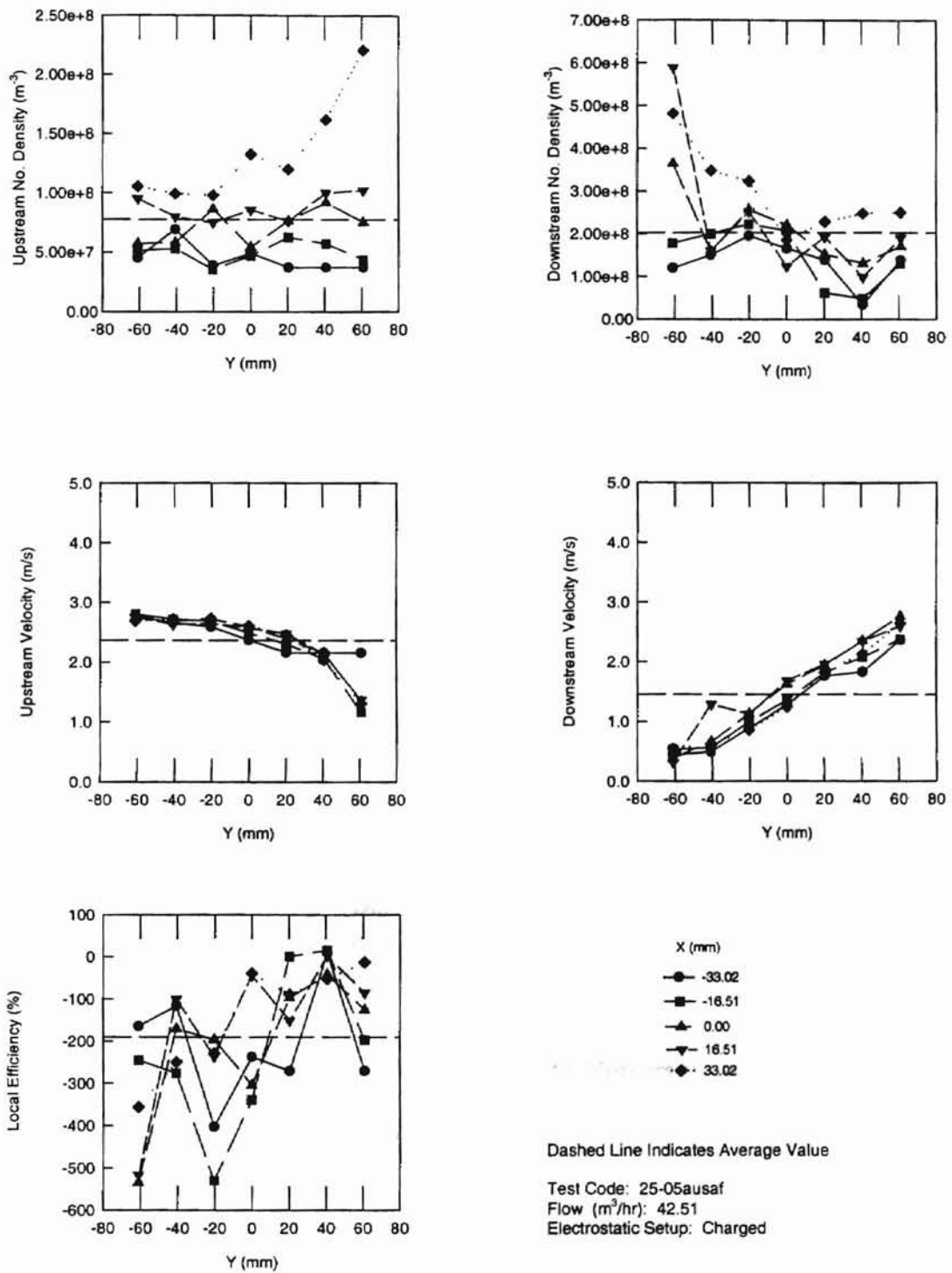


Figure J-9 Results for 0.505 Micron Diameter Aerosols using a Charged Setup for a Flow Rate of 42.51 m³/hr in the Simulated Automotive Filter Housing (25-05ausaf)

VITA

Ram Srinivasan

Candidate for the Degree of

Master of Science

Thesis: EFFECT OF CHARGE NEUTRALIZATION, PARTICLE SIZE AND
BIDISPERSE AEROSOL FRACTIONS ON THE EFFICIENCY OF
FIBROUS AUTOMOTIVE AIR FILTERS USING LASER DOPPLER
VELOCIMETRY

Major Field: Mechanical Engineering.

Biographical:

Personal Data: Born in Pune, India, on June 23, 1973

Educational: Graduated from St. Vincents Junior College of Education, Pune, India in 1991. Received Bachelor of Technology degree in Mechanical Engineering from Banaras Hindu University, Varanasi, India in January 1996. Completed the requirements for the Master of Science degree with a major in Mechanical Engineering at Oklahoma State University in May, 2000.

Experience: Employed by Oklahoma State University as a graduate research assistant from January, 1998 to November, 1999; worked as a Mechanical Engineer with Development Consultants Ltd., India from June, 1995 to December, 1997.

Professional Memberships: Student Member, ASME